# Evolution and Ecomorphology of the Avian Foot:
## The morphology of the tarsometatarsus in birds and its responses to evolutionary changes in foot use

Brigit Tronrud
Linacre College
University of Oxford

A thesis submitted for the degree of
Doctor of Philosophy
Michaelmas Term 2022

Supervised by:
Roger Benson
Graham Taylor

# Abstract

Accipitriformes, Strigiformes, and Falconiformes are the three extant raptorial avian clades, most members of which use their feet to kill and carry prey. The disparate grouping of these clades with similar foot use has been hypothesised to result from retention of raptoriality from a telluravian ancestor, which has not been tested using ecomorphological methods. I evaluated the hypothesis by testing the anatomical correlates of raptoriality and other foot uses in extant birds using geometric morphometrics and phylogenetic comparative shape analysis on first the entire tarsometatarsus bone, and then on the proximal articular surface and hypotarsus (a plantar channel through which flexor tendons run). I then mapped the ancestral states of raptoriality across the phylogeny, including fossil taxa, as well as the ancestral states of 14 other foot uses. Centroid size, body mass, flightlessness, zygodactyl digit orientation, force grip foot use, and raptoriality all had significant and independent effects on whole tarsometatarsus shape, and explain approximately 26% of tarsometatarsus shape variation. Hypotarsus shape is a statistically significant indicator of raptoriality in birds: raptorial birds tend to possess a deep and wide monosulcate hypotarsus. This relationship can be used to infer raptorial foot use in stem taxa throughout Telluraves known only from fossils. Using these inferred states in ancestral character estimation demonstrates that all extant raptorial groups have convergently evolved raptoriality, contradicting existing hypotheses of a raptorial ancestry of Telluraves as a whole. However, this does not rule out the occurrence of carnivory in the ancestor of Telluraves. Cursoriality, ability to hold down objects, digital manipulation, scansoriality, and hanging and clinging behaviour were determined to be convergent within Telluraves. Force grip foot use, walking ability, perching ability, and anisodactyl digit orientation were determined to be ancestral to Telluraves.

# Acknowledgements

I must thank a number of influential people who have helped this thesis come to life, in various ways and in no particular order.

Firstly, to my supervisors: Roger Benson, who always provided the most creative ways of looking at things; Graham Taylor, who gave sage advice, and crucially let me hold a Harris's hawk at Wytham Woods; and unofficially, Daniel Field, who encouraged my budding love of birds, and who thought I'd made a great joke when I said the Egyptian goose "doesn't look that bad". All of your ongoing feedback, assistance, and reassurance kept the creation of this work on the rails of an ever-changing track.

Secondly, to my family: my parents, who let me phone them at all hours, and my brother Thor, who cheered me on while he was simultaneously doing his own PhD. Thanks also go to my grandmother, who passed in 2019, as it was her weekly updates on knitting projects that kept me going through a challenging time.

Thirdly, to my friends: Josie Paton, for her patience in living with me for the last two years; Claudine Tinsman, for her uncanny ability to know which evenings I might like to escape; Alyssa Sanchez, for letting me video chat with her cats; and Jay L. Colbert, Danielle Ellis, and numerous other new and old long-distance friends for many wondrous and delightful reminders that the world is very big, and also very kind.

Fourthly, to the members of the office: Alice Turner, Duhita Naware, Mhairi Reid, and Gwen Antell, for their brilliant support and positivity, and for letting me distract them from their research (important scientific advancements) with my research (videos of birds).

Fifthly, to the paleontological community at Oxford: Elsa Panciroli, for her friendliness, openness, and her live commentary of the Scottish Highlands and Islands; Han Hu, for her fossil bird knowledge and invitations to play tennis; Hilary Ketchum, for sharing her enthusiasm in museum collections and her incredible mentorship; and to all the members of Oxford Palaeo Club for much-needed end-of-Tuesday illumination.

Lastly, many thanks go to the museum collections staff who generously provided images of their fossil tarsometatarsi during a global pandemic: Julien Lalanne (RBINS), Annelise Folie (RBINS), and Loïc Costeur (NMB).

I'm immensely grateful to all those listed here, as well as to the inhabitants of the last four years who have shaped my life, and therefore this dissertation, in one way or another. Including the birds. Thank you.

Brigit Tronrud
September, 2022

# Contents

List of Figures……*i*

Introduction

A. Background……... 1
B. Raptoriality……2
C. The Tarsometatarsus…… 4
D. Ecomorphology……6
E. Geometric Morphometrics…….8
F. Phylogenetic Comparative Analyses…… 10
G. Ancestral Character Estimation…… 11
H. Outline……...12

Chapter 1

1.1 Introduction……..15
1.2 Material and Methods
1.2.1 Terminology……..22
1.2.2 Data Collection…… 22
1.2.3 Ecological Foot Use Characters……23
1.2.4 Landmarking……43
1.2.5 Generalized Procrustes Analysis, and Principal Components Analysis…… 70
1.2.6 Phylogenetic Framework…….. 71
1.2.7 Phylogenetic Regression and Visualization: Shape Analysis……... 71
1.2.8 Phylogenetic Regression: Size Analysis……... 72
1.3 Results
1.3.1 Principal Components Analysis…… 73
1.3.2 Phylogenetic Regression: Size Analysis……... 79
1.3.3 Phylogenetic Regression: Shape Analysis Using Size-Related Traits……79
1.3.4 Phylogenetic Regression: Shape Analysis of All Traits…….... 80
1.3.5 Shape Variation Associated with Foot Use Traits…… 86
1.4 Discussion…… 106

Chapter 2

2.1 Introduction……..113
2.1.1 Initial Survey……115
2.1.2 Raptoriality in Extinct Species……..119
2.2 Material and Methods

2.2.1 Terminology……..121
2.2.2 Data Collection……. 121
2.2.3 Qualitative Classification……..122
2.2.4 Phylogenetic Frameworks…….125
2.2.5 Geometric Morphometrics: Taxon Sample……...134
2.2.6 Geometric Morphometrics: Landmarking…… 134
2.2.7 Generalized Procrustes Analysis, and Principal Components Analysis…… 137
2.2.8 Statistical Analyses……... 138
2.2.9 Analysis of Soft Tissue……. 139
2.3 Results
2.3.1 Analysis of Extant Taxa: Principal Components Analysis……... 143
2.3.2 Analysis of Extant Taxa: Generalized Procrustes Analysis……..146
2.3.3 Analysis of Fossil Taxa: Principal Components Analysis…… 148
2.3.4 Discriminant Function Analyses……...148
2.3.5 Analysis of Soft Tissue……. 150
2.4 Discussion
2.4.1 Raptoriality and Hypotarsus Shape in Extant Taxa…….. 153
2.4.2 Discriminant Analysis of Fossil Taxa……...153
2.4.3 Foot Tendon Comparison……. 157
2.4.4 Implications for Telluravian Ancestry…….. 158

Chapter 3
3.1 Introduction……..162
3.2 Material and Methods
3.2.1 Terminology……..165
3.2.2 Data Collection……. 166
3.2.3 Taxa and Character Scoring……..167
3.2.4 Phylogenetic Frameworks…….167
3.2.5 Ancestral Character Estimation…… 169
3.3 Results
3.3.1 Raptoriality……... 169
3.3.2 Force Grip……. 175
3.3.3 Zygodactyly…….. 177
3.3.4 Anisodactyly……. 180
3.3.5 Heterodactyly…… 182
3.3.6 Pamprodactyly…….. 182
3.3.7 Documented Walking Ability……... 184
3.3.8 Terrestrial vs. Arboreal……. 186
3.3.9 Hanging and Clinging Behaviour……. 188

3.3.10 Scansoriality……190
3.3.11 Digital Manipulation……...192
3.3.12 Ability to Hold Down Objects…… 195
3.3.13 General Perching Ability…… 197
3.3.14 Hopping Ability…….. 199
3.3.14 Cursoriality……. 201
3.4 Discussion……203
3.4.1 Ancestral Foot Use of Telluraves……. 209

Conclusion
A. Summary……...210
B. Caveats……..211
C. Future Directions……...212
D. Synthesis……... 213

Appendices
A. Supporting Charts for the Introduction
A.1 Tables……..216
B. Supporting Charts for Chapter 1
B.1 Tables…….. 230
B.2 Data……. 244
C. Supporting Charts for Chapter 2
C.1 Figures……245
C.2 Tables…….. 260
C.3 Data……. 269
D. Supporting Charts for Chapter 3
D.1 Figures……270
D.2 Tables……..309
D.3 Data……311

References……...312

# List of Figures

## Chapter 1

1. Simplified phylogeny of Telluraves……...15
2. Variation in morphology and foot use across Aves (1)…… 18
3. Variation in morphology and foot use across Aves (2)…… 19
4. Variation in morphology and foot use across Aves (3)…… 20
5. Semi-landmark series 1……...……...44
6. Semi-landmark series 2, Landmarks 1, 2……...45
7. Landmarks 3–6……...46
8. Semi-landmark series 3, Landmarks 7, 8……...47
9. Semi-landmark series 4, Landmarks 9, 10…….48
10. Landmarks 11, 12…….48
11. Landmarks 13, 14…….49
12. Semi-landmark series 5, Landmarks 15, 16…….50
13. Landmarks 17, 18…….50
14. Semi-landmark series 6, Landmark 19…… 51
15. Semi-landmark series 6, *Columba palumbus* and *Tockus nasutus*…….. 52
16. Semi-landmark series 7, Landmarks 1, 20……...53
17. Semi-landmark series 7, Landmark 20, *Climacteris melanurus*……..54
18. Semi-landmark series 8, Landmarks 21, 22…….56
19. Semi-landmark series 8, Landmark 21, Probosciger aterrimus……... 57
20. Semi-landmark series 8, *Regulus ignicapilla*……...58
21. Semi-landmark series 9, 10……..59
22. Landmarks 23–26…….60
23. Landmarks 27–29…….61
24. Landmarks 27–29, *Urocolius macrourus*…… 62
25. Semi-landmark series 9, 11, Landmarks 30, 31……...63
26. Semi-landmark series 10, 12, Landmarks 32, 33…….64
27. Semi-landmark series 10, 12, Landmarks 32, 33, *Falco sparverius*……65
28. Semi-landmark series 2, 13, Landmarks 34, 35……...66
29. Semi-landmark series 14, 15, Landmarks 36, 37…….68
30. Semi-landmark series 14, 15, Landmarks 36, 37, *Archilochus colubris*……. 69
31. Visualisation of minimum values of Principal Component 1……..74
32. Visualisation of maximum values of Principal Component 1……. 74
33. Visualisation of minimum values of Principal Component 2……..75
34. Visualisation of maximum values of Principal Component 2……. 76
35. Visualisation of minimum values of Principal Component 3……..77
36. Visualisation of maximum values of Principal Component 3……. 77
37. Mean body mass shape deformations…….. 87

38. Centroid size shape deformations…… 89
39. Centroid size shape deformations, scaled to input centroid sizes……91
40. Force grip foot use and raptoriality shape deformations……. 93
41. Flightlessness shape deformations……...100
42. Zygodactyl shape deformations, with force grip foot use = 0……. 103
43. Zygodactyl shape deformations, with force grip foot use = 1……. 104
44. Podicipediformes tarsometatarsus morphology……...109
45. Aquatic taxa tarsometatarsus morphology……...110

## Chapter 2

1. Hypotarsus shape categories……..114
2. Phylogenetic tree of Aves showing trends of raptoriality and monosulcate hypotarsus shape…… 117
3. Phylogenetic tree of Accipitriformes showing trends of raptoriality and monosulcate hypotarsus shape……...118
4. Monosulcate hypotarsi across Aves……...120
5. Fossil hypotarsi (1)…… 127
6. Fossil hypotarsi (2)…… 130
7. Hypotarsus landmarking scheme……... 134
8. Cross-sectional imaging of flexor tendons (1)……...141
9. Cross-sectional imaging of flexor tendons (2)……...142
10. Principal components plot of extant taxa……145
11. pGLS hypotarsus shape deformations……. 146
12. LM hypotarsus shape deformations……147
13. Raptorial foot use plotted against regression axis……147
14. Principal components plot of extant and fossil hypotarsus shape……148
15. Phylogenetic tree of Aves showing raptoriality in extant and fossil taxa……155

## Chapter 3

1. Phylogenetic tree of Accipitriformes showing ancestral character estimation for raptoriality in extant taxa……... 171
2. Phylogenetic tree of Aves showing ancestral character estimation for raptoriality in extant and fossil taxa…….....172
3. Phylogenetic tree of Strigiformes showing ancestral character estimation for raptoriality in extant and fossil taxa……...173
4. Phylogenetic tree of Accipitriformes showing ancestral character estimation for raptoriality in extant and fossil taxa……...174
5. Phylogenetic tree of Aves showing ancestral character estimation for force grip foot use in extant taxa……176
6. Phylogenetic tree of Accipitriformes showing ancestral character estimation for

force grip foot use in extant taxa……... 177
7. Phylogenetic tree of Aves showing ancestral character estimation for zygodactyly in extant taxa……..179
8. Phylogenetic tree of Aves showing ancestral character estimation for anisodactyly in extant taxa……..181
9. Phylogenetic tree of Aves showing ancestral character estimation for heterodactyly and pamprodactyly in extant taxa…….. 183
10. Phylogenetic tree of Aves showing ancestral character estimation for walking ability in extant taxa…….. 185
11. Phylogenetic tree of Aves showing ancestral character estimation for terrestriality vs arboreality in extant taxa……... 187
12. Phylogenetic tree of Aves showing ancestral character estimation for hanging and clinging behaviour in extant taxa…… 189
13. Phylogenetic tree of Aves showing ancestral character estimation for scansoriality in extant taxa……..191
14. Phylogenetic tree of Aves showing ancestral character estimation for digital manipulation in extant taxa……193
15. Phylogenetic tree of Accipitriformes showing ancestral character estimation for digital manipulation in extant taxa……194
16. Phylogenetic tree of Aves showing ancestral character estimation for ability to hold down objects in extant taxa……196
17. Phylogenetic tree of Aves showing ancestral character estimation for perching ability in extant taxa……...198
18. Phylogenetic tree of Aves showing ancestral character estimation for hopping ability in extant taxa……...200
19. Phylogenetic tree of Aves showing ancestral character estimation for cursoriality in extant taxa……..202
20. Extant force grip foot use tarsometatarsus morphology…….. 204
21. Force grip foot use shape deformations……...205
22. Fossil taxa labelled with force grip foot use morphology (1)……..207
23. Fossil taxa labelled with force grip foot use morphology (2)……..208

## Appendices

C.1 Extant hypotarsi morphology (1)…… 246
C.2 Extant hypotarsi morphology (2)…… 248
C.3 Extant hypotarsi morphology (3)…… 250
C.4 Extant hypotarsi morphology (4)…… 252
C.5 Extant hypotarsi morphology (5)…… 254
C.6 Extant hypotarsi morphology (6)…… 256
C.7 Visualisation of minimum and maximum values of Principal Component 1……. 257

C.8 Visualisation of minimum and maximum values of Principal Component 2……. 258
C.9 Visualisation of minimum and maximum values of Principal Component 3……. 259
D.1 Phylogenetic tree of Aves showing ancestral character estimation for raptoriality in extant taxa……..271
D.2 Phylogenetic tree of Aves showing ancestral character estimation for raptoriality in extant and fossil taxa……. 273
D.3 Phylogenetic tree of Aves showing ancestral character estimation for raptoriality in extant and fossil taxa, including *Messelastur gratulator*……...275
D.4 Phylogenetic tree of Aves showing ancestral character estimation for force grip foot use in extant taxa……277
D.5 Phylogenetic tree of Aves showing ancestral character estimation for zygodactyly in extant taxa……..279
D.6 Phylogenetic tree of Aves showing ancestral character estimation for anisodactyly in extant taxa, using ER model reconstruction…….. 281
D.7 Phylogenetic tree of Aves showing ancestral character estimation for anisodactyly in extant taxa, using ARD model reconstruction……...283
D.8 Phylogenetic tree of Aves showing ancestral character estimation for heterodactyly in extant taxa……..285
D.9 Phylogenetic tree of Aves showing ancestral character estimation for pamprodactyly in extant taxa……287
D.10 Phylogenetic tree of Aves showing ancestral character estimation for walking ability in extant taxa, using ER model reconstruction……...289
D.11 Phylogenetic tree of Aves showing ancestral character estimation for walking ability in extant taxa, using ARD model reconstruction……291
D.12 Phylogenetic tree of Aves showing ancestral character estimation for terrestriality vs arboreality in extant taxa……...293
D.13 Phylogenetic tree of Aves showing ancestral character estimation for hanging and clinging behaviour in extant taxa…… 295
D.14 Phylogenetic tree of Aves showing ancestral character estimation for scansoriality in extant taxa……..297
D.15 Phylogenetic tree of Aves showing ancestral character estimation for digital manipulation in extant taxa……299
D.16 Phylogenetic tree of Aves showing ancestral character estimation for ability to hold down objects in extant taxa……301
D.17 Phylogenetic tree of Aves showing ancestral character estimation for perching ability in extant taxa……...303
D.18 Phylogenetic tree of Aves showing ancestral character estimation for hopping ability in extant taxa……...305
D.19 Phylogenetic tree of Aves showing ancestral character estimation for cursoriality in extant taxa……..307

# Introduction

## A. Background

The three major groups of predatory birds in Aves are Accipitriformes (hawks, eagles, and vultures), Strigiformes (owls), and Falconiformes (falcons). These orders fall alongside other predatory clades, such as Cariamiformes (seriemas), and many other vertebrate-feeding groups within Telluraves, or "land birds". In addition to carnivory, Accipitriformes, Strigiformes, and Falconiformes share a number of traits, such as large and strongly curved talons, increased visual acuity, and prey capture using the feet, and these morphological and ecological similarities have caused historical studies of classification to often propose that they are very closely related to each other. For example, Garrod (1874) hypothesised that the group "Accipitres" contained both the families Falconidae and Strigidae, that Cathartidae (New World vultures) was a separate "cohort", and that both these groups were all contained within Ciconiiformes (now storks). These merged classifications persisted in various phylogenetic arrangements until the emergence of molecular phylogenetic studies (e.g. Wink et al., 1998), and then in Hackett et al. (2008), which showed through genome-based phylogenetic analysis that Accipitriformes, Strigiformes, and Falconiformes are separate orders, sharing a common ancestor only at the very base of Telluraves. This placement raises intriguing possibilities about the ecological ancestry of land

birds; it has been suggested that raptoriality could be ancestral, not only to the currently disparate extant raptorial groups, but for all landbirds (Jarvis et al., 2014; Prum et al., 2015). Alternatively, raptoriality may have evolved independently three times within Telluraves, providing a striking example of convergent evolution.

However, these hypotheses remain uncertain, in part due to the ambiguity of meaning among different uses of the term "raptoriality", and in part due to the uncertain ecologies of fossil species. In this thesis, I use the morphology of the tarsometatarsus bone to explore the varied foot uses of Aves, including raptoriality, and ultimately test the hypothesis of raptorial ancestry in Telluraves.

## B. Raptoriality

The terms "raptorial" and "predatory" have often been used interchangeably in descriptions of bird ecology, along with the term "bird of prey". The predatory nature of "raptors" such as Accipitriformes, Falconiformes, and Strigiformes, and the enduring usage of the term in colloquial circumstances has resulted in widely varying formal definitions of "raptoriality" in studies of avian ecology, ecomorphology, and palaeobiology. This term has been used to describe avian features ranging from specifications in diet, relative size to prey, beak shape, wing shape, and visual acuity (e.g. Burton, 1989; Habib and Ruff, 2007; Tsang and McDonald, 2019). There is also a tendency to subdivide the term further by either diurnal or nocturnal behaviour, depending on the inclusion of owls in research (e.g. Hertel, 1995; Mayr, 2006; Tsang and McDonald, 2019).

With the exception of cases where "raptors" are nebulously (and tautologically) defined as "birds of prey", or simply left undefined, uses of "raptor" and "raptoriality" in the literature fall broadly into two categories: taxonomic and foot-use based definitions. For example, several

articles of the mid-2000s (Appendix Table A.1) which use the term "raptor" define it as those taxa within the now obsolete order Falconiformes, which has been since split into the two distinct orders Accipitriformes and Falconiformes. McClure et al. (2019) came to the conclusion that qualitative foot morphology and behaviour was too ambiguous to be useful in defining the term, and so suggested that it refer to the taxonomic orders evolved from raptorial landbirds in which the majority of species have "maintained their raptorial lifestyle" (McClure et al., 2019; p.426). This type of definition further varies in its inclusion of taxa. Some authors have included Cariamiformes (seriemas) in the purview of "raptorial ecology" (e.g. Jarvis et al., 2014; Prum et al., 2015; McClure et al., 2019), whereas others either include or exclude owls and vultures, depending on the focus of the study (e.g. Negro et al., 2006; Hertel et al., 2015).

Few studies remark on the "highly evolved senses" (Tsang and McDonald, 2019) or the "highly efficient predatory characteristics" (Ward et al., 2002) of "raptors" which they subsequently list by species or group. These characteristics include strongly curved beaks, enhanced visual, aural, or olfactory capabilities, and sharp talons, as well as powerful hindlimbs, all for the efficient capture of prey. However, the particular usage of hindlimbs and feet in definitions of raptorial birds in the literature is relatively uncommon.

Of those raptorial definitions which do involve foot use, two are notably applicable here. Mayr et al. (2013) defined raptoriality in birds as the use of feet to manipulate animal prey; Zeffer et al. (2003) defined their bird of prey "habitat group" as those birds which seize prey from or out of the air and carry it with their feet. It is a combination of these uses which I adapted into the working definition of raptoriality, specifically in terms of foot use: birds which kill and carry their prey with their feet. I use this definition of the term raptoriality for two reasons. Firstly, this definition distinguishes between "raptoriality" (as a foot use) and

"carnivory" (as a dietary category). This is important because carnivory has a shared meaning across all vertebrates and should be used as such in birds. Secondly, restricting raptoriality to birds which use their feet to kill and carry prey renders the concept into a testable form-function hypothesis.

This working definition means that vultures, often grouped ecologically with other Accipitriformes as "raptors", are not considered raptorial here, as they do not actively kill their prey, and have relatively weak feet in terms of grasping (Birds of the World, 2020). In Zeffer et al. (2003), in which taxa were given primary ecological designations, the vultures in their dataset were categorised as "ground birds", whereas other Accipitriformes were categorised as "birds of prey". Furthermore, although seriemas (Cariamiformes) have been included in some general concepts of "raptorial" bird (Jarvis et al., 2014; Prum et al., 2015; McClure et al., 2019), they also do not kill or carry their prey with their feet, and so are not here considered as being raptorial. Both of these non-raptorial yet raptor-adjacent groups are carnivorous, and share some physical and behavioural characteristics with raptorial taxa. However, there are many other carnivorous species within Telluraves, which also do not exhibit raptorial foot use (e.g. Laniidae, Corvidae, Trogoniformes, Galbuliformes; Appendix Table A.2). By analysing the characteristics and evolutionary lineages of raptoriality through a definition focussed on foot usage, I am able to discern the morphological effects of the optimization of raptoriality, rather than the optimization of carnivory.

## C. The Tarsometatarsus

This thesis focusses on the ecomorphology of the tarsometatarsus, with a specific focus on its potential use for inferring raptoriality in fossil species. The tarsometatarsus of birds is a fusion of distal tarsal and metatarsal bones in the avian foot, articulating with the tibiotarsus at its

proximal end, and with the second, third, and fourth digits at its distal end. In those species which possess a hallux (first toe), this phalanx also articulates with the tarsometatarsus at a fossa a short distance above the distal end along the shaft (Baumel and Witmer, 1993). Non-avian theropods and many Mesozoic birds have separate tarsal and metatarsal bones that became fused to form the tarsometatarsus in Aves (Ostrom, 1976; Raikow, 1985).

Because of its location between the digits and the ankle joint, the morphology of the tarsometatarsus is intrinsic to any foot use, and unlike the phalanges, has sufficiently distinct and highly variable morphological features which reflect the overall structure and function of the foot. It has been proposed to have strong links to ecology in functional morphology (e.g. Bock and Miller, 1959; Gatesy and Middleton, 1997; Zeffer and Norberg, 2003; Sustaita et al., 2013) and palaeontology (e.g. Ksepka and Clarke, 2012; Mayr, 2016; Ksepka et al., 2017). Furthermore, it is a robust bone that is commonly well-preserved in fossil skeletons. All these factors make the tarsometatarsus an ideal individual anatomical structure for studying the ecomorphology of Telluraves and other birds.

As we will see in Chapter 2, a significant structure of the tarsometatarsus bone is the hypotarsus, a protrusion on the proximal plantar end that acts as a channel for the digital flexor tendons. The hypotarsus varies in shape across the extant and extinct avian phylogeny and has been used to assess the phylogenetic affinities of extant avian groups (Mayr, 2008; Mayr, 2011; Mayr, 2019). Evolutionary literature on the hypotarsus of fossil taxa is limited: Manegold (2004) analysed the hypotarsus of fossil songbirds in comparison to those of extant Eupasseres in order to assess the evolution of hypotarsus shape in that clade; Ksepka et al. (2013) performed a phylogenetic analysis of morphological data in order to make insights into the evolution of fossil and extant Podicepidiformes by assessing key hypotarsal structures. In Chapter 2, I investigate

the use of the hypotarsus as a morphological indicator for raptoriality in extinct fossil taxa, based on the reoccurrence of monosulcate hypotarsus shape in extant raptorial species across orders.

## D. Ecomorphology

Ecomorphology pertains to the shapes of structures within an organism, their functions, and their relationships to behaviour and ecology (Olson and Miller, 1958; Karr and James, 1975; James, 1982; Leisler and Winkler, 1985). Skeletal structures of animals are exposed to selective pressures and constraints which reflect aspects of their ecology, such as diet and locomotion. The most recent form of study on this connection between shape and ecology is multivariate analysis, in which linear measurements or coordinate shape data are collected on a bone or structure, and subsequently analysed as a statistical hypothesis test, often taking additional factors such as phylogenetic bias into account.

In both fossil and extant birds, ecomorphological studies have been performed on many anatomical regions. For example, among recent works: Hinić-Frlog and Motani (2010) used the linear measurements of the appendicular skeletons of birds to discriminate between swimming modes; Taylor and Thomas (2014) tested variation in wing morphology as it relates to flight ecology and behaviour; Benson et al. (2017) investigated how aspects of the inner ear semicircular canals are influenced by wing kinematics and flight style; Bright et al. (2019) analysed the effect of mechanical resistance in diet to psittaciform cranial morphology; Navalón et al. (2019) examined skull shape in relation to feeding ecology; and Orkney et al. (2021) examined major aspects of the avian skeleton for ecomorphological relationships both between and within body regions. Most recently, Lowi-Merri et al. (2021) conducted the first ecomorphological investigation of the avian sternum as it relates to both terrestrial and aerial locomotion.

A vital part of ecomorphological studies lies in the categorisation of ecological predictors of morphology, to be tested for their impact on shape. The foot uses of the extant radiation of over 10,000 bird species are varied and simultaneous; for example, in addition to being raptorial, birds can perch or run, climb and grip, or walk, hop, and swim. The basis of ecomorphology is the concept that all of these foot uses factor into the shape of a bird's body. The categorization of bird foot uses is therefore both vital and complex in the investigation of the independent effects of foot use on foot morphology, and in subsequent analysis of the foot morphologies of stem fossil taxa. For the majority of the literature, birds are categorised into mutually exclusive groups based on their primary ecological behaviour (e.g. seed-eating, pelagic soaring, surface swimming). However, in reality the behaviour of an individual bird is complex and varied, in that a bird is capable of more than one behaviour within a broader ecological context that is not readily classified into a single category. There are classification schemes available to capture multiple behaviours, which make use of individual characters scored as a binary for the presence (1) or absence (0) of a behaviour or ecology for each taxon. Taylor and Thomas (2014) made use of this style of classification scheme in order to capture the multiple different flight styles exhibited by birds. This approach was used subsequently by Benson et al. (2018) and Lowi-Merri et al., (2021). There is a similar plasticity of foot uses in birds, so it is appropriate to use this comprehensive method of ecological classification.

Ecomorphology as it specifically relates to the study of the tarsometatarsus bone is not a new area of avian research. For example, Bock and Miller (1959) explored the relationship between scansoriality, zygodactyl digit arrangement, and perching foot use in Piciformes (woodpeckers and allies). Their work was primarily qualitative, and observed the relative orientation of the toes to the tarsometatarsus, but many studies since have incorporated

quantitative measurements. For example, Zeffer et al. (2003) examined the basic functional correlation between habitat use and leg morphology in birds, sorting the taxa into exclusive ecological groups according to leg use (including aerial, ground, and tree species, birds of prey, swimming and wading species) and analysing length measurements of the femur, tibiotarsus, and tarsometatarsus using multiple regression (without taking phylogeny into consideration). Most studies of tarsometatarsus ecology so far has been quantitative and/or two-dimensional (e.g. Barbosa and Moreno, 1997; Einoder and Richardson, 2007; Degrange, 2017, De Mendoza and Gomez, 2022). This type of information represents only parts of the structure, and unless analyses are focussed on specific anatomical structures of the tarsometatarsus, cannot fully capture the most variable and functionally relevant aspects of the entire bone.

Morphology is one of the primary sources of information a fossil can provide. Investigating significant relationships between an extant bird's tarsometatarsus morphology and its ecology/foot uses allows us to observe similar morphological characteristics in extinct taxa known only from fossils, and make inferences as to their past ecology.

## E. Geometric Morphometrics

In this thesis, the shape of the tarsometatarsus (Chapter 1) and its proximal end (Chapter 2), is quantified using landmark points and semi-landmark series which are then analysed using geometric morphometrics. Morphometrics is the study of the shape and variation of shape of a biological structure, as well as the study of covariance between the shape of a biological structure and external factors (Webster and Sheets, 2010). Geometric morphometrics makes use of landmarks, which describe two- or three-dimensional coordinates, placed on repeatable (biologically homologous) points on a structure (Bookstein, 1991; Webster and Sheets, 2010); here the tarsometatarsus. Sliding semilandmarks, which are set series of landmarks placed along

curves or surfaces, also capture homologous structures that would be difficult to landmark as a traditional, singular point (Webster and Sheets, 2010). Sliding semilandmarks allow points to slide along their tangent vectors in order to minimise bending energy differences from the mean shape. This removes the effect of their initial differences in placement, spacing, and number on individual specimens, so that all landmarks may be treated equally in later statistical analyses (Gunz and Mitteroecker, 2013).

The use of geometric morphometrics for analysis of the tarsometatarsus is not as common as for studies of cranial morphology in birds (e.g. Kulemeyer et al., 2009; Sun et al., 2018; Navalon et al., 2019), but has been performed before. Provini et al. (2013) conducted 3D geometric morphometric comparisons of the intertarsal joint between two species of birds (the common quail (*Coturnix coturnix*), and the ringed teal (*Callonetta leucophrys*)), and compared the size and shape of the tibiotarsus and tarsometatarsus between the two taxa. The testing of their hypothesis that the difference in ankle joint shape is due to the difference in their styles of terrestrial locomotion produced inconclusive results. In 2015, Kirchner-Smith used a grid of landmarks and sliding semilandmarks over 3D models of loons (*Gavia*), grebes (*Podiceps*), and hesperornithiforms (*Hesperornis*) to evaluate the effectiveness of variation in tarsometatarsus morphology for interspecies identification of *Hesperornis* fossil taxa. However, the research concluded that tarsometatarsus shape alone was insufficient in identifying discrete species due at least in part to the large amount of intraspecific variation present in both extant and extinct taxa studied. De Mendoza and Gomez (2022) also analysed the ecomorphology of members of Anseriformes using 2D geometric morphometrics on their tarsometatarsi, with respect to categorical locomotory habits, and were able to infer the locomotory habits of extinct Anseriformes known only from fossils.

## F. Phylogenetic Comparative Analyses

I evaluate the relationship between tarsometatarsus shape and ecology using the comparative approach, drawing data from species rather than from independent experimental trials. Comparative statistical analysis of interspecific data can be biased by the different durations of shared evolutionary ancestry among pairs of species (Felsenstein, 1985). This bias is addressed by incorporating phylogenetic information into multivariate analyses of ecomorphological models. Scaling parameters, such as Pagel's λ (Pagel, 1999) take into account the phylogenetic closeness of taxa when analysing their trait similarity, and essentially act as an estimator of phylogenetic signal. Phylogenies with well-resolved internal nodes, as few polytomies as possible, and accurate branch lengths are able to provide important interspecific relational data that lays the groundwork for valid models of evolutionary comparison (Felsenstein, 1985; Purvis et al., 1994).

Phylogenetic regression (also known as Phylogenetic Generalized Least Squares, or PGLS; Grafen and Hamilton, 1989) can analyse the evolutionary covariation between dependent (tarsometatarsus shape) and independent traits (foot uses) in order to investigate macroevolutionary hypotheses (Adams and Collyer, 2018). Many studies have used this phylogenetically informed method of analysis in combination with geometric morphometrics and have robustly determined the ecomorphology of extant taxa (e.g. Navalón et al., 2019; Choiniere et al., 2021; Lowi-Merri et al., 2021; De Mendoza and Gomez, 2022). The use of 3D and 2D landmark data across the tarsometatarsus and my multiple foot use character scoring system yields a comprehensive basis for determining the relationship between the foot uses of all extant bird groups and the morphology of their tarsometatarsi.

Once ecomorphological relationships are known, the same phylogenetic information can also be used for inference of the ecologies of extinct species known only from fossils. Several discriminant function analyses were tested in this study, using known information about the raptoriality of extant taxa to predict the likelihood of raptoriality in fossil taxa based on statistical shape comparisons. A phylogenetic flexible discriminant analysis (phyFDA; Motani and Schmitz, 2011) was performed twice, to test the effects of phylogenetic signal (Pagel's λ) on the model's predictive power.

## G. Ancestral Character Estimation

The assumption that the phylogenetic relationships between taxa are as accurate as possible is the basis of every ancestral reconstruction. Maximum likelihood methods in Ancestral Character Estimation (ACE) provide a measure of statistical uncertainty and take into account prior ancestral probabilities and time available for change to occur (Schluter et al., 1997; Cunningham et al., 1998; Pagel, 1999). A phylogeny populated with known ancestral states contributes to the elimination of some of the uncertainty of a clade (Pagel, 1999). This is how the inclusion of fossil material at or near decisive ancestral nodes of a phylogeny can result in significantly different ancestral character estimations.

The addition of fossil taxa at multiple nodes across a phylogeny can "minimize the biases caused by directional trends" (Finarelli and Flynn, 2006), and the information these fossil taxa provide helps to inform and constrain the value of estimates at those nodes (Garland et al., 1999). Using ACE with relevant stem fossils of telluravian groups has the potential to constrain the timing of and variation in raptoriality in such telluravian clades regardless of a convergent or ancestral outcome.

In the case of Prum et al. (2015), their phylogeny is the most up-to-date understanding of extant avian relationships, based on analyses of genomic data from an extensive and well-represented taxon sample. It resolves uncertainties inherent to previous hypotheses of bird phylogenies, such as the placement of Tinamidae as sister to cassowary and emu, the Aequorlitornithes as a comprehensive clade of waterbirds, and the hoatzin (*Opisthocomus hoazin*) as sister to all of Telluraves (Prum et al., 2015).

## H. Outline

I aim to investigate the hypothesised links between morphology of the avian tarsometatarsus, with the potential to provide a tool by which to infer raptoriality in extinct birds, allowing a test of the hypothesis of a raptorial telluravian ancestor. The contents of this thesis will synthesize and apply this background knowledge in testing the hypothesis of ancestral telluravian raptoriality.

**Chapter 1** pertains to the amount of variation in the overall shape of the tarsometatarsus which can be explained by a bird's foot use traits and other aspects, such as allometry, as well as the independent effects on tarsometatarsus shape of distinct foot use traits, including raptoriality. I use a combination of 3D shape data of extant taxa, and foot use and ecology character scorings to produce a phylogenetically-informed linear model to address these questions statistically and quantitatively. I also examine these results from the perspective of functional morphology to address the questions qualitatively.

**Chapter 2** addresses the amount of variation in hypotarsus shape that can be explained by raptoriality using a combination of 2D shape data of extant taxa and hypotarsus shape character scorings to produce a phylogenetically-informed linear model. Inferences for raptoriality in taxa known only from fossils are made using the statistical relationship between

raptoriality and hypotarsus shape, and 2D shape data of fossil taxa in discriminant function analyses.

**Chapter 3** investigates the likelihood of raptoriality in the common ancestor of Telluraves using ancestral character estimation. I also test the effects of incorporating fossil taxa in the prediction of an ancestral character state, with raptoriality inferred based on hypotarsus morphology found in Chapter 2. This will provide a strong test of the hypothesis that the ancestor of Telluraves was raptorial. I also estimate the ancestry of 14 other telluravian foot uses and ecologies based only on extant taxa, to provide additional contextual information on the ancestry of Telluraves.

# Chapter 1:

## The effects of foot use on variation in tarsometatarsus shape in extant birds

## 1.1 Introduction

Telluraves, or "land birds", is a group of birds (Aves) that encompasses Accipitriformes, Strigiformes, Coraciimorphae, Falconiformes, Psittaciformes, and Passeriformes. The exceptional diversity of Telluraves spans a broad range of ecologies and flight forms, and includes Passeriformes, the most species-rich avian order. Several aspects of the early evolution of Telluraves remain unclear, in part because relationships within Telluraves, and even the existence of the group were uncertain until recently (Hackett et al., 2008; Yuri et al., 2013). Nevertheless, recent phylogenetic research has substantially clarified telluravian relationships, providing initial steps towards understanding the lifestyle and ecology of the common telluravian ancestor.

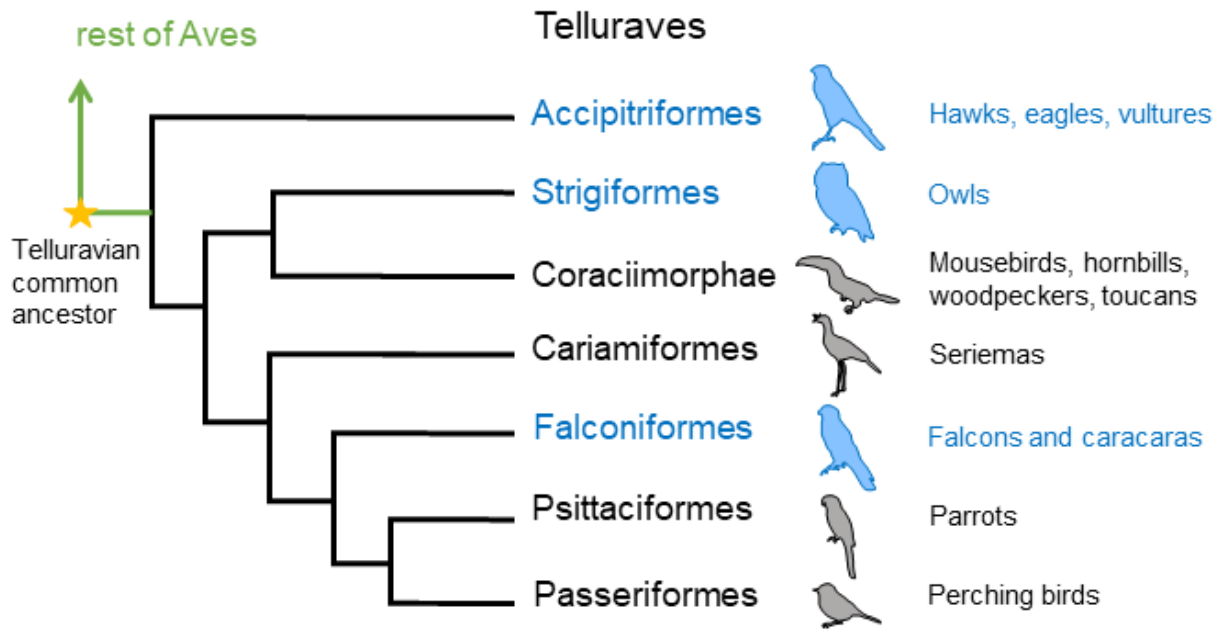


**Figure 1.** Simplified phylogenetic tree of Telluraves based on Prum et al. (2015). Raptorial groups are in blue text.

The genomic phylogenies of Jarvis et al, (2014) and Prum et al. (2015), revealed a surprising pattern of relationships among telluravian subclades. Extant raptorial groups

(Accipitriformes, Strigiformes, and Falconiformes) are not closely related to each other, and do not form a single clade. Instead, they are dispersed throughout the phylogeny, generally as sister to non-raptorial groups: Acciptriformes as sister to the rest of Telluraves, Strigiformes as sister to Coraciimorphae, Falconiformes as sister to Psittacopasseres (Figure 1). Based on this result, Prum et al. (2015) proposed that the ancestor of all Telluraves may have been raptorial. Wu et al. (2020) examined this hypothesis using a comparative phylogenetic analysis of genes relating to major aspects of ecology (e.g. vision, hearing, temperature sensation, digestion), and found that among the digestion-related genes, all three branches of extant raptorial groups possess selectively intensified genes for fat digestion and absorption. Their ancestral trait reconstruction results also suggest that these abilities might have been present in the common ancestor of Telluraves, in the form of intensified selection of the genes relating to fat digestion and absorption. Their findings therefore suggest that a carnivorous diet was already present in ancestral telluravians and was independently lost in two descendent lineages: 1) On the line leading to Coraciimorphae, which includes such groups as Coliiformes, Coraciiformes, and Piciformes; and 2) On the line leading to Psittacopasseres, the clade comprising Psittaciformes (parrots) and Passeriformes (passerines).

Observations of modern species therefore raise the possibility that the presence of raptoriality in extant Accipitriformes (hawks, eagles, kites), Strigiformes (owls), and Falconiformes (falcons) reflects retention of a primitive trait rather than independent evolutionary acquisition (Prum et al, 2015; Wu et al., 2020). However, support for this hypothesis from fossil species has yet to be evaluated. Studies so far have used evidence from extant species to infer these evolutionary events in deep time (e.g. Jarvis et al., 2014; Prum et al., 2015). The fossil record provides unique evidence of such events in deep time, and could be a

powerful tool for testing these hypotheses. Such an assessment would require robust skeletal correlates of raptoriality that could be evaluated in key fossil species.

'Carnivory' here is taken to mean the consumption of vertebrates in any percentage of overall diet. Among extant Telluraves, carnivory is present in a large number of groups; in addition to Strigiformes, Falconiformes, and Accipitriformes, seven orders and 49 families within Telluraves have taxa with diets consisting primarily of other vertebrates. These carnivorous groups are diverse (Appendix Table A.2), and many are not considered to be 'raptorial,' in either a colloquial or zoological sense (e.g. Habib and Ruff, 2007; Hertel et al., 2015; Navalón et al., 2018). The groups most commonly referred to as being 'raptorial' share a suite of adaptations that includes short, hooked bills, long, sharp talons, keen eyesight, and often kill and carry prey with the feet (Zeffer et al., 2003; Backus et al., 2015; Tsang and McDonald, 2019). Raptoriality can therefore be considered a foot-use trait that is possessed by select carnivorous telluravian taxa (e.g. Strigiformes, Falconiformes, and Accipitriformes, excluding Old and New World vultures), and is an important ecological specialisation that should be evident in the skeleton, particularly in the morphology of the foot bones. The morphology of the tarsometatarsus bone is likely especially important, as it is an integral component of all foot uses, and exhibits considerable variation in morphology among species and groups of birds (Figures 2-4). The tarsometatarsus also has good representation in the avian fossil record, and so is a reliable subject of study in both extant and extinct species.

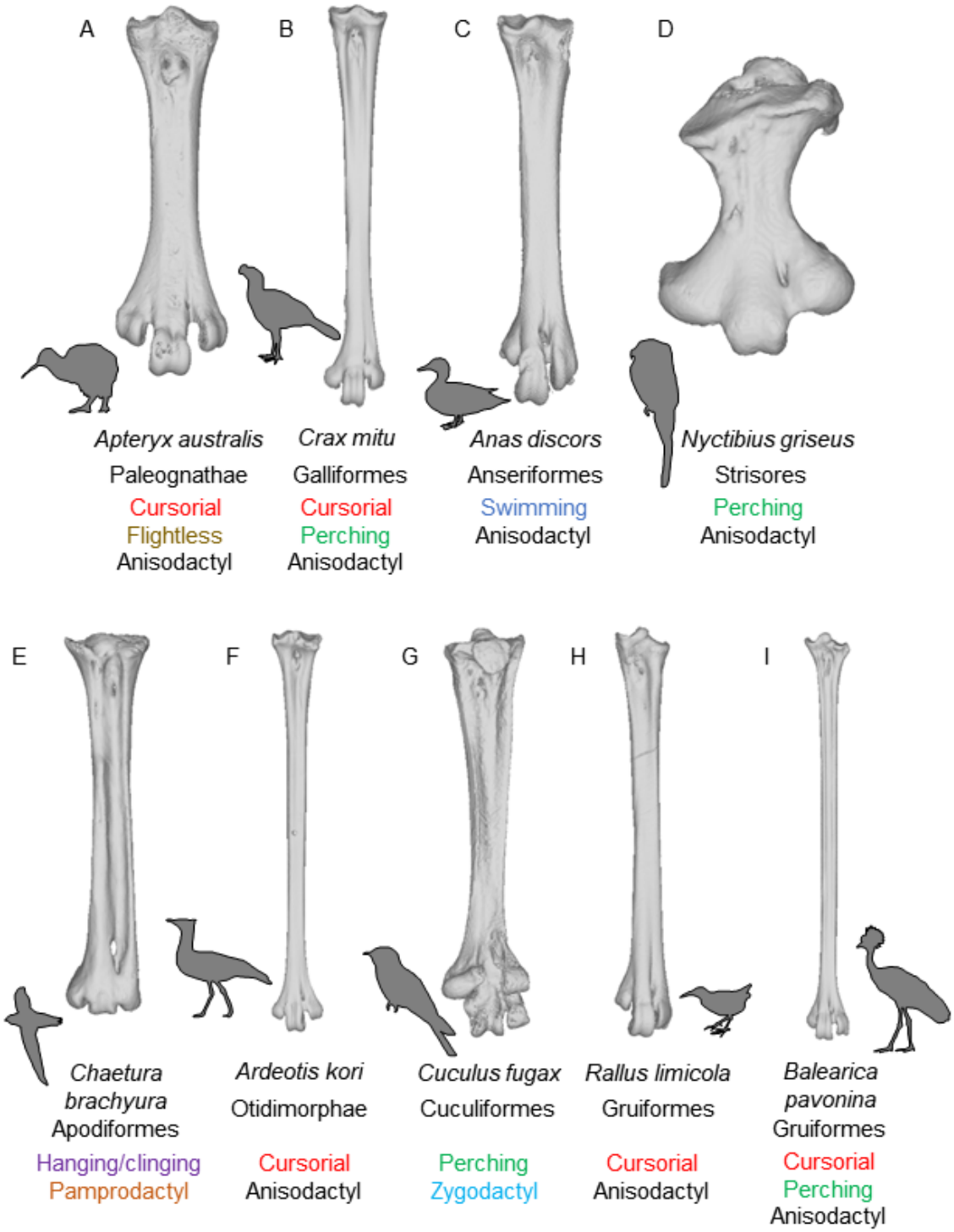


**Figure 2.** Entire left tarsometatarsi (3D models) showing the variation in morphology and foot use across Aves; not to scale. A) Dorsal view of *Apteryx australis* (Southern brown kiwi; FMNH 391011); B) Dorsal view of *Crax mitu* (Razor-billed curassow; FMNH 320386); C) Dorsal view of *Anas discors* (Blue-winged teal; NHMUK S2001.41.5); D) Dorsal view of *Nyctibius griseus* (Common potoo; UMMZ 136371); E) Dorsal view of *Chaetura brachyura* (Short-tailed swift; UMMZ 157689); F) Dorsal view of *Ardeotis kori* (Kori bustard; UMMZ 210444); G) Plantar view of *Cuculus fugax* (Malaysian hawk-

cuckoo; FMNH 357420); H) Dorsal view of *Rallus limicola* (Virginia rail; FMNH 501812); I) Dorsal view of *Balearica pavonina* (Black-crowned crane; NHMUK 1859.10.26.5).

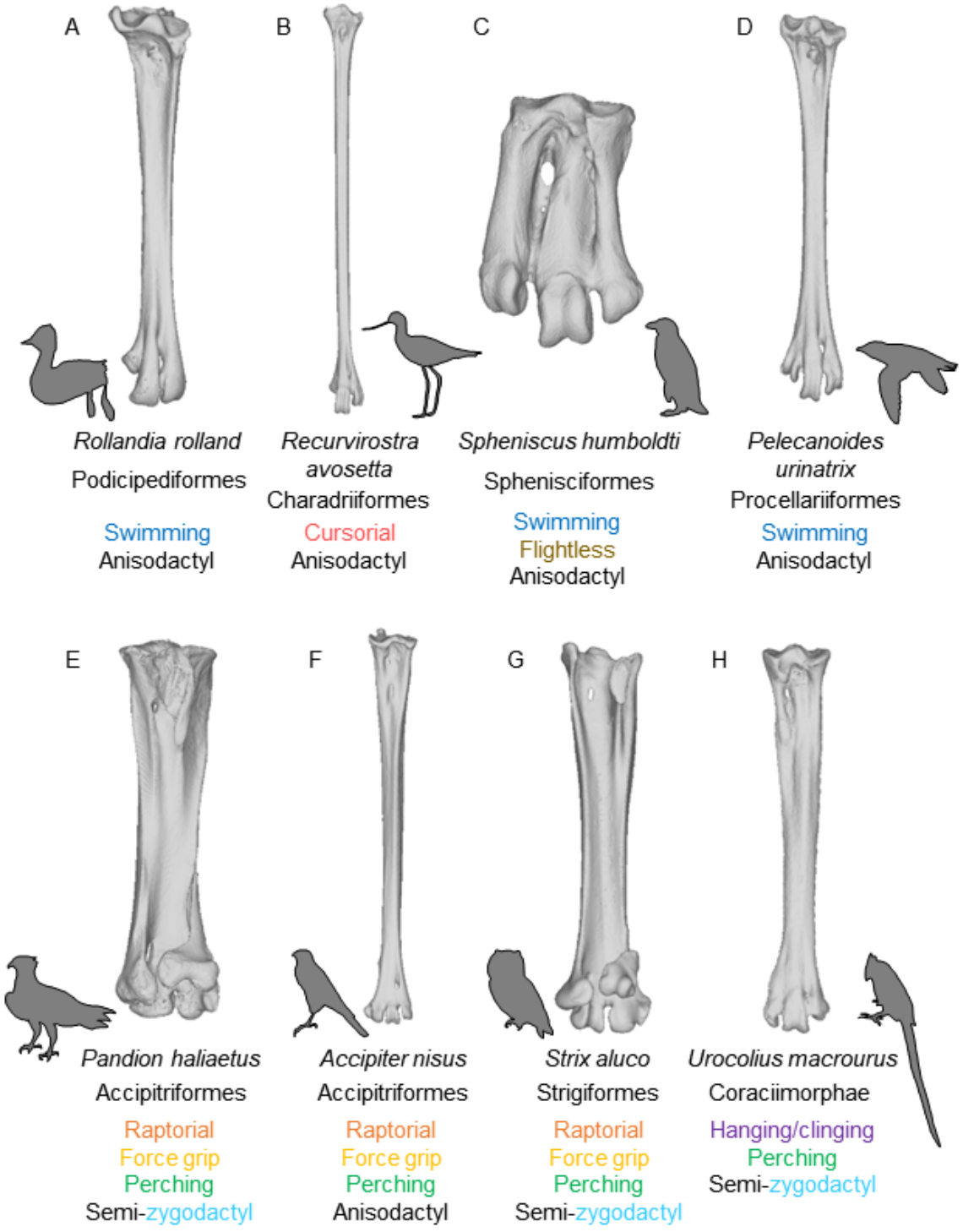


**Figure 3.** Entire left tarsometatarsi (3D models) showing the variation in morphology and foot use across Aves; not to scale. A) Dorsal view of *Rollandia rolland* (White-tufted grebe; UMMZ 156975); B) Dorsal view of *Recurvirostra avosetta* (Pied avocet; NHMUK S1962.10.1); C) Dorsal view of *Spheniscus humboldti* (Humboldt penguin; NHMUK S2000.7.1); D) Dorsal view of *Pelecanoides urinatrix*

(Common diving-petrel; NHMUK S2006.1.14); E) Plantar view of *Pandion haliaetus* (Osprey; FMNH 437336); F) Dorsal view of *Accipiter nisus* (Eurasian sparrowhawk; NHMUK S1982.149.1); G) Plantar view of *Strix aluco* (Tawny owl; NHMUK S2001.38.1); H) Dorsal view of *Urocolius macrourus* (Blue-naped mousebird; FMNH 368959).

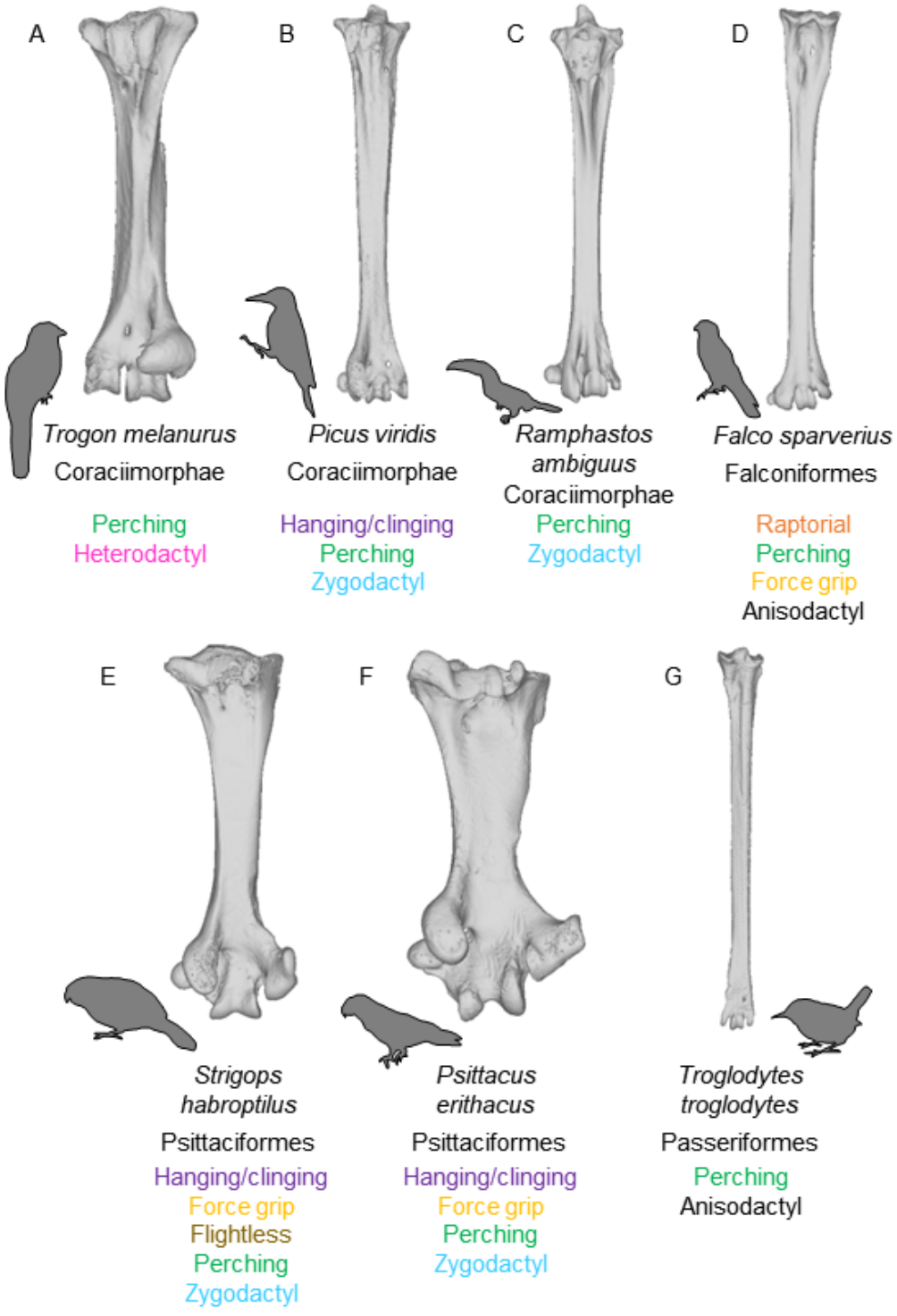


**Figure 4.** Entire left tarsometatarsi (3D models) showing the variation in morphology and foot use across Aves; not to scale. A) Plantar view of *Trogon melanurus* (Black-tailed trogon; FMNH 290496); B)

Plantar view of *Picus viridis* (Eurasian green woodpecker; NHMUK S1982.5.1); C) Plantar view of *Ramphastos ambiguus* (Yellow-throated toucan; NHMUK 2002.21.2); D) Dorsal view of *Falco sparverius* (American kestrel; UMMZ 154462); E) Plantar view of *Strigops habroptilus* (Kākāpō; NHMUK 1881.1.17.71); F) Plantar view of *Psittacus erithacus* (Grey parrot; NHMUK S1992.41.60); G) Dorsal view of *Troglodytes troglodytes* (Eurasian wren; NHMUK 1963.23.2).

Many previous studies have proposed links between tarsometatarsus morphology and foot use traits in birds, including, among other traits, scansoriality and zygodactyl digit arrangements (Bock and Miller, 1959), locomotion performance in wading birds (Barbosa and Moreno, 1999), and lift-based foot-propelled swimming in grebes (Johansson and Norberg, 2001). However, aside from locomotory habit in Anseriformes (de Mendoza and Gomez, 2022), these ecomorphological hypotheses are so far untested using quantitative comparative methods beyond external linear measurements. In this chapter, I evaluate the ecomorphological relationship between the tarsometatarsus bone and foot use in extant birds using three-dimensional (3D) geometric morphometrics and multivariate phylogenetic comparative methods to answer the following questions:

**1)** How much of the variation in general shape of the tarsometatarsus can be explained by a bird's foot use traits and other aspects, such as allometry?

**2)** What are the independent effects on tarsometatarsus shape of distinct foot use traits, including raptoriality?

The elucidation of these two questions will provide an important basis for the subsequent ecomorphological analysis of fossil taxa and telluravian roots. In order to address the question of the ancestral ecomorphology of Telluraves, raptorial or otherwise, it is key to look at the complexities of foot uses and states in relation to each other, and identify which aspects of a bird's ecology might have a significant influence on the shape of a bone.

## 1.2 Material and Methods

### 1.2.1 Terminology

Most anatomical nomenclature is used as per Baumel and Witmer (1993). Both Latin and English equivalents are used interchangeably for muscular and osteological structures. Terminology relating to geometric morphometrics and related statistical analyses is collated from multiple sources, namely Bookstein (1997), Zelditch et al. (2004), Webster and Sheets (2010), Grafen and Hails (2002), and Burnham and Anderson (2002). The Latin names used for extant bird species are in accordance with their information as currently listed in the online *Birds of the World* (ed. Billerman et al., 2021).

### 1.2.2 Data Collection

I used 179 three-dimensional computer models of avian tarsometatarsi, many of which were collected from the TEMPO project library on morphosource (https://www.morphosource.org/projects/00000C420/about; see also Bjarnason and Benson, 2021), made from x-ray microcomputed tomography scans (CT scans) of museum specimens. These CT scan images were processed using ImageJ software (Schneider et al., 2012), and segmented, visualized and turned into 3D models using Avizo Lite software (v.9.7.0). In-person, qualitative observations were made on skeleton specimens at the Oxford University Museum of Natural History (OUMNH) and the Natural History Museum (NHMUK) at Tring.

*Institutional abbreviations*—**FMNH**, Field Museum of Natural History, Chicago; **NHMUK**, Natural History Museum of London; O**UMNH**, Oxford University Museum of Natural History; **UMMZ**, University of Michigan Museum of Zoology; **UMZC**, University Museum of Zoology, Cambridge; **YPM**, Yale Peabody Museum, Connecticut.

The complete list of taxa and their foot use character scorings can be found in the Appendices (Appendix Data B.1).

### 1.2.3 Ecological Foot Use Characters

I scored each taxon for a set of ecological foot use characters covering a wide range of capabilities observed among extant birds. This data was used previously in a broad statistical study of bird ecomorphology (Tronrud in Orkney et al., 2021). My approach is similar to that in several recent studies of bird flight capabilities (Taylor, 2014), labyrinth morphology (Benson et al., 2018), and sternal morphology (Lowi-Merri et al., 2021), which also scored each bird species against a list of many separate ecological capabilities. This differs from the approach of older studies which scored each species as having a single ecological type (e.g. Zeffer and Norberg, 2002; Zeffer et al., 2003; Hinić-Frlog and Motani, 2010; Close and Rayfield, 2012; de Mendoza and Gomez, 2022).

I took an inclusive approach to trait selection, with the intention of statistically asking which had the strongest relationships to morphology of the tarsometatarsus, and eliminating redundant or uninformative traits using a statistical model selection process. For example, many of the foot use categories relate to aquatic behaviour, yet not all are expected to return significant independent effects on tarsometatarsus shape. Characters that embody specific foot uses (e.g. foot-propelled underwater locomotion; see Character 22, below), or morphologies (e.g. digital webbing; see Character 20, below) may be hypothesised to affect variation in tarsometatarsus morphology in different ways. I am able to test whether one character contributes significant independent effects on tarsometatarsus shape to a larger degree than another, with the expectation that neither foot use will provide wholly discrete explanatory power from the other.

The ecological information used to score the extant taxa for each character was collected from Birds of the World, the Internet Bird Collection (IBC), and published ornithological accounts (e.g. Townsend, 1909; Miller, 1919; Brooks, 1945; Schreiber and Woolfenden, 1975; Grémillet, 1998; Garthe et al., 2000; Barber and Robbins, 2002; Fry and Fry, 2010), through written statements and observed in photographic or video evidence. Therefore the scoring of characters in this work is reliant on and limited to those foot uses which have been recorded for each species analysed, or at times when species information is unavailable, at the genus level.

***1.*** *Documented walking ability*: Absent, taxon has been clearly documented as having inability to walk (0); Present, taxon either can walk or has not been clearly documented as having inability to walk (1).

A bird that can stride, hop or otherwise step while holding their body off of the ground can be here categorised as having ground walking ability. This character may correspond with Character 2, which elaborates on the habitat use of birds either as terrestrial or arboreal (see below).

Most extant birds have the ability to walk on the ground, yet many arboreal birds rarely do so, and it is difficult to obtain specific information about whether they are capable of ground-walking or not. The sedentary nature of many arboreal birds, and/or the relative inaccessibility of nocturnal or geographically sparse species means that the data included herein is as complete as possible given the current availability of such documented evidence. Examples of such taxa from this dataset include the Northern saw-whet owl (*Aegolius acadicus*) and the common sunbird-asity (*Neodrepanis coruscans*). These taxa were treated as having insufficient documentation of walking inability, and were therefore scored as state 1 (walking ability present). Notably, all taxa

in this dataset which had such scoring difficulties due to lack of documentation lead predominantly arboreal lifestyles (see below: Character 2, state 0).

In addition, some aquatic birds that either spend the majority of their time in the water or in the air have become so specialised to those locomotory modes that their ability to walk is substantially hindered. Loons (Gaviidae) are able to push themselves along the ground when necessary with their body in contact with the ground, but are incapable of holding their bodies off of the ground (Birds of the World; ed. Billerman, 2021), and so would be scored for character 1 as state 0. The Ascension Frigatebird (*Fregata aquila*) comes ashore only for breeding, and is only able to perch while on land (Wanless, 2002), and is likewise scored as state 0 (walking ability absent).

Some other well-documented examples of birds that cannot walk include swifts (Apodidae), many hummingbirds (Trochilidae), and trogons (Trogonidae) (Birds of the World; ed. Billerman, 2021).

***2.*** *Terrestrial vs. Arboreal*: Taxon is predominantly terrestrial (or aquatic) (0); 'Mixed' state: taxon has approximately equal preference for terrestrial and arboreal spaces (1); Taxon is predominantly arboreal (2).

This character scores taxa on their preferred substrate when on land, either on the ground or water (state 0), or above ground (state 2). Arboreality and terrestriality are commonly used as ecological traits in literature on birds and other animals (e.g. hominids: Gebo, 1996; Crompton et al., 2010; lizards: Collar et al., 2010), and are important considerations in the debate on the origin of bird flight (e.g. Ostrom, 1974; Padian and Chiappe, 1998; Dececchi and Larsson, 2011; Field et al., 2018). This character is used here to supplement the information scored in the

general walking ability character; birds for which it was difficult to find a clearly documented ability or inability to walk were all scored in this dataset as arboreal (state 2).

In this dataset, a taxon may be scored as both arboreal (state 2) and able to walk on the ground (Character 1, state 1), such as the Eurasian Sparrowhawk (*Accipiter nisus*), or they may be scored as both arboreal (state 2) and unable to walk on the ground (Character 1, state 0), such as the Short-tailed Swift (*Chaetura brachyura*) and the Ascension Frigatebird (*Fregata aquila*). Likewise, a taxon may be scored as both terrestrial (state 0) and able to walk on the ground (Character 1, state 1), such as the New Zealand Rockwren (*Xenicus gilviventris*). Through the inclusion of primarily aquatic birds, a taxon in this dataset may also be scored as terrestrial (state 0) and unable to walk (Character 1, state 0), such as the Red-throated Loon (*Gavia stellata*). Additionally, some taxa in this dataset have been scored as having 'mixed' stratification (state 1), in that they spend a non-preferential amount of time in both terrestrial and arboreal spaces. Such taxa include the Common Woodpigeon (*Columba palumbus*) and the American Crow (*Corvus brachyrhynchos*).

***3.*** *Nesting substrate*: Taxon nests on the ground and/or non-arboreal horizontal surface (0); 'Mixed' state: taxon has non-preferential substrate for nesting (1); Taxon nests above ground, in tree or on vertical surface (2).

Regardless of the scoring of character 2, a taxon may construct or position a nesting site either on the ground or on a level, terrestrial surface (state 0), or in a tree or attached to a vertical surface (state 2). Ground nesting may refer to mounds, burrows, or nests positioned on the water surface. Tree nesting may refer to nests on branches or tree cavities, in arboreal termitaria, on the walls of chimneys or other similar vertical structures, or any nest suspended above the ground surface.

In this dataset, a taxon may be scored as both ground nesting (state 0) and terrestrial (Character 2, state 0), such as geese (*Anser*) and the Lesser Yellow-headed Vulture (*Cathartes burrovianus*), or both ground nesting (state 0) and arboreal (Character 2, state 1), such as the Common Kingfisher (*Alcedo atthis*). Likewise, a taxon in this dataset may be scored as both tree nesting (state 2) and predominantly arboreal (Character 2, state 2), such as the Green Woodhoopoe (*Phoeniculus purpureus*) and the Tawny Owl (*Strix aluco*), or may be scored as both tree nesting (state 2) and terrestrial (Character 2, state 0), such as the Grey-winged Trumpeter (*Psophia crepitans*), and the Secretarybird (*Sagittarius serpentarius*). Some nest structures of note, which were ultimately scored as state 2 (above ground), were those of the Collared Crescentchest (*Melanopareia torquata*), which builds its nest low in a grass tussock (Gressler and Marini, 2008), and the Thrush-like Antpitta (*Myrmothera campanisona*), which is similar in behaviour to the Tepui Antpitta (*Myrmothera simplex*) in constructing nests in the leaf-bases of philodendron plants (Barber and Robbins, 2002). As well, the Limpkin (*Aramus guarana*) is notable in its disparity of nesting substrates, including on floating vegetation, in shrubs, and high on tree branches (Walkinshaw, 1982), and so was scored as the only 'mix' (state 1) for this character.

***4.*** *Cursorial*: Absent, taxon not specialised for running efficiency (0); Present, taxon specialised for running efficiency (1).

Birds categorised as cursorial are those which have adapted to running as their preferred method of locomotion, regardless of wing function or other foot use. Their tarsometatarsi (and lower leg bones in general) tend to be longer and thinner in proportion (Gatesy & Middleton, 1997). This elongation of both tibiotarsus and tarsometatarsus allows the femur to remain in horizontal position with distal end situated anteriorly, while the rest of the leg rotates at the knee

joint for the running motion (Bennet, 1996; Jones et al., 2007). Taxa were scored on video observation of locomotion (IBC).

In the case of Galliformes, Gruiformes, Ciconiiformes, Procellariiformes, and Charadriiformes, which are known for their walking behaviours, cursoriality has been scored on the basis of their behaviour during flight take-off from a solid substrate. Taxa such as herons and bitterns (Ardeidae), shoebills (Balaenicipitidae), and partridge (*Rollulus*) do not run before taking flight, only jumping once into the air, and so are scored as non-cursorial (state 0). Conversely, killdeer (Charadriidae), godwits (*Limosa*), avocets (Recurvirostridae), Secretarybirds (*Sagittarius*), guineafowl (Numididae) and cranes (Gruidae) do break into a run when they take flight, and are scored as cursorial (state 1). If a taxon has well-documented running ability, such as seriemas (Cariamidae), which have a moment during full speed cursorial locomotion when both feet are off the ground (Silva et al., 2016), then they may be scored as cursorial (state 1) regardless of flight take-off movements. Waterfowl such as ducks, geese, and swans (Anseriformes), although occasionally running for take-off, have not adapted to and do not prefer running or walking as their primary mode of locomotion, and so are scored as state 0. In an study concerning the allometry of the hindlimb in cursorial birds, Maloiy et al. (1979) studied a small number of taxa which are known to walk and run, and which run rather than fly as a first resort when disturbed. After scoring the taxa in this dataset on the character rules stated above, the coding scheme reached following my specifications was similar to that applied by Maloiy et al. (1979).

All cursorial birds in this dataset have well-documented ground walking ability (Character 1, state 1; above), as well as a range of perching abilities, but none in this dataset are scored as being able to digitally manipulate objects (Character 11, state 1), having webbed feet

(Character 20, state 1) or are scored as scansorial (Character 15, state 1). All taxa scored as cursorial have anisodactyl digit arrangements (Character 7, state 1).

As explained above, examples of cursorial birds from this dataset include the Southern Brown Kiwi (*Apteryx australis*) and the Secretarybird (*Sagittarius serpentarius*). Examples of non-cursoriality in this dataset include taxa such as the Red-fan Parrot (*Deroptyus accipitrinus*) and the Black-spotted Barbet (*Capito niger*). It is also possible for a bird to be habitually ground-walking (Character 1, state 1) and lack cursoriality, such as the Little Bittern (*Ixobrychus minutus*).

***5.*** *Hopping*: Absent, taxon does not hop as primary form of ground locomotion (0); Present, taxon hops, with either one or two feet, as primary form of ground locomotion (1).

Birds categorised as having hopping ability are those which can hop on either one or both feet and become momentarily airborne, as their primary mode of locomotion along a ground surface without the use of wings for lift. This character is unrelated to general ground walking ability. Both in-phase and out-of-phase hopping are counted as overall hopping ability (Hayes & Alexander, 1982).

Birds with hopping ability from this dataset include the Collared Crescentchest (*Melanopareia torquata*) and the Black-spotted Barbet (*Capito niger*). Birds in this dataset scored as state 0 either make primary use of walking (Character 1, state 1) or running (Character 4, state 1) gaits for ground locomotion, such as the Hamerkop (*Scopus umbretta*), or lead primarily stationary or arboreal lifestyles (Character 2, state 2).

***6.*** *General perching*: Absent, taxon cannot perch (0); Present, taxon can perch (1)

Birds here characterized as having perching ability are able to hold onto a branch or structure at any height above ground, provided that their toes are curving and grasping onto the

branch rather than merely standing and balancing. Most species within Telluraves are capable of perching; examples of birds without perching abilities include swifts (Apodidae), most waterbirds (Aequorlitornithes; Prum et al., 2015), Galloanserae, and Paleognathae (HBW). The primary element of the foot that allows birds to perch is the opposable, or "reversed" hallux (digit 1; Raikow, 1985; Middleton, 2001), and its overall strength as a digit. Taxa were primarily scored using documented evidence of bird habits from Birds of the World (ed. Billerman, 2021) and IBC.

*Digit Arrangement Characters 7-10*

Bird species vary in the orientations of their pedal digits, and these arrangements assist in the performance of foot-related behaviours, such as locomotion, perching, and manipulation of objects (Bock & Miller, 1959; Raikow, 1985; Sustaita et al. 2013). Some taxa, such as owls (Strigiformes) and mousebirds (Coliiformes), show behavioural variability, in which certain digit arrangements may be employed facultatively, in addition to one or many other arrangements. For example, owls are described as having "semi-zygodactyl" (Raikow, 1985) arrangements, which describes that a single individual can use either anisodactyl or zygodactyl digit arrangements, depending on the functional requirements of specific actions (Bock & Miller, 1959; Raikow, 1985). The positions of digits may influence the morphology of the tarsometatarsus, especially if digit arrangement has significant implications for function across multiple independently evolved groups.

Each arrangement (anisodactyly, zygodactyly, heterodactyly, pamprodactyly) has been separated into its own binary character. Species with facultative arrangements (e.g. semi-zygodactyly) are scored as state 1 (present) for each relevant digit arrangement. For example, in

the case of semi-zygodactyly, the taxon is scored as state 1 for both anisodactyly (Character 7) and zygodactyly (Character 8).

***7.*** *Anisodactyly*: Absent, taxon is not capable of anisodactyl digit orientation (0); Present, taxon is capable of anisodactyl digit orientation (1).

Birds that are able to arrange their toes such that digit 1 (hallux) is directed posteriorly, and digits 2, 3, and 4 are directed anteriorly. Most extant bird taxa have this digit arrangement.

***8.*** *Zygodactyly*: Absent, taxon is not capable of zygodactyl digit orientation (0); Present, taxon is capable of zygodactyl digit orientation (1).

Birds that are able to arrange their toes such that digits 1 (hallux) and 4 are directed posteriorly, and digits 2 and 3 are directed anteriorly. Examples of taxa from this dataset with zygodactyl arrangements include parrots (Psittaciformes), cuckoos (Cuculiformes), and woodpeckers, jacamars, and allies (Piciformes) (Birds of the World ed. Billerman, 2021; Mayr, 2002). Taxa with facultatively zygodactyl arrangements include owls (Strigiformes), mousebirds (Coliiformes), turacos (Musophagiformes)(Birds of the World ed. Billerman, 2021; Mayr, 2002), and kites (*Elanus*)(Negro et al., 2006).

***9.*** *Heterodactyly*: Absent, taxon is not capable of heterodactyl digit orientation (0); Present, taxon is capable of heterodactyl digit orientation (1).

Birds that are able to arrange their toes such that digits 1 (hallux) and 2 are directed posteriorly, and digits 3 and 4 are directed anteriorly. The heterodactyl arrangement is unique to trogons (Trogonidae) among extant birds (Birds of the World ed. Billerman, 2021; Raikow, 1985; de los Monteros, 2000).

***10.*** *Pamprodactyly*: Absent, taxon is not capable of pamprodactyl digit orientation (0); Present, taxon is capable of pamprodactyl digit orientation (1).

Birds that are able to arrange their toes such that all digits 1 to 4 are directed anteriorly. This configuration of digits is seen facultatively in both swifts (Apodidae), and mousebirds (Coliiformes) (Birds of the World ed. Billerman, 2021; Raikow, 1985).

***11.*** *Digital manipulation*: Absent, taxon does not digitally manipulate prey and/or objects (0); Present, taxon does manipulate prey and/or objects (1)

Birds with digital manipulation ability are here defined as using their feet and toes to manipulate objects such as food items.

Most extant bird species, including many falconiforms and accipitriforms, do not use their feet for digital manipulation. However, examples of those that do (state 1) from this dataset are parrots (Psittaciformes), owls (*Aegolius*, *Tyto*) and the falconiform Crested Caracara (*Caracara cheriway*) (Birds of the World ed. Billerman, 2021; IBC; Sustaita et al., 2013).

***12.*** *Ability to hold down objects*: Absent, taxon does not hold down objects (0); Present, taxon does hold down objects (1).

This variable refers to birds that hold or pin down prey or other objects with force and bodyweight while picking at it with the beak. The action is a prolonged, forceful step onto the prey, to counteract pulling force from the beak. This action is judged independently of foot grip strength (Character 13), because there are non-raptorial species which routinely exhibit hold-down behaviour (ex. black crowned crane (*Balearica pavonina*)), as well as species whose grips are weak yet nevertheless exhibit hold-down behaviour (ex. new world vultures (Cathartidae)). The amount of force put on the feet in the hold-down position, for an important activity such as feeding, should exert some amount of influence in the shape of the foot bones in species which hold down objects (Madan et al. 2017).

Most taxa in this dataset scored with the ability to hold down objects (state 1) are raptorial (Character 18, state 1) and have a force grip (Character 13, state 1), and all such taxa are scored as being able to perch (Character 6, state 1). Most have ground walking ability (Character 1, state 1; e.g. *Balearica pavonina*), and few can digitally manipulate objects (Character 11, state 1; e.g. Psittaciformes). There is a mix of anisodactyl and zygodactyl digit arrangements among these taxa (Characters 7 and 8). None are scored as scansorial (Character 15, state 0), but parrots (Psittaciformes) exhibit hanging and clinging behaviour (Character 14, state 1). None are flightless (Character 23, state 0) or swimming (Character 19, state 0).

***13.*** *Force grip*: Absent, taxon does not grip objects forcefully (0); Present, taxon does grip objects forcefully (1)

A "force grip" is here defined as the use of a foot or the feet in order to grip onto an object, usually in the capture and carry of prey, exerting force and closing talons to maintain grasp. This ability is commonly associated with structures such as digital tendon locking mechanisms (Quinn and Baumel, 1990), so that the force behind such a grip can be efficiently maintained (Einoder & Richardson, 2007). Like perching, forceful gripping is also facilitated by the reversal of the hallux (Sustaita et al., 2013), as well as by certain digital arrangements such as anisodactyly and zygodactyly (Bock & Miller, 1959; Ksepka & Clarke, 2012; Carril et al., 2014).

All taxa in this dataset scored as having a force grip (state 1) also have the ability to perch (Character 6, state 1), and to hold down objects (Character 12, state 1). Most taxa with a force grip are also scored as raptorial (Character 18, state 1), with the exception of parrots (Psittaciformes). Most are anisodactyl; the parrots (Psittaciformes) and owls (Strigiformes) are zygodactyl and semi-zygodactyl respectively. Only one taxon, the Secretarybird (*Sagittarius*

*serpentarius*) is scored as cursorial (Character 4, state 1). None are flightless (Character 23, state 0) or swimming (Character 19, state 0).

The majority of extant bird species do not exhibit forceful gripping behaviour; examples of taxa from this dataset which do employ force grips include most members of raptorial clades (Accipitriformes, Falconiformes, Strigiformes) as well as parrots (Psittaciformes).

***14.*** *Hanging and clinging behaviour*: Absent, taxon does not use the feet to hang or cling on branches or vertical surfaces (0); Present, taxon does use the feet to hang or cling on branches or vertical surfaces (1).

Zeffer and Norberg (2003) determined that hanging locomotion results in varied moment arms and relative tarsometatarsus lengths among parrots (Psittacidae), tits (*Parus*), and goldcrests (*Regulus*). However, in combination with feeding movements, these taxa may rely more on stability of the tarsometatarsus (Zeffer & Norberg, 2003), in the form of shorter overall bone length (Norberg, 1979).

Taxa with hanging and clinging behaviour are mixed in other shared ecological categories in this dataset: none are here scored as cursorial (Character 4, state 0), raptorial (character 18, state 0), flightless (Character 23, state 0), or swimming (Character 19, state 0); only some exhibit scansoriality (Character 15, state 1) in addition to hanging and clinging behaviour; all but swifts (Apodidae) are able to perch (Character 6, state 1) as well as hang and cling; all share a mix of anisodactyl and zygodactyl digit arrangements (Characters 7 and 8, state 1), apart from the swifts (Apodidae) and mousebirds (Coliiformes), which are capable of pamprodactylous (Character 10, state 1) toe configurations in addition to anisodactyly.

Extant birds from this dataset that hang from branches include parrots (Psittaciformes) and mousebirds (Coliidae); birds that cling to vertical surfaces include swifts (Apodidae).

***15.*** *Scansoriality*: Absent, taxon does not climb vertical surfaces (0); Present, taxon does climb vertical surfaces (1)

Scansorial birds climb vertical surfaces by hopping or walking upwards. The use of this term signifies only the presence of vertical climbing behaviour, not necessarily a primary or frequent preference for this style of locomotion, as the term has been used in other research. Zeffer and Norberg (2003) determined that climbing locomotion correlates with higher than average distances between the eminentia intercotylaris and the m. tibialis cranialis insertion point, resulting in a focus on force production during ankle flexion, rather than speed.

In this dataset, only four taxa are scored as scansorial. All four share a number of other ecological scores. All can hang and cling (Character 13, state 1), perch (Character 6, state 1), and have standard walking ability (Character 1, state 1). There is a mix of anisodactyl and zygodactyl digit arrangements (Characters 7 and 8, state 1) in this category; the Black-tailed Treecreeper (*Climacteris melanurus*) and the Common Hoopoe (*Upupa epops*) are anisodactylous (Character 7, state 1), and the Least Honeyguide (*Indicator exilis*) and the Eurasian Wryneck (*Jynx torquilla*) are zygodactylous (Character 8, state 1). None of the taxa scored here as scansorial are also scored as cursorial (Character 4, state 0), raptorial (Character 18, state 0), flightless (Character 23, state 0) or swimming (Character 19, state 0).

***16.*** *Centroid size*: continuous variable

The centroid size of a specimen is the square root of the sum of squared distances of each landmark from the centroid of the total landmark configuration (Bookstein, 1991). Centroid size aids in indexing size of the tarsometatarsus. When included as an explanatory variable alongside individual size (mean body mass; Character 17, see below), it indexes the proportional size of the tarsometatarsus. Centroid size is generally considered to be independent of shape (Zelditch et al.,

2004). However, it may still have a relationship with tarsometatarsus shape due to allometry (Mitteroecker et al., 2013). It is also argued that the use of real biological data to calculate landmark configurations and centroid size results in natural and slight variation. This suggests that centroid size cannot be entirely unrelated to the shape of an object (Mitteroecker et al., 2013). For example, proportional elongation of the tarsometatarsus, or similar shape variation should result in an increase in centroid size. The sampled tarsometatarsi span centroid sizes from 3.2 mm (*Archilochus colubris*) to 209.2 mm (*Sagittarius serpentarius*). Centroid size data has therefore been $\log_{10}$-transformed so analyses are effectively conducted on a proportional scale that avoids inflation of residuals with increasing absolute size.

***17.*** *Mean body mass*: continuous variable

The average of male and female body masses of each species, in grams (measurements used from Birds of the World; ed. Billerman, 2021) are used to index estimated individual size. This is appropriate, given that only adult specimens were scanned, without data on specimen sex. This size measurement differs from centroid size in that it is independent of both landmark placement and proportional size of the tarsometatarsus within the body. The relationship between body mass and morphology takes into account the proportions of the entire bird, unlike that of centroid size and morphology. Body mass data was $\log_{10}$-transformed prior to analysis (see above).

***18.*** *Raptoriality*: Absent, taxon does not strike and carry prey with the feet (0); Present, taxon does strike and carry prey with the feet (1)

Despite their widespread use in classification or as behavioural categories, the terms ‘raptor’ or ‘bird of prey’ are not well-defined. Zeffer and Norberg (2003) defined a subsection of birds of prey as those species which “carry their prey close to the body with the claws during

flight," (p. 1086) to avoid drag and parasitism from other birds. Zeffer et al. (2003) described their bird of prey category as those birds which "strike and carry prey with the feet," (p. 462), but excluded certain taxa (such as new and old world vultures, and Secretarybirds) to a terrestrial category instead. Ward et al. (2002) referred to the term "raptor" in connection to predatory efficiency, and the dependency on the use of hindlimbs to catch prey. Many works refer to specific taxonomic orders to define raptoriality: the Accipitriformes, Falconiformes, and Strigiformes. For the purposes of this work, which focuses on the uses of the foot in a bird's lifestyle, the definition of raptorial behaviour will follow the Zeffer et al. (2003) description of striking and carrying prey with the feet. However, unlike the classification of Zeffer et al. (2003), Secretarybirds (*Sagittarius serpentarius*) are included in this category, as they are observed to strike and carry prey with the feet; they are also scored independently as terrestrial and cursorial, which is permitted by the multivariate classification scheme used here.

Although vultures are colloquially referred to as birds of prey, the emphasis of this research on foot use must exclude them from the raptorial foot use category, despite their vernacular status as raptors. Vultures do not use their feet for the hunting and killing of prey unlike other Accipitriformes. Indeed, they do not have the appropriate foot grip strength to perform this behaviour (Birds of the World; ed. Billerman, 2021). Most vultures primarily scavenge for carrion prey; although a carrion diet would not preclude their inclusion in the raptorial category outright, and although some vultures hunt and kill live prey with varying degrees of frequency, it is both unclear and unlikely that any vulture taxon uses its feet for striking in the same way that other raptors do.

Einoder and Richardson (2007) concluded that prey type and killing technique exert selective pressures on the hindlimb morphology of raptors. The impact on owl (Strigiformes)

tarsometatarsi of penetrating snow or leaf litter and the force required to securely hold prey is benefited by an abundance of sesamoids and a shorter, more robust tarsometatarsus (Ward et al., 2002; Madan et al., 2017). Likewise, the agile, high velocity pursuit demonstrated by many Accipitriformes and Falconiformes, followed by either a forceful capture impact and subsequent bites (Falconiformes: Goslow, 1971; Csermely et al., 1998) or a kneading compression grasp (Accipitriformes: Goslow, 1971; Einoder and Richardson, 2007) is generally aided by a longer and thinner tarsometatarsus (Ward et al., 2002; Einoder and Richardson, 2007).

Raptorial birds in this dataset all also share the ability to hold down objects (Character 12, state 1), usually combined with the use of a force grip (Character 13, state 1). All taxa are either anisodactyl or semi-zygodactyl, with a varied mix of cursoriality (Character 5, state 1) and ground walking ability (Character 1, state 1). None are scansorial (Character 15, state 0) or flightless (Character 23, state 0). Ospreys (Pandionidae) are the only taxon scored intermediately for swimming ability (Character 19, state 1) as they are briefly and partially submerged after a plunging dive to catch fish (Birds of the World; ed. Billerman, 2021).

***19.*** *Swimming ability*: Absent, taxon cannot swim (0); Mixed, Taxon exhibits plunging behaviour, i.e. briefly submerged after a dive (1); Present, taxon exhibits a full swimming mode of locomotion (2).

Birds here characterized as having full swimming ability are able to both suspend and propel themselves through water with any aquatic mode of locomotion. This includes birds which swim on the surface of water as well as those which swim with their bodies submerged. Scores of this character are independent of the mechanism of propulsion through the water (i.e. including both strictly wing-based locomotion as well as foot-based locomotion). The scoring of this category is designed to be as inclusive as possible, to test the hypothesis of the independent

effect of general swimming ability on morphology of the tarsometatarsus. Other characters in this list are used to test the hypothesised independent effects of more specific swimming behaviours (see below).

The intermediate scoring of plunging behaviour includes taxa which do not otherwise have a full swimming locomotion mode, yet nonetheless interact with the water as a major aspect of their behaviour. For example, the kingfishers included in this dataset (*Chloroceryle*, *Alcedo*) plunge for fish and are briefly submerged (Fry and Fry, 2010), but do not continue to propel themselves either under the water or on top of it (IBC), and so have intermediate scoring. The brown pelican (*Pelecanus occidentalis*) exhibits a similar plunging technique, yet also rests on top of the water with foot-propelled surface swimming (IBC), and so is scored as having full swimming ability.

Apart from the Hoatzin (*Opisthocomus hoazin*) and the Virginia Rail (*Rallus limnicola*) all taxa in this dataset with full swimming mode have webbed feet (Character 20, state 1 or 2) and are not scored as cursorial (Character 4, state 0). All fully swimming taxa have anisodactyl digit arrangements (Character 7, state 1), and none are scored as raptorial (Character 18, state 0). Some examples of taxa from this dataset that are defined as non-swimming include wading birds such as bitterns, herons, and egrets (Ardeidae), and most Passeriformes. Most shorebirds (Charadriiformes) included in this dataset have surface swimming ability (state 2), and at least some sandpipers (*Actitis*, *Tringa*) are able to dive and propel themselves using both feet and wings (Birds of the World; ed. Billerman, 2021).

***20.*** *Webbed feet*: Absent, taxon does not have webbed feet or feet with toe lobes (0); Present, taxon has feet with toe lobes (1); Present, taxon has webbed feet (2).

Webbed feet are linked with aquatic behaviour in birds. They are found in Anseriformes, Phoenicopteriformes, Phaethoniformes, Gaviiformes, Sphenisciformes, Procellariiformes, Pelecaniformes, and Suliformes. The triangular shape and surface area of webbed feet provide efficient propulsion for swimming (Johannes & Norberg, 2003). Most taxa with swimming ability have either webbed feet or feet with toe lobes. Toe lobes, found in grebes (Podicepedidae), finfoots (Heliornithidae), coots (*Fulica*), and phalaropes (*Phalaropus*, *Steganopus*) are here categorized as an intermediate score between non-webbed and webbed feet, in case there is a statistically significant distinction between morphologies.

All taxa with toe lobes or webbed feet have anisodactyl digit arrangements (Character 7, state 1; Raikow, 1985), and all except for the Ascension frigatebird (*Fregata aquila*) swim (Character 19, state 0; Wanless, 2002). In this dataset, it appears that most taxa with toe lobes or webbed feet perform foot-propelled surface swimming (Character 21, state 1), and a smaller subset perform submerged foot-propelled swimming (Character 21). All taxa with toe lobes or webbed feet in the current dataset are able to fly (Character 23, state 0), apart from the Humboldt Penguin (*Spheniscus humboldti*); there are a number of flightless aquatic taxa with toe lobes or webbed feet, such as the Flightless Cormorant (*Nannopterum harrisi*) and the Titicaca Grebe (*Rollandia microptera*). Most taxa scored as state 1 or 2 are able to walk on the ground (Character 1, state 1), with the exception of the Ascension Frigatebird (*Fregata aquila*) and the Red-throated Loon (*Gavia stellata*).

The Virginia Rail (*Rallus limnicola*) is an example of a taxon within this dataset which is able to swim but does not have webbed feet, whereas the Frigatebird (*Fregata aquila*) does not swim (Wanless, 2002) but does have webbed feet. Taxa within this dataset which have feet with toe lobes include the African Finfoot (*Podica senegalensis*), and the White-tufted Grebe

(*Rollandia rolland*). The Magpie Goose (*Anseranas semipalmata*), which has "semipalmated" feet (Birds of the World, ed. Billerman, 2021; Miller, 1919), has here been scored as state 2, due to the presence of webbing, regardless of relative amount.

***21.*** *Foot-propelled surface swimming*: Absent, taxon does not propel itself along water surface using feet (0); Present, taxon does propel itself along water surface using feet (1).

Foot-propelled surface swimming describes the locomotion of a bird which sits on top of the water surface, and uses its legs and feet underneath to propel itself forward. All surface swimmers, with the exception of the Southern Brown Kiwi (*Apteryx australis*), the Hoatzin (*Opisthocomus hoazin*), and the Virginia Rail (*Rallus limnicola*) have toe lobes or webbed feet (Character 20, state 1 or 2), have anisodactyl digit arrangements (Character 7, state 1), and are able to fly (Character 23, state 0).

Examples of birds which use surface foot-propulsion include the pelican (*Pelecanus*), and ducks, geese, and swans (Anatidae). An example of a bird from this dataset which does not employ this method of locomotion is the Amazon Kingfisher (*Chloroceryle amazona*).

***22.*** *Foot-propelled submerged swimming*: Absent, taxon does not propel itself through water using feet while fully submerged (0); Present, taxon does propel itself through water using feet while fully submerged (1).

State 1 of this character describes the locomotion of a bird which submerges its body fully under the surface of the water, and then propels itself with the use of legs and feet. The taxa in this dataset which do engage in submerged foot propelled swimming have also been scored as having webbed feet or toe lobes (Character 20, state 1 or 2) (Birds of the World, ed. Billerman, 2021; Clifton and Biewener, 2018), anisodactyl digit arrangements (Character 7, state 1), ability

to fly (Character 23, state 0), and ability to swim on the water surface with foot-propulsion (Character 21, state 1).

Examples of birds in this dataset which employ this method of locomotion include grebes (Podicipedidae) and ducks (Anatidae). Birds such as penguins (Spheniscidae) and gulls (*Larus*) are capable of swimming, but penguins do not propel with the hindlimbs, and gulls do not swim while submerged (Birds of the World; ed. Billerman, 2021). Plunge-divers such as pelicans (Schreiber and Woolfenden, 1975) and aquatic kingfishers become either partially or fully submerged during their dive, but do not exhibit forms of forward or upward propulsion while submerged. The Short-tailed Shearwater (*Ardenna tenuirostris*) and the Masked Booby (*Sula dactylactra*) use a combination of foot and wing propulsion (Birds of the World; ed. Billerman, 2021) during submerged swimming to lengthen their plunge dives, and are here scored as state 1 (present).

***23.*** *Flightlessness*: Absent, bird is able to fly in any capacity (0); Present, bird is unable to fly (1).

Birds defined here as flightless are physically incapable of aerial flight, regardless of preference or facultative ability. Flightless birds tend to have more robust hindlimbs, as they must rely on and invest in their legs for locomotion (e.g. Heers and Dial, 2015).

Birds which are considered flightless in this dataset include the Humboldt Penguin (*Spheniscus humboldti*) and the kiwi (*Apteryx*). Both taxa are able to walk (Character 1, state 1) and swim (Character 19, state 2), to varying extents of proficiency in each, although swimming ability for other flightless ratites is likely not common.

### 1.2.4 Landmarking

I used 37 point landmarks and 15 semi-landmark series to quantify tarsometatarsus shape with geometric morphometrics (e.g. Bookstein, 1991; Gunz and Mitteroecker, 2013). These were placed on the 3D models using the analysis software Avizo Lite (v.9.7.0). Each landmark was manually placed, in accordance with the landmark scheme and subsequent placement rules. The landmarks were then read from Avizo and converted to a format that could be analysed in R package geomorph (version 4.0.1; Adams et al., 2021). Reading from Avizo was achieved using a set of R functions provided by R. Benson, which use functions from the packages geomorph and stringdist (version 0.9.8; van der Loo, 2020). I prepared my 3D shape data so that all right and left landmarked tarsometatarsi were flipped to left sides. I placed arbitrary numbers of points in each semi-landmark series, which were then standardised to equal counts in all specimens using the geomorph function digit.curves (version 3.2.1; Adams, 2020).

***SL1.*** *Metatarsal I fossa*

The semi-landmark series 1 (SL1; Figure 5A) starts from the most proximal point of the lip of the fossa, traces around the lateral edge in a proximal-to-distal direction, then circles around the distal end and traces around the medial edge in a distal-to-proximal direction, ending just medial to the starting point. This landmark series shows where the metatarsal I (hallux) attaches to the tarsometatarsus, and to a certain extent also helps in the inference of the orientation of digits (Middleton, 2001). The semi-landmark loop around the perimeter describes the shape of the entire attachment area. Many of the muscles controlling the hallux attach directly to the phalanx, and not to the joint (Raikow, 1985).

For taxa with poorly defined fossa edges, such as the mousebirds (Coliidae), landmarks for this series were estimated, following in-person examinations of articulated osteological specimens (Figure 5B).

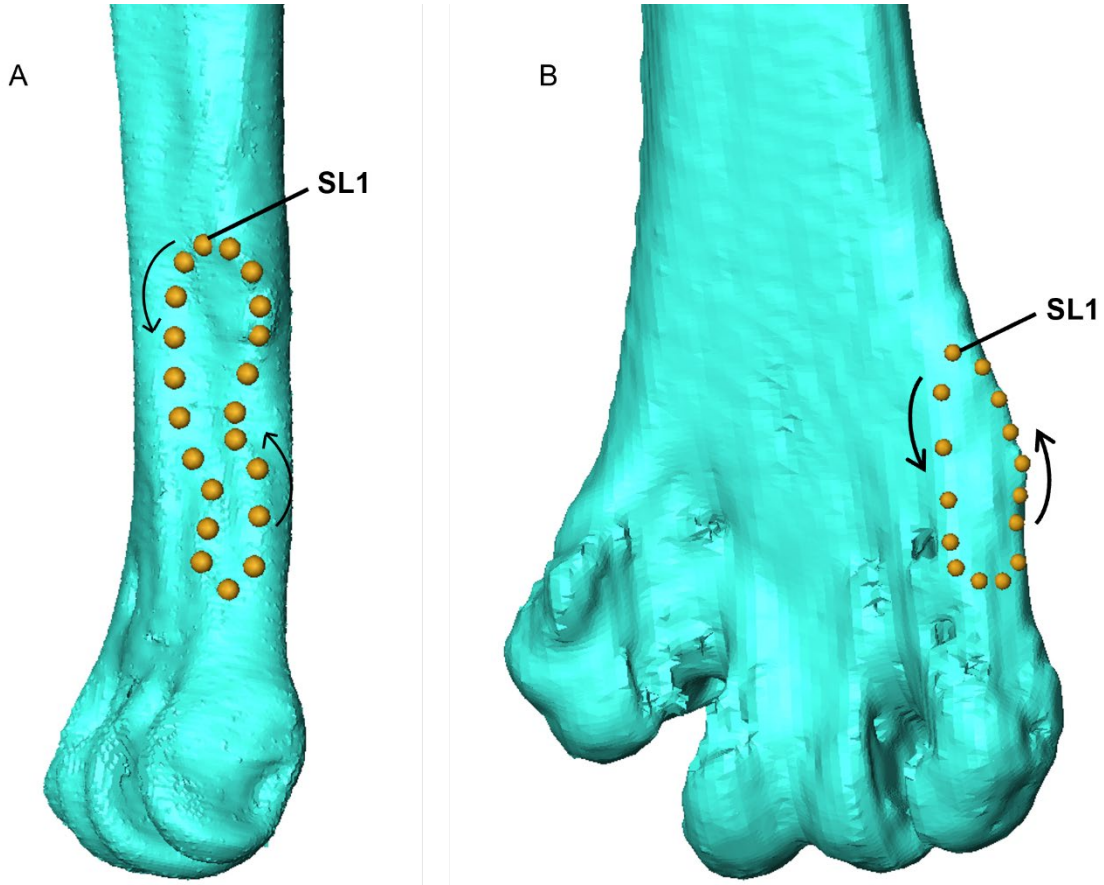


**Figure 5.** A) Distal end of left tarsometatarsus (3D model) of *Corvus albus* (NHMUK 1866.8.6.13) in medial view showing semi-landmark series around metatarsal I fossa (SL1) landmarked with orange points. B) Distal end of left tarsometatarsus (3D model of *Urocolius macrourus* (FMNH 368959) in plantar view showing semi-landmark series around metatarsal I fossa (SL1) landmarked with orange points.

***L1, L2, SL2.*** *Metatarsal IV trochlea*

SL2 (Figure 6) starts from the most proximal point of the lateral edge of trochlea metatarsi IV on the plantar surface (L1), follows the edge in a proximal-to-distal direction, then in a plantar-to-dorsal direction on the distal surface, and then a distal-to-proximal direction on

the dorsal surface, looping around at the most proximal point of the metatarsi to curve back along the medial edge of the condyle, ending at the proximal-most point of this medial edge on the plantar surface (L2).

***L3, L4.*** *Lateral intertrochlear incisura*

Two point-landmarks mark the deepest point of the lateral intertrochlear incisura on both the plantar (L3) and dorsal (L4) sides (Figure 7).

***L5, L6.*** *Metatarsal IV trochlea condyle*

Two point landmarks mark the deepest points on both the lateral (L5) and medial (L6) sides of the individual condyle (Figure 7). The lateral side of trochlea IV is an attachment area for the ligaments which lead to the digit IV phalanges (Raikow, 1985).

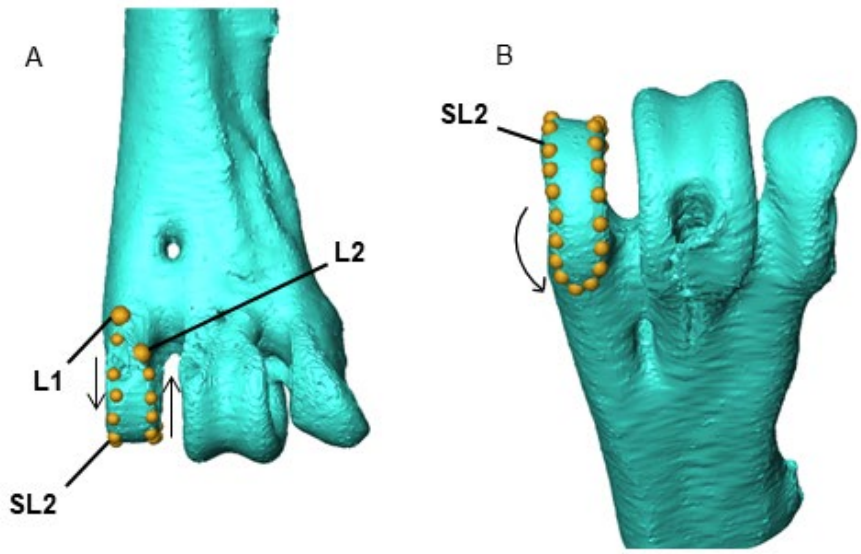


**Figure 6.** A) Distal end of left tarsometatarsus (3D model) of *Corvus albus* (NHMUK 1866.8.6.13) in dorsal view showing point landmarks and semi-landmark series around metatarsal IV trochlea (SL2, L1, L2) landmarked with orange points. B) Distal end of left tarsometatarsus (3D model) of *Corvus albus* (NHMUK 1866.8.6.13) in distal view showing semi-landmark series around metatarsal II trochlea (SL2) landmarked with orange points.

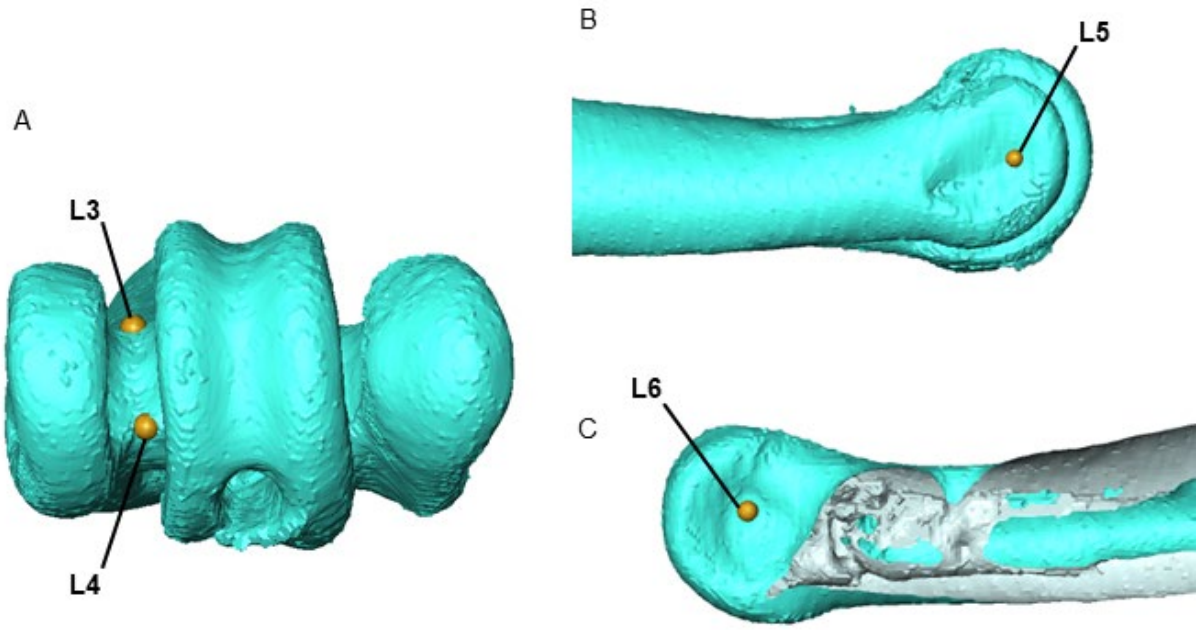


**Figure 7.** A) Distal end of left tarsometatarsus (3D model) of *Corvus albus* (NHMUK 1866.8.6.13) in distal view showing point landmarks of the lateral intertrochlear incisura (L3, L4) landmarked with orange points. B) Distal end of left tarsometatarsus (3D model) of *Corvus albus* (NHMUK 1866.8.6.13) in lateral view showing lateral point landmark of the metatarsal IV trochlea condyle (L5) landmarked with orange point. C) Distal end of left tarsometatarsus (3D model) of *Corvus albus* (NHMUK 1866.8.6.13) in medial view showing medial point landmark of the metatarsal IV trochlea condyle (L6) landmarked with orange point.

***L7, L8, SL3.*** *Metatarsal III trochlea*

SL3 (Figure 8) starts at the proximal-most point of the lateral edge on the plantar side of trochlea metatarsi III (L7), following the edge in a proximal-to-distal direction, then in a plantar-to-dorsal direction on the distal surface, and then a distal-to-proximal direction on the dorsal surface, looping around the proximal most point of the metatarsi to curve back along the medial edge, ending at the proximal-most point on the plantar side (L8).

***L9, L10, SL4.*** *Metatarsal III trochlear furrow*

A separate semi-landmark series (SL4; Figure 9) starts at the most proximal point of the middle of the metatarsal III trochlea (L9), and follows a similar path down the local minimum of the groove or furrow between the lateral and medial edges along the full articular surface of the metatarsi, ending on the dorsal side at the furthest point created by the path that runs around the medial and lateral ridges (L10).

***L11, L12.*** *Medial intertrochlear incisura*

The same point-landmarks as those on trochlea metatarsi IV have been placed on local minimums in the medial intertrochlear incisura (L11; L12; Figure 10).

***L13, L14.*** *Metatarsal IV trochlea condyle*

Two point landmarks mark the deepest points on both the lateral (L13; Figure 11A) and medial (L14; Figure 11B) sides of the individual condyle. These also function as digit III ligament attachment areas (Raikow, 1985).

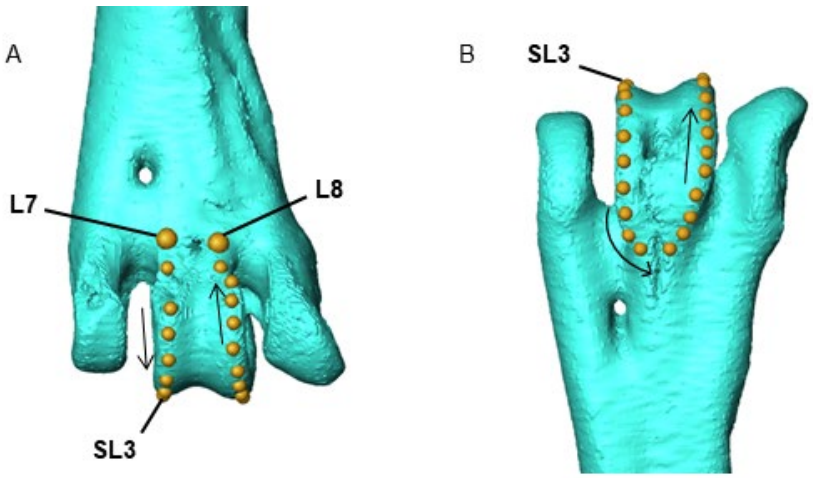


**Figure 8.** A) Distal end of left tarsometatarsus (3D model) of *Corvus albus* (NHMUK 1866.8.6.13) in plantar view showing point landmarks and semi-landmark series of the metatarsal III trochlea (SL3, L7,

L8) landmarked with orange points. B) Distal end of left tarsometatarsus (3D model) of *Corvus albus* (NHMUK 1866.8.6.13) in dorsal view showing semi-landmark series of the metatarsal III trochlea (SL3) landmarked with orange points.

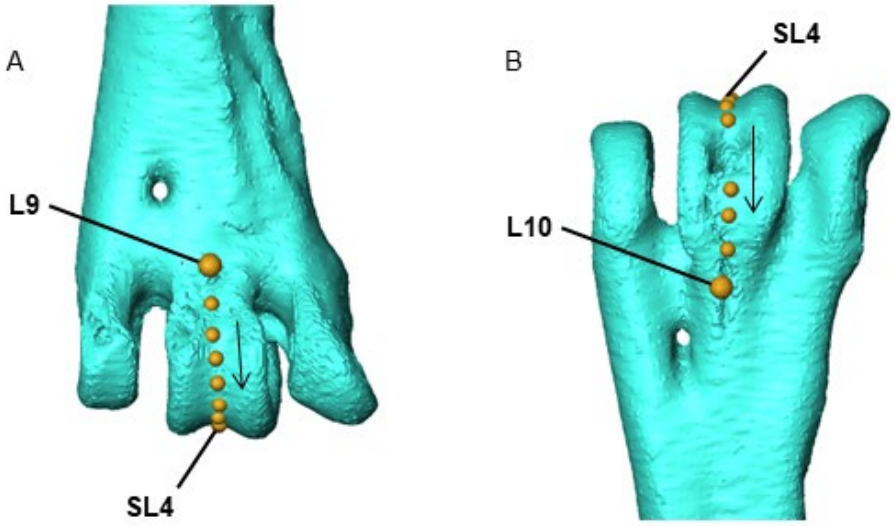


**Figure 9.** A) Distal end of left tarsometatarsus (3D model) of *Corvus albus* (NHMUK 1866.8.6.13) in plantar view showing point landmark and semi-landmark series of the metatarsal III trochlea furrow (SL4, L9) landmarked with orange points. B) Distal end of left tarsometatarsus (3D model) of *Corvus albus* (NHMUK 1866.8.6.13) in dorsal view showing point landmark and semi-landmark series of the metatarsal III trochlea furrow (SL4, L10) landmarked with orange points.

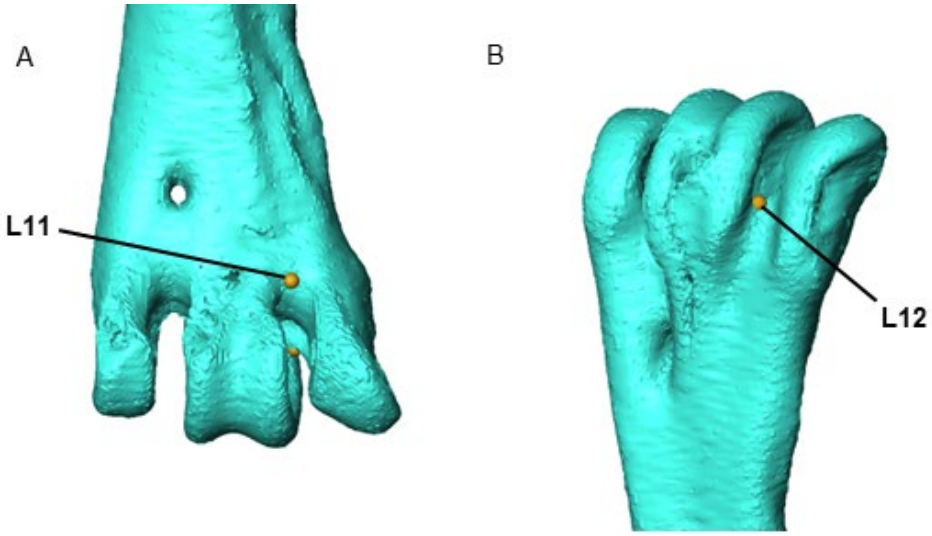


**Figure 10.** A) Distal end of left tarsometatarsus (3D model) of *Corvus albus* (NHMUK 1866.8.6.13) in plantar view showing point landmark medial intertrochlear incisura (L11) landmarked with orange point. B) Distal end of left tarsometatarsus (3D model) of *Corvus albus* (NHMUK 1866.8.6.13) in dorsal view showing point landmark of the medial intertrochlear incisura (L12) landmarked with orange point.

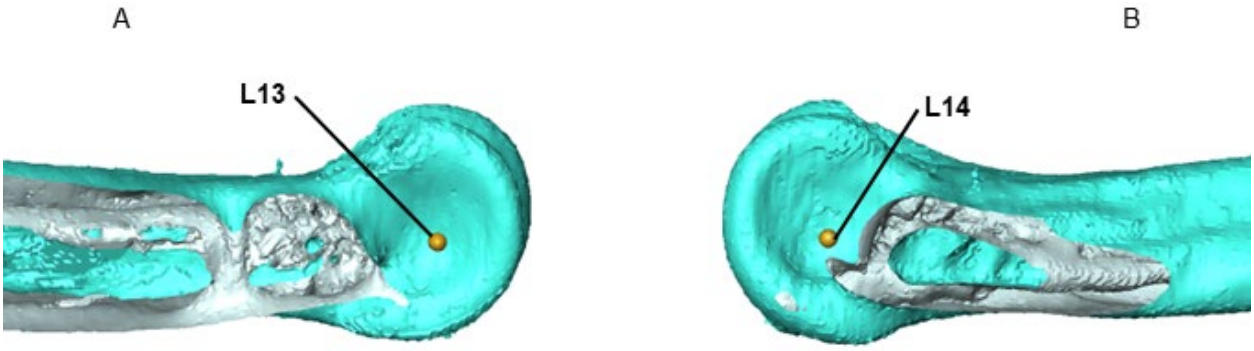


**Figure 11.** A) Distal end of left tarsometatarsus (3D model) of *Corvus albus* (NHMUK 1866.8.6.13) in lateral view showing point landmark of the metatarsal III trochlea condyle (L13) landmarked with orange point. B) Distal end of left tarsometatarsus (3D model) of *Corvus albus* (NHMUK 1866.8.6.13) in medial view showing point landmark of the metatarsal III trochlea condyle (L14) landmarked with orange point.

***L15, L16, SL5.*** *Metatarsal II trochlea*

SL5 (Figure 12) starts from the proximal-most point of the lateral edge of the TM II on the plantar surface (L15), following the edge in a proximal-to-distal direction, in a plantar-to-dorsal direction on the distal surface, and then a distal-to-proximal direction on the dorsal surface, looping around the proximal-most point of the metatarsi to follow the medial-most curve of the medial ridge of the condyle (L16).

***L17, L18.*** *Metatarsal II trochlea condyle*

The same point-landmarks as trochlea metatarsi III and IV mark the local minima on the sides of the condyle (L17; L18; Figure 13). There is a ligament attachment area on the medial side of the tarso-phalangeal joint. The tendon for M. abductor digiti II slides over the trochlea (from the dorsomedial surface of tarsometatarsus) in order to attach to the first phalanx (Raikow, 1985).

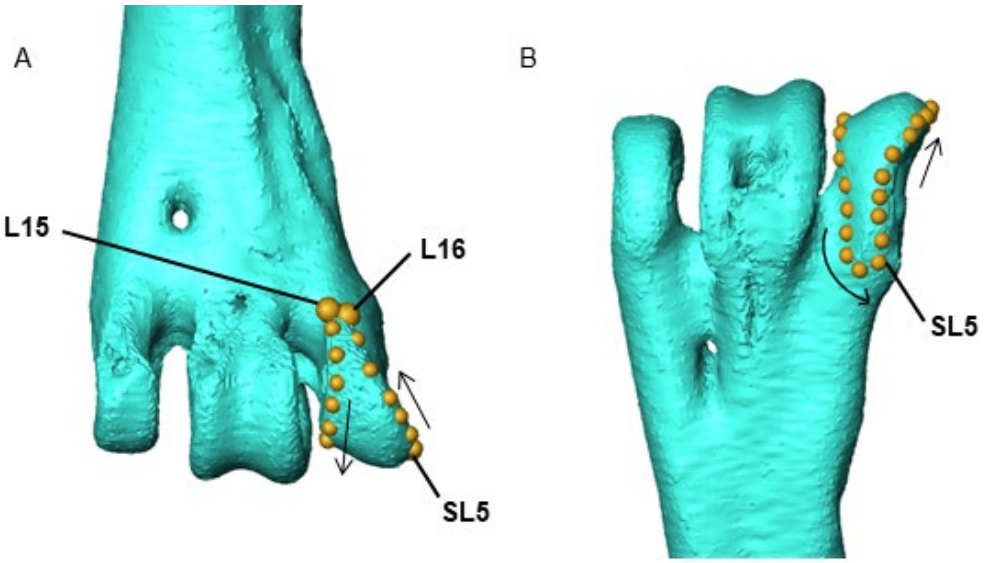


**Figure 12.** A) Distal end of left tarsometatarsus (3D model) of *Corvus albus* (NHMUK 1866.8.6.13) in plantar view showing point landmarks and semi-landmark series of the metatarsal II trochlea (SL5, L15, L16) landmarked with orange points. B) Distal end of left tarsometatarsus (3D model) of *Corvus albus* (NHMUK 1866.8.6.13) in dorsal view showing semi-landmark series of the metatarsal III trochlea (SL3) landmarked with orange points.

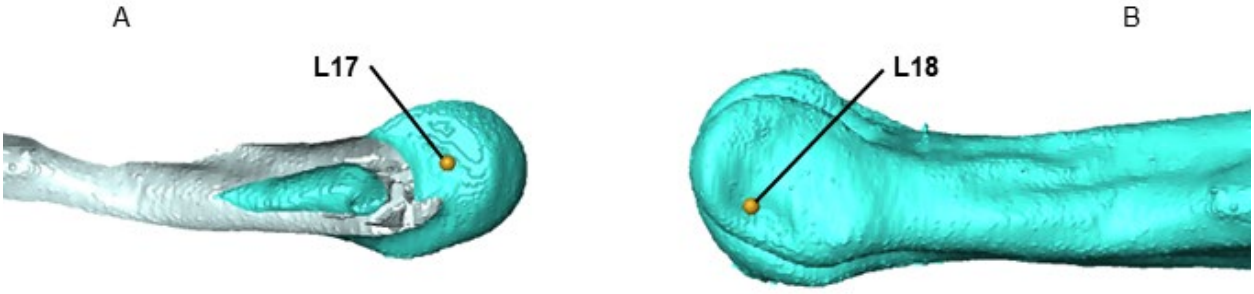


**Figure 13.** A) Distal end of left tarsometatarsus (3D model) of *Corvus albus* (NHMUK 1866.8.6.13) in lateral view showing point landmark of the metatarsal II trochlea condyle (L17) landmarked with orange point. B) Distal end of left tarsometatarsus (3D model) of *Corvus albus* (NHMUK 1866.8.6.13) in medial view showing point landmark of the metatarsal II trochlea condyle (L18) landmarked with orange point.

***L19, SL6.*** *Distal vascular foramen*

On the dorsal side of the tarsometatarsus, there is a point-landmark at the distal-most point of the distal vascular foramen (L19; Figure 14A). On the plantar side, there is a closed loop

of semi-landmarks which follow the perimeter of the foramen (SL6; Figure 14B), starting at the most proximal point and following down the lateral side first. The distal vascular foramen forms the passage for the dorsal metatarsal artery, which traverses through the foramen in a plantar-to-distal direction (Midtgård, 1982).

For cases in which the plantar side of the distal edge of the foramen is poorly defined, as in the Common Wood Pigeon (*Columba palumbus*) and the plain-breasted ground dove (*Columbina minuta*), an ovular, elongated loop of semi-landmarks were placed on the plantar side of the foramen, from the proximal edge of the foramen to just proximal to the plantar point landmark for the lateral intertrochlear incisura (Figure 15A). For cases in which the distal vascular foramen is obscured due to either the aeration of the bone (as in the African Grey Hornbill (*Tockus nasutus*)) or the closeness of the metatarsal trochleas (as in the Common Little Bittern (*Ixobrychus minutus*)), it is necessary to use the 3D analysis software to clip through the model of the bone in order to track the vascular path to find the correct opening (Figure 15B).

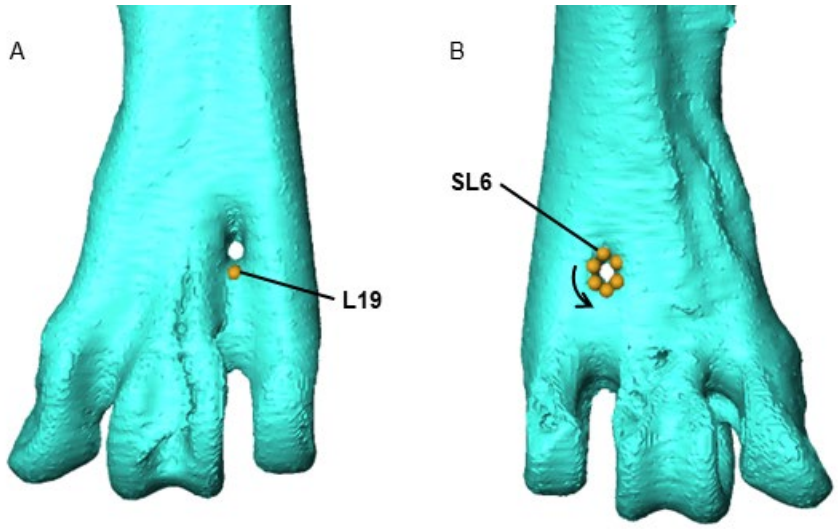


**Figure 14.** A) Distal end of left tarsometatarsus (3D model) of *Corvus albus* (NHMUK 1866.8.6.13) in dorsal view showing point landmark of the distal vascular foramen (L19) landmarked with orange point. B) Distal end of left tarsometatarsus (3D model) of *Corvus albus* (NHMUK 1866.8.6.13) in plantar view showing semi-landmark series of the distal vascular foramen (SL6) landmarked with orange points.

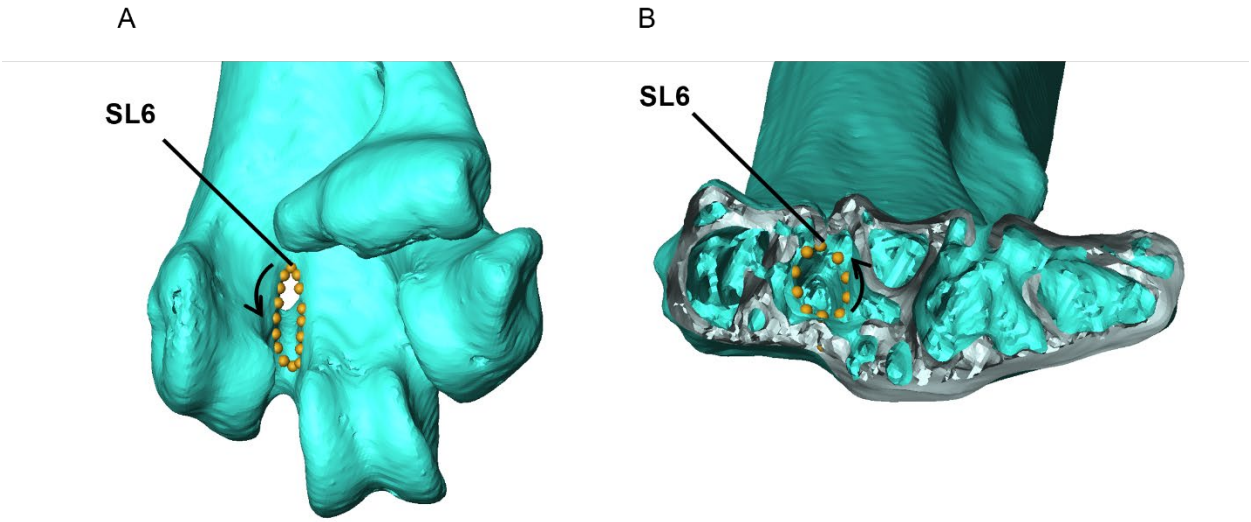


**Figure 15.** A) Distal end of left tarsometatarsus (3D model) of *Columba palumbus* (UMZC 409A) in plantar view showing semi-landmark series of the distal vascular foramen (SL6) landmarked with orange points. B) Distal end of left tarsometatarsus (3D model) of *Tockus nasutus* (NHMUK S1989.2.2) in plantar view showing semi-landmark series of the distal vascular foramen (SL6) landmarked with orange points.

***L1, L20, SL7.*** *Lateral plantar ridge*

SL7 (Figure 16) starts on the point at which the lateral plantar ridge meets the lateral hypotarsal cotyle (L20; Figure 16C). SL7 runs in a distal direction which bypasses the lateral hypotarsal crest (crista lateralis hypotarsi) on the plantar side, ending at the point where the ridge meets the most proximal point on plantar lateral edge of metatarsal IV (L1; Figure 16D). This structure forms one side of the sulcus flexorius, which guides the muscles, tendons and ligaments that attach to the digits after they pass through the hypotarsus (Raikow, 1985).

For cases in which the lateral hypotarsal crest joins smoothly with the lateral plantar ridge such that it's difficult to ascertain the distinct features (as in the Black-tailed Treecreeper (*Climacteris melanurus*)), it is possible with 3D analysis software to follow the faint edge of the lateral plantar ridge down from its starting point at the lateral cotyle in a distal direction which bypasses the hypotarsal canals and crests, eventually connecting with the bottom of the lateral hypotarsal crest (Figure 17).

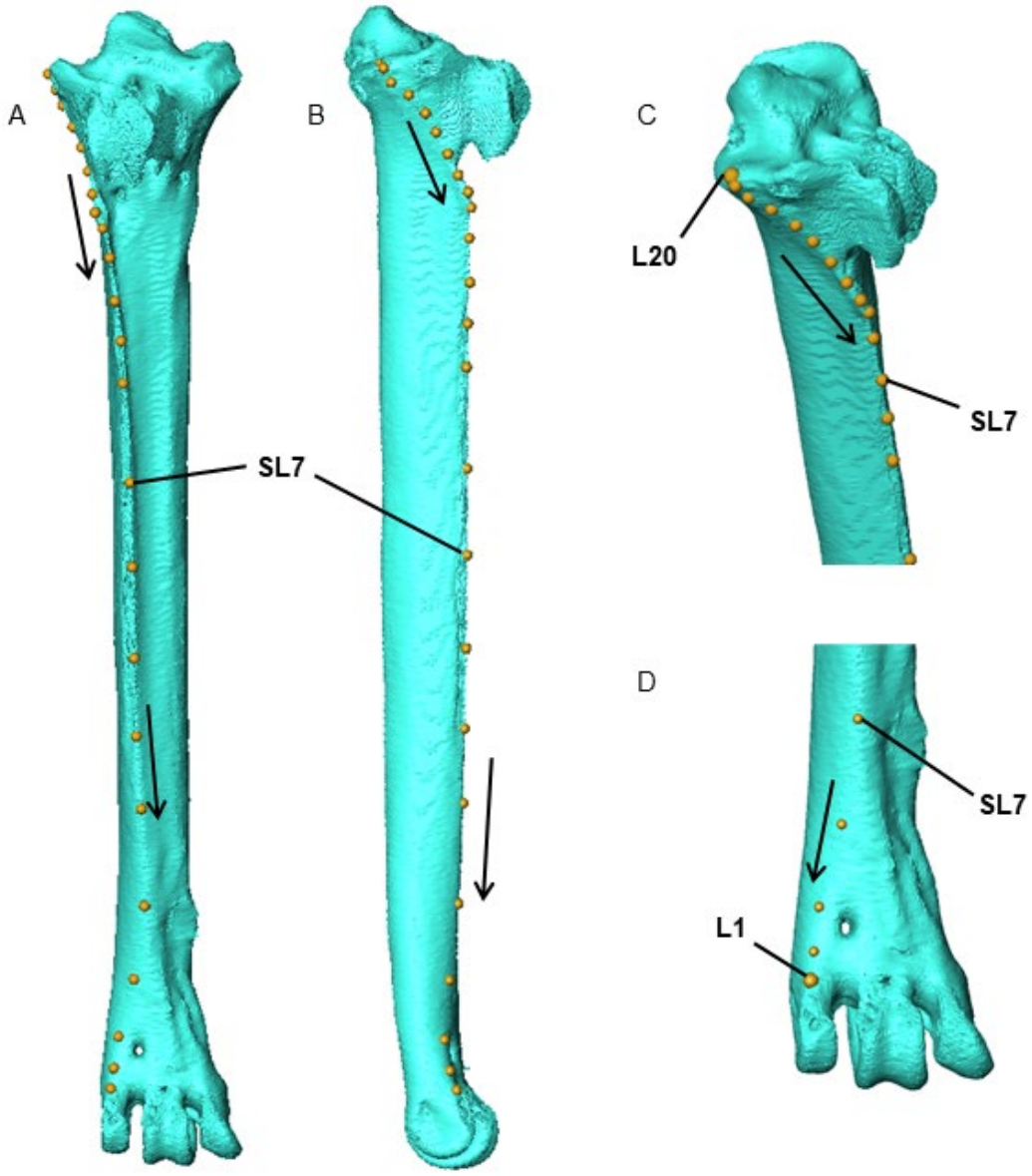


**Figure 16.** A) Entire left tarsometatarsus (3D model) of *Corvus albus* (NHMUK 1866.8.6.13) in plantar view showing semi-landmark series of the lateral plantar ridge (SL7) landmarked with orange points. B) Entire left tarsometatarsus (3D model of *Corvus albus* (NHMUK 1866.8.6.13) in lateral view showing semi-landmark series of the lateral plantar ridge (SL7) landmarked with orange points. C) Proximal end of left tarsometatarsus (3D model) of *Corvus albus* (NHMUK 1866.8.6.13) in oblique lateral view showing point landmark and semi-landmark series of the lateral plantar ridge (SL7, L20) landmarked with orange points. D) Distal end of left tarsometatarsus (3D model) of *Corvus albus* (NHMUK 1866.8.6.13) in plantar view showing point landmark and semi-landmark series of the lateral plantar ridge (SL7, L1) landmarked with orange points.

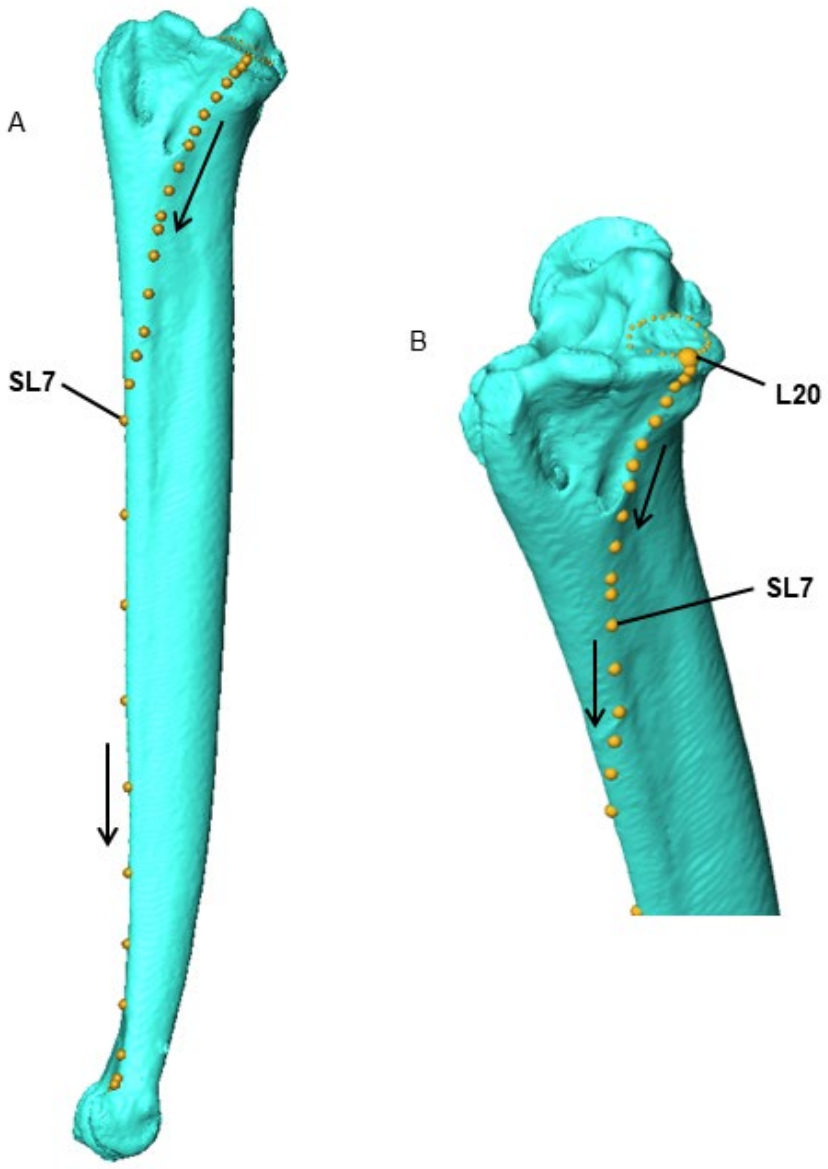


**Figure 17.** A) Entire right tarsometatarsus (3D model) of *Climacteris melanurus* (UMMZ 214303) in lateral view showing semi-landmark series of the lateral plantar ridge (SL7) landmarked with orange points. B) Proximal end of right tarsometatarsus (3D model) of *Climacteris melanurus* (UMMZ 214303) in oblique lateral view showing point landmark and semi-landmark series of the lateral plantar ridge (SL7, L20) landmarked with orange points.

***L21, L22, SL8.*** *Medial plantar ridge*

Similar to above, the semi-landmarks for SL8 (Figure 18) run in a distal direction along the ridge that starts at the edge of the medial hypotarsal cotyle (L21; Figure 18C), bypassing the medial hypotarsal crest on the plantar side, ending where the ridge meets the metatarsal I fossa

(L22; Figure 18D). It forms one side of the sulcus flexorius, which guides the muscles, tendons, and ligaments that attach to the digits after they pass through the hypotarsus (Raikow, 1985).

In some cases, the starting point and the path of the semi-landmark series for the medial plantar ridge is much more dorso-medially situated than in the majority of taxa, as in the Australian Ringneck (*Barnardius zonaris*), the Palm Cockatoo (*Probosciger aterrimus*), and the Grey Parrot (*Psittacus erithacus*) (Figure 19). In the Common Firecrest (*Regulus ignicapilla*), a short, proximo-medial protrusion is bypassed by the medial plantar ridge semi-landmark series, as it is neither a structure of the hypotarsal crest structure nor the medial plantar ridge (Figure 20).

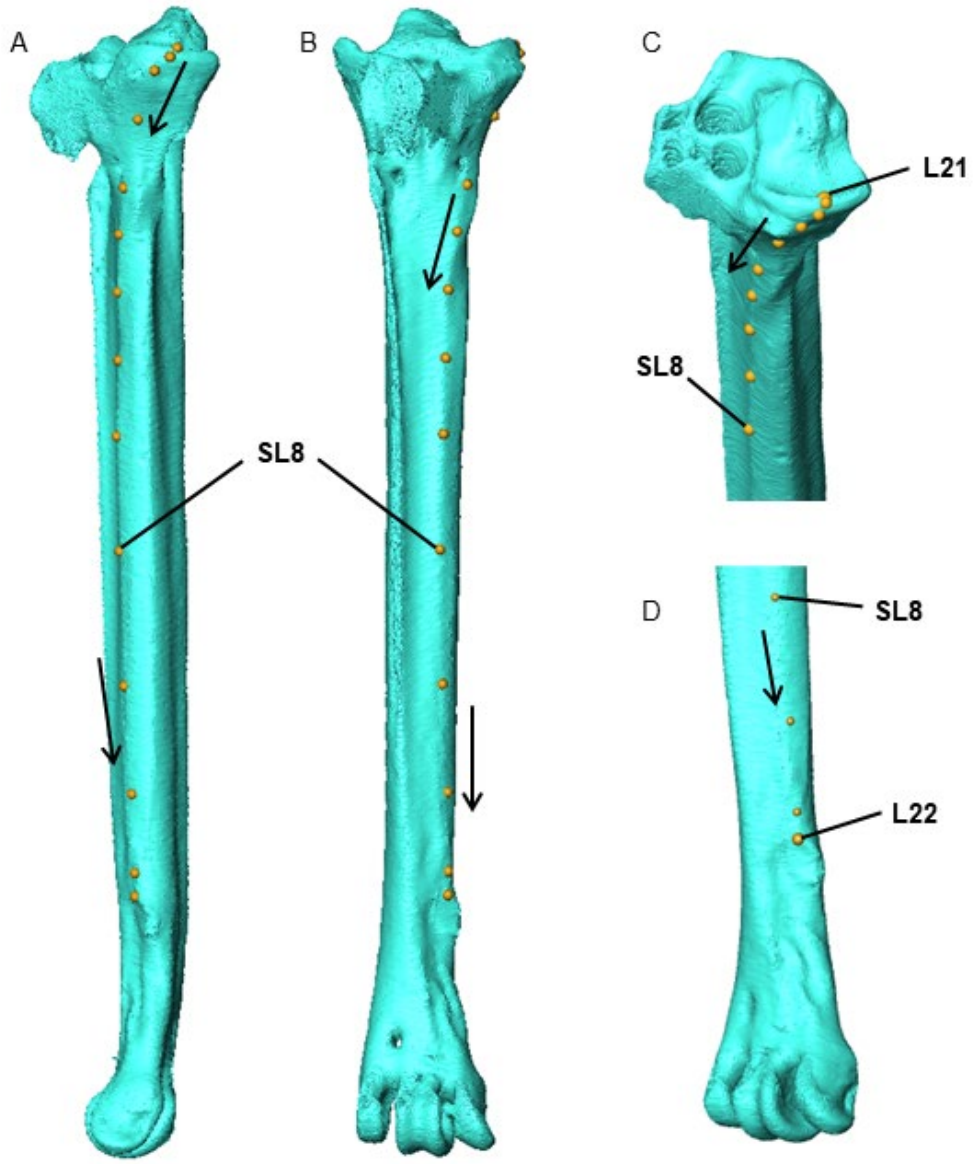


**Figure 18.** A) Entire left tarsometatarsus (3D model) of *Corvus albus* (NHMUK 1866.8.6.13) in medial view showing semi-landmark series of the medial plantar ridge (SL8) landmarked with orange points. B) Entire left tarsometatarsus (3D model) of *Corvus albus* (NHMUK 1866.8.6.13) in plantar view showing semi-landmark series of the medial plantar ridge (SL8) landmarked with orange points. C) Proximal end of left tarsometatarsus (3D model) of *Corvus albus* (NHMUK 1866.8.6.13) in oblique medial view showing point landmark and semi-landmark series of the medial plantar ridge (SL8, L21) landmarked with orange points. D) Distal end of left tarsometatarsus (3D model) of *Corvus albus* (NHMUK 1866.8.6.13) in plantar view showing point landmark and semi-landmark series of the medial plantar ridge (SL8, L22) landmarked with orange points.

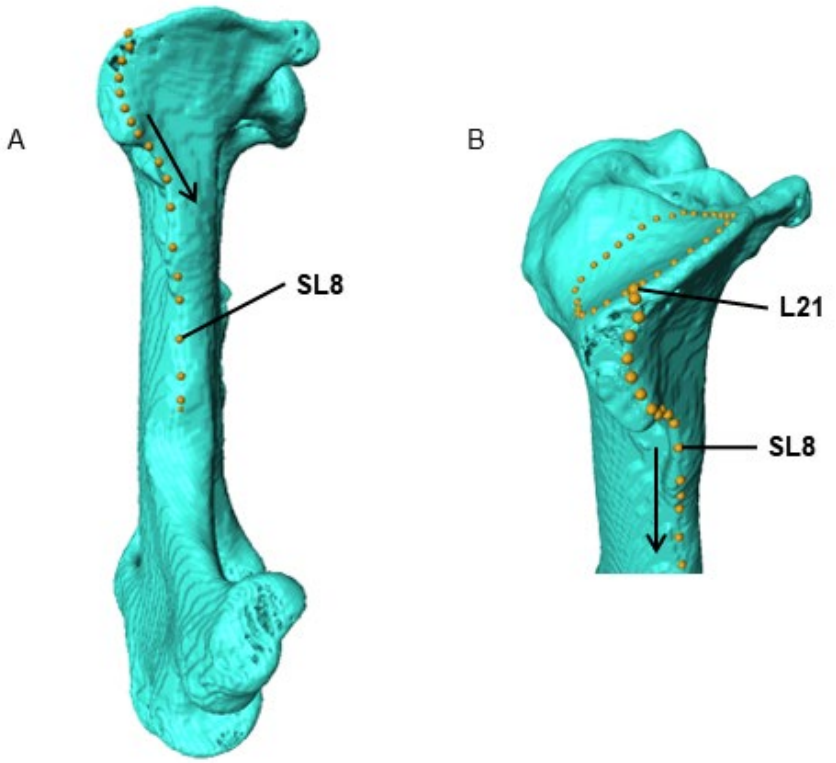


**Figure 19.** A) Entire right tarsometatarsus (3D model) of *Prosobsciger aterrimus* (NHMUK S2006.15.5) in medial view showing semi-landmark series of the medial plantar ridge (SL8) landmarked with orange points. B) Proximal end of right tarsometatarsus (3D model) of *Prosobsciger aterrimus* (NHMUK S2006.15.5) in oblique medial view showing point landmark and semi-landmark series of the medial plantar ridge (SL8, L21) landmarked with orange points.

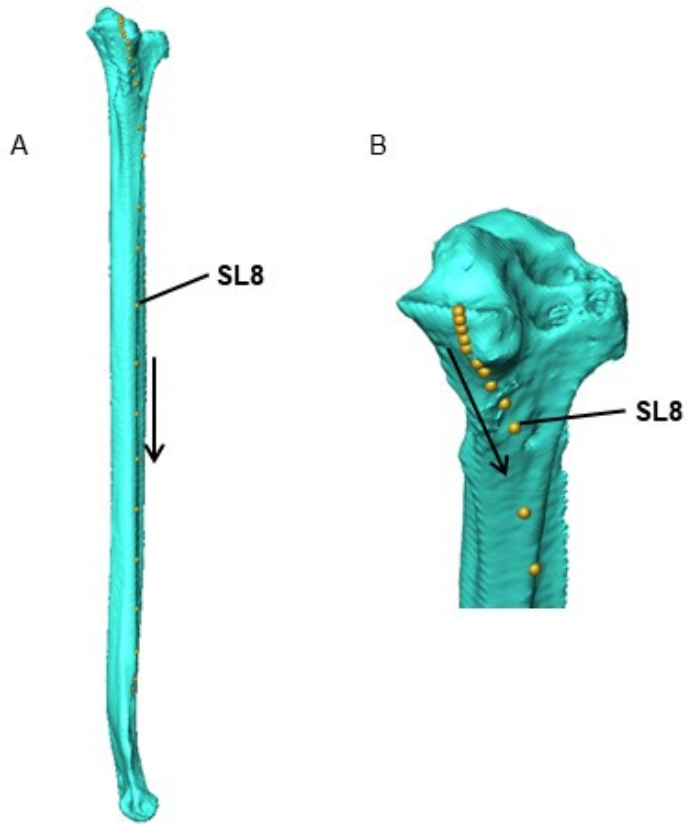


**Figure 20.** A) Entire right tarsometatarsus (3D model) of *Regulus ignicapilla* (NHMUK S1952.2.662) in medial view showing semi-landmark series of the medial plantar ridge (SL8) landmarked with orange points. B) Proximal end of right tarsometatarsus (3D model) of *Regulus ignicapilla* (NHMUK S1952.2.662) in oblique medial view showing semi-landmark series of the medial plantar ridge (SL8) landmarked with orange points.

***SL9, SL10.*** *Medial and lateral cotyles*

These semi-landmark series (SL9, SL10; Figure 21) separately trace the ovular shapes of the medial and lateral cotyles, which articulate with the medial and lateral condyles of the tibiotarsus. The loop starts at the plantar-medial most point on the outer edge of the medial cotyle, and the plantar-lateral most point on the outer edge of the lateral cotyle.

For the medial cotyle, the series runs in a plantar-to-dorsal direction around the medial edge of the cotyle, then medial-to-lateral along the dorsal edge, dorsal-to-plantar along the lateral edge, and lateral-to-medial along the plantar edge, ending just lateral to the starting point.

For the lateral cotyle, the series runs in a lateral-to-medial direction along the plantar edge, then a plantar-to-dorsal direction along the medial edge, then medial-to-lateral along the dorsal edge, and finally dorsal-to-plantar along the lateral edge, ending just dorsal to the starting point. The cotyles form an articular surface for the tibiotarsal condyles along with articular cartilage (Cracraft, 1971). Medial and lateral ligaments related to the intertarsal joint connect on medial and lateral sides of the cotyles, as continuations of the intertarsal joint capsule, and all limit the range of extension of the foot. (Cracraft, 1971).

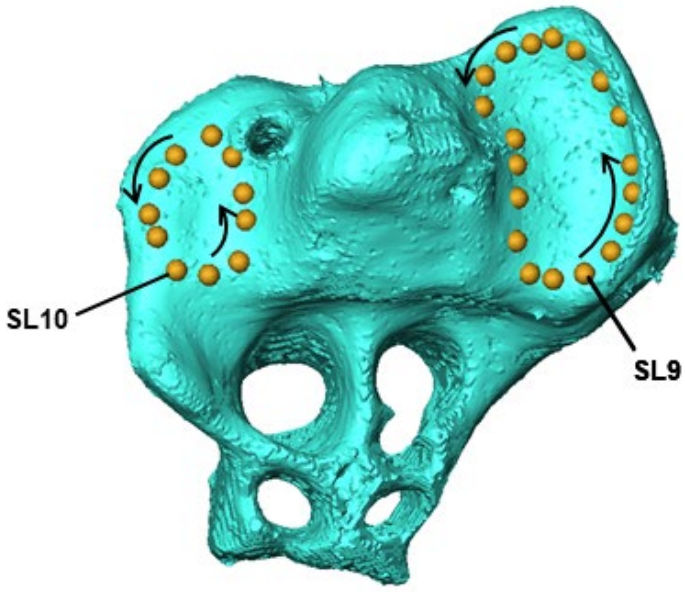


**Figure 21.** Proximal end of left tarsometatarsus (3D model) of *Corvus albus* (NHMUK 1866.8.6.13) in proximal view showing semi-landmark series of the medial (SL9) and lateral (SL10) cotyles landmarked with orange points.

***L23, L24, L25, L26.*** *Proximal vascular foramen*

The proximal vascular foramen point-landmarks function as they do on the distal vascular foramen, to mark size and placement. Two point-landmarks are placed on the proximal (L23; Figure 22A) and distal (L24; Figure 22A) positions of the perimeter of the foramen on the dorsal side of the tarsometatarsus, and two are placed in similar positions on the plantar side (L25; L26; Figure 22B).

For cases in which there are two or more foramina present, as in the majority of telluravian taxa, the most medial foramen is chosen for landmarking as it is the foramen which most commonly leads through to a visible opening on the plantar side. Both the lateral and medial proximal vascular foramina are the channels which the bifurcating branches of the plantar tarsal artery traverse in a dorsal-to-plantar direction after crossing the intertarsal joint (Thorp, 1988).

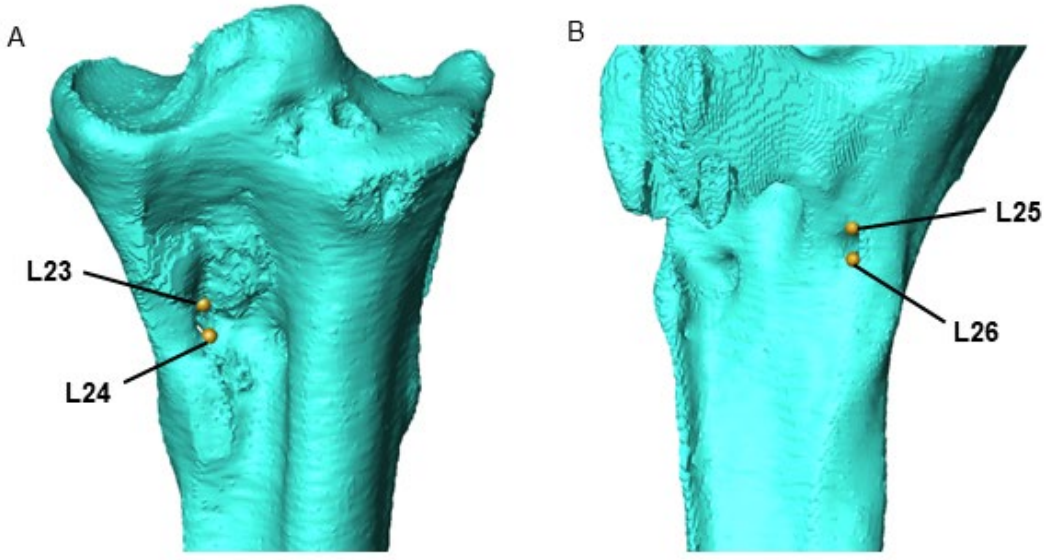


**Figure 22.** A) Proximal end of left tarsometatarsus (3D model) of *Corvus albus* (NHMUK 1866.8.6.13) in dorsal view showing point landmarks of the proximal vascular foramen (L23, L24) landmarked with orange points. B) Proximal end of left tarsometatarsus (3D model) of *Corvus albus* (NHMUK 1866.8.6.13) in plantar view showing point landmarks of the proximal vascular foramen (L25, L26) landmarked with orange points.

***L27, L28, L29.*** *Tuberositas m. tibialis cranialis*

The tuberositas m. tib. cranialis has three point-landmarks, one each marking the proximal (L27) and distal (L28) points of the protrusion and one marking the point of greatest dorsal projection (L29; Figure 23). The tuberositas is the insertion point for the M. tibialis cranialis (or tibialis anterior) which originates on the femur and runs down the tibiotarsus and across the intertarsal joint. This muscle helps to flex the ankle, and can generate considerable forces (Raikow, 1985).

For some taxa, such as swifts (Apodidae) and mousebirds (Coliidae), the protrusion of the tuberositas is not positioned in the dorsal infracotyle fossa, but rather along the medial side of the sulcus extensorius further distally on the shaft (Figure 24).

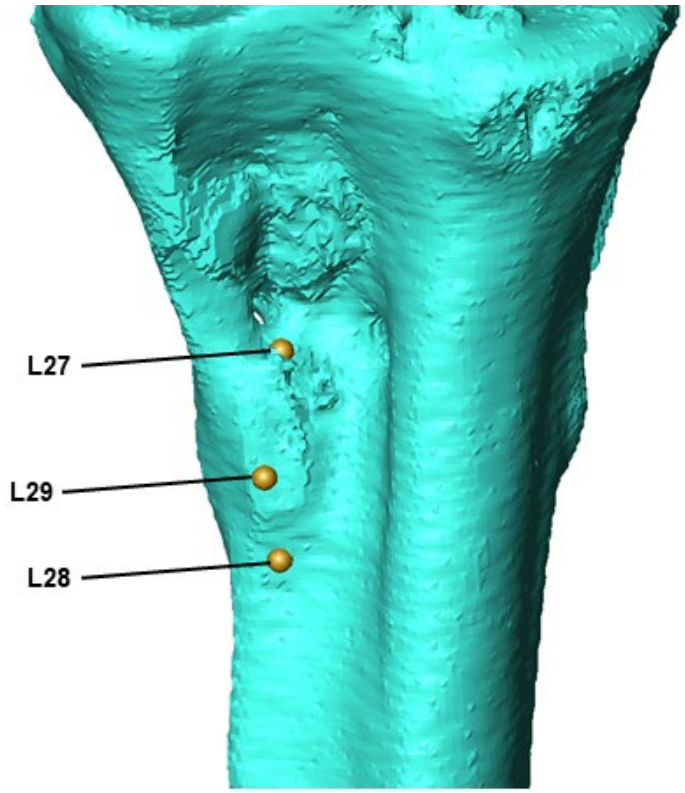


**Figure 23.** Proximal end of left tarsometatarsus (3D model) of *Corvus albus* (NHMUK 1866.8.6.13) in dorsal view showing point landmarks of the tuberositas m. tib. cranialis (L27, L28, L29) landmarked with orange points.

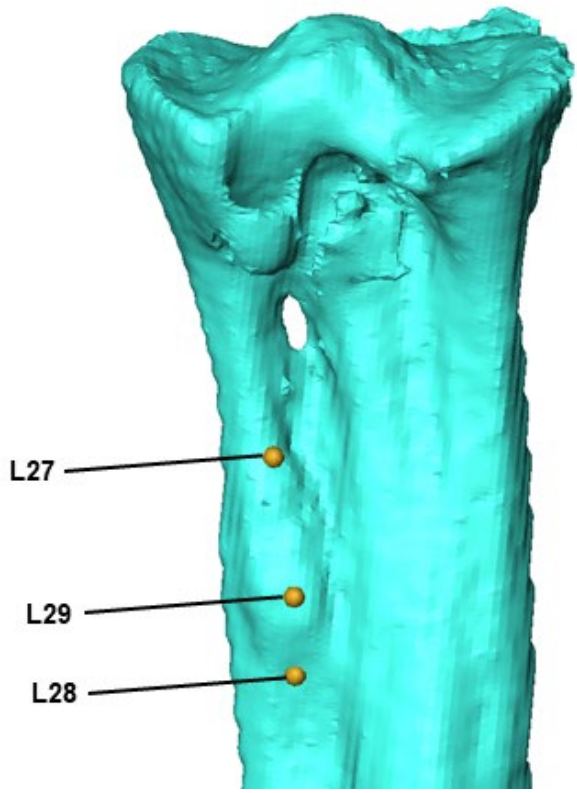


**Figure 24.** Proximal end of left tarsometatarsus (3D model) of *Urocolius macrourus* (FMNH 368959) in dorsal view showing point landmarks of the tuberositas m. tib. cranialis (L27, L28, L29) landmarked with orange points.

***L30, L31, S11.*** *Medial hypotarsal crest*

A semi-landmark series (SL11; Figure 25) marks the exterior ridge shape of the crest, starting at the junction of the medial edge of the crest and the medial cotyle (L30; Figure 25B), moving in a dorsal-to-plantar direction along the medial edge of the ridge, around the curve of the structure in a distal direction, and ending at the point when the crest has been fully assimilated into the plantar shaft surface (L31; Figure 25A). All three parts of the m. gastrocnemius combine to form a tendon of insertion that crosses the intertarsal joint and attaches to the plantar surface of the medial hypotarsal crest. The “externus” muscle part is suggested to extend the ankle/tarsometatarsus, and possibly absorb most of the shock of landing and stops tarsometatarsus flexion (Raikow, 1985). The “internus” muscle part resists flexion and maintains posture, contributing minimal force during tarsometatarsus extension (Raikow, 1985).

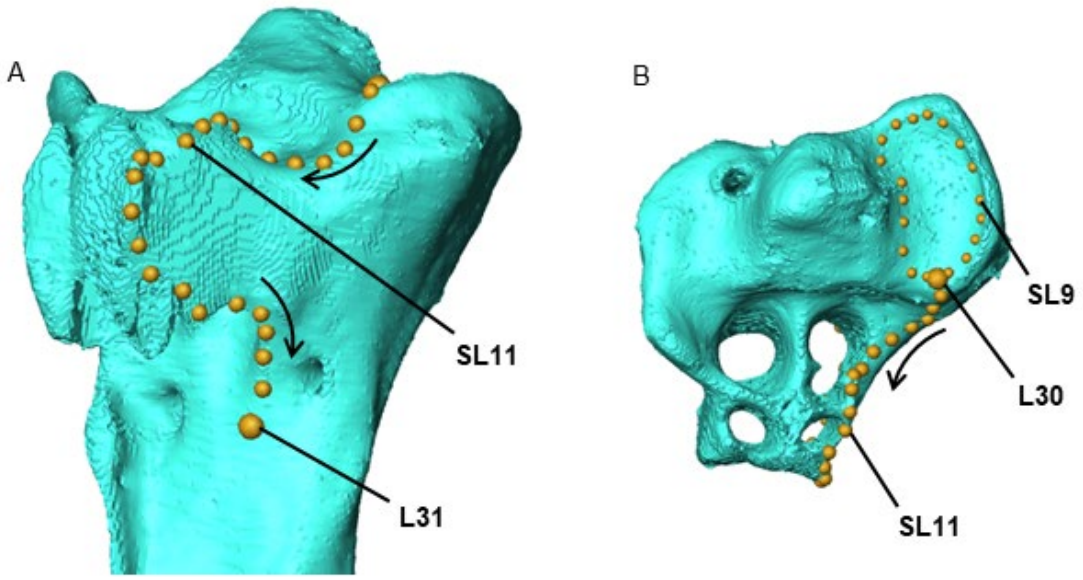


**Figure 25.** A) Proximal end of left tarsometatarsus (3D model) of *Corvus albus* (NHMUK 1866.8.6.13) in oblique plantar view showing point landmark and semi-landmark series of the medial hypotarsal crest (SL11, L31) landmarked with orange points. B) Proximal end of left tarsometatarsus (3D model) of *Corvus albus* (NHMUK 1866.8.6.13) in proximal view showing point landmark and semi-landmark series of the medial hypotarsal crest (SL11, L30) and the medial cotyle (SL9) landmarked with orange points.

***L32, L33, SL12.*** *Lateral hypotarsal crest*

The semi-landmark series for the lateral hypotarsal crest (S12; Figure 26) logically follows a similar route as the medial hypotarsal crest (S11), starting at the junction of the lateral edge of the lateral hypotarsal crest and the lateral cotyle (L32; Figure 26A), running in a dorsal-to-plantar direction along the lateral edge of the crest, then down along this edge, following any curves in a proximal-to-distal direction, finally ending at the point when the crest has been fully assimilated into the plantar shaft surface (L33; Figure 26B).

This lateral part of the hypotarsal structure is suggested to have less functional importance than the medial hypotarsal crest (Raikow, 1985), yet it does serve to guide the various muscles, tendons and ligaments of the leg through the intertarsal joint, down the plantar side (Raikow, 1985).

For cases in which the lateral hypotarsal crest is only a relatively small protrusion, such as in the Crested Caracara (*Caracara cheriway*), the American Kestrel (*Falco sparverius*), and, to a lesser extent, the Black-crowned Crane (*Balearica pavonina*i), it is still possible to follow along the lateral edge of the crest much like any other taxon (Figure 27).

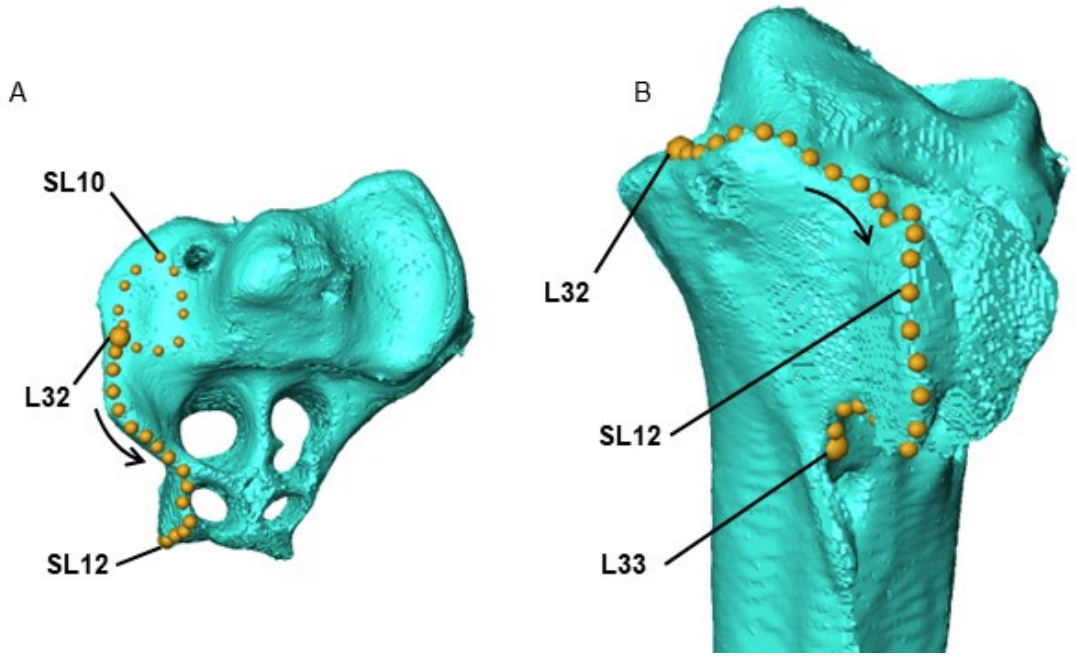


**Figure 26.** A) Proximal end of left tarsometatarsus (3D model) of *Corvus albus* (NHMUK 1866.8.6.13) in proximal view showing point landmark and semi-landmark series of the lateral hypotarsal crest (SL12, L32) and lateral cotyle (SL10) landmarked with orange points. B) Proximal end of left tarsometatarsus (3D model) of *Corvus albus* (NHMUK 1866.8.6.13) in oblique plantar view showing point landmarks and semi-landmark series of the lateral hypotarsal crest (SL12, L32, L33) landmarked with orange points.

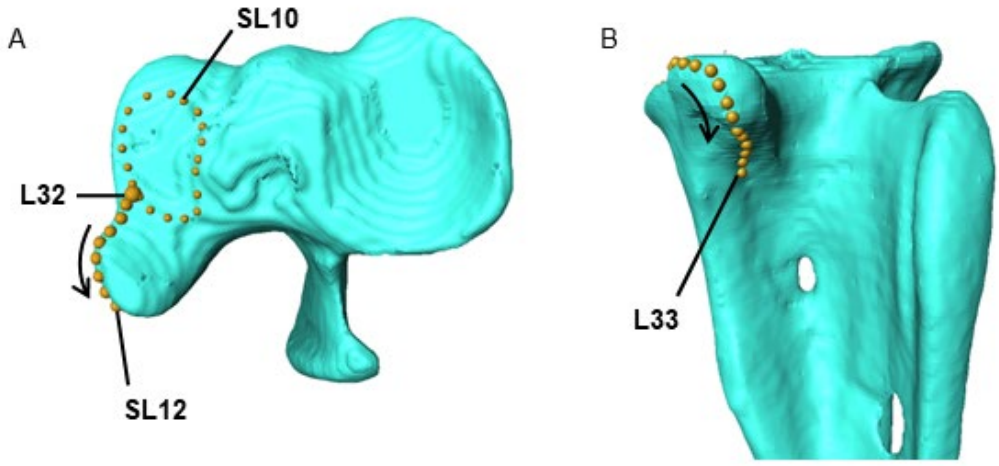


**Figure 27.** A) Proximal end of left tarsometatarsus (3D model) of *Falco sparverius* (UMMZ 154452) in proximal view showing point landmark and semi-landmark series of the lateral hypotarsal crest (SL12, L32) and lateral cotyle (SL10) landmarked with orange points. B) Proximal end of left tarsometatarsus (3D model) of *Falco sparverius* (UMMZ 154452) in oblique plantar view showing point landmark and semi-landmark series of the lateral hypotarsal crest (SL12, L33) landmarked with orange points.

***L34, L35, SL13.*** *Lateral extensorial ridge*

SL13 (Figure 28) marks the most prominent ridge on the dorsal side of the tarsometatarsus, from the dorso-lateral point of the lateral cotyle edge (L34; Figure 28B), running towards the distal point above where the lateral edge of trochlear metatarsi IV starts (L35; Figure 28C). It has been colloquially named the 'lateral extensorial ridge' in this work for clarification of its purpose; it is a sufficiently consistent anatomical feature throughout the avian phylogeny, and neighbours the sulcus extensorius, which is not landmarked. This facies provides a convenient surface in order to track the shape of the tarsometatarsal shaft.

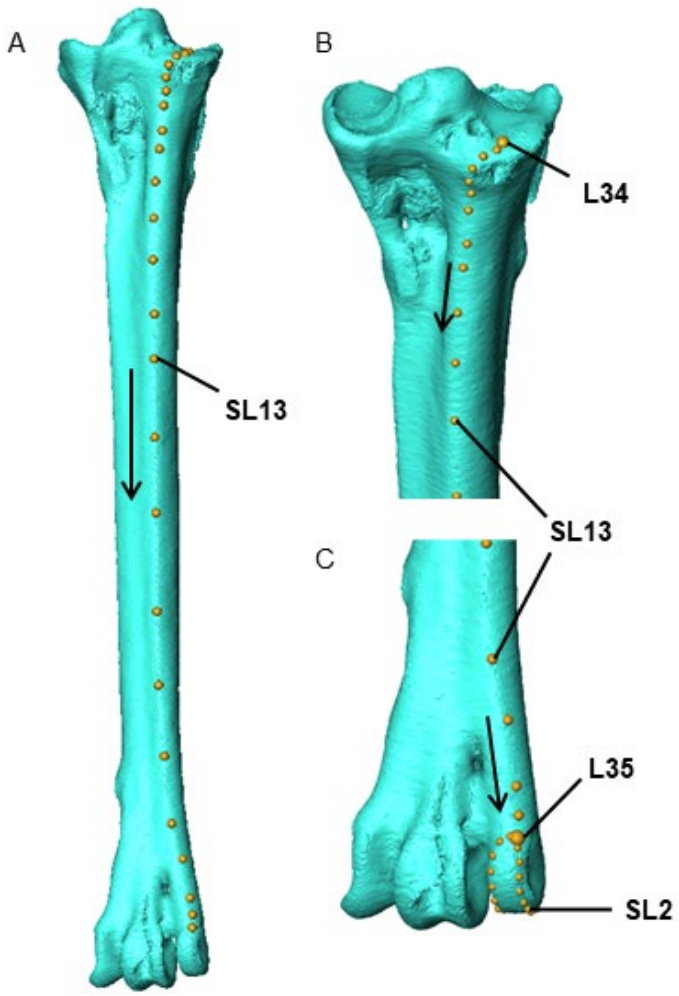


**Figure 28.** A) Entire left tarsometatarsus (3D model) of *Corvus albus* (NHMUK 1866.8.6.13) in dorsal view showing semi-landmark series of the lateral extensorial ridge (SL13) landmarked with orange points. B) Proximal end of left tarsometatarsus (3D model) of *Corvus albus* (NHMUK 1866.8.6.13) in oblique dorsal view showing point landmark and semi-landmark series of the lateral extensorial ridge (SL13, L34) landmarked with orange points. C) Distal end of left tarsometatarsus (3D model) of *Corvus albus* (NHMUK 1866.8.6.13) in dorsal view showing point landmark and semi-landmark series of the lateral extensorial ridge (SL13, L35) and metatarsal IV trochlea (SL2) landmarked with orange points.

***SL14.*** *Circum-proximal series*

Starting at the junction of medial hypotarsal crest and medial cotyle ridge, SL14 (Figure 29) runs outside the medial edge of the hypotarsus (including the entire proximal articular surface) in a dorsal direction, then along the dorsal edge in a medial-to-lateral direction, then along the lateral edge in a dorsal-to-plantar direction, then bypassing the lateral and medial

hypotarsal crests the series runs along the plantar edge of the hypotarsus in a lateral-to-medial direction, ending just lateral to starting point.

***L36, L37, SL15.*** *Intercotylar eminentia*

The intercotylar eminentia is marked with a semi-landmark series (SL15; Figure 29B) which starts at the centre point of the circum-proximal series on the dorsal edge (L36; Figure 29C), runs along the path of most proximal points along the eminentia and the intercotylar area, ending at a central circum-proximal semi-landmark on the plantar side (L37; Figure 29D). The intercotylar eminentia is the attachment area for medial and lateral menisci, and is a prominent component of the intertarsal joint (Cracraft, 1971).

For cases in which the eminentia is poorly defined, as in the Ruby-throated Hummingbird (*Archilochus colubris*), then the semi-landmark series takes the most direct path from dorsal to plantar sides of the hypotarsal surface (Figure 30).

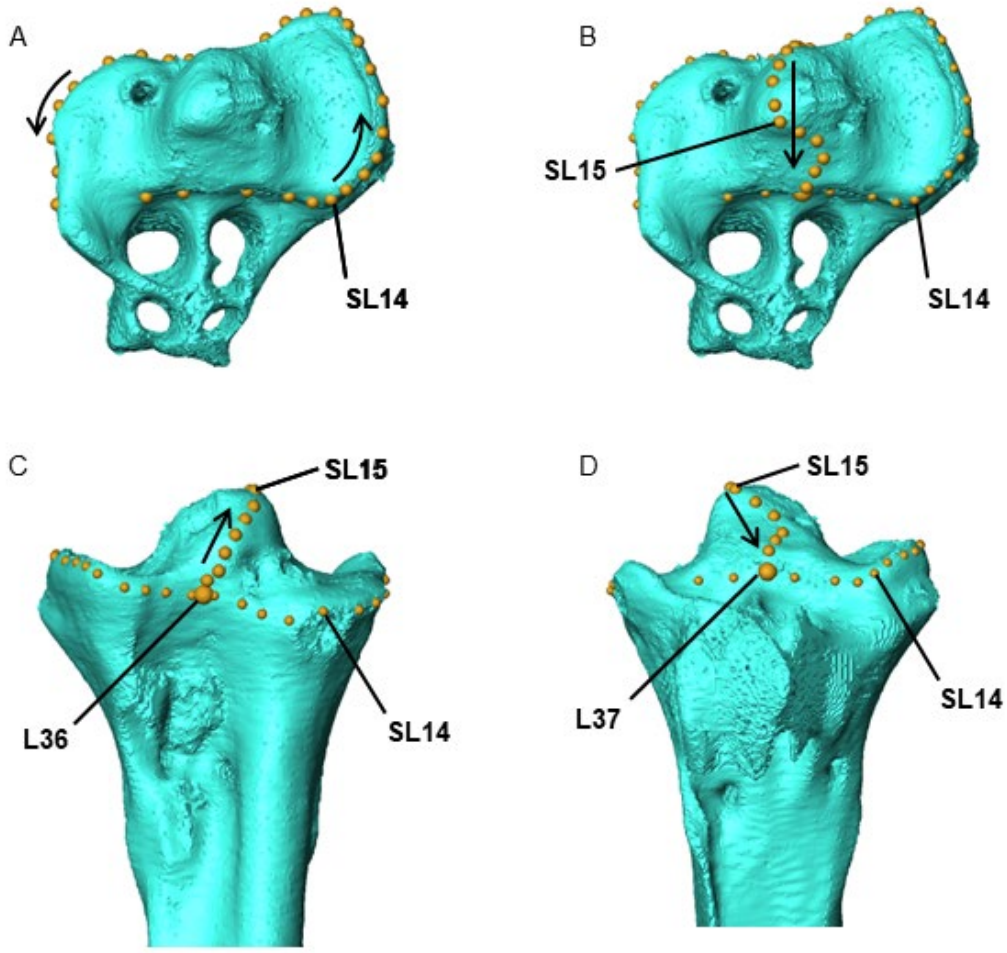


**Figure 29.** A) Proximal end of left tarsometatarsus (3D model) of *Corvus albus* (NHMUK 1866.8.6.13) in proximal view showing semi-landmark series of the circum-proximal series (SL14) landmarked with orange points. B) Proximal end of left tarsometatarsus (3D model) of *Corvus albus* (NHMUK 1866.8.6.13) in proximal view showing semi-landmark series of the circum-proximal series (SL14) and intercotylar eminentia (SL15) landmarked with orange points. C) Proximal end of left tarsometatarsus (3D model) of *Corvus albus* (NHMUK 1866.8.6.13) in dorsal view showing point landmark and semi-landmark series of the circum-proximal series (SL14) and intercotylar eminentia (SL15, L36) landmarked with orange points. D) Proximal end of left tarsometatarsus (3D model) of *Corvus albus* (NHMUK 1866.8.6.13) in plantar view showing point landmark and semi-landamark series of the circum-proximal series (SL14) and intercotylar eminentia (SL15, L36) landmarked with orange points.

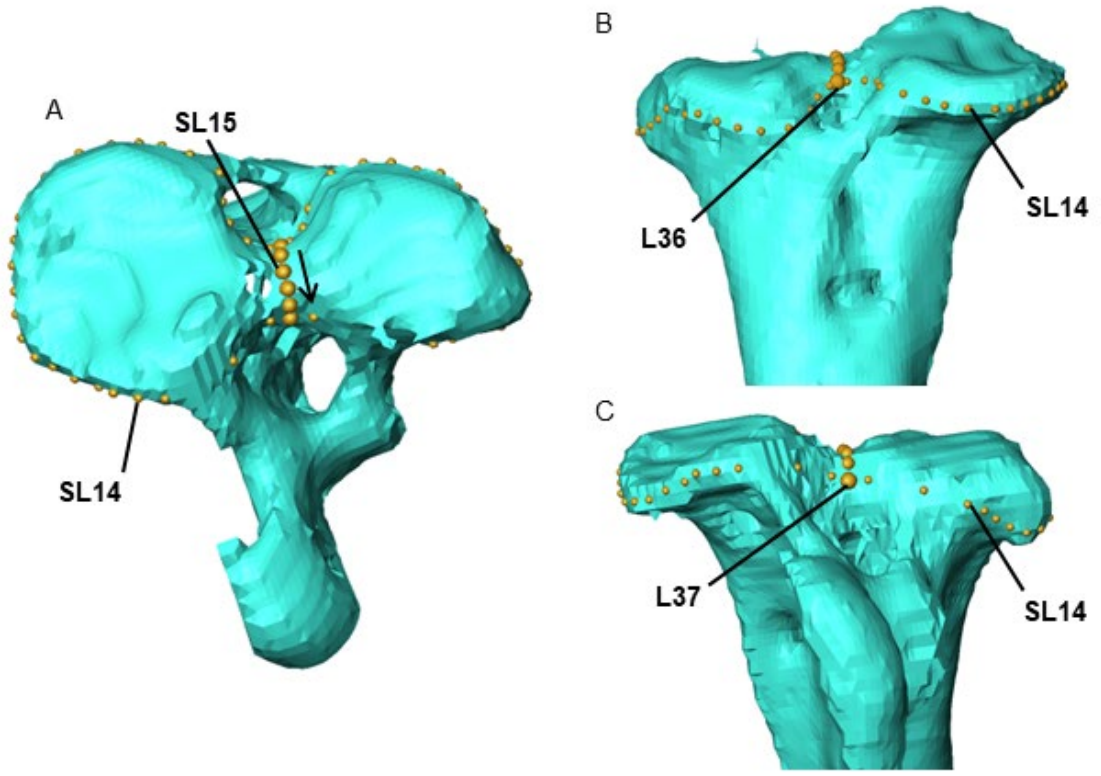


**Figure 30.** A) Proximal end of right tarsometatarsus (3D model) of *Archilochus colubris* (FMNH 484738) in proximal view showing semi-landmark series of the circum-proximal series (SL14) and intercotylar eminentia (SL15) landmarked with orange points. B) Proximal end of right tarsometatarsus (3D model) of *Archilochus colubris* (FMNH 484738) in dorsal view showing point landmark and semi-landmark series of the circum-proximal series (SL14) and intercotylar eminentia (SL15, L36) landmarked with orange points. C) Proximal end of right tarsometatarsus (3D model) of *Archilochus colubris* (FMNH 484738) in plantar view showing point landmark and semi-landmark series of the circum-proximal series (SL14) and intercotylar eminentia (SL15, L37) landmarked with orange points.

### 1.2.5 Generalized Procrustes Analysis, and Principal Components Analysis

Generalized Procrustes Analysis (GPA) is a normalization process in which shape data undergoes translation, rotation and scaling to make the shape data statistically comparable. I used sliding semi-landmarks, which allow points to slide along their tangent vectors in order to minimise bending energy differences from the mean shape. I performed GPA using a set of R functions provided by R. Benson, which use functions from the packages geomorph (Adams et al., 2021) and stringdist (van der Loo, 2020). GPA results in a set of Procrustes coordinates (shape data) which are used as the dependent variable in all subsequent analyses, and a set of

centroid sizes, which are used as the explanatory variable in some analyses. Shape data variation was visualized along the primary axes of variation in a Principal Components analysis of the Procrustes coordinates, using geomorph's gm.prcomp function (Collyer and Adams, 2021).

### 1.2.6 Phylogenetic Framework

Phylogenetic data was obtained from birdtree.org (Jetz et al., 2012), using the supertree based on the Hackett et al. (2008) backbone.

### 1.2.7 Phylogenetic Regression and Visualization: Shape Analysis

The shape data was used as a dependent variable in linear models with the foot use characters as explanatory variables to evaluate the significance of their independent effects using phylogenetic regression for Procrustes shape variables (Adams, 2014; procD.pgls; geomorph package; Adams, 2021), and a Randomized Residuals Permutation Procedure (RRPP; Collyer and Adams, 2020). This method was chosen because it is appropriate for large, multivariate data relative to sample size; it exhibits increasing statistical power with increasing counts of points in the landmark data, compared to older methods that showed decreasing power with increasing counts of points (Adams, 2014). I also used a marginal sum of squares for each model, which evaluates the effects of each individual variable as if the effects of all other variables in the model have been accounted for.

Model selection parameters such as Akaike Information Criterion (AIC) or corrected Akaike Information Criterion (AICc) are not currently available for procD.pgls. Therefore, model selection was performed manually, in which an initial 'lenient' stage tested individual foot use variables for their independent effects on tarsometatarsus shape. Variables were discarded only if the p-value was greater than 0.1. Subsequent combinations of remaining foot use

variables were submitted to the same process, and explanatory variables were discarded in models in which their independent effects became obsolete ($p > 0.05$) in the presence of other foot uses or factors (e.g. proportional elongation and allometry). No mathematical correction was made for multiple comparisons; only the preliminary model selection stage evaluated the significance of each of the 21 foot use variables with centroid size and body mass taken into account, and from then onwards model selection grouped similar foot use variables together with the intention of discarding variables that became redundant in the presence of others.

The model with the highest overall adjusted-$R^2$ value for which all explanatory variables remained significant was selected as the 'best' model. If in future AIC and AICc become available for procD.pgls, the 'best' model may change, as a model selection method that controls for the effects of additional parameters (i.e. penalizes increases in number of parameters) may result in a final model with fewer foot use variables.

Each variable in the model produces a vector of coefficients that describe the independent effect of that variable on the 3D coordinates of each landmark and semi-landmark point, as deviations from the mean (baseline) shape. I visualised an 'idealised' shape deformation representing the independent effect of the selected explanatory foot use character by introducing combinations of general coefficients to the model which represent the absence or presence of each foot use. These general coefficients (zeros or ones) select which of the variables' vector of coefficients to compute to transform the mean shape, the results of which are plotted three-dimensionally to observe the shape deformations.

### 1.2.8 Phylogenetic Regression: Size Analysis

I also performed a set of phylogenetic regressions to explain variation in centroid size of the tarsometatarsus (used as a dependent variable). To do this, I used phylogenetic generalised

least squares regression (pGLS; Grafen, 1989), implemented via the gls function from the package nmle (version 3.1-153; Pinheiro et al., 2020), using correlation structures from the package ape (version 5.6-1; Paradis and Schliep, 2019) and the AICc function from the package qpcr (version 1.4-1; Spiess, 2018) to calculate AICc values for each regression. I used models of the form 'centroid size ~ species mean body mass + foot use trait 1 + …' to test the hypothesis that the relative size of the tarsometatarsus, in relation to mean body mass, is independently affected by my foot use traits.

Centroid size as a function of mean body mass and a combination of ecological variables was investigated, using Pagel's λ to infer phylogenetic signal (Pagel, 1999), and AICc to select the best model. Models with lower AICc scores, AIC weight values nearest to 1, and significant ecological trait variables best fit the relationship between relative centroid size and ecological traits. There is also a difference in AICc score between ordinary least squares regression models and the models taking phylogenetic relationships into account, which implies that there is a non-zero amount of phylogenetic signal for the ecological traits tested here.

Size model selection was based on AICc score, pairing each of the 19 ecological foot use traits with mean body mass, to determine which foot uses had significant or marginally non-significant independent effects on the variation in relative centroid size once the independent effect of mean body mass was taken into account. Logical pairings of these traits were then combined in models with mean body mass to test for redundancies between variables.

## 1.3 Results

### 1.3.1 Principal Components Analysis

The Procrustes-transformed landmark constellations represent a size-free measure of tarsometatarsus shape and were reoriented using Principal Components analysis to illustrate the primary axes of variation in tarsometatarsus shape.

The principal components analysis provides an ordination of my 3D shape data, and describes the distribution of 179 extant species with reference to major aspects of tarsometatarsus shape variation. Principal component 1 (PC1) represents approximately 51.6% of the shape variation in the tarsometatarsus. PC2 and PC3 represent 18.0% and 6.7% of the variation respectively.

PC1 describes variation in relative robusticity, or the mediolateral and dorsoventral width proportional to length. The negative values of PC1 (Figure 31) correspond to tarsometatarsi with proportionally narrow features, such as those of primarily cursorial or other birds with proportionally elongate tarsometatarsi (e.g. seriemas, secretarybirds, egrets). The tarsometatarsus representing the minimum values of PC1 possesses short and closely spaced metatarsal trochleae, a narrow and prominent eminentia intercotylaris, and a lateral extensorial ridge which runs down the midline of the shaft before curving back to the lateral side on the distal end. Positive values of PC1 (Figure 32) correspond to tarsometatarsi with proportionally wide features, such as those of parrots, penguins, and kingfishers. The tarsometatarsus representing the maximum values of PC1 possesses widely splayed metatarsal trochleae, a distally placed tuberositas tibialis cranialis, and a shallow eminentia intercotylaris.

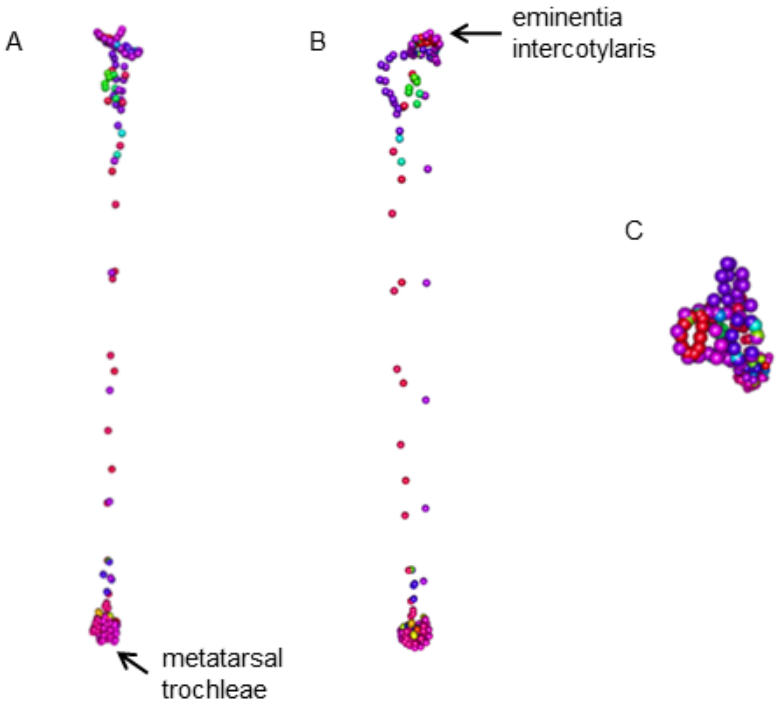


**Figure 31.** Visualisation of the tarsometatarsus representing the minimum values of Principal Component 1, shown in A) dorsal view; B) medial view; C) proximal view.

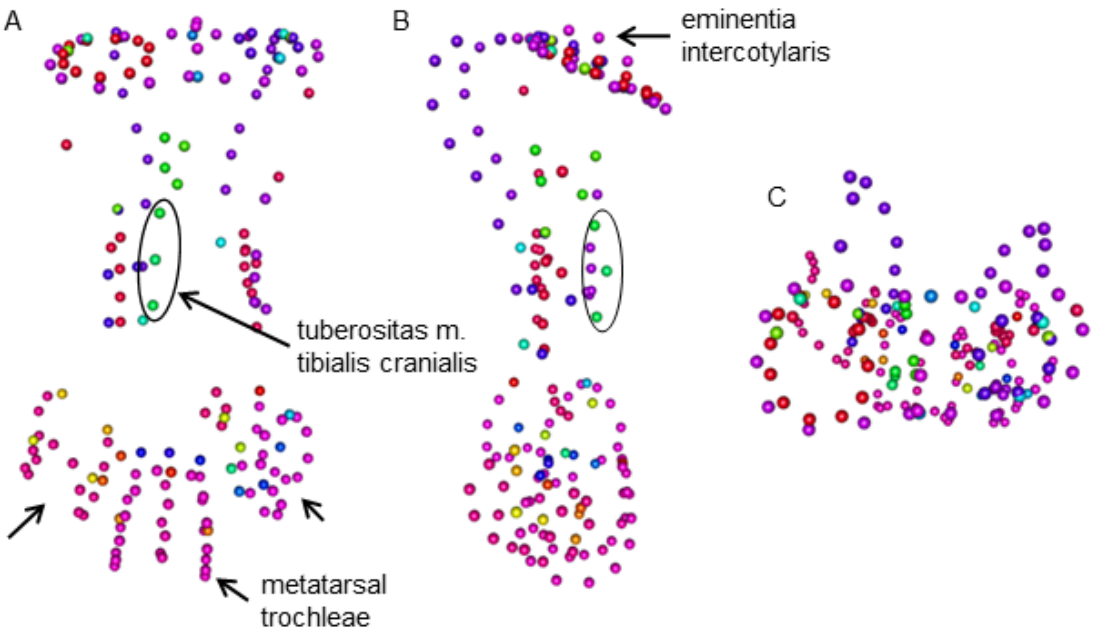


**Figure 32.** Visualisation of the tarsometatarsus representing the maximum values of Principal Component 1, shown in A) dorsal view; B) medial view; C) proximal view.

PC2 describes variation in the hypotarsal crest shape, and the relative widths of intertrochlear incisura and the metatarsal trochleae. The negative values of PC2 (Figure 33) correspond to tarsometatarsi with proximodistally short hypotarsal crests, a mediolaterally wide hypotarsal sulcus, and more mediolaterally splayed metatarsal trochleae. The positive values of PC2 (Figure 34) correspond to tarsometatarsi with proximodistally long hypotarsal crests, a mediolaterally narrow or non-existent hypotarsal sulcus, and less mediolaterally splayed metatarsal trochleae.

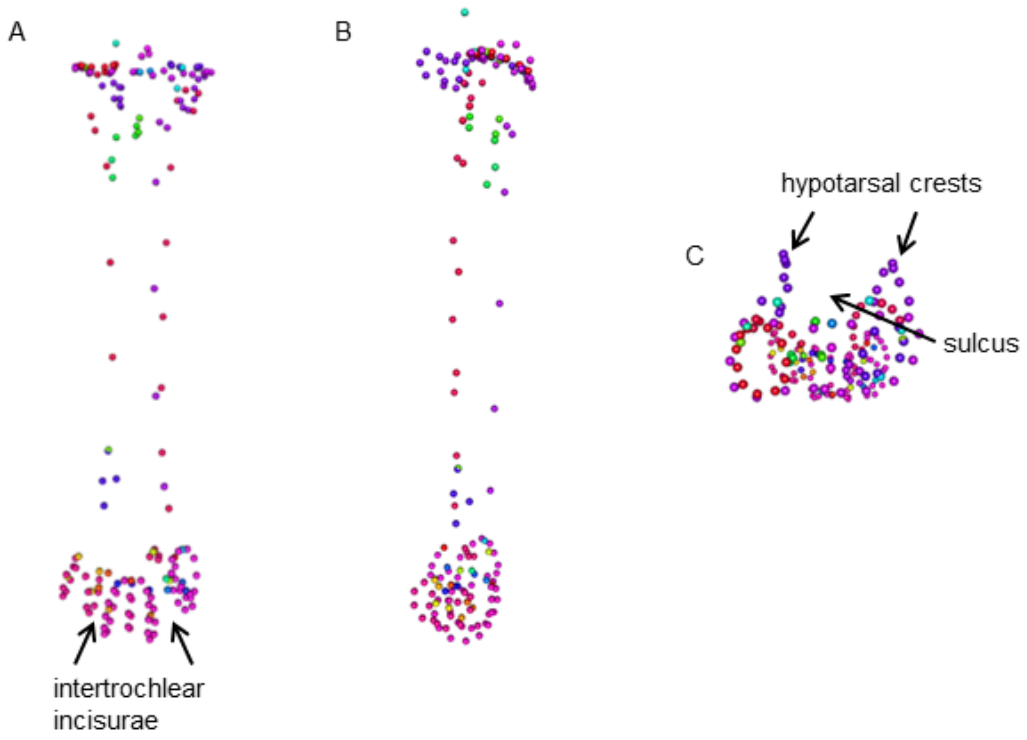


**Figure 33.** Visualisation of the tarsometatarsus representing the minimum values of Principal Component 2, shown in A) dorsal view; B) medial view; C) proximal view.

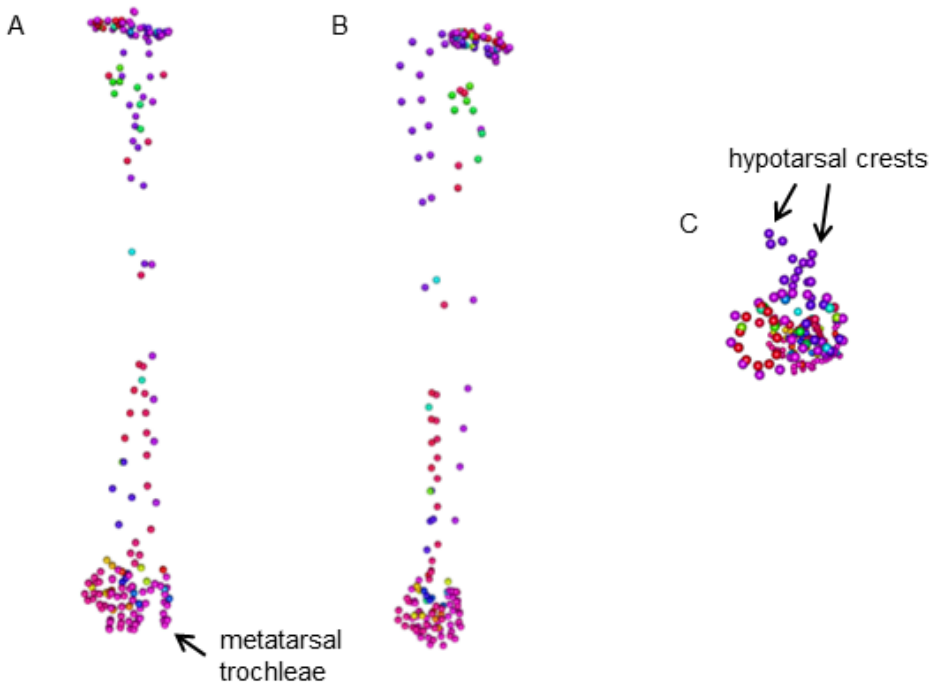


**Figure 34.** Visualisation of the tarsometatarsus representing the maximum values of Principal Component 2, shown in A) dorsal view; B) medial view; C) proximal view.

PC3 primarily describes variation in the metatarsal trochleae, the placement of the metatarsal 1 fossa, and the dorsoventral width of the shaft. The negative values of PC3 (Figure 35) correspond to tarsometatarsi with a proximodistally lifted and rotated plantarward metatarsal trochlea 4, a further distally positioned metatarsal 1 fossa, and a dorsoventrally narrower shaft. The positive values of PC3 (Figure 36) correspond to tarsometatarsi with a proximodistally lifted metatarsal trochlea 2, a further proximally positioned metatarsal 1 fossa, and a dorsoventrally wider shaft. There is also a variation in hypotarsal arrangement described by PC3, in that negative PC3 values correspond to proximodistally shorter and mediolaterally wider hypotarsi, whereas positive PC3 values correspond to the opposite.

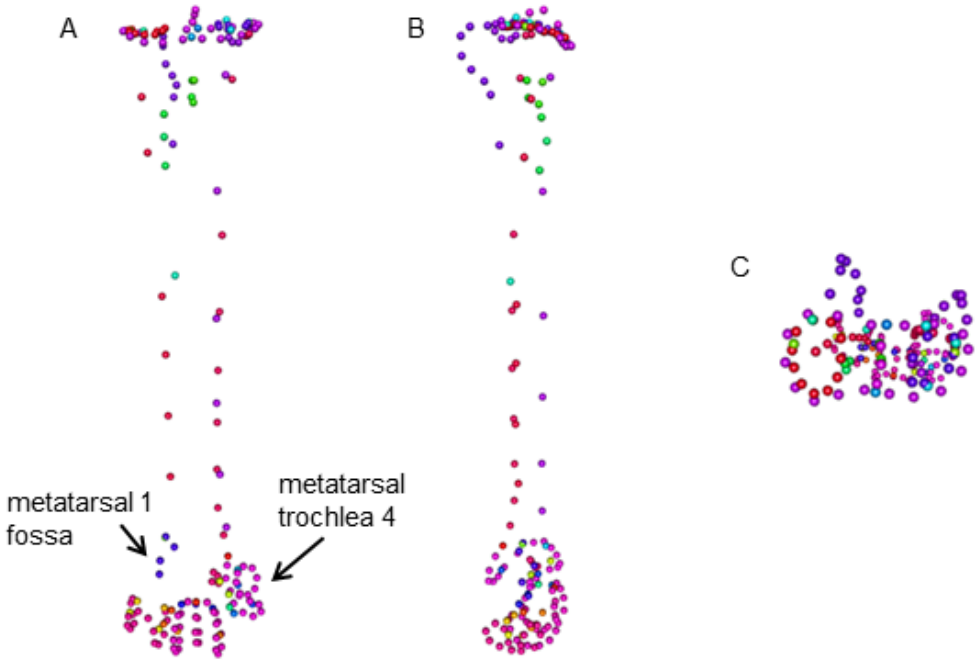


**Figure 35.** Visualisation of the tarsometatarsus representing the minimum values of Principal Component 3, shown in A) dorsal view; B) medial view; C) proximal view.

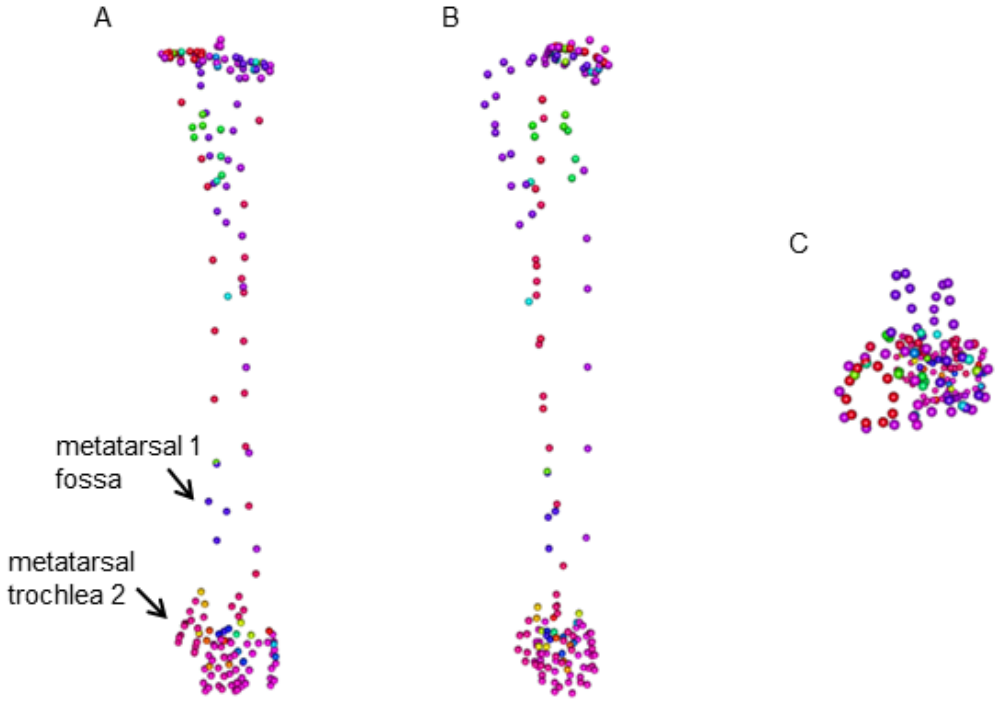


**Figure 36.** Visualisation of the tarsometatarsus representing the maximum values of Principal Component 3, shown in A) dorsal view; B) medial view; C) proximal view.

### 1.3.2 Phylogenetic Regression: Size Analysis

The model with lowest AICc for tarsometatarsus centroid size included the dependent variables mean body mass, terrestrial/arboreal ecology, and webbed feet (AICc = –76.6; $\lambda$ = 1.01) (Appendix Table B.1). This 'best' model has an AICc weight of 0.84, whereas the next highest model AICc weight was 0.055. Body mass, terrestrial/arboreal ecology and webbed feet all had significant p-values in the 'best' model. The coefficients for terrestrial/arboreal ecology and webbed feet in this model are both small and negative; birds with arboreal ecology have slightly shorter relative tarsometatarsus centroid size (coefficient = -0.08), and among terrestrial birds, those with webbed feet have much shorter relative centroid size (coefficient = -0.11).

Of the models with higher AICc scores and lower AICc weights, variation in relative centroid size as explained by mean body mass and webbed feet was the best fit (model 2; AICc= –71.2), followed closely by mean body mass and terrestrial/arboreal ecology (model 3; AICc= –70.7). Both terrestrial/arboreal ecology and webbed feet variables were always found to be significant both on their own and in models combined with other variables. Cursoriality, anisodactyly and zygodactyly were significant until included in models with mean body mass and terrestrial/arboreal ecology, at which point they became redundant. Swimming ecology also became redundant once included in a model with mean body mass and webbed feet.

### 1.3.3 Phylogenetic Regression: Shape Analysis Using Size-Related Traits

Centroid size of the tarsometatarsus has a significant but weak relationship with tarsometatarsus shape on its own ($R^2$ = 0.079; p = 0.001; Appendix Table B.2). In contrast, mean body mass on its own has no relationship with tarsometatarsus shape ($R^2$ = 0.007; p = 0.239; Appendix Table B.2). However, when both are included together as explanatory variables to explain tarsometatarsus shape, their relationship strengthens considerably (centroid size: $R^2$ =

0.23; p = 0.001; body mass: $R^2 = 0.16$; p = 0.001; Appendix Table B.2). This indicates that proportional centroid size of the tarsometatarsus, after accounting for body mass, has a strong and significant independent effect on tarsometatarsus shape, which is described below.

Because I documented relationships of relative centroid size with terrestrial/arboreal habits (Character 2) and webbed feet (Character 20), I also tested the following models:

(1) $$tarsometatarsus\ shape \sim centroid\ size\ +\ mean\ body\ mass\ +\ terrestrial/arboreal\ +\ webbed\ feet$$

(2) $$tarsometatarsus\ shape \sim mean\ body\ mass\ +\ terrestrial/arboreal\ +\ webbed\ feet.$$

The first model had an overall adjusted-$R^2$ of 0.23, and although centroid size remained significant, its explanatory strength within the model was weaker ($R^2 = 0.18$) than it was in a model that did not include the foot use traits ($R^2 = 0.23$; Appendix Table B.2). Therefore, a small portion of the size-related shape variation is explained by relative-size-related foot-use traits.

The second model had an overall adjusted-$R^2$ of 0.05, and the foot-use traits become significant (terrestrial/arboreal p = 0.001; webbed feet p = 0.002), where they were not in the first model (terrestrial/arboreal p = 0.059; webbed feet p = 0.149). The explanatory power of tarsometatarsus shape weakens considerably when centroid size is removed from the model. This suggests that tarsometatarsus centroid size is important and the ecological traits are not.

### 1.3.4 Phylogenetic Regression: Shape Analysis of All Traits

Regression model comparisons carried out as described in the Methods suggest that the most important variables for explaining variation in tarsometatarsus shape are centroid size, mean body mass, flightlessness, zygodactyl digit arrangement, force grip foot use, raptoriality, and digital manipulation foot use (Appendix Table B.2). This was selected as the ‘best’ model

because it had the highest overall adjusted-$R^2$ value for which all explanatory variables remained significant.

There is some correlation between the ecological trait variables, as found using cor() (stats package; version 4.1.2) and rcorr() (Hmisc package; version 4.7-1) with Pearson parametric correlation testing, which measures the linear dependence between two variables. The majority of my variables became redundant when paired in phylogenetic regression models with the variables they were found to be most significantly correlated with, negating any effects of autocorrelation in downstream analyses. Force grip and raptoriality have a significant correlation ($r = 0.78$, $p = 0.00$), but their independent effects on shape variation as found with the phylogenetic regression are still valid, as I used marginal sum of squares in my phylogenetic regression models. This evaluates the effects of each variable as if all other variable effects have been accounted for.

As discussed in the centroid size regression model fitting results, centroid size has a significant but weak relationship with tarsometatarsus shape on its own (Appendix Table B.2; model 43: adj-$R^2$=0.074, p=0.001), whereas mean body mass has no relationship to tarsometatarsus shape on its own (Appendix Table B.2; model 54: adj-$R^2$=0.002, p=0.239). Once paired in a model together, both relative centroid size and mean body mass have significant and strong independent effects on tarsometatarsus shape (Appendix Table B.2; model 39: adj-$R^2$=0.229).

Models 40-42 (Appendix Table B.2), which include documented walking ability, hopping gait, and raptoriality, were all non-significant upon the inclusion of relative centroid size and mean body mass to the model. These three models also had a lower adjusted-$R^2$ than the initial model “shape ~ centroid size + mean body mass”. This suggests that walking ability and hopping

gait have no influence on tarsometatarsus shape. Despite its non-significant results in these test models, the raptorial foot use trait was experimented with as an addition in later models, particularly paired with force grip foot use, because of their ecological similarity.

Models 28-35 (Appendix Table B.2), which include heterodactyly, webbed feet, swimming ecology, solely foot-propelled submerged swimming, cursoriality, scansoriality, nesting substrate, perching ability, and hanging or clinging foot use were non-significant once the independent effects of relative centroid size and mean body mass were accounted for in their individual test models. This suggests that these foot uses have redundant influence on tarsometatarsus shape, that is accounted for by centroid size and mean body mass. The resulting non-significant p-values of the ecological foot use trait variables ranged from 0.2 to 0.35, and the adjusted-$R^2$ of the test models were all approximately around 0.23.

Models 15, 21-23 and 25-28 (Appendix Table B.2), which include digital manipulation, flightlessness, anisodactyly, zygodactyly, terrestrial/arboreal ecology, foot-propelled surface swimming, hold-down and force grip foot use either remained significant once the independent effects of relative centroid size and mean body mass were accounted for, or had a sufficiently low p-value to be considered only marginally non-significant and retained for the next round of model comparisons. This suggests that these foot uses have some independent influence on tarsometatarsus shape. Models 15 and 21-23 (Appendix Table B.2), which include flightlessness, zygodactyly, anisodactyly, and digital manipulation had the highest adjusted-$R^2$ of the individual test models, and had entirely significant ecology and foot use trait variables.

The second set of test models (Appendix Table B.2; models 8-14, 16-20 and 24), which combined pairs of foot use traits with a constant inclusion of centroid size and mean body mass, confirmed redundancies and introduced surprising additions. Once experimentally paired

together with relative centroid size and mean body mass, the independent effects of force grip foot use and of raptorial ecology became significant in model 20 (Appendix Table B.2). The $R^2$ of both raptoriality and force grip foot use also increased greatly from their individual test models (Appendix Table B.2; models 25 and 42) once paired together. This suggests that the independent effects of raptoriality and force grip foot use are additive when combined, and have a significant influence on tarsometatarsus shape.

Although the p-value of terrestrial/arboreal ecology in model 26 (Appendix Table B.2) was sufficiently close to 0.05 to retain for the second set of test models (p=0.077), none of the subsequent model pairs with flightlessness, anisodactyly, and digital manipulation (Appendix Table B.2; models 8, 16, 17) resulted in an $R^2$ greater than 0.008, or a significant p-value. This seems to confirm that the independent effect of terrestrial/arboreal ecology is redundant with variation due to relative centroid size of the tarsometatarsus, regardless of additional foot use trait variables.

Foot-propelled surface swimming likewise remained non-significant in each of its paired test models with flightlessness and anisodactyly (Appendix Table B.2; models 10, 18), and its $R^2$ remained at approximately 0.007. It is unclear why this occurs, as it doesn't have a significant relationship with centroid size, was greatly non-signficant on its own (Appendix Table B.2; model 55: adj-$R^2$=0.001), and only nominally non-significant once the independent effects of relative centroid size and mean body mass were accounted for.

Anisodactyl and zygodactyl digit arrangement were paired together (Appendix Table B.2; model 19) to confirm that they overlap in information and render each other redundant when combined in a test model. It seems overall that zygodactyl digit arrangement has a stronger $R^2$ than anisodactyl digit arrangement, in their paired model as well as pairs with other variables.

Interestingly, when zygodactyly was paired with digital manipulation foot use (Appendix Table B.2; model 9), both variables were significant with relatively strong $R^2$, but when anisodactyly was paired with digital manipulation (Appendix Table B.2; model 12), digital manipulation became non-significant ($p = 0.052$). This suggests that the independent effect of digital manipulation on tarsometatarsus shape can be better explained in a model by the independent effect of anisodactyl digit orientation.

The independent effect of digital manipulation also became redundant with the variation due to flightlessness accounted for (Appendix Table B.2; model 11). As mentioned above, the addition of raptorial ecology to a model with force grip appears to improve the strength of the model further than merely adding another variable. The individual $R^2$ of both force grip (0.016) and digital manipulation (0.015) in model 7 increase from their values in model 14 (force grip $R^2 = 0.010$; digital manipulation $R^2 = 0.014$), where raptorial ecology was not included. The total adjusted-$R^2$ of model 7 (0.249) is also slightly stronger than that of model 14 (0.242). This further suggests that the additive effect of combining raptorial and force grip foot uses have greater influence on tarsometatarsus shape than when left separate.

When flightlessness is paired with the combination of raptorial ecology and force grip foot use (Appendix Table B.2; model 4), the resulting model is stronger (adj-$R^2 = 0.253$) than when digital manipulation foot use was paired with the same combination (Appendix Table B.2; model 7; adj-$R^2 = 0.249$). This suggests that the flightlessness is a stronger explanatory variable than digital manipulation.

An interesting phenomenon occurred in which the separate additions of either flightlessness (Appendix Table B.2; model 11) or anisodactyl digit arrangement (Appendix Table B.2; model 12) renders the independent effect of digital manipulation redundant. When

flightlessness is paired with anisodactyly, however (Appendix Table B.2; model 6), all variables in the model are significant (p = 0.001–0.026), and their individual $R^2$ values are stronger than those from the models paired with digital manipulation. Regardless, zygodactyl digit arrangement (Appendix Table B.2; model 5) makes for a slightly stronger model with flightlessness than anisodactyly does (Appendix Table B.2; $R^2$=0.252).

A large model was tested which included all seven previously determined important variables (Appendix Table B.2; model 1), which resulted in the best fitting model in terms of overall adjusted-$R^2$ (0.268). This is likely due to the pseudo-strengthening that occurs from an increased number of explanatory variables in a regression model. With the inclusion of both digital manipulation and flightlessness in the model, digital manipulation is non-significant (p = 0.510), as seen in the previous test model with that pair of variables (model 11; digital manipulation p = 0.106).

The impact of removing either digital manipulation or flightlessness from this large model were compared, resulting in models 2 and 3 (Appendix Table B.2). Model 2 describes tarsometatarsus shape as a function of relative centroid size, mean body mass, flightlessness, raptorial ecology, force grip foot use, and zygodactyl digit orientation, but excluding digital manipulation. The overall adjusted-$R^2$ of model 2 (0.262) is slightly lower than that of model 1 (adj-$R^2$ = 0.268), although this could just be due to the removal of an explanatory variable. All of the explanatory variables in model 2 are significant, and the $R^2$ of relative centroid size (0.194) and mean body mass (0.117) stay approximately the same as in model 1. The $R^2$ of flightlessness increases marginally in model 2 (model 1 $R^2$ = 0.015; model 2 $R^2$ = 0.019), and its p-value lowers as well (model 1 p = 0.015; model 2 p = 0.002). The $R^2$ of raptorial ecology and force grip foot use decrease in model 2 (raptoriality $R^2$ = 0.011; force grip foot use $R^2$ = 0.014), and their p-

values increase (model 2 raptoriality p = 0.027; force grip foot use p = 0.023). The $R^2$ (0.012) and p-value (model 1 p = 0.021; model 2 p = 0.023) of zygodactyly remain approximately the same.

Model 3 (Appendix Table B.2) describes tarsometatarsus shape as a function of the same foot use variables as model 2, except flightlessness is replaced with digital manipulation. The overall adjusted-$R^2$ of model 3 (0.257) is lower than that of model 2 (0.262), which has the same number of explanatory variables. All of the variables are significant, yet the $R^2$ of relative centroid size increases from 0.19 to 0.21, and the $R^2$ of mean body mass increases from 0.11 to 0.14 in this model compared to models 1 and 2. Unsurprisingly, the $R^2$ of digital manipulation ($R^2$ = 0.015; p = 0.033) is slightly stronger in this model than in model 1 ($R^2$ = 0.010; p = 0.510), now that it is no longer redundant from the independent effect of variation due to flightlessness. The $R^2$ values of raptorial foot use and force grip foot use are only marginally better in model 3 (raptoriality $R^2$ = 0.011; force grip foot use $R^2$ = 0.015) than in model 2 (raptoriality R2 = 0.011; force grip foot use $R^2$ = 0.014), yet their p-values are higher (model 3 raptoriality p = 0.037; force grip foot use p = 0.016). Zygodactyl digit arrangement experiences a nominal increase in $R^2$ in model 3 (0.01204) compared to model 2 ($R^2$ = 0.01201). The $R^2$ values of raptorial ecology, force grip foot use and zygodactyly in model 3 are all lower than those resulting from model 1.

### 1.3.5 Shape Variation Associated with Foot Use Traits

The PGLS model used to visualise the shape deformation of the tarsometatarsus due to ecology and foot use is:

$$shape \sim centroid\ size\ +\ mean\ body\ mass\ +\ flightlessness\ +\ force\ grip\ +\ raptoriality\ +\ zygodactyly$$

which is indexed as Model 2 (Appendix Table B.2). Despite having a higher adjusted-$R^2$, Model 1 was not used because the variable 'digital manipulation' was non-significant, and its independent effect had previously been redundant in models where variation due to flightlessness had already been accounted for. The intercept value was set to 1 for all shape deformation analyses, and centroid size and mean body mass were set to their mean values (32 mm centroid size; 1034 g body mass) and log-transformed.

For the analyses of the shape variation associated with proportional centroid size, and shape variation associated with mean body mass, all foot use trait coefficients were set to 0, as this is the most common scoring for each trait within my dataset.

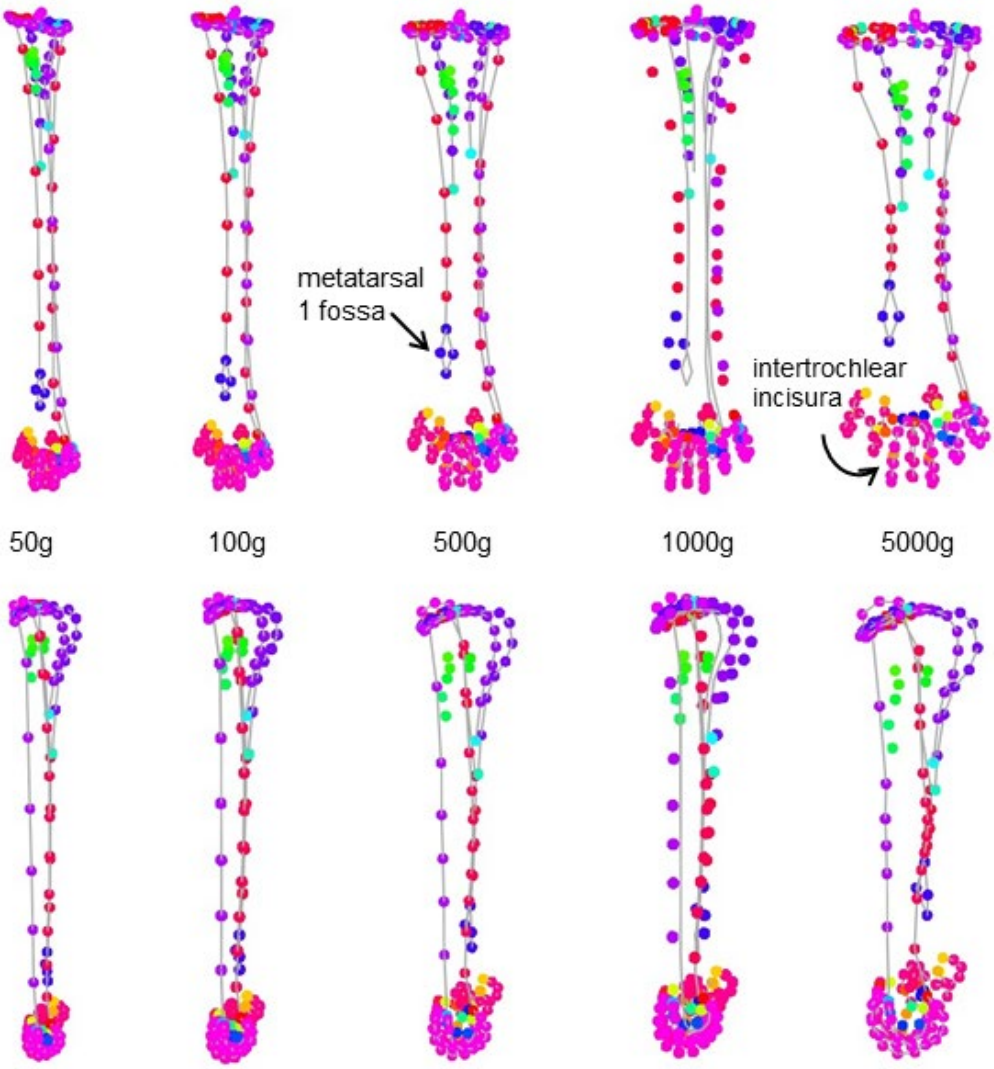


**Figure 37.** Shape deformations depicting the variation associated with mean body mass holding all other variables constant, with centroid size set to mean value of 34 mm and all foot use traits set to 0. Shape deformations compare the effects of setting $\log_{10}$-mean body mass to the log-values of 50g, 100g, 500g, 1000g, 5000g.

*Shape variation associated with mean body mass*

Quantitative shape deformations of the tarsometatarsus associated with variation in species mean body mass represent the independent effects of scaling relationships that have universal allometric effects among birds (Appendix Table B.2; shape ~ mean body mass: $R^2$ = 0.007, p = 0.239; Model 2: $R^2$ = 0.117, p = 0.001). To visualise the independent effects of a

range of body masses on tarsometatarsus shape, I generated several idealised shapes, setting the value of $\log_{10}$-mean body mass from 50g – 5000g to represent proportionally small and proportionally large body masses (Figure 37).

The overall trend in shape variation with increasing mean body mass is an increase in robustness, entailing an increase in relative mediolateral and anteroposterior width in comparison to proximodistal length. This definition of increasing robustness is also applicable for the later uses of the term in the results. Additional shape variation associated with this increase in relative robustness includes widening intertrochlea incisurae, increasingly plantarward prominence of the hypotarsal crests, and increasingly large and proximal placement of the metatarsal 1 fossa. There is also a noticeable decrease in the proximal projection of the medial side of the proximal articular surface, resulting in a proximal articular surface that is oriented more closely perpendicular to the long axis of the tarsometatarsus as mean body size increases. There is no discernible difference in the arrangement of the metatarsal trochleae, the relative placement of the tuberositas m. tibialis cranialis, proximal and distal vascular foraminae, or the height of the eminentia intercotylaris.

Scaling relationships predict that an increase in body mass results in an increase of the relative cross-sectional area of weight-supporting limb bones as a result of allometric scaling. In allometric scaling, the volume of the bone acting as a support must increase in proportion to the body mass to the power of 1.33 (Schmidt-Nielsen, 1984, p.44). The increase in robustness seen in the proportionally enlarging condyles and muscle attachment areas provide increased space for soft tissue support.

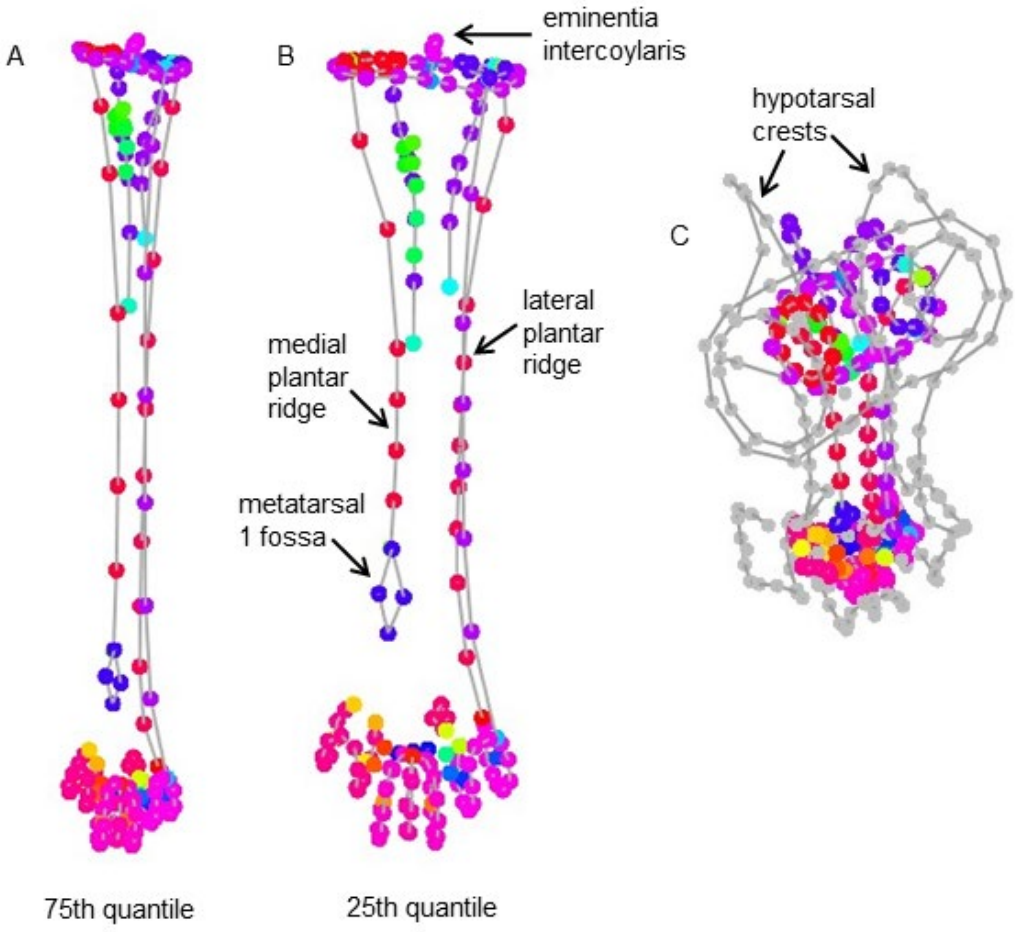


**Figure 38.** Shape deformations depicting the variation associated with proportional centroid size holding all other variables constant, with mean body mass set to mean value of 1034 g and all foot use traits set to 0. Shape deformations compare the effects of setting $\log_{10}$-centroid size to the A) 75th quantile (36 mm), and B) 25th quantile (13 mm) values to represent proportionally small and proportionally large tarsometatarsi; C) grey points depict the 25th quantile shape, coloured points depict the 75th quantile shape.

*Shape variation associated with proportional centroid size*

To visualize allometric shape deformations associated with the variation in proportional size of the tarsometatarsus, I used the coefficients of centroid size from within the final pGLS model (Appendix Table B.2; model 2). This model documents the independent effects of relative variation in tarsometatarsus size because it includes terms for both mean body mass and tarsometatarsus centroid size. I generated two idealised shapes, setting the value of $\log_{10}$-centroid

size to its 25th quantile to represent proportionally small centroid sizes, and to its 75th quantile to represent proportionally large centroid sizes. These correspond to centroid sizes of approximately 13mm and 36mm respectively.

The most conspicuous difference between the two resulting shapes is in their apparent relative robustness. The shape associated with proportionally small centroid size (Figure 38B) appears proportionally wide, widening further at proximal and distal ends. The shape associated with proportionally large centroid size (Figure 38A) appears comparatively slender. However, this difference in proportional robustness results from variation in proximodistal elongation rather than variation in cross-sectional diameters. This is seen in visualizations of the shape deformations re-scaled by their associated input centroid sizes, after which the midshaft widths of each shape do not differ (Figure 39).

Proportionally small tarsometatarsi also appear to have a larger and more proximally positioned metatarsal 1 fossa. The metatarsal 1 fossa may become smaller and more distally positioned in those species with proportionally larger centroid sizes in order to group all four toes together for balance, especially combined with wider intertrochlear incisura. Other differences include the occurrence of relatively wider intertrochlear incisurae, plantarward curving and greater proximal separation of the medial and lateral plantar ridges, and a more proximally projecting eminentia intercotylaris in proportionally large tarsometatarsi. Furthermore, the hypotarsal crests and the plantar area between them cover approximately two-thirds of the total width of the proximal end of proportionally small tarsometatarsi, whereas this space spans only approximately half the total width of proportionally large tarsometatarsi. Aspects of the shape deformations that do not differ, or differ with only slight nuance include the

shape of each trochlea metatarsi, the hypotarsal crests, and the proximal asymmetrical articular surfaces.

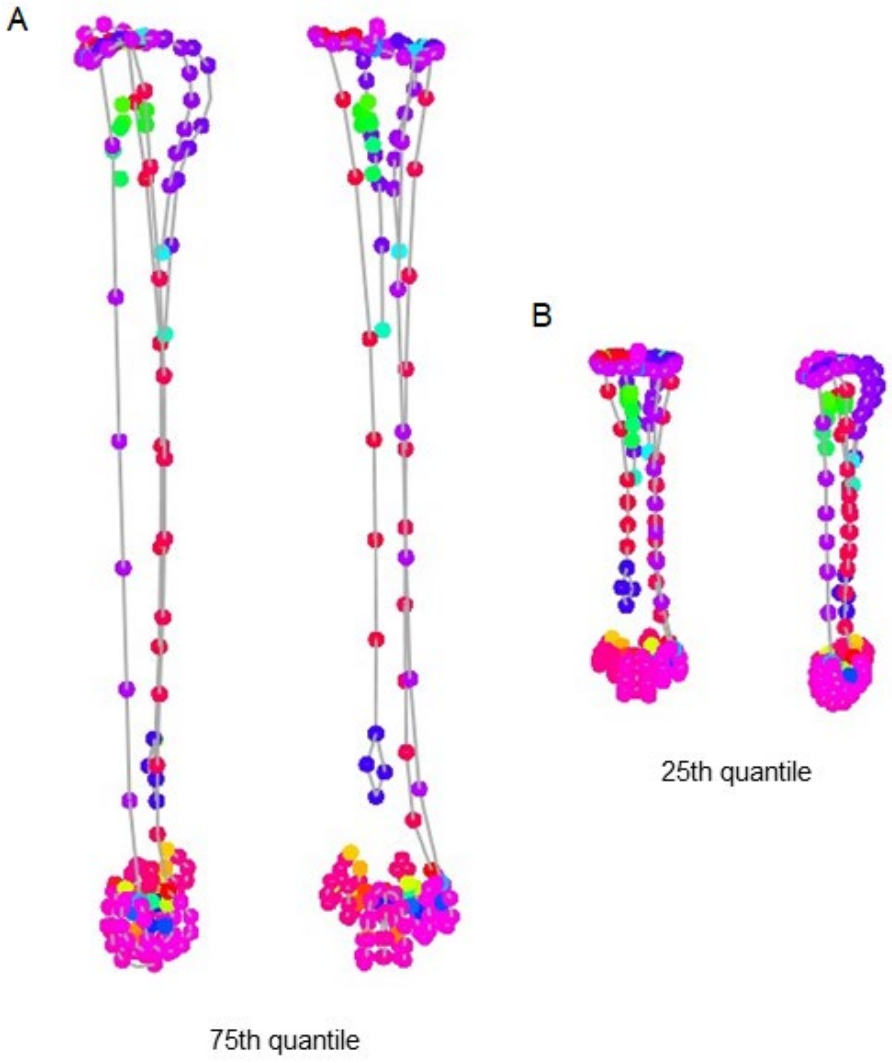


**Figure 39.** Shape deformations depicting the variation associated with proportional centroid size, re-scaled to input centroid sizes, A) 36mm, 75th quantile; B) 13mm, 25th quantile.

The extremes of variation in centroid size are represented by birds that have proportionally long and proportionally short tarsometatarsi. Previous hypotheses tend to predict that "ground species" (Zeffer et al., 2003) or birds which rely on terrestrial locomotion generally

possess longer hindlimbs. In their research on the indexing of avian leg length independent of body mass in different ecological groups, Zeffer et al. (2003) found that their "leg length index" of species defined as "ground-based" was no higher than that for other ecological groups, possibly due to the diversity of the range of birds included in the group. They also found that wading birds had a higher index for leg length. Zeffer and Norberg (2003) found that both birds of prey and birds categorised as "fast swimmers" also have longer tarsometatarsi in relation to body size.

The results of phylogenetic regression (pGLS) of centroid size in this work only partly follow along these lines, excepting that I have slightly different categorisation (my terrestrial versus arboreal categorical variable is similar to "ground species", but my webbed foot anatomy variable is different than their "wading birds" category). Both terrestrial/arboreal ecology and webbed foot anatomy have slight negative relationships to centroid size (coefficients of -0.08 and -0.11 respectively). In other words, the tarsometatarsi of arboreal birds tend to have smaller relative centroid sizes than those of terrestrial birds, and birds with webbed feet have smaller tarsometatarsus centroid sizes to a slightly stronger degree. Mean body mass also has a positive relationship with tarsometatarsus centroid size; birds with larger body mass will have proportionally greater tarsometatarsus centroid size. The coefficient of this relationship (coefficient = 0.33) indicates positive allometry. As described above, other ecological variables had slight positive independent effects on centroid size, including cursoriality and anisodactyly, but these effects became redundant upon the inclusion of webbed foot anatomy and terrestrial/arboreal ecology variables.

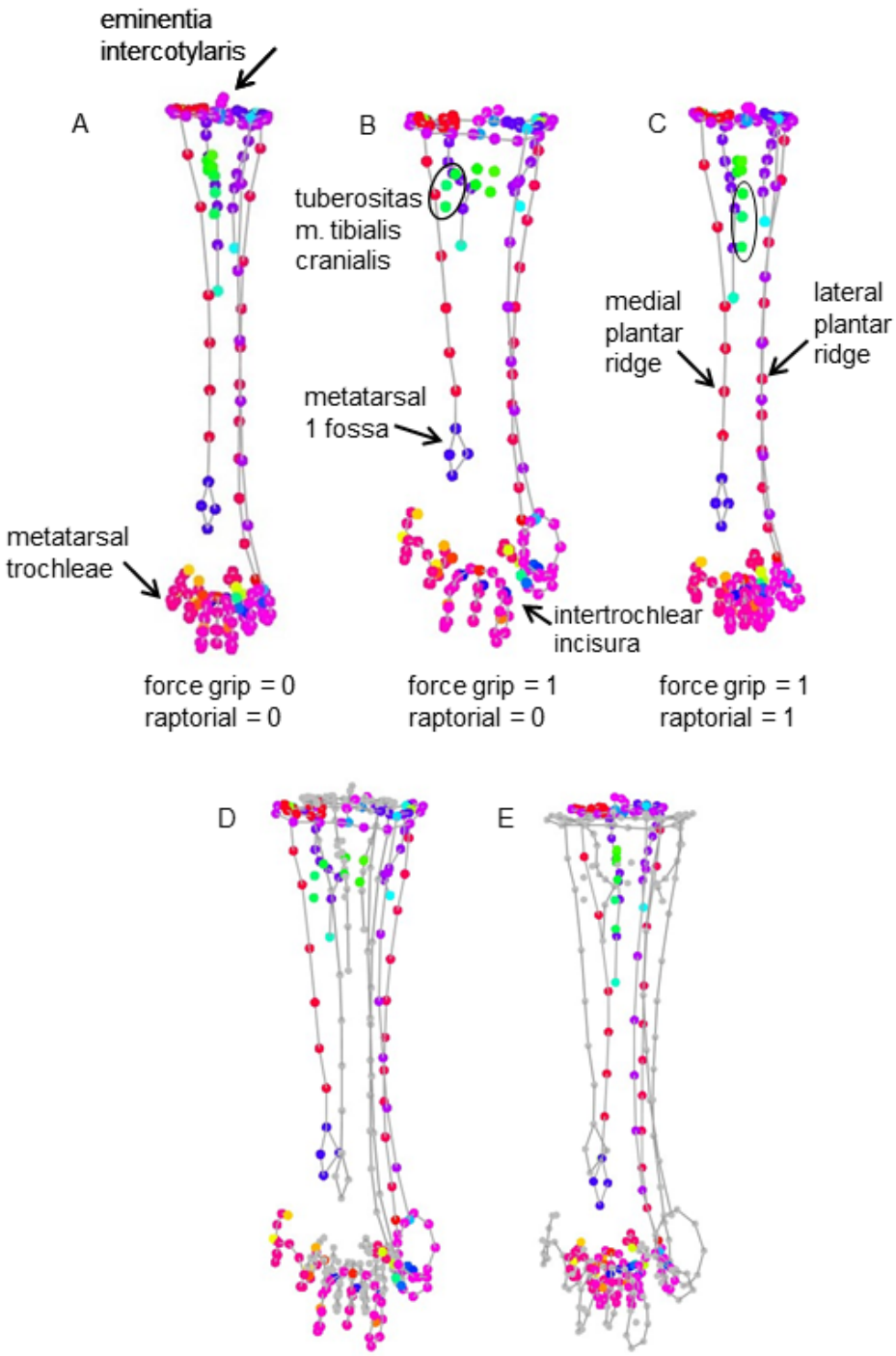


**Figure 40.** Shape deformations depicting the variation associated with force grip foot use and raptoriality holding all other variables constant, with centroid size set to mean value of 34 mm, mean body mass set to mean value of 1034 g, and all other foot use traits set to 0. Although the majority of birds with force grip are also raptorial (12 out of 18 taxa), there is no data to support a plausible morphological output of a raptorial bird without force grip foot use, as raptorial has been defined here. A-C) compared presence/absence (1/0) of force grip foot use and raptoriality; D) Visualisation of the independent effect of force grip foot use with grey points depicting the baseline shape ( with force grip = 0), coloured points

depicting the force grip shape; E) Visualisation of the independent effect of raptoriality with grey points depicting the baseline shape (with raptorial = 0), coloured points depict the raptorial shape (with force grip = 1).

*Shape variation associated with force grip foot use*

I find strong evidence for a relationship between tarsometatarsus morphology and force grip foot use (shape ~ force grip foot use: $R^2 = 0.009$, $p = 0.174$; model 2: $R^2 = 0.014$, $p = 0.023$).

The main result of force grip foot use on tarsometatarsus morphology is an increase in robustness as a proportional mediolateral and anteroposterior widening of features along the length of the bone. Both the trochlea metatarsae and the intertrochlea incisurae between them are widened both mediolaterally and anteroposteriorly in the force grip foot use shape (Figure 40B, D). The fourth trochlea metatarsi is notably large and anterioposteriorly flattened, in addition to being slightly rotated laterally plantarward. Other differences in the force grip foot use shape include the mediolaterally wider and more proximally positioned metatarsal 1 fossa, the more medially positioned m. tibialis cranialis tuberositas, and the less pronounced eminentia intercotylaris, as well as the angular and less prominently plantarward hypotarsal crests.

The groups that utilise force grip foot use in my analysis are Psittaciformes, Strigiformes, and many Accipitriformes and Falconiformes. Grasping in birds enables hanging, clinging, climbing, and prey-gripping foot uses (Sustaita et al., 2013). The plantar rotation of trochlea metatarsal 4 associated with force grip foot use in my analyses is seen most clearly in parrots (Psittaciformes), and to a lesser extent in owls (Strigiformes) and the osprey (Pandionidae). This is similar to, but independent of, the effect of zygodactyl digit arrangement on tarsometarsus morphology (described below) and I suggest that it assists with grasping function: either perching or grasping an object forcefully (Mourer-Chauviré, 1994; Sustaita et al., 2013).

Past literature has emphasised the role of the hallux in digital manipulation as well as in forceful gripping (Sustaita et al., 2013), and the muscles involved with the hallux and distal portions of the foot generally tend to increase in cross-sectional area with evolutionary increases in these foot uses (Backus et al., 2015). This observation may explain the proportional enlargement of the metatarsal 1 fossa articulation surface shown associated with the force grip foot use shape from my analysis, reflecting the need for stability in grip strength. The main focus of past literature on avian grasping is on the phalanges rather than the tarsometatarsus, but the proportions of distal tendons (e.g. flexor hallucis longus, flexor digitorum longus) and other soft tissue associated with grasping are increased in forcefully grasping species such as raptors (Backus et al., 2015). The mediolateral and anteroposterior widening of the trochlea metatarsae and the intertrochlea incisurae associated with force grip here likely creates ample space for stable toe articulation, and further room for flexion of tendons, respectively, and may also increase the physical span of the foot when the toes are extended.

An increase in overall robusticity of the tarsometatarsus associated with force grip, including mediolateral widening and anteroposterior deepening of the proximal and distal ends, likely aids in other factors of force grip foot use. The mediolateral spread of trochlea metatarsae is hypothesised to improve prey grasping and/or perching capabilites in Strigiformes (Mourer-Chauviré, 1994). The increased robusticity of digits 3 and 4, as well as the increased size of digital muscles assists in overall grip strength in parrots, as well as mousebirds (Sustaita et al., 2013), which are not scored as having force grip foot use in this analysis, but which do engage in other activities such as hanging and clinging which likely requires similar muscle structure, if not similar muscle strength or bone robusticity. According to Volkov (2004), a robust intertarsal joint is needed for the stabilisation of overall grip strength of arboreal/perching birds, as well as

for the seizing of prey items in raptors. An adaptation hypothesised by Volkov (2004) to increase the amount of force applied to gripping an object is a further distal placement of the tuberositas m. tibialis cranialis, in the "second third" of the tarsometatarsus shaft; this may only be applicable to strigiform tarsometatarsus morphology, as it is not seen in my force grip foot use shape model. Mayr et al. (2020) hypothesised that a widened trochlea metatarsi 2 with a flattened articular surface, found in many fossil owl tarsometatarsi, better stabilises the toe joint against torsion during grasping activity. This could also be true of the force grip foot use shape, for which all trochlea metatarsae are widened in all directions.

*Shape variation associated with raptoriality*

I find strong evidence for a relationship between raptorial foot use and tarsometatarsus morphology only when also including force grip foot use in the model (shape ~ raptorial: $R^2$=0.006, p=0.352; model 2: $R^2$=0.011, p=0.027). This suggests that raptorial foot use represents a modification of shape from that associated with forceful gripping.

In order to more thoroughly examine the independent effect of raptorial foot use on tarsometatarsus morphology, I have compared the raptorial tarsometatarsus shape to both a non-raptorial force grip foot use shape (Figure 40B) as well as a non-raptorial, non-force grip shape (Figure 40A). This is because the raptorial shape, by necessity, has a non-zero value for its force grip foot use coefficient. The raptorial shape appears overall much more similar to the non-raptorial, non-force grip shape more than it does to the non-raptorial, force grip foot use shape, confirming that the independent effect of raptoriality on a tarsometatarsus are much different than the effects of solely force grip foot use.

The primary difference of the independent effect of raptoriality is that the raptorial + force grip foot use shape (Figure 40C, E) is more gracile along its length than the non-raptorial,

force grip foot use shape. From a dorsal view, it is slender in the middle of the shaft and becomes only slightly wider at the proximal and distal ends. Compared to the non-raptorial, non-force grip tarsometatarsus shape however, the raptorial shape is thicker, and the medial and lateral plantar ridges curve further outwards in a plantar direction, and so the raptorial shape appears anteroposteriorly deeper. The metatarsal 1 fossa is positioned slightly further distally in the raptorial shape, and the proximal vascular foramen and tuberositas m. tibialis cranialis are positioned more centrally on the bone than for either non-raptorial shape. Furthermore, the hypotarsal crests are asymmetrical in the raptorial shape, and the crests extend further distally along the shaft than in the non-raptorial, force grip foot use shape. The raptorial hypotarsal crests are much more similar to those of the non-raptorial, non-force grip shape, but the lateral hypotarsal crest is much less prominent in the raptorial shape, and the crests are mediolaterally spaced further apart. The intertrochlea incisurae are much narrower in the raptorial than the non-raptorial, force grip foot use shape, and are still slightly more narrow than in the non-raptorial, non-force grip shape. The trochlea metatarsae are smaller in the raptorial shape than the non-raptorial, force grip foot use shape, but are larger than those of the non-raptorial, non-force grip shape. The raptorial shape lacks the lateral, plantarward rotation of trochlea metatarsal 4 found in the non-raptorial, force grip foot use shape, which contributes to its overall gracility. The distal end of the tarsometatarsus has a curved mediolateral widening resulting in trochlea metatarsae 2 and 4 to appear similar to the flanges found in semi-zygodactyl species (Strigiformes, Pandionidae).

Less conspicuous differences include the straightened and low eminentia intercotylaris in the raptorial shape, and the lack of noticeable distal angling of the dorsal side of the proximal articular surface.

The results described here represent the independent effect of raptoriality on tarsometatarsus shape, independent of variation related to body mass, tarsometatarsus size, and forceful gripping, depicting a generalised shape deformation under the independent effect of raptorial foot use among birds, rather than a lineage-specific descriptions of raptorial bird tarsometatarsi (e.g. in owls; Madan et al., 2017). This goes beyond past analyses of raptor tarsometatarsi which used either basic linear measurements or qualitative descriptive terms, often in relation to body mass (e.g. Zeffer and Norberg, 2003) or focussed on the talons (e.g. Einoder and Richardson, 2007). Madan et al. (2017) hypothesise that the tarsometatarsus is the primary hindlimb structure for withstanding functional loading in owls, which they use to explain the relative robusticity of owl tarsometatarsi compared to the more gracile accipitrid tarsometatarsi. My pGLS analyses (see above) indicate a lack of correspondence between centroid size of the tarsometatarsus with raptoriality (size ~ body mass + raptoriality; $p = 0.308$, AICc = -63.466). This reflects variation in relative tarsometatarsus length among raptors.

Sustaita et al. (2013) suggested that "enhanced digital force production" (p.390) specifically in raptors is aided by various arrangements of digital flexor muscles and tendons. These are not directly observed in osteological data used here, but interact with osteology in ways that could explain aspects of my findings. This force production is potentially linked to the distally extended hypotarsal crests and the mediolaterally widened space between them, in that they form a channel for hypertrophied digital flexor tendons used in their prey capture grasping foot use (Sustaita et al., 2013). Ward et al. (2007) hypothesised two ways for raptors to close the foot on prey; one using the previously mentioned flexor tendons, and the other using the m. tibialis cranialis to flex the intertarsal (ankle) joint, pulling the tendons taut and closing the foot. Having a more mediolaterally central positioned tuberositas m. tibialis cranialis as found in the

raptorial foot use shape potentially aids in the efficiency of this motion. The relationship between the hypotarsal crests, the tendons they channel, and raptorial foot use are investigated in Chapter 2.

Notably, the intertrochlea incisurae of the raptorial shape are even more narrow than in the non-raptorial, default coefficient shape. This could be an idiosyncracy of the shape deformation, as the trochlea metatarsae are larger and flanged, but the spaces between these condyles are smaller. A wider spread of digits for raptorial foot use is hypothesised to aid in prey capture (Einoder and Richardson, 2007), whereas a narrower foot and distal end of the tarsometatarsus is hypothesised to help the foot reach prey in small crevices (Burton, 1978). However, wider distances between the toes is most prominent in owl feet, and could be attributed to zygodactyl digit arrangement, and in those cases of particularly distally narrowed tarsometatarsi, there are much more noticeable changes to the structure of the trochlea metatarsi than what is found in my raptorial shape. Overall, the relative widths of the trochlea metatarsi and the intertrochlear incisurae have not been examined in this method before, and so it is both difficult and premature to utilise the terminology of relative widths and spacing from literature focussed solely at the family, genus, or species level.

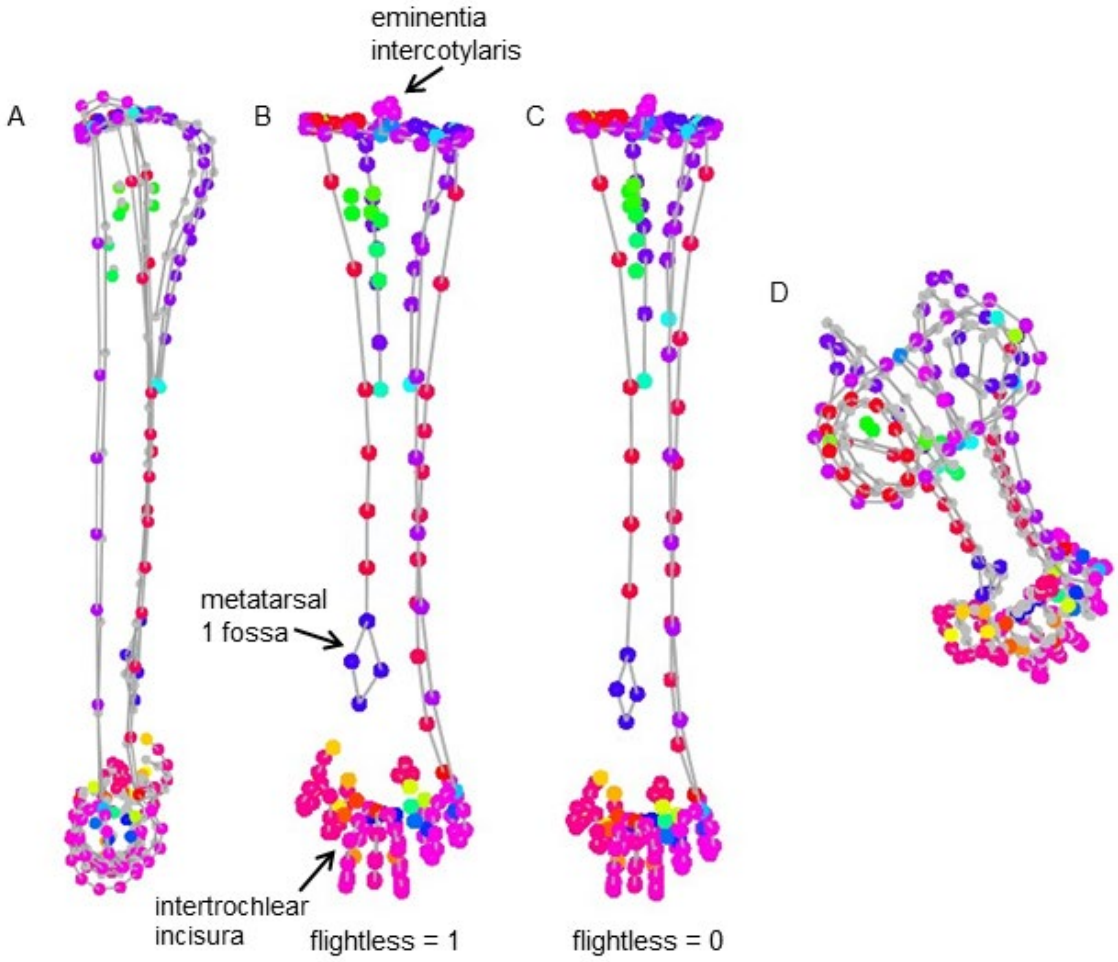


**Figure 41.** Shape deformations depicting the variation associated with flightlessness holding all other variables constant, with centroid size set to mean value of 34 mm, mean body mass set to mean value of 1034 g, and all other foot use traits set to 0. A) Lateral view of shape representing the effect of flightlessness; B, C) compared presence/absence (1/0) of flightlessness; D) Visualisation of the effect of flightlessness with grey points depicting the baseline shape (with flightlessness = 0), coloured points depicting the flightless shape.

*Shape variation associated with flightlessness*

I find strong evidence of a relationship between flightlessness and tarsometatarsus shape (shape ~ flightlessness: $R^2$= 0.046, p= 0.001; model 2: $R^2$ = 0.019, p = 0.002). Flightless taxa in my analysis are spread among several groups, representing 10 independent origins of flightlessness from volant ancestors across Paleognathiformes, Anseriformes, Gruiformes, Sphenisciformes, Psittaciformes, and Passeriformes.

Overall, the shape representing the independent effect of flightlessness (Figure 41A, B, D) has widened features at both the proximal and distal ends of the tarsometatarsus. In particular, the intertrochlea incisurae are more widely spaced, and the distal articular surfaces of the trochlea metatarsae are also larger both mediolaterally and anteroposteriorly. At the proximal end of the tarsometatarsus, both the articular cotyles and the hypotarsal crests are set mediolaterally wider apart, and the eminentia intercotylaris of the flightless tarsometatarsus shape is slightly taller. The shaft of the flightless tarsometatarsus shape model is also slightly mediolaterally wider along its entire length, but not deeper anteroposteriorly. The metatarsal 1 fossa is larger and positioned slightly more proximally in the flightless shape than that of the volant model. There is no discernable difference between the flightless and the volant shape in the extent to which the hypotarsal crests project plantarward, although the lateral hypotarsal crest of the flightless model extends further distally along the shaft.

There is no one foot use singularly associated with avian flightlessness, as its secondary evolution occurs in many groups with a range of ecological origins, including in foot-propelled divers such as *Rollandia microptera* (Titicaca Grebe), force grip foot users such as *Strigops habrotila* (Kakapo), wing-propelled divers such as *Spheniscus humboldti* (Humboldt Penguin), and cursorial specialists such as *Dromaius novaehollandiae* (Emu). Flightless birds either run, walk, or swim, locomotion modes which likely influence the shape of hindlimbs in varying ways, but are not generally found to have statistically significant, predictable independent effects on tarsometatarsus shape by my analyses. Flightlessness is also associated with increased body size and cross-sectional areas of hindlimb elements in many avian groups (Feduccia, 1999; Gaspar et al., 2020). My analyses account for variation in body mass separately by including species mean body mass as an explanatory variable. Therefore, the shape deformations

associated with flightlessness here represent the independent effect of flightlessness after accounting for variation in body mass.

Flightlessness appears to result in an increase in overall robusticity, relative size of the proximal articular surface, and relative size and spacing of the distal articular condyles, all of which would ensure increased stability in the hindlimb, particularly the ankle and digit joints. In non-swimming birds such as *Dromaius novaehollandiae* (Emu), this could assist in combatting dynamic forces on joints during running, or in general structural support of increased body mass, which tends to occur in flightless birds such as paleognaths. In swimming birds, there is a notable increase in limb bone density and bone wall thickness in response to flightlessness (Habib and Ruff, 2008; Mendoza and Tambussi, 2015), but it is unclear which morphological aspects of the flightless tarsometatarsus shape may function to the benefit of swimming foot uses. However, even though the volant relatives of these flightless birds also dive and/or swim, variation in flightlessness should be considered independent of swimming ability. There may be higher variability in tarsometatarsus shapes for swimming birds because of the convergent evolution of foot-propelled swimming modes. Thus, it's possible that the foot of a swimming bird may already be specialized for a flight-irrelevant locomotion mode, resulting in nominal effects from the addition of flightlessness, apart from perhaps an increase in bone density or general robusticity.

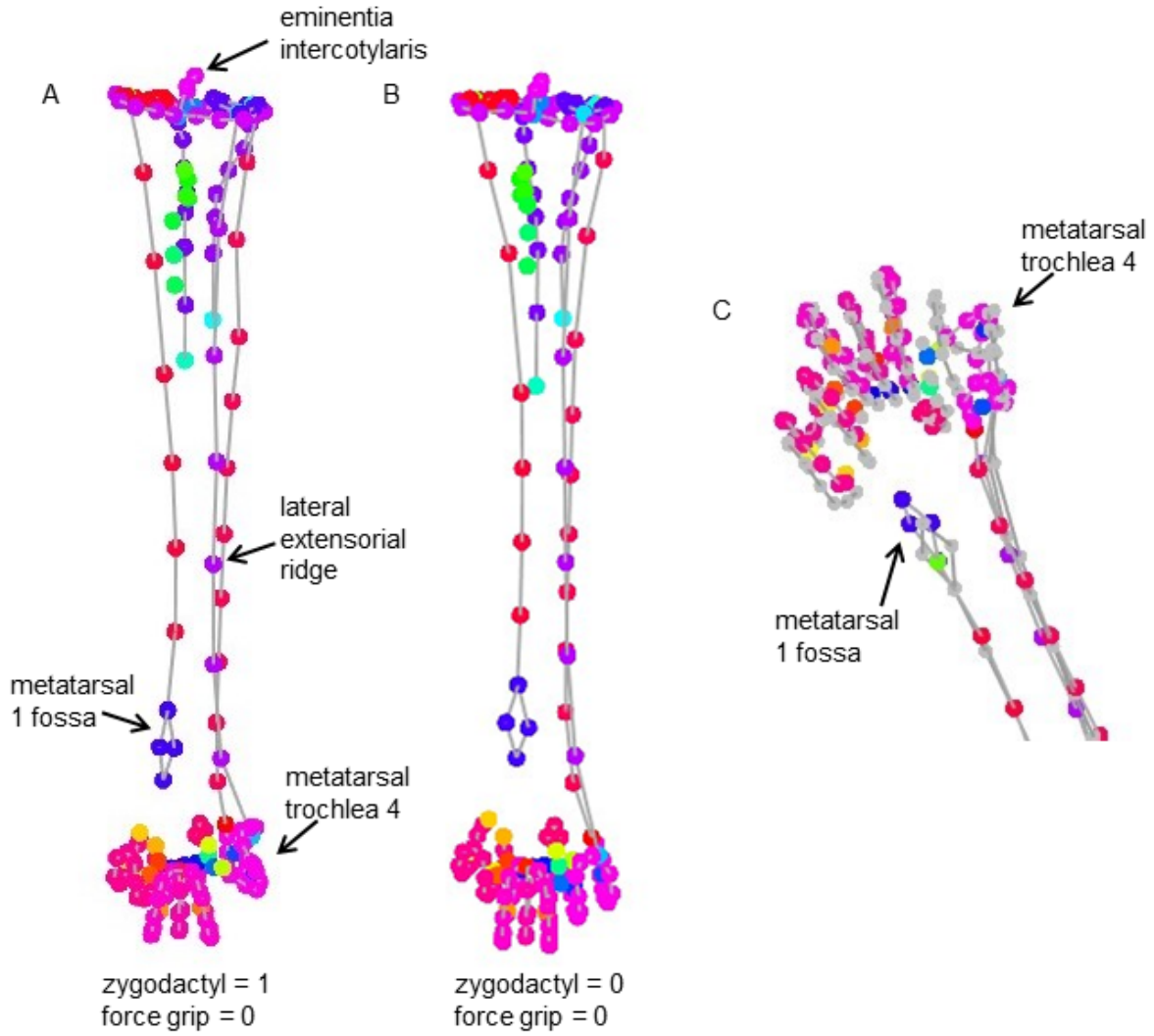


**Figure 42.** Shape deformations depicting the variation associated with zygodactyly holding all other variables constant, with centroid size set to mean value of 34 mm, mean body mass set to mean value of 1034 g, and all other foot use traits set to 0. A, B) Compared zygodactyl presence/absence (1/0); C) Visualisation of the effect of zygodactyly with grey points depicting the baseline shape (with zygodactyl = 0), coloured points depicting the zygodactyl shape in the absence of force grip foot use. 12 of the 22 species in the dataset with the ability to assume a zygodactyl digit arrangement also had force grip foot use. However, only 5 out of the 22 birds with zygodactyly in this dataset are also raptorial, so the raptorial variable was set to a constant of 0.

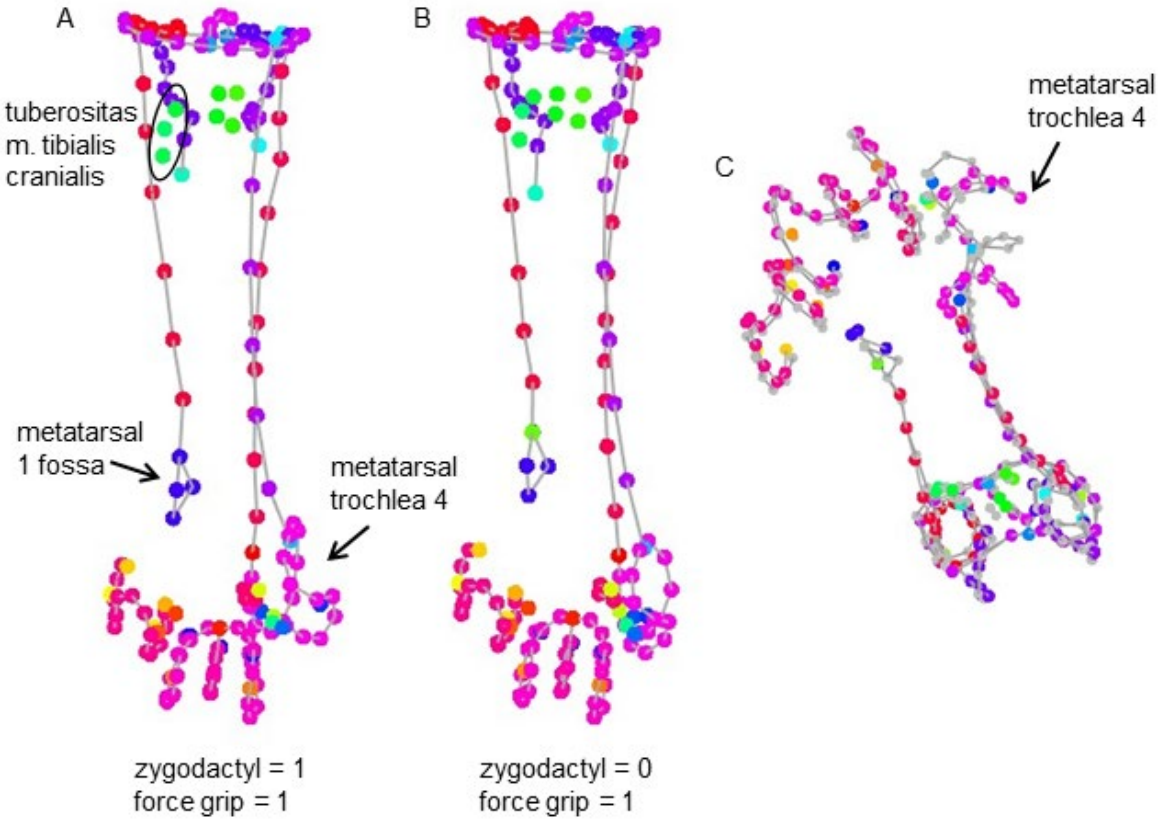


**Figure 43.** Shape deformations depicting the variation associated with zygodactyly holding all other variables constant, with centroid size set to mean value of 34 mm, mean body bass set to mean value of 1034 g, flightlessness and raptoriality set to 0, and force grip foot use set to 1. A, B) Compared zygodactyl presence/absence (1/0); C) Visualisation of the effect of zygodactyly with grey points depicting the baseline shape (with zygodactyl = 0), coloured points depicting the zygodactyl shape in the presence of force grip foot use.

*Shape variation associated with zygodactyly*

I find strong evidence of a relationship between tarsometatarsus morphology and zygodactyl digit arrangement (shape ~ zygodactyly: $R^2$=0.016, p=0.035; model 2: $R^2$=0.012, p=0.023).

The primary independent effect of the presence of zygodactyl digit arrangement on tarsometatarsus shape is the plantarward lateral rotation of metatarsal trochlea 4 (Figures 42A, 43A). In addition, the metatarsal 1 fossa is positioned further distally, and there is a mediolateral

widening in the curve of the plantar ridges near the proximal end of the shaft. In the zygodactyl shape for which force=0 (Figure 42A), the eminentia intercotylaris is slightly higher, trochlea metatarsi 3 is wider, and the medial intertrochlear incisura is narrower, or trochlea metatarsi 2 is slightly longer and rotated plantarwards toward the centre. Along the shaft, both the lateral plantar ridge and the lateral extensorial ridge narrow in a distal direction, before flaring out to accommodate the plantarward rotation of trochlea metatarsi 4. The tuberositas m. tibialis cranialis is also positioned slightly more mediodistal in the zygodactyl shape. Otherwise, both the zygodactyl and non-zygodactyl shapes are very similar, particularly the hypotarsal crests.

The plantarward lateral rotation of trochlea metatarsi 4 accommodates the rotation of the fourth toe, either for constant zygodactyly as for parrots (Psittaciformes), semi-zygodactyly as for owls (Strigiformes), ospreys (Pandionidae) and mousebirds (Coliiformes), or the intermediate temporary position assumed by woodpeckers (Picidae), for which the fourth toe is positioned perpendicular to the forward-facing second and third toes (Bock and Miller, 1959). The distally shifted metatarsal 1 fossa seems to benefit mousebirds in their ability to configure their digits into many different arrangements (Berman and Raikow, 1982). The m. tibialis cranialis is a tarsometatarsus flexor, and is larger when required for hanging foot use (Berman and Raikow, 1982), and/or object manipulation (Carril et al. 2014). The tuberositas m. tibialis cranialis is this muscle's attachment site, and so is more developed and distally placed in mousebirds and parrots.

## 1.4 Discussion

My analysis aimed to quantitatively test the relationship between tarsometatarsus morphology and foot use in birds. I used 3D geometric morphometrics and phylogenetic

comparative analysis to see which specific foot uses have a significant impact on the shape of the tarsometatarsus bone, and how much of the variation in bone shape could be explained by a combination of independent effects of foot uses.

Tarsometatarsus centroid size, taxon mean body mass, flightlessness, zygodactyl digit orientation, raptoriality, and force grip foot use each have significant independent effects on tarsometatarsus shape. Approximately 26% of the variation in tarsometatarsus shape is explained by these foot uses and ecologies. In addition, variation in tarsometatarsus centroid size can be explained by a combination of taxon mean body mass, arboreality, and the presence of webbed feet. This suggests that different factors influence tarsometatarsus size compared to those that influence tarsometatarsus shape, with potentially different functional and/or evolutionary implications (e.g. phylogenetic signal).

Overall, these results suggest that there is a considerable link between foot use and tarsometatarsus shape, and to a certain extent, foot use and tarsometatarsus size. I was also able to visualize and identify the independent effects of individual foot uses on tarsometatarsus shape. Past ecomorphological studies, as well as qualitative comparisons and explanations of the shape changes associated with foot uses tend to state their results in terms of scale rather than shape. For example, research describing the effect of flightlessness on skeletal morphology frames changes in the hindlimb as changes in proportional elongation, and/or changes in body mass. Common descriptors of the tarsometatarsus of extant and extinct flightless birds are “short,” “stout,” or “robust,” either in comparison to other hindlimb elements, or in comparison to the tarsometatarsus of close relatives (e.g. Alcover et al., 2015; Olson and Wingate, 2001; Livezey, 1992a; Gaspar et al., 2020). The results of these studies are more directly indicative of the independent effects of shifts in body mass than of the direct effects of flightlessness on

tarsometatarsus shape independent of these other factors. The anatomical conclusions of the effect of flightlessness on birds reached by these studies are therefore primarily based on the effects of other variables, that are taken into account separately in my analysis, as independent factors. I was able to distinguish here between the independent effect on tarsometatarsus shape that is explained by flightlessness versus other factors such as terrestriality, tarsometatarsus centroid size and body mass variation.

Zygodactyl digit arrangement has a statistically stronger relationship with tarsometatarsus shape than do other digit orientations. This may be possible because zygodactyly corresponds with a more consistent tarsometatarsus shape over a sufficiently large number of taxa, unlike other variation in digit orientations such as heterodactyly (present only in Coliiformes and Trogoniformes), and pamprodactyly (present only in Coliiformes and Apodidae). Anisodactyly is the most widespread digit orientation in extant Aves, and had a significant independent effect on tarsometatarsus shape, as it shares similar explanatory power as zygodactyl digit orientation.

I found evidence for an important interplay between raptorial foot use and force grip foot use. This interplay results from the fact that the capability to exert a forceful grip with the foot is closely related to raptorial foot uses; all 12 raptorial taxa in the dataset exhibit force grip foot use, and these 12 raptorial taxa comprised two-thirds of all dataset taxa with force grip foot use (the others being Psittaciformes). The strength of the pGLS shape model as well as the significance of the independent foot use variables increased for both foot uses when both were included in the model, so the information they contribute individually to the explanation of tarsometatarsus shape variation must benefit the statistical strength of each other. Raptoriality and force grip foot use are strongly connected in birds in an ecological sense as well, outside of the realm of quantitative analysis. It was not possible to analyse the effects of an interaction term

between these raptorial and force grip foot use variables due to the invariant state of force grip foot use for all raptorial taxa. The independent effects of raptorial foot use and force grip foot use have an additive impact on tarsometatarsus shape, but they cannot interact in a statistical sense.

I found no evidence of a significant relationship found between tarsometatarsus shape and any aquatic-related foot use variable. This is despite the occurrence of distinctive tarsometatarsus morphologies in some foot-propelled aquatic divers such as the distinct tarsometatarsus shape best exemplified in Podicipediformes (i.e. proximally raised trochlea metatarsal 2, torqued shaft; Figure 44; Lovvorn, 1991; Johansson and Norberg, 2001). The aquatic groups possess different morphologies for similar ecologies, rather than converging on the same morphology (Figure 45). From a functional perspective, it is likely that different diving birds use their feet differently, therefore evolving different tarsometatarsus shapes.

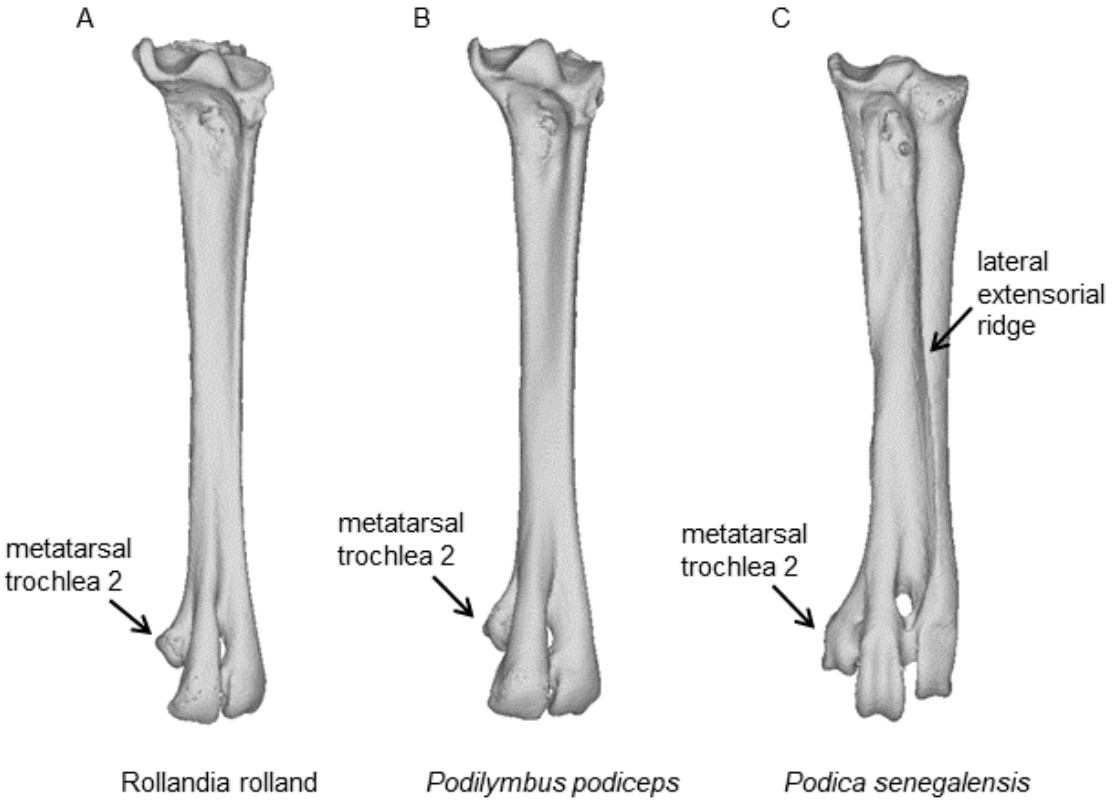


**Figure 44.** Tarsometatarsi not to scale. A) Entire left tarsometatarsus (3D model) of *Rollandia rolland* (UMMZ 156975) in dorsal view showing aspects of podicipediform morphology; B) Entire left tarsometatarsus (3D model) of *Podilymbus podiceps* (UMMZ 205087) in dorsal view showing aspects of podicipediform morphology; C) Entire left tarsometatarsus (3D model) of *Podica senegalensis* (UMZC 209A) in dorsal view showing aspects of podicipediform morphology.

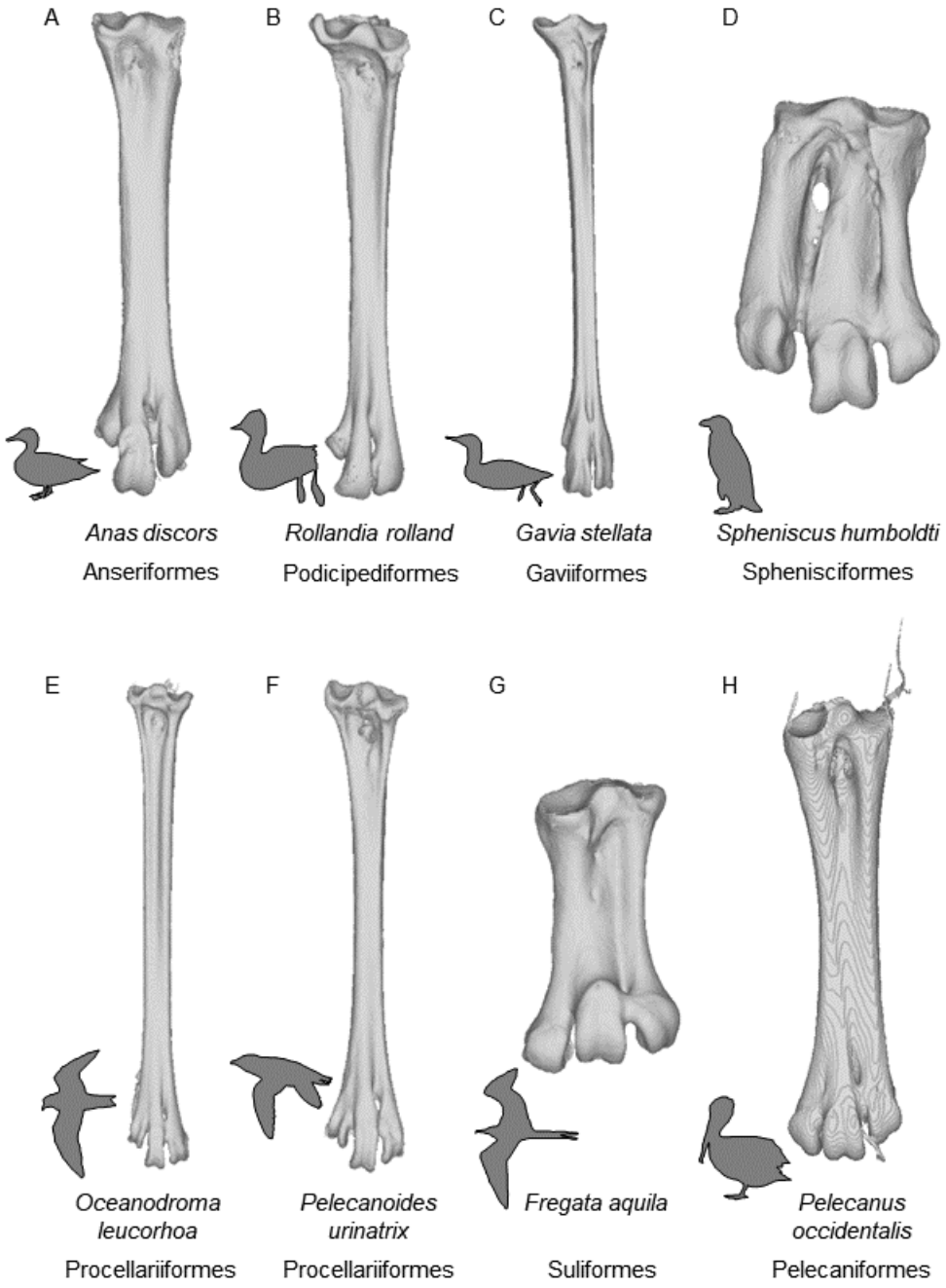


**Figure 45.** Entire left tarsometatarsi (3D models) in dorsal view showing the variation in morphology across swimming taxa; not to scale. A) *Anas discors* (NHMUK S2001.41.5); B) *Rollandia rolland* (UMMZ 156975); C) *Gavia stellata* (NHMUK 1891.7.20.132); D) *Spheniscus humboldti* (NHMUK S2000.7.1); E) *Oceanodroma leucorhoa* (NHMUK S1953.3.10); F) *Pelecanoides urinatrix* (NHMUK S2006.1.14); G) *Fregata aquila* (NHMUK 1890.11.3.3); H) *Pelecanus occidentalis* (NHMUK S1973.66.16).

The significant relationship of centroid size with presence of webbed feet indicates that swimming birds typically have proportionally shortened tarsometatarsi. Nevertheless, the independent effect of this shortening on the tarsometatarsus would be redundant with the independent effect of variation in centroid size in the final model. Any independent effect contributed by swimming variables would have been rendered obsolete in the presence of centroid size, which has a much larger amount of explanatory power.

There is a general assumption that if only approximately 26% of variation in tarsometatarsus shape can be explained by select foot uses, then there is approximately 74% of this variation left "unexplained" by any foot use, and must be accounted for by other specific ecological or phylogenetic factors. The reality is that a large amount of natural and random variation is to be expected, especially considering the general interaction among body parts in an organism, and the as-of-yet unidentifiable influence this has on individual bone shape. A small amount of variation may have been introduced by the process of manually positioning landmarks, and by landmarks which were difficult to place (e.g. the distal vascular foramen; Figures 14 and 15). As well, 26% of variation is specifically a minimum amount, explained by foot uses where they have one-to-one relationships with form, rather than many-to-one.

# Chapter 2:

## The effects of raptorial foot use on variation in hypotarsus shape in extant and fossil birds

## 2.1 Introduction

Modern birds number over 10,000 extant species, the majority of which are in Telluraves, which includes Accipitriformes, Strigiformes, Coraciimorphae, Falconiformes, Psittaciformes, and Passeriformes. Telluravians have adapted to many different flight styles, terrestrial locomotion methods, and diets. As a result, they have adapted their skeletal morphologies in response to ecological constraints. Ecomorphology studies the relationship between an organism's morphology and aspects of its ecology, and can be examined in a robust statistical manner using multivariate phylogenetic comparative methods, which use phylogenetic relationships, two- or three-dimensional shape data, and ecological trait scores.

It was shown in Chapter 1, through 3D geometric morphometrics and phylogenetic generalized least squares (pGLS) analysis, that the shape of the tarsometatarsus bone varies with its centroid size, mean body mass, flightlessness, force grip foot use, raptoriality, and zygodactyly. These results were based on landmarks across all areas of the tarsometatarsus. However, due to difficulties in reproducibility and analogous point placements, it was not possible to landmark details of the hypotarsus. Nevertheless, the hypotarsus structure may have great functional relevance to foot use in birds due to its role in guiding tendons which control pedal digit flexion (Raikow, 1985). Therefore it is a vital functional aspect of the tarsometatarsus osteology, which is investigated here.

The hypotarsus is a plantarward extension of the proximal end of the plantar surface of the tarsometatarsus, and consists of crests with guiding structures in the form of sulci, canals, or block-like protrusions (synonymous with the calcaneus; Baumel and Witmer, 1993). The tendons of several hindlimb muscles pass through or along these structures on their way to attachment sites on the digits (Raikow, 1985). There are many different shapes of hypotarsi (Baumel and

Witmer, 1993; Mayr, 2016), resulting from different patterns of loss and modification from an ancestral morphology formed from the distal tarsal bone and separate crests on metatarsals II, III, and IV (Baumel and Witmer, 1993; Ossa-Fuentes et al., 2020). This makes it difficult to establish homology between hypotarsal structures of different birds which in turn makes shape analysis methods requiring homology between taxa difficult. So far, literature on the hypotarsus has primarily focussed on the use of qualitative hypotarsus shape characteristics in assessing the phylogenetic affinities of extant avian groups (Mayr, 2008; Mayr, 2011; Mayr, 2019). Mayr (2016) composed a comprehensive survey of hypotarsus morphology in extant birds, and devised a nomenclature for the six major types of hypotarsus shape, defining each by the presence and/or number of sulci or canals (A-, mono-, bi-, or trisulcate, or mono- or bicanaliculate; Figure 1). Manegold et al. (2004) analysed the hypotarsus of fossil songbirds in comparison to those of extant Eupasseres in order to assess the evolution of hypotarsus shape in that clade. Ksepka et al. (2013) performed a phylogenetic analysis of morphological data in order to make insights into the evolution of fossil and extant Podicepidiformes by assessing key hypotarsal structures.

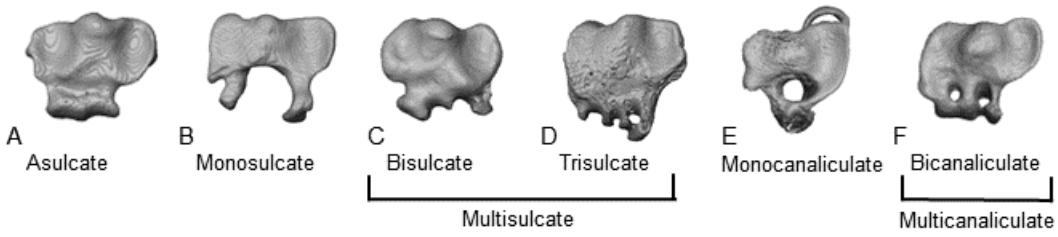


**Figure 1.** Examples of hypotarsus shapes, left sides, labelled according to Mayr 2016 classifications. Proximal views of 3D models of: A) asulcate hypotarsus of *Cathartes burrovianus*; B) monosulcate hypotarsus of *Accipiter nisus*; C) bisulcate hypotarsus of *Phaethon lepturus*; D) trisulcate hypotarsus of *Anas discors*; E) monocanaliculate hypotarsus of *Pandion haliaetus*; F) bicanaliculate hypotarsus of *Leptosomus discolor*.

Recent genome-based phylogenies (Jarvis et al., 2014; Prum et al., 2015) hypothesised that the ancestor to all Telluraves had a raptorial ecology, but did not explain how they defined

this ecological trait. My research focusses primarily on foot uses, using a working definition of raptoriality as the behaviour of killing and carrying prey with the feet (see Chapter 1). Those birds which exhibit this behaviour are thus referred to here as raptorial, and are described as exhibiting raptorial foot use. I avoid colloquial usage of the term "raptorial", which includes use of the term to refer to phylogenetic groups including Accipitriformes, Strigiformes, and Falconiformes, and use of the term to refer to traits such as carnivory, or strongly curved talons and beaks. Here, I use these definitions only sparingly, and in conjunction with past literature.

Raptoriality has been shown to have a significant but small effect on 3D shape variation of the tarsometatarsus, when not including information about the hypotarsus (see Chapter 1). However, given its role as a channel through which tendons pass, as well as its general similarity in shape across raptorial taxa, hypotarsus morphology may provide stronger evidence of raptoriality in birds. Variation in hypotarsus structure among Telluraves may therefore hold information on the relationship between raptoriality and tarsometatarsus shape among extant species, allowing for inferences of raptoriality (and non-raptoriality) in fossil species, and providing a test for the occurrence of raptoriality at earlier nodes in the tree. I approach this question using a combination of geometric morphometrics, generalized Procrustes analysis, and discriminant function analyses.

### 2.1.1 Initial Survey

I conducted an initial survey of the general trends of raptoriality and hypotarsus shape in Telluraves (Figure 2), scoring raptoriality using my definition above, and hypotarsus morphology using terminology adapted from Mayr (2016). Based on this survey, it appears that the monosulcate condition (sensu Mayr 2016; see Figure 1B) has at least a loose correspondence with the presence of raptoriality. Monosulcate hypotarsi possess no canals and, as the name

suggests, only one sulcus, framed on either side by the medial and lateral hypotarsal crests (Figure 1B). Almost all raptorial species shown here, including Strigiformes, Falconiformes, and most raptorial members of Accipitriformes, possess the monosulcate condition, even in those species not formally analysed in this research (pers. obs.). Ospreys (Accipitriformes, Pandionidae) provide one notable exception to this general association between raptorial foot use and the monosulcate hypotarsus because they are raptorial but possess a monocanaliculate condition (possessing one canal and no sulci). The monosulcate hypotarsus is also present in some non-raptorial birds, including apodids (swifts) and ciconiids (storks), which also provides exceptions to a potential association of the monosulcate hypotarsus to raptoriality.

New World vultures (Accipitriformes, Cathartidae) and seriemas (Cariamiformes) are carnivorous or partly-carnivorous birds which do not exhibit raptorial foot use and have an asulcate condition in the hypotarsus (possessing no canals or sulci, only a block-like protrusion). In contrast, species of Old World vultures, and the Palm-nut vulture, *Gypohierax*, which both also lack raptorial foot use but are nested deeply within raptorial Accipitriformes, have a monosulcate condition (Figure 3). This partial overlap of hypotarsus shape between raptorial and non-raptorial accipitriforms raises interesting questions about the history of raptorial foot use and the possibility of accompanying morphological changes within the phylogeny.

Based on this initial survey, it is likely that the monosulcate condition arose after New World vultures split from the rest of Accipitriformes, approximately 57 Ma (Prum et al., 2015). If so, then the presence of the asulcate condition (and absence of the monosulcate condition) in New World vultures reflects the retention of a primitive condition. In contrast, a monosulcate hypotarsus would have been retained from raptorial ancestors in Old World and Palm-nut vultures when they arose later, approximately 20Ma (Mindell et al., 2018).

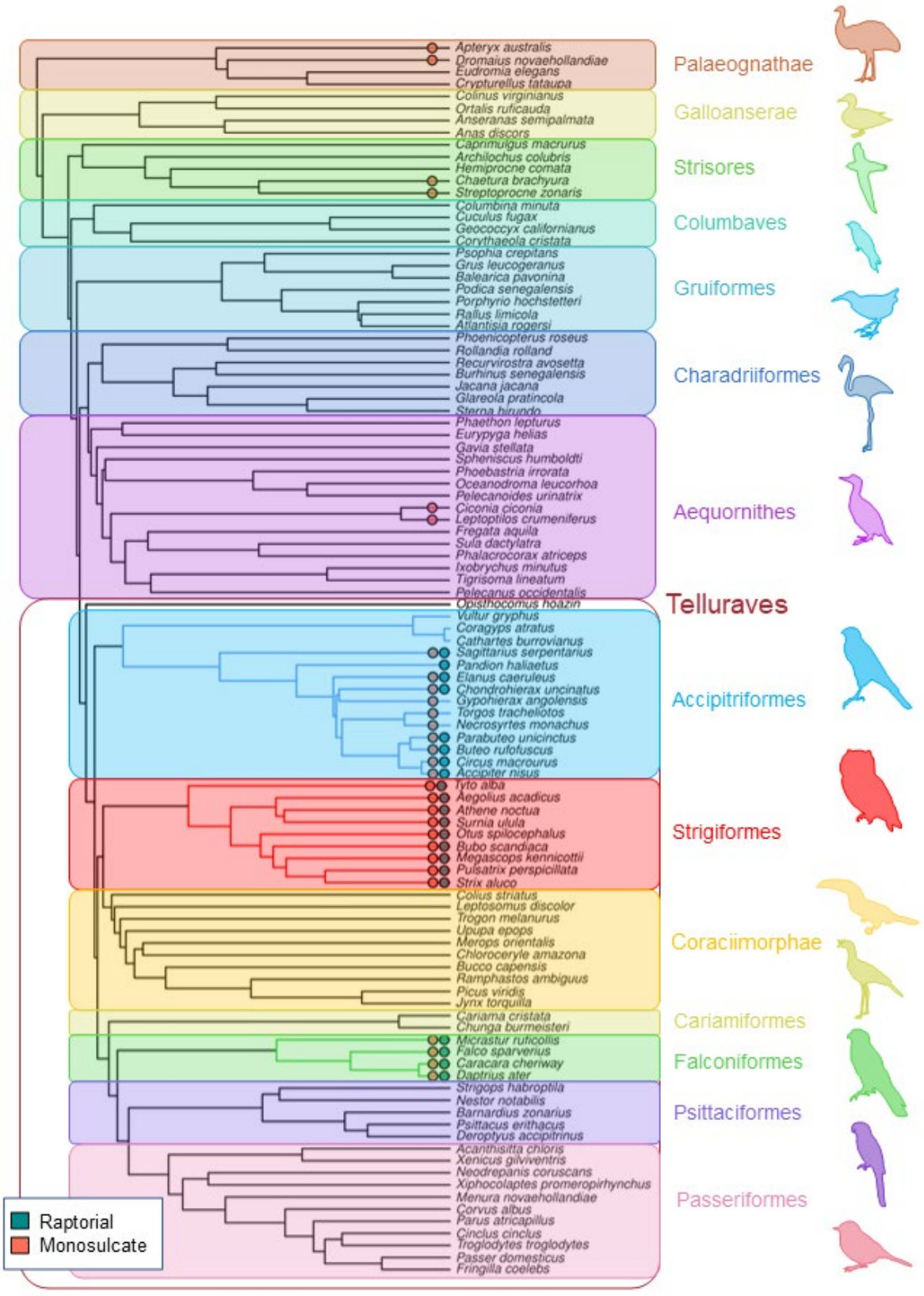


**Figure 2.** Phylogenetic tree of 179 avian taxa showing raptoriality and monosulcate hypotarsus shape.

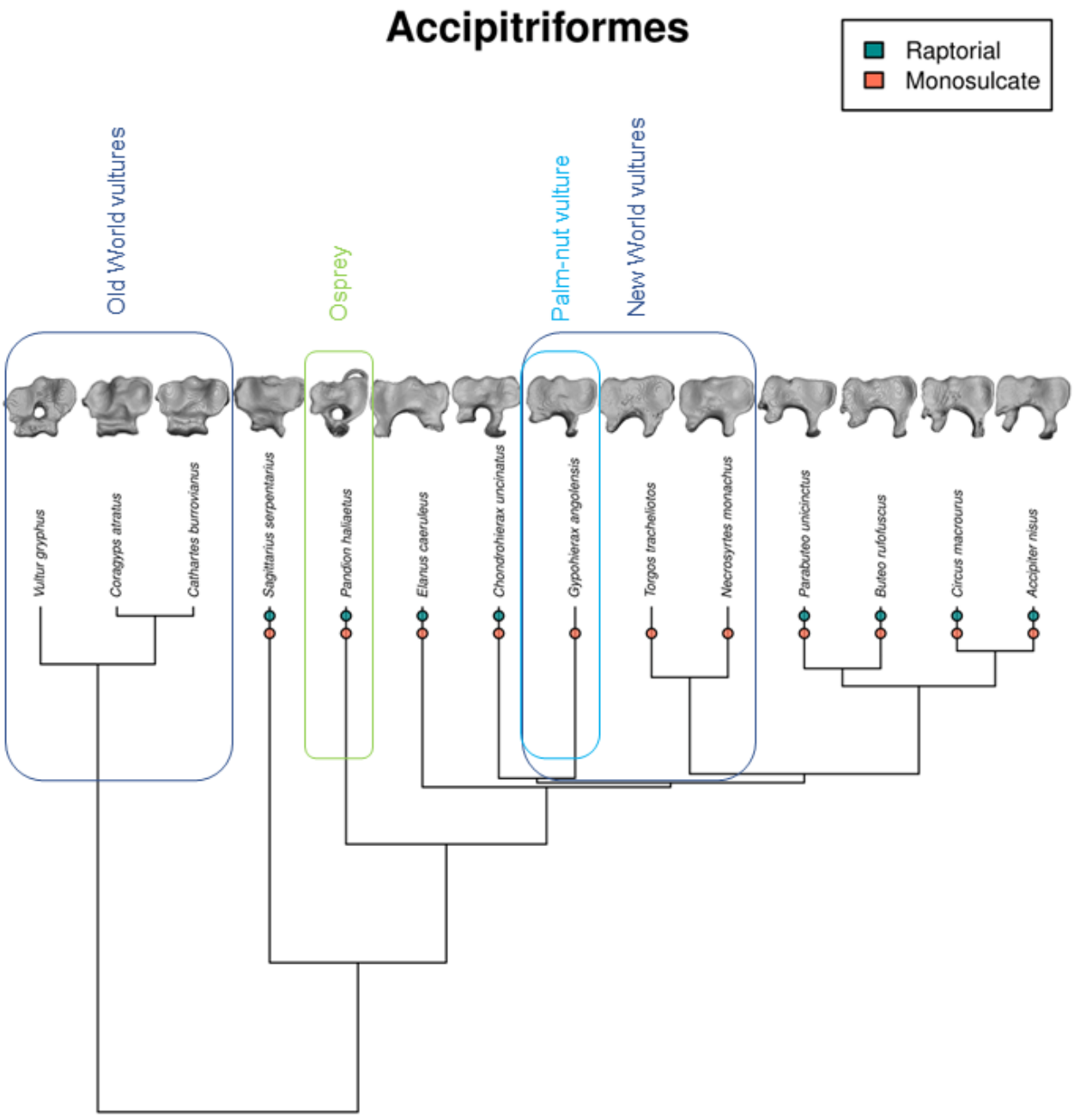


**Figure 3.** Phylogenetic tree of 14 accipitriforms, showing raptoriality and monosulcate hypotarsus shape. Proximal views of 3D models for all taxa shown. Note that the hypotarsus for *Vultur gryphus* does not possess a canal; the specimen (NHMUK S.1955.5.11) has had a hole drilled through its proximal end.

### 2.1.2 Raptoriality in Extinct Species

The hypothesis that Telluraves were primitively raptorial can be tested through evaluation of the occurrence of raptoriality among early stem-members of telluravian subclades, not only in the extant raptorial groups (Accipitriformes, Strigiformes, Falconiformes), but also the non-raptorial groups (e.g. Coraciimorphae, Psittaciformes, Passeriformes). It is also likely that this evaluation would be considerably enhanced by the incorporation of fossil evidence of the potential for raptorial foot use in the early, stem-group members of these clades. The proximity of the order Accipitriformes to the base of Telluraves puts the clade in a pivotal position in approaching the question of raptorial ancestry posed by Jarvis et al. (2014) and Prum et al. (2015). If raptorial foot use was found to be present as far stemward in Accipitriformes as their initial branching, then it is more likely that raptorial foot use was present in the common ancestor of Telluraves. If raptoriality is found to have arisen at a later point within Accipitriformes, it is most likely that raptorial foot use was converged upon by the other raptorial groups within Telluraves, and was not an ancestral trait.

To evaluate the occurrence of raptoriality in extinct species known only from fossils requires a rigorous test of the potential link between raptoriality and the monosulcate hypotarsus condition. So far, I have described the presence of a monosulcate hypotarsus in various raptorial taxa. However, the monosulcate condition also occurs in some non-raptorial birds: in Apodidae (swifts), Ciconiidae (storks), Paleognathae (ratites), and some species within Sphenisciformes (penguins). However, these monosulcate conditions are noticeably different than those of raptorial taxa, usually extending further in a plantar direction so that the deepest point of the hypotarsal sulcus is separated from the primary articular/cotylar surface by a section of solid bone (i.e. the hypotarsal sulcus is shallower; Figure 4). These observations prompted the use of

geometric morphometrics to capture shape differences of the hypotarsus and statistically interrogate the link between hypotarsus morphology and raptorial foot use, with the potential to infer raptoriality in extinct species known only from fossils.

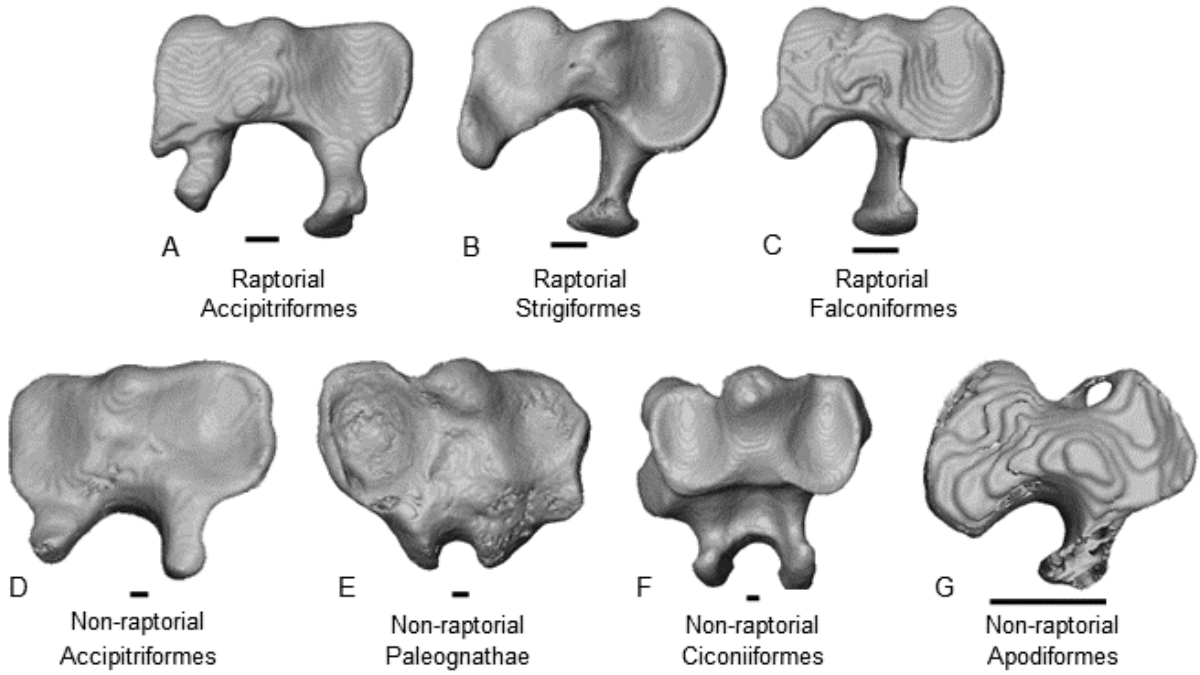


**Figure 4.** Shape comparison of 3D models of monosulcate hypotarsi in extant raptorial and non-raptorial taxa. All left sides or mirrored to left sides, scale bar is 1mm. A) *Accipiter nisus* (Eurasian Sparrowhawk; Accipitriformes); B) *Athene noctua* (Little Owl; Strigiformes); C) *Falco sparverius* (American Kestrel; Falconiformes); D) *Necrosyrtes monachus* (Hooded Vulture; Accipitriformes); E) *Apteryx australis* (Southern Brown Kiwi; Paleognathae); F) *Ciconia ciconia* (White Stork; Ciconiiformes); G) *Chaetura brachyura* (Short-tailed Swift; Apodiformes).

In this chapter, I aim to answer the following questions, using a combination of 2D geometric morphometrics and phylogenetically-informed comparative shape analysis, as well as the application of discriminant function analyses:

**1)** What is the relationship between hypotarsus shape and raptoriality?

**2)** Can the relationship between raptoriality and hypotarsus shape be used to predict the occurrence of raptoriality in telluravian fossil taxa?

By examining the tendon anatomy through the hypotarsus across six entire extant specimens each representing one of the main telluravian groups, I am also able, provisionally, to address an additional question;

**3)** Is a relationship between relative tendon size and raptoriality a possible explanation for shared hypotarsus morphology?

## 2.2 Material and Methods

### 2.2.1 Terminology

Most anatomical nomenclature is used as per Baumel and Witmer (1993). Both Latin and English equivalents are used interchangeably for muscular and osteological structures. Terminology relating to geometric morphometrics and related statistical analyses is collated from multiple sources, namely Bookstein (1997), Zelditch et al. (2004), Webster and Sheets (2010), Grafen and Hails (2002), and Burnham and Anderson (2002). The Latin names used for extant bird species are in accordance with their information as currently listed in the online *Birds of the World* (ed. Billerman et al., 2021).

### 2.2.2 Data Collection

Tarsometatarsi of extant bird skeleton and spirit specimens were imaged using x-ray microcomputed tomography scans (CT scans). These CT scan images were processed using ImageJ software (Schneider et al., 2012), and segmented, visualized and turned into 3D models using Avizo Lite software (v.9.7.0). These models are stored on the open-access digital archive Morphosource (morphosource.org). 2D images of the proximal ends of 29 fossil specimens were collected from both the literature and from museum collections.

*Institutional abbreviations*—**AMNH**, American Museum of Natural History; **BSP**, Bayerische Staatssammlung für Paläontologie und Geologie, Munich; **BMS**, Buffalo Museum of Science, New York; **FMNH**, Field Museum of Natural History, Chicago; **IRSNB**, Royal Belgian Institute of Natural Sciences; **ML**, Musée des Confluences, Lyon; **MNHN**, Musée National d'Histoire Naturelle, Paris; **MPM**, Museo Regional Provincial Padre Molina, Santa Cruz; **NHMUK**, Natural History Museum of London; **NMB**, Naturhistorisches Museum Basel; **NMA**, Naturmusuem Augsberg; **NMMNH**, New Mexico Museum of Natural History; O**UMNH**, Oxford University Museum of Natural History; **PIN**, Paleontological Institute, Russian Academy of Sciences; **UF**, University of Florida Museum of Natural History; **UMMZ**, University of Michigan Museum of Zoology; **UMZC**, University Museum of Zoology, Cambridge; **UNSM**, University of Nebraska State Museum of Natural History; **YPM**, Yale Peabody Museum, Connecticut.

The complete list of extant and fossil taxa can be found in the Appendices (Appendix Data B.1)

### 2.2.3 Qualitative Classification

The hypotarsus shape of 305 extant taxa were scored based on a classification scheme for hypotarsus morphology (Appendix Data B.1). Three of the five anatomically descriptive terms used for hypotarsal structures are adapted from Mayr (2016) (Figure 1). The primary components of the hypotarsus used for character scoring are sulci and canals. These structures are inherently framed by the lateral and medial hypotarsal crests (cristae lateralis and medialis hypotarsi; Baumel and Witmer, 1993). The two main, "deep" muscles that pass through or along the hypotarsal structures are the m. flexor hallucis longus and the m. flexor digitorum longus, even in those birds which do not possess a hallux/hindtoe (Mayr, 2016). In addition, the hypotarsus

guides a small number of superficial flexor tendons for each toe, although those for digit 2 are more frequently guided through the hypotarsus than those for digits 3 and 4 (Mayr, 2016).

Unlike the foot use scoring scheme described in Chapter 1, the scoring of the hypotarsus into just one of a mutually-exclusive set of categories excludes the possibility of one tarsometatarsus possessing multiple characters. Therefore, I used a set of separate characters, in case further research arises for which individual binary characters are required.

***1.*** *Presence of canals*: No, taxon hypotarsus does not possess canals (0); Yes, taxon hypotarsus possesses one or more canals (1).

The presence of canals through the hypotarsus does not preclude the presence of sulci (Figure 1D-F). The canal or canals may guide one or more of the muscles and tendons which pass along the plantar side of the tarsometatarsus.

***2.*** *Asulcate* (Mayr, 2016): No, taxon hypotarsus is not asulcate (0); Yes, taxon hypotarsus is asulcate (1).

An asulcate hypotarsus is defined as block-like and without canals or sulci, protruding from the articular surface of the proximal end of the tarsometatarsus, sometimes possessing very shallow furrows for flexor tendons (Figure 1A). This form of hypotarsus structure can be found in Cariamidae (seriemas), for example.

***3.*** *Monosulcate* (Mayr, 2016): No, taxon hypotarsus is not monosulcate (0); Yes, taxon hypotarsus is monosulcate (1).

A monosulcate hypotarsus is defined as a single, wide, “open” hypotarsal sulcus through which all flexor tendons pass (Figure 1B). This form of hypotarsus structure can be found in Accipitridae (hawks, eagles, and kites), for example.

***4.*** *Multisulcate*: No, taxon hypotarsus is not multisulcate (0); Yes, taxon hypotarsus is multisulcate (1).

A multiculcate hypotarsus is defined here as the presence of more than one hypotarsal sulcus, which may or may not also possess one or more canals (Figure 1C). This form of hypotarsus structure can be found in Anatidae (ducks and geese), for example.

***5.*** *Monocanaliculate* (Mayr, 2016): No, taxon hypotarsus is not monocanaliculate (0); Yes, taxon hypotarsus is monocanaliculate (1).

A monocanaliculate hypotarsus is defined here as the presence of only a single hypotarsal canal, through which all tendons pass (Figure 1E). A hypotarsus possessing one canal in addition to sulci may be scored as multisulcate, rather than monocanaliculate. This form of hypotarsus structure can be found in Gaviidae (loons), for example. Although the hypotarsi of members of Coliidae (mousebirds) and Musophagidae (turacos) are described by Mayr (2016) as being monocanaliculate, in these cases only one muscle or tendon passes through this single canal, either m. flexor hallucis longus, in the case of Coliidae (Berman and Raikow, 1984), or m. flexor digitorum longus, in the case of Musophagidae (Berger, 1960). This arrangement leaves the other muscles and tendons to pass along additional sulci, and so these taxa are instead scored as multisulcate.

***6.*** *Multicanaliculate*: No, taxon hypotarsus is not multicanaliculate (0); Yes, taxon hypotarsus is multicanaliculate (1).

A multicanaliculate hypotarsus is defined here as the presence of multiple canals through which all tendons pass, with no discernable sulci (Figure 1F). This form of hypotarsus structure can be found in most families within the order Passeriformes, for example.

The hypotarsus shape scores of 102 extant taxa were mapped onto an adapted phylogeny by Prum et al. (2015). The hypotarsus morphology and preservation state of the fossil taxa were also scored (Appendix Table C.2).

### 2.2.4 Phylogenetic Frameworks

A phylogeny of 102 extant taxa from birdtree.org (Jetz et al. 2012; based on the Hackett et al., 2008 backbone) was modified using Mesquite (Maddison and Maddison, 2019) to match higher-level relationships recovered by Prum et al. (2015). This was used to perform the phylogenetically-informed GLS analysis.

The phylogenetic information of 23 fossil taxa was included into another version of this phylogeny, so that it could be used for the phylogenetic Flexible Discriminant Analysis (PhyFDA). Inclusion of the fossil species was based on a comprehensive survey of the literature, identifying all fossil Telluraves from the Paleocene to Pleistocene for which well-preserved hypotarsus morphology has been illustrated in proximal view (N = 29 species). However, not all of these could be included in the phylogeny; of the six excluded fossil specimens, two were repeated genera and therefore redundant (*Berruornis orbisantiqui*, *Pulchrapollia* sp.), three were taxa whose affinities were too uncertain affinities to be included in the phylogeny (*Paleopsittacus georgei*, *Horusornis vianeyliandae*, Coraciiform sp.A (Lyon PQ1216)), and one taxon was too deformed to provide reliable shape data (*Messelastur gratulator*). In addition to the information in cited literature, and general temporal reasoning, the phylogenetic relationships, node and tip ages of the following fossil taxa were estimated with the aid of The Paleobiology Database (paleobiodb.org). Explanations of how fossil species were incorporated into the phylogeny are given below:

*Accipitriformes*

Accipitrid sp. (IRSNB Av0182; Figure 5A) was described as belonging generally within Accipitridae by Mayr and Smith (2019). It was originally described as having an age of 52-50 Ma (Eocene; Mayr and Smith, 2019) and was thus placed as the sister taxon to Sagittaridae, Pandionidae, and Accipitridae based on temporal reasoning, in order to accommodate the node ages resolved by Prum et al. (2015). This specimen is the proximal end of a right tarsometatarsus, free of matrix, with slightly eroded hypotarsal crests.

*Anchigyps voorhiesi* (UNSM 62877; Figure 5B) was described as belonging within Gypaetinae by Zhang et al. (2012), with an estimated age of 13.6-10.3Ma (Miocene). It was positioned as sister taxon to extant *Gypohierax angolensis* Rüppell, 1836, using their provided phylogenetic information as well as that found by Mindell et al. (2018). This specimen is a right tarsometatarsus with an entire proximal end, free of matrix.

*Gymnogyps kofordi* (UF 63512; Figure 5C) was described by Emslie (1988) as belonging to Cathartidae alongside the extant members of the genus, with an estimated age of 1.8-0.3Ma (Pleistocene). It was positioned as sister taxon to extant *Vultur gryphus* Linnaeus, 1758, using the phylogeny constructed by Johnson et al. (2016). This specimen is an entire right tarsometatarsus, free of matrix.

*Strigiformes*

*Berruornis orbisantiqui* (MNHN L3096; Figure 5D) was described by Mourer-Chauviré (1987, 1994) as having an age of 58.7-55.8Ma (Paleocene; Mourer-Chauviré, 1987, 1994) and was positioned as sister taxon to the clade comprising *Sophiornis quercynus* Mourer-Chauviré, 1987, and *Palaeobyas cracrafti* Mourer-Chauviré, 1987, to form the family Sophiornithidae (Mourer-Chauviré, 1987). Sophiornithidae is sister clade to *Eostrix tsaganica* Kurochkin and

Dyke, 2011, and the rest of Strigiformes. This specimen of *B. orbisantiqui* is a cast of an entire right tarsometatarsus, free of matrix.

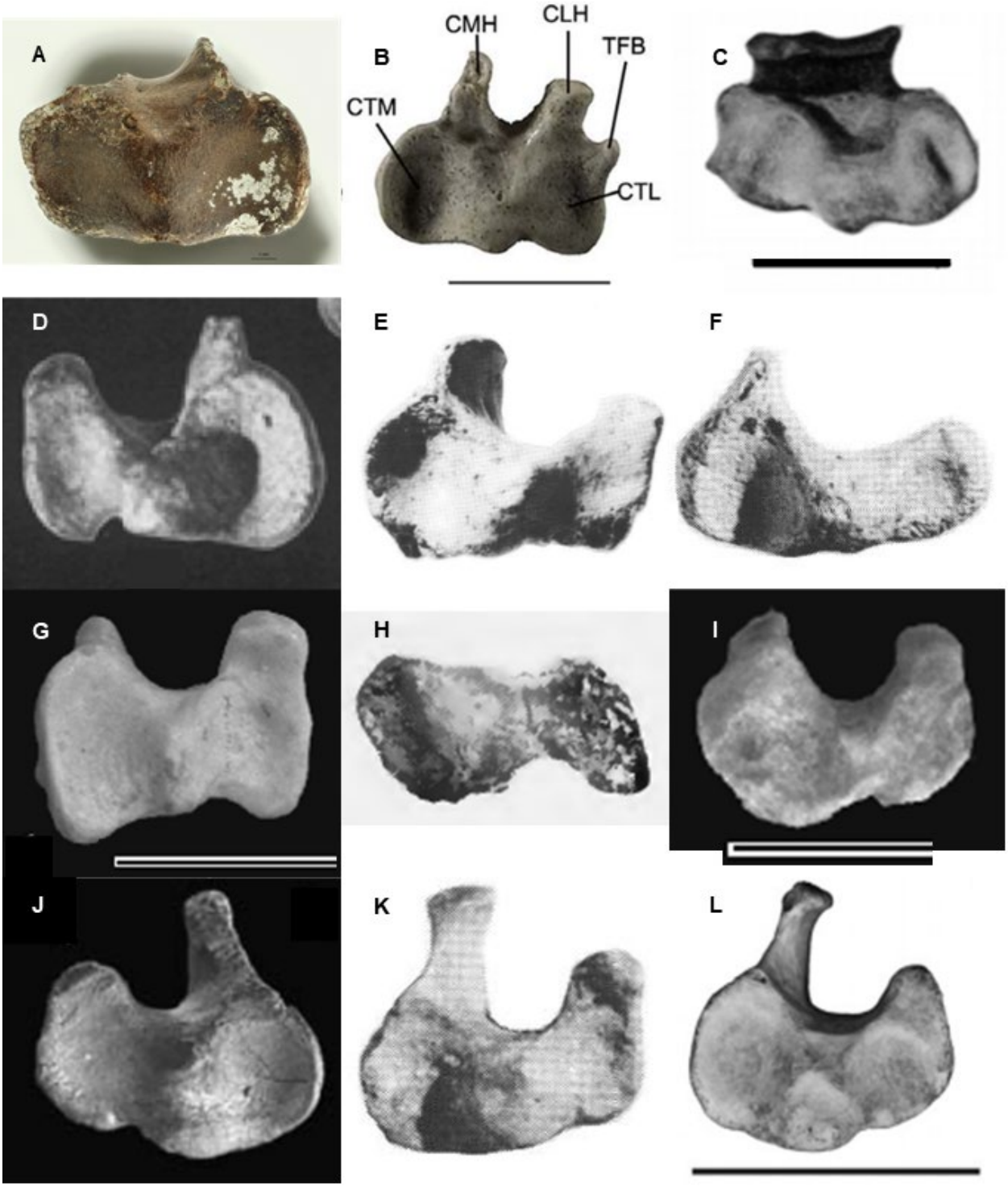


**Figure 5.** Proximal views of fossil hypotarsi analysed herein. Scale bars included where part of the original image, specimen mediolateral width given for those without. A) Accipitrid sp. (IRSNB Av0182),

right side, 1mm scale; B) *Anchigyps voorhiesi* (UNSM 62877), right side, 1cm scale; C) *Gymnogyps kofordi* (UF 63512), right side, 2cm scale; D) *Berruornis orbisantiqui* (MNHN L3096), right side, 19.4mm width; E) *Sophiornis quercynus* (Lyon PQ1202), left side, 19.9mm width; F) *Palaeobyas cracrafti* (MNHN QU15746), left side, 16.5mm width; G) *Eostrix tsaganica* (PIN 3104-147), left side, 10mm scale; H) *Ogygoptynx wetmorei* (AMNH 2653), right side, 9mm width; I) *Heterostrix tatsinensis* (PIN 3211-35), left side, 12.5mm scale; J) *Selenornis steendorpensis* (IRSNB Av84a+b), right side, 5mm scale; K) *Necrobyas harpax* (MNHN QU15695 (3195)), left side, 10.2mm width; L) *Tyto sanctialbani* (NHMUK A305), left side, 10mm scale.

*Sophiornis quercynus* (Lyon PQ1202; Figure 5E) was also described by and phylogenetically positioned by Mourer-Chauviré (1987), with an estimated age of 33.8-30Ma (Oligocene). It was positioned as sister taxon to *P. cracrafti*. This specimen is a near-complete left tarsometatarsus with an entire proximal end, free of matrix.

*Palaeobyas cracrafti*'s (MNHN QU15746; Figure 5F) exact phylogenetic position is uncertain, but was estimated by Mlikovsky (2002) to be a member of Sophiornithidae. This taxon has an estimated age of 42-30Ma (Eocene-Oligocene; Mourer-Chauviré, 1987) and was positioned as sister taxon to *S. quercynus*. This specimen is an entire left tarsometatarsus with slightly eroded hypotarsal crests, free of matrix.

*Eostrix tsaganica* (PIN 3104-147; Figure 5G) was described by Kurochkin and Dyke (2011) as belonging to its own family, Protostrigidae, which Kurochkin and Dyke (2011) estimated to be phylogenetically positioned between Sophiornithidae and Ogygoptingidae. It has an estimated age of 55.8-48.6Ma (Eocene) and was positioned as sister taxon to *Ogygoptynx wetmorei* and the rest of Strigiformes. This specimen of *E. tsaganica* is the entire proximal end of a left tarsometatarsus, free of matrix.

*Ogygoptynx wetmorei* (AMNH 2653; Figure 5H) was described by Rich and Bohaska (1976) as belonging to its own family, Ogygoptingidae, with an estimated age of 61.7-56.8Ma (Paleocene-Eocene). It was positioned as sister taxon to *Heterostrix tatsinensis* Kurochkin and

Dyke, 2011, and the rest of Strigiformes. This specimen is a near-complete right tarsometatarsus with eroded hypotarsal crests, free of matrix.

*Heterostrix tatsinensis* (PIN 3211-35; Figure 5I) was described and positioned phylogenetically by Kurochkin and Dyke (2011), within its own family, Heterostrigidae, with an estimated age of 33.9-28.4Ma (Oligocene). It was positioned as sister taxon to the family Strigidae. This specimen is an entire left tarsometatarsus free of matrix.

*Selenornis steendorpensis* (IRSNB Av84a+b; Figure 5J) was described by Mayr (2009a) with an estimated age of 31-28Ma (Oligocene). It was positioned as sister taxon to *Necrobyas harpax* Milne-Edwards, 1892, and the rest of Tytonidae based on phylogenetic estimations by Mayr (2009article). This specimen is an entire right tarsometatarsus free of matrix.

*Necrobyas harpax* Milne-Edwards, 1892, was described as having an estimated age of 37-33.8Ma (Eocene-Oligocene) and was positioned as sister taxon to *Tyto sanctialbani* and the rest of Tytonidae based on the phylogeny constructed by Mourer-Chauviré (1987). This specimen of *N. harpax* (MNHN QU15695 (3195); Figure 5K) is an entire left tarsometatarsus free of matrix.

*Tyto sanctialbani* (NHMUK A305; Figure 5L) was described by Pavia and Mourer-Chauviré (2011) with an estimated age of 12.75-9.7Ma (Miocene). It was positioned as sister taxon to the rest of extant Tytonidae based on information from Pavia and Mourer-Chauviré (2011). This specimen is an entire left tarsometatarsus free of matrix.

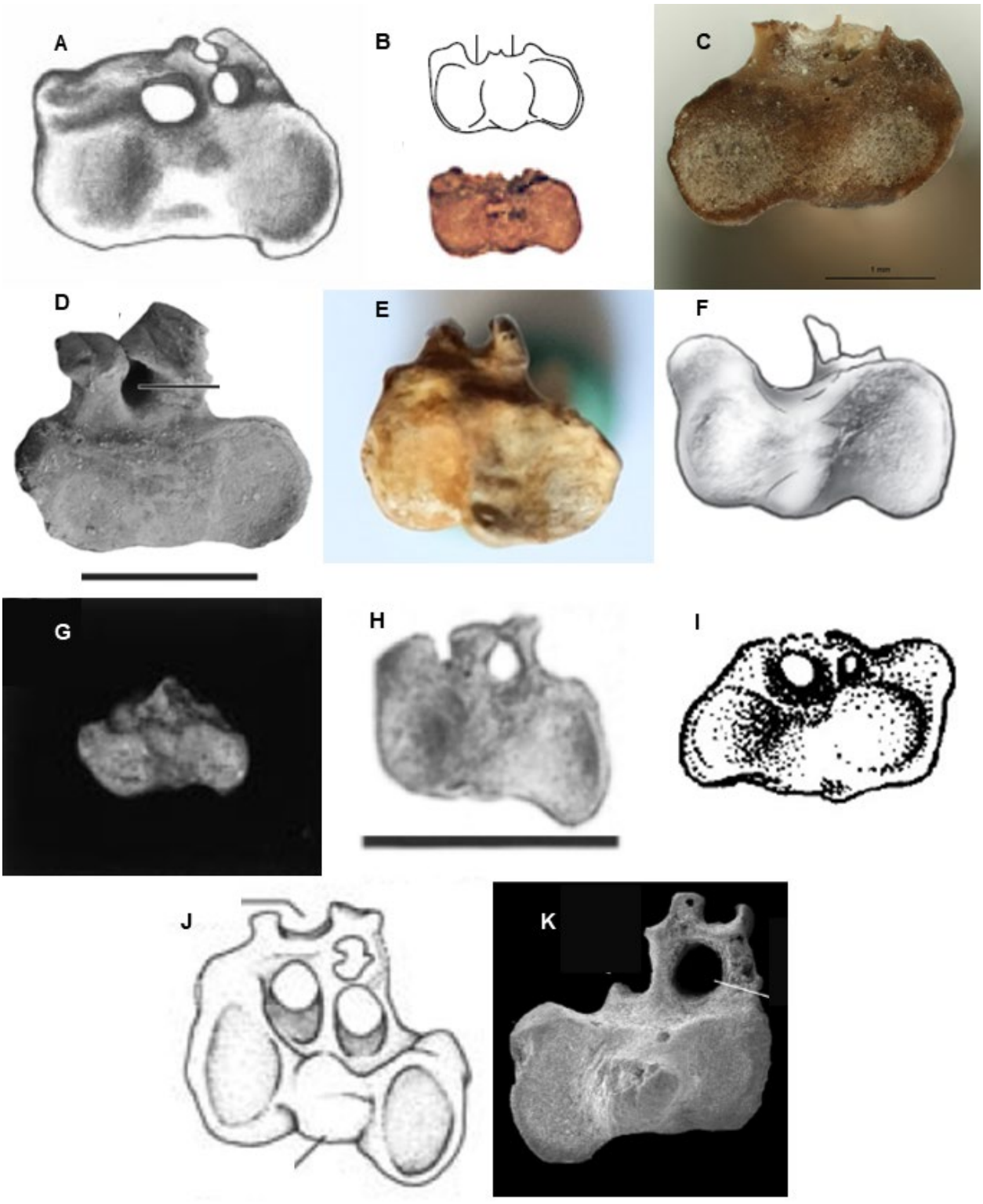


**Figure 6.** Proximal views of fossil hypotarsi analysed herein. Scale bars included where part of the original image, specimen mediolateral width given for those without. A) *Anneavis anneae* (BMS E25337), right side, 5.8mm width; B) *Tsidiiyazhi abini* (NMMNH P54128), left side, 5mm scale; C) Alcediniform sp.A (IRSNB Av0188), left side, 1mm scale; D) *Septencoracias* sp. (IRSNB Av0191), right side, 2.5mm scale; E) *Elaphrocnemus phasianus* (NMB QH158a), left side, 10mm width; F) *Thegornis*

*musculosis* (MPM PV-3443), right side, 17.1mm width; G) *Pulchrapollia gracilis* (BMNH PVA6207), right side, 4.4mm width; H) London Clay sp. A (WN 89627A), right side, 5mm scale; I) *Bavaripsitta ballmanni* (BSP 1970XVIII899), left side, 3.5mm width; J) *Certhiops rummeli* (NMA 2007.51.2021), right side, 2.5mm width; K) *Miocorvus larteti* (MNHN SA1263c), left side, 1mm scale.

*Coraciimorphae*

*Anneavis anneae* (BMS E25337; Figure 6A) was described by Houde and Olson (1992) as belonging to Sandcoleiformes, with an estimated age of 63-54Ma (Paleocene-Eocene). It was positioned within a clade with *Tsidiiyazhi abini* Ksepka et al., 2017, which was sister to Coliidae based on the phylogeny constructed by Ksepka et al. (2017). This specimen of *A. anneae* is composite illustration of a presumed entire right tarsometatarsus, embedded in a flat slab of matrix along with other articulated post-cranial elements.

*Tsidiiyazhi abini* (NMMNH P54128; Figure 6B) was described by Ksepka et al. (2017) with an estimated age of 62.2-62.5Ma (Paleocne). It was positioned as sister taxon to *A. anneae* within Sandcoleiformes based on the phylogeny constructed by Ksepka et al. (2017). This specimen is the proximal and distal ends of a left tarsometatarsus, free of matrix, with eroded and/or broken hypotarsal crests.

Alcediniform sp.A (IRSNB Av0188; Figure 6C) was described by Mayr and Smith (2019) with an estimated age of 54-51Ma (Eocene). It was positioned within Coraciimorphae as sister taxon to extant *Chloroceryle amazona* Latham, 1790, based on temporal reasoning and the phylogeny constructed by Ksepka et al. (2017). This specimen is an entire left tarsometatarsus with slightly eroded hypotarsal crests, free of matrix.

*Septencoracias* sp. (IRSNB Av0191; Figure 6D) was described by Bourdon et al. (2016) with an estimated age of 54-48Ma (Eocene). It was positioned within Coraciidae as sister taxon to extant *Merops orientalis* Latham, 1801, based on information from Mayr and Smith (2019)

and Ksepka et al. (2017). This specimen is a right tarsometatarsus lacking one of the distal trochlea, free of matrix.

*Cariamiformes*

*Elaphrocnemus phasianus* Milne Edwards, 1891, was reassigned by Mayr (2009b) as belonging to the Cariamiformes, with an estimated age of 35.5-32Ma (Eocene-Oligocene). It was positioned as sister taxon to the rest of extant Cariamiformes based on this phylogenetic reassignment (Mayr, 2009book) and temporal reasoning. This specimen of *E. phasianus* (NMB QH158a; Figure 6E) is an entire left tarsometatarsus with slightly eroded hypotarsal crests, free of matrix.

*Falconiformes*

*Thegornis musculosis* Ameghino, 1894, was described by Noriega et al. (2011) with an estimated age of 17.5-16.3Ma (Miocene). It was positioned within the family Falconidae as sister taxon to *Micrastur ruficollis* based on phylogenetic estimations by Noriega et al. (2011). This specimen of *T. musculosis* (MPM PV-3443; Figure 6F) is a right tarsometatarsus lacking one of its distal trochlea, with a broken medial hypotarsal crest, free of matrix.

*Psittaciformes*

*Pulchrapollia gracilis* (BMNH PVA6207; Figure 6G) was described by Dyke and Cooper (2000) and Ksepka and Clarke (2012) with an estimated age of 53-52Ma (Eocene). It was positioned within Halcyornithidae (Harrison and Walker, 1972) as sister taxon to Psittaciform sp.A (WN 89627A) and the rest of Psittaciformes based on phylogenetic estimations by both Dyke and Cooper (2000) and Ksepka and Clarke (2012). This specimen is an entire right tarsometatarsus with slightly eroded hypotarsal crests, free of matrix.

Psittaciform sp.A, or London Clay sp.A (WN 89627A; Figure 6H) was described by Mayr and Daniels (1998) with an estimated age of 55.8-48.6Ma (Eocene). It was positioned as sister taxon to the rest of Psittaciformes based on phylogenetic estimations by Ksepka and Clarke (2012). This specimen is a presumed entire right tarsometatarsus, free of matrix.

*Bavaripsitta ballmanni* (BSP 1970XVIII899; Figure 6I) was described by Mayr and Gohlich (2004) and Waterhouse (2006) with an estimated age of 15-13.5Ma (Miocene). It was positioned within the extant family Cacatuidae as sister taxon to the clade of *Barnardius* + *Deroptyus* + *Psittacus* based on the phylogeny constructed by Crouch et al. (2019). This specimen is an illustration of a presumed entire left tarsometatarsus free of matrix with slight erosion on the medial hypotarsal crest.

*Passeriformes*

*Certhiops rummeli* (NMA 2007.51.2021; Figure 6J) was described by Manegold (2008) with an estimated age of 20.5-18Ma (Miocene). It was positioned within Certhioidea as sister taxon to *Troglodytes troglodytes* Linnaeus, 1758, using temporal reasoning and phylogenetic estimations by Manegold (2008). This specimen is an illustration of a near-complete right tarsometatarsus, free of matrix.

*Miocorvus larteti* (MNHN SA1263c; Figure 6K) was described by Manegold et al. (2004) with an estimated age of 15-3Ma (Miocene-Pliocene). It was positioned within the extant family Corvidae as sister taxon to extant *Corvus albus* Muller, 1776, based on phylogenetic estimations by Mourer-Chauviré (2004). This specimen is the proximal end of a left tarsometatarsus, free of matrix.

### 2.2.5 Geometric Morphometrics: Taxon Sample

I selected 102 extant taxa for morphometric analysis, spanning a broad range of ecologies and hypotarsus types across the extant avian tree, based on screenshots in orthogonal view (i.e. lacking parallax) of the proximal surface (Appendix Figures C.1-6). Images of the proximal ends of 29 fossil specimens were collected from both published articles and museum collections. The fossil taxa span from the Early Paleocene to the Late Miocene in age, and cover the stem lineages of all telluravian groups except for Passeriformes.

### 2.2.6 Geometric Morphometrics: Landmarking

These images were then landmarked according to the hypotarsus landmarking scheme below (Figure 7), using Avizo visualization and analysis software. Sliding semilandmarks were used so that the effect of initial differences in landmark placement, spacing, and number along the curved surface of individual specimens, could be removed, and the landmarks could be treated equally in subsequent statistical analyses (Gunz and Mitteroecker, 2013).

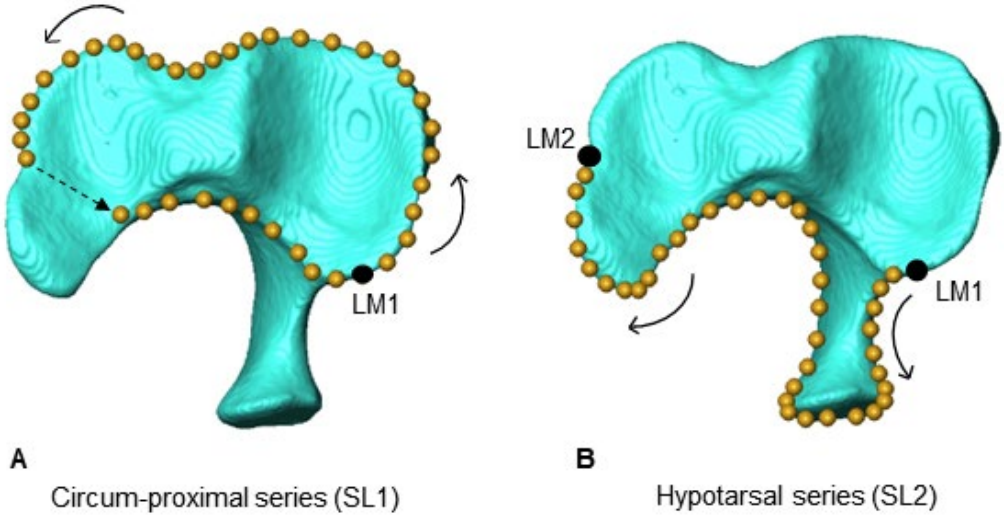


**Figure 7.** The hypotarsus landmarking scheme shown on the proximal view of 3D model of *Nyctea scandiaca*, left side. A) The circum-proximal semilandmark series, with landmark 1 (junction of medial

hypotarsal crest and medial cotyle ridge) marked; B) The hypotarsal semilandmark series, with landmark 1 (junction of medial hypotarsal crest and medial cotyle ridge) and landmark 2 (junction of the lateral hypotarsal crest and the lateral cotyle ridge).

The nature of geometric morphometrics requires the landmarks used to be placed on biologically homologous points on the structure or shape to be studied. A compromise must be made in the case of structures which often lack homology between species, such as the hypotarsus on the tarsometatarsus. Sliding semi-landmarks (set series of landmarks placed along curves or surfaces) assist in this compromise, as they are able to follow shape outlines without necessarily requiring the use of fixed point, homologous landmarks. The absence of homology between all types of hypotarsal structures means that the closest method to capture the shape variation with geometric morphometrics involves the landmarking of only external, or outlining shapes/surfaces. It is impossible to capture internal form (i.e. hypotarsal canals) in a homologous manner because canals vary in presence, absence and number among the species studied here. The discrete character system (above) is able to provide supplementary shape information to the 2D landmarks, particularly the character scoring the presence of canals. Without the scoring of this character it would otherwise be impossible to differentiate between asulcate and mono- or multicaniculate hypotarsi, for example.

It is not possible to place 2D landmarks along the hypotarsus in multiple semi-landmark series (such as separate medial and lateral series, or series of individual hypotarsal protrusions), because these are non-homologous structures across taxa. The potential advantages of enabling the capture of multiple semi-landmark series are greatly outweighed by the difficulties that may arise. Deciding which hypotarsal structures belong to medial or lateral sides in non-monosulcate hypotarsi, or remaining consistent between taxa with differing numbers of hypotarsal protrusions, would become too subjective, and this cannot be done in practice.

Therefore, the approach used here for external 2D semi-landmarking involves the use of two semi-landmark series. One series is a closed loop which outlines the proximal end of the tarsometatarsus, but excludes the external hypotarsus shape, similar to the semi-landmark series used in the Chapter 1 section on tarsometatarsus shape analysis. The other series is an open-ended outline of the hypotarsal crests. The detailed description of these semi-landmark series is as follows:

*Semi-landmark series 1. Circum-proximal series*

This semi-landmark series starts at the junction of the medial hypotarsal crest and medial cotyle ridge. It runs outside the medial edge of the entire proximal articular surface in a dorsal direction, then along the dorsal edge in a medial-to-lateral direction, then along the lateral edge in a dorsal-to-plantar direction. Bypassing the lateral and medial hypotarsal crests, the series then runs along the plantar edge of the hypotarsus in a lateral-to-medial direction. It terminates just lateral to the starting point. This series was resampled to an equal count of 40 equally-spaced points in all species studied here using the function digit.curves from the R package geomorph (version 3.2.1; Adams, 2020).

For taxa which possess a canal on the dorsal side of the proximal end of the tarsometatarsus, for the extensor digitorum longus tendon to pass through (e.g. *Pandion haliaetus* or *Aegolius acadicus*), the semilandmark series follows the plantar side of the canal, as this is homologous to the semilandmark path on taxa which do not possess the canal.

*Semi-landmark series 2. Hypotarsal series*

This semi-landmark series starts at the point-landmark junction of medial hypotarsal crest and medial cotyle ridge. It runs outside the medial edge of the medial hypotarsal crest in a plantar direction, and follows this outside edge of the hypotarsal structure in a medial-to-lateral

direction. The series follows any inward curves that are accessible as external edges, and terminates at the point-landmark junction of the lateral hypotarsal crest and the lateral cotyle ridge. This series was resampled to an equal count of 32, equally-spaced points in all species studied here using the function digit.curves from the R package geomorph (version 3.2.1; Adams, 2020).

The landmarks were read from Avizo and converted to a format that could be analysed in R package geomorph (version 4.0.1; Adams et al., 2021). Reading from Avizo was achieved using a set of R functions provided by R. Benson, which use functions from the packages geomorph and stringdist (version 0.9.8; van der Loo, 2020). I prepared my 2D shape data so that all right and left landmarked hypotarsi were flipped to left sides. This landmark data was subsequently processed using generalized Procrustes analysis (GPA) using the gpagen function of the R package geomorph version 3.2.1 (Adams, 2020). This procedure removes differences in landmark configuration due to rotation, translation, and scale information of the 2D landmark constellations, allowing for hypotarsus shape (Procrustes coordinates) to be analysed independently of these factors.

### 2.2.7 Generalized Procrustes Analysis, and Principal Components Analysis

Shape data from the landmarks were read from Avizo, resampled to equal point counts, and then processed in a generalized Procrustes analysis using the geomorph (Adams, 2021) and stringdist (van der Loo, 2020) packages, in specialized R code provided by R. Benson. The Procrustes shape data was visualized along the primary axes of variation in a Principal Components analysis using geomorph's gm.prcomp function (Collyer and Adams, 2021).

A principal components analysis (PCA) was performed on the 2D shape data of extant taxa using the gm.prcomp function of geomorph (Adams, 2020) to visualise overall patterns of

shape variation. A PCA reordinates data points along the primary axes of variation in the data, and this process better visualized the largest ranges in morphology among the taxa.

### 2.2.8 Statistical Analyses

The shape data for extant taxa was then used as the dependent variable in a statistical model to test the effects of raptoriality, centroid size, and mean body mass on hypotarsus shape. The model was a phylogenetically informed regression with Procrustes shape variables, via the procD.pgls function of geomorph (Adams, 2014; 2020), which took shape data, raptoriality scoring, and body mass measurement, and performed a linear regression that took phylogenetic distance between taxa into account. The outputs of this analysis were a set of coefficients for each variable, and an ANOVA table with $R^2$ and p-values to indicate a variable's significance and strength in the model. A non-phylogenetic linear model, without potential correction from phylogenetic bias, was also conducted, using the procD.lm function of geomorph (Adams, 2014; 2020). No mathematical correction was made for multiple comparisons; only six planned comparisons between raptoriality, centroid size, and mean body mass were performed using procD.pgls, and only the model describing the effects of raptoriality on variation in hypotarsus was performed using procD.lm.

Idealised shape deformations were created using the coefficients of the best procD.pgls and procD.lm models, inputting the presence or absence of raptoriality, and plotting the resulting landmark constellations. This process visualizes the independent effects of raptorial foot use on hypotarsus shape. Model regression scores were also plotted against input raptorial foot use scores to visualise the shape-space relationship between foot use and hypotarsus shape, and the potential overlap of hypotarsus shapes belonging to raptorial and non-raptorial species in my extant sample.

Hypotarsus shape data from both the extant and fossil taxa were used in a linear discriminant analysis (lda, MASS package; Ripley, 2021), a flexible discriminant analysis, (fda, mda package; Hastie and Tibshirani, 2020), a mixed discriminant analysis (mda, mda package), and finally a phylogenetic flexible discriminant analysis (PhyFDA; Motani and Schmitz, 2011) to predict the likelihoods of raptoriality for each fossil taxon. Discriminant function analyses take a set of sample data for which the classification is known, and predict the classification of a set of test data based on statistical similarities to the sample data. In this case, the extant taxa provide the sample set of hypotarsus shapes, because their raptoriality is known, and the raptoriality of fossil taxa are predicted based on the similarity of their hypotarsus shapes to known raptorial, extant taxa. Prior probabilities for all analyses were set at 80% non-raptorial to 20% raptorial given the counts of 81 non-raptorial and 21 raptorial extant species in the data set. Posterior correct classification rate of the test set was determined by confusion matrices.

### 2.2.9 Analysis of Soft Tissue

To investigate differences in relative tendon sizes and the possibility that these differences might explain the occurrence of monosulcate hypotarsi or other hypotarsal traits of raptorial birds, the tarsometatarsi and distal flexor tendons of six extant birds (*Accipiter nisus, Corvus corone, Falco tinnunculus, Lorius garrulus, Picus viridis, Strix aluco*) representing the six main phylogenetic groups within Telluraves were scanned and segmented into 3D models using Avizo software. Two cross-sectional images of tendon and bone were taken perpendicular to the long axis of the tarsometatarsus. The first image was taken at the proximal “entrance” of tendons into the hypotarsus (i.e. the top of the hypotarsal crests; Figure 8), as well as at the distal “exit” of tendons from the hypotarsus (i.e. the bottom of the hypotarsal crests; Figure 9). These

points in relation to hypotarsal crest morphology were determined by the same definition as used in the 3D landmarking scheme of Chapter 1.

Cross-sectional area measurements were taken using the point-counting method, in which a grid pattern is overlaid on the image, and the number of squares for which the tendon or bone comprises over half of the square's area is counted. Using the scalebars of the original image, the cross-sectional area of both bone and tendon was calculated from the point counts, across both top and bottom image slices for each species. In addition, cross-sectional measurements for specifically the flexor digitorum longus and flexor hallucis longus tendons were taken, as these are the tendons primarily associated with the forceful grasping displayed by raptorial birds (Raikow, 1985; Sustaita et al., 2013). These bone and tendon measurements were also compared to the total body mass of the dry specimens, as well as to the average species masses (Birds of the World; ed. Billerman, 2021) in a linear regression model using procD.pgls to account for phylogenetic relationships in a measure of the relative variation in tendon size across the six representative species.

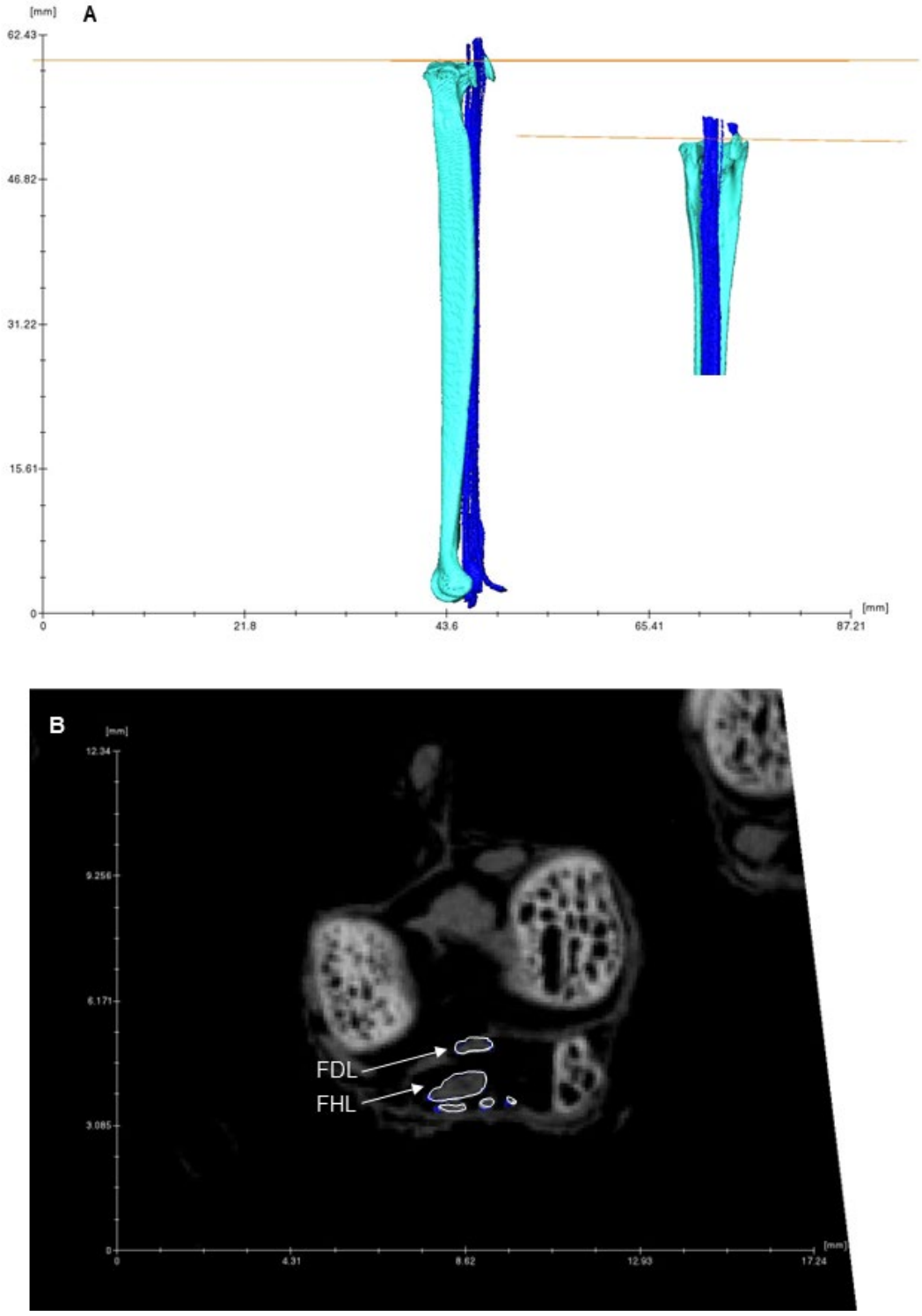


**Figure 8.** A) Lateral view of the 3D model of *Accipiter nisus* tarsometatarsus (green) and flexor tendons (blue). Red line indicates where the top cross-sectional image was taken. Inset image shoes plantar view of the model and line. B) Proximal cross-section view of the CT scan of *Accipiter nisus* tarsometatarsus and soft tissue. Flexor digitorum longus (FDL) and flexor hallucis longus (FHL) are labelled, and all flexor tendons are outlined in white.

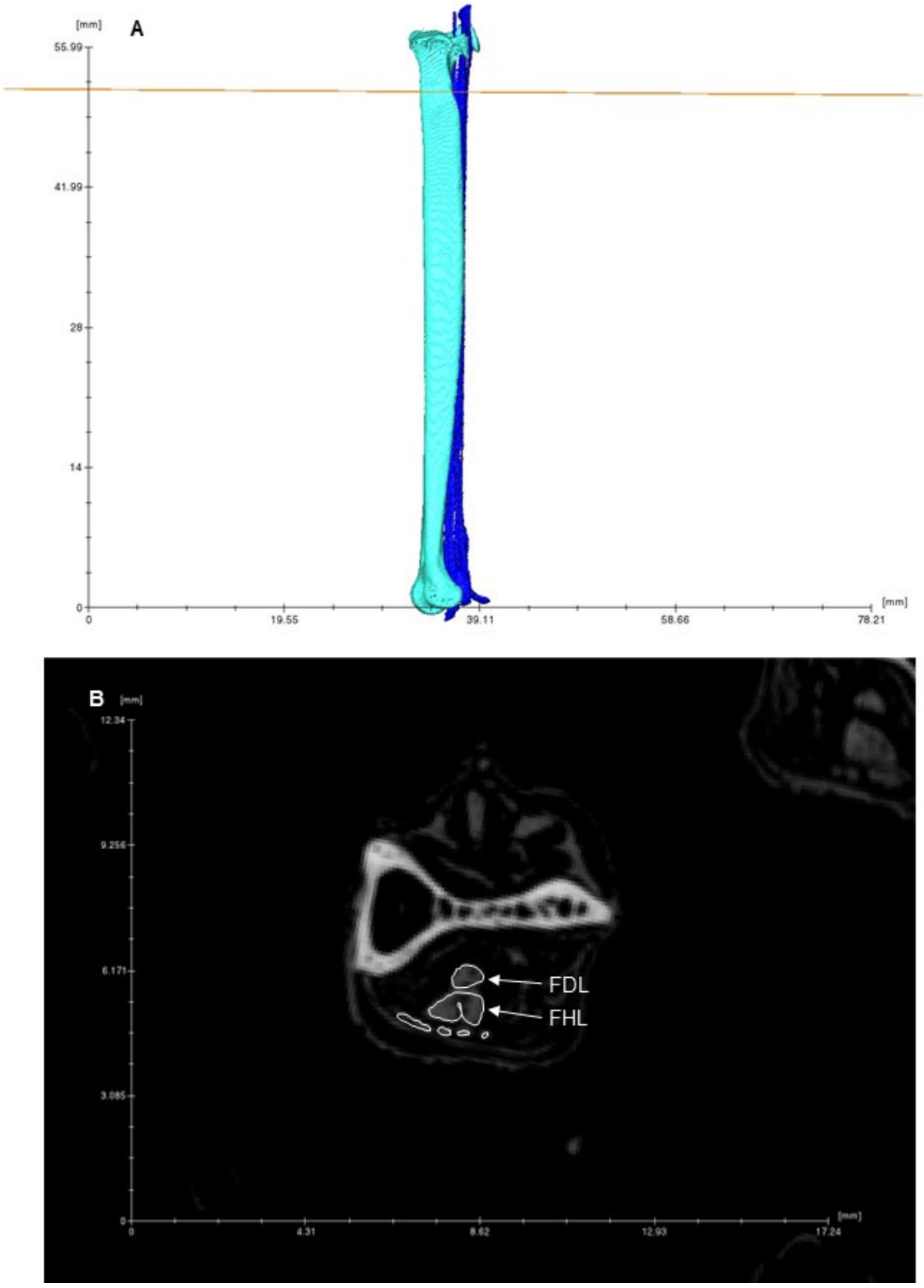


**Figure 9.** A) Lateral view of the 3D model of Accipiter nisus tarsometatarsus (green) and flexor tendons (blue). Red line indicates where the bottom cross-sectional image was taken. B) Proximal cross-section view of the CT scan of Accipiter nisus tarsometatarsus and soft tissue. Flexor digitorum longus (FDL) and flexor hallucis longus (FHL) are labelled, and all flexor tendons are outlined in white.

## 2.3 Results

### 2.3.1 Analysis of Extant Taxa: Principal Components Analysis

The principal components analysis of extant birds provides an ordination of my 2D shape data, describing the distribution of species with reference to major aspects of hypotarsus shape variation. Principal component 1 (PC1) represents approximately 35.14% of the shape variation in the hypotarsus. PC2 and PC3 subsequently represent 17.12% and 11.39% of the variation respectively.

PC1 (Figure 10; Appendix Figure C.7) describes a shift in the relative width of the space between the medial and lateral hypotarsal crests (i.e. the hypotarsal sulcus). The negative values of PC1 correspond to hypotarsi with a wide and deep hypotarsal sulcus, which curves in to meet the proximal articulating surface. Positive values of PC1 correspond to hypotarsi which lack a sulcus, with the two hypotarsal crests instead forming one singular plantar prominence which is squared-off at its plantar end. As well, Positive values of PC1 correspond to hypotarsi with a dorsoventrally wider lateral side of the articular surface, whereas negative values correspond to a much more rounded shape of this feature.

PC2 (Figure 10; Appendix Figure C.8) primarily describes variation in the range of squareness of the articular surface, a mediolateral shift in positioning of the hypotarsal crests, and the presence of a hypotarsal sulcus. Negative values of PC2 correspond to proximal ends of the tarsometatarsus with a more rounded articular surface, a centrally positioned hypotarsus, and a shallow hypotarsal sulcus created by the plantarward prominence of the medial hypotarsal crest. Positive values of PC2 correspond to proximal ends with a more rectangular articular surface, a much more laterally positioned hypotarsus, and no hypotarsal sulcus.

PC3 (Figure 10; Appendix Figure C.9) primarily describes variation in the width of the hypotarsus relative to the proximal articular surface, and the presence of a hypotarsal sulcus as it relates to the mediolateral positioning of the hypotarsal crests. Negative values of PC3 correspond to hypotarsi which join to the articular surface at its medial and lateral edges, and lack a hypotarsal sulcus. The extent of the hypotarsus in this case covers the entire plantar side of the proximal articular surface. Positive values of PC3 correspond to hypotarsi which join to the articular surface on its plantar side, and which possess a shallow hypotarsal sulcus. The extent of the hypotarsus for positive values of PC3 leave the most medial and lateral portions of the plantar side of the proximal articular surface exposed.

### 2.3.2 Analysis of Extant Taxa: Generalized Procrustes Analysis

My procD.pgls analysis indicates that 2.4% of the variation in the hypotarsus shape of extant Telluraves can be explained by the independent effects of raptoriality (adj-$R^2$ = 0.024; p = 0.002*; Appendix Table C.1). In contrast, the effects of centroid size and mean body mass on hypotarsus shape are not significant, suggesting no role for static allometry in determining hypotarsus shape in Telluraves. The coefficients of raptoriality in my model "shape ~ raptoriality" demonstrate that raptorial foot use is associated with hypotarsus shape deformations that give rise to a deeply monosulcate condition in raptorial taxa compared to their non-raptorial relatives, which possess non-monosulcate, or only shallow monosulcate hypotarsi (Figure 11a).

Because PhyFDA indicated an optimal λ value of zero in the relationship between hypotarsus shape and raptorial foot use (see below), an ordinary (i.e. non-phylogenetic) linear model of the shape data was also evaluated, to examine the relationship between raptorial foot use and hypotarsus shape without the influence of phylogenetic signal. The results indicate that

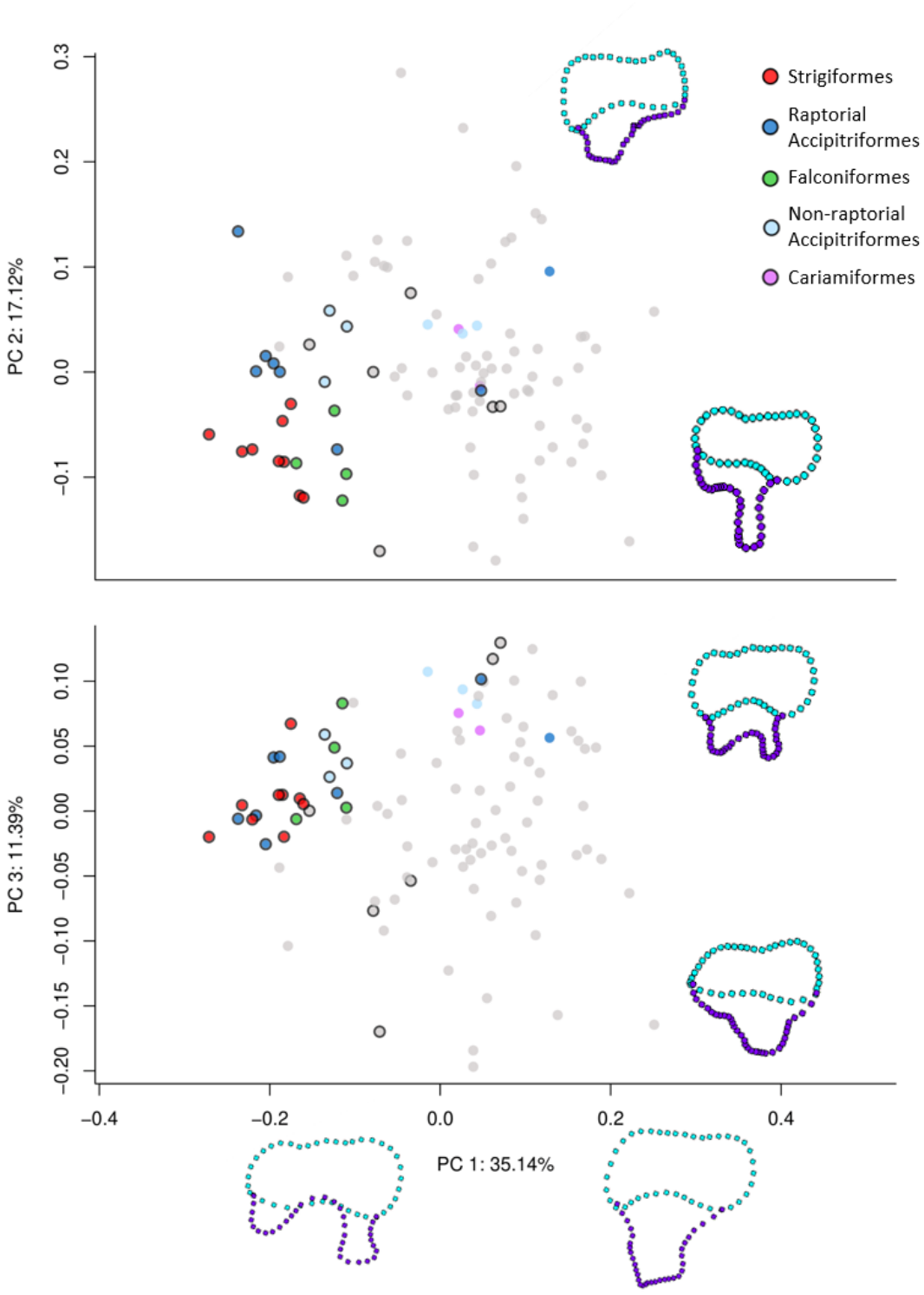


**Figure 10.** Principal components plot of extant taxa (N = 102). Bolded outlines refer to monosulcate hypotarsus shape. Superimposed hypotarsus landmark shapes represent the negative and positive values of each principal component, and describe the range in shape variation. All hypotarsus landmark shapes are left sides.

16% of the variation in hypotarsus shape can be explained by raptorial foot use (adj-$R^2$ = 0.16; p = 0.001*; Appendix Table C.1). The coefficients of raptoriality in this model also demonstrate that raptorial foot use is associated with a deeply monosulcate hypotarsal condition (Figure 12a). This idealised hypotarsus from the ordinary GLS model possessed an even deeper sulcus than the shape produced from the pGLS model.

The regression scores from both the pGLS model (procD.pgls) and the ordinary GLS model (procD.lm) were plotted against the raptorial foot use scores. These plots suggests that, in spite of the relatively small proportion of overall tarsometatarsus shape variation explained by raptoriality, raptorial hypotarsi show little overlap with non-raptorial hypotarsi in shape space (Figure 13). This finding suggests that hypotarsus shape could be used to make confident predictions of raptoriality in fossil species. This hypothesis was evaluated using discriminant function analysis (see below).

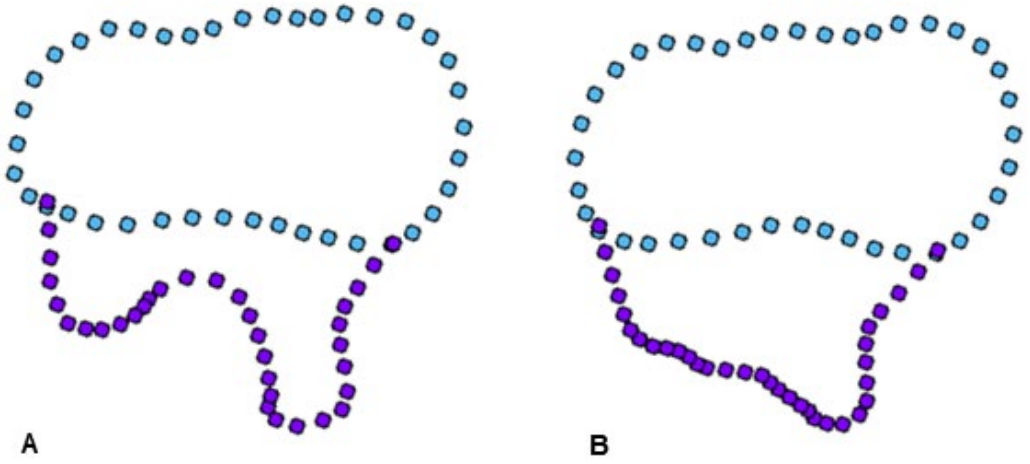


**Figure 11.** Hypotarsus landmark idealized shape deformations using the coefficients of the procD.pgls model "shape ~ raptoriality". Hypotarsi are left sides. A) the independent effects of raptoriality on hypotarsus shape; B) non-raptorial hypotarsus shape.

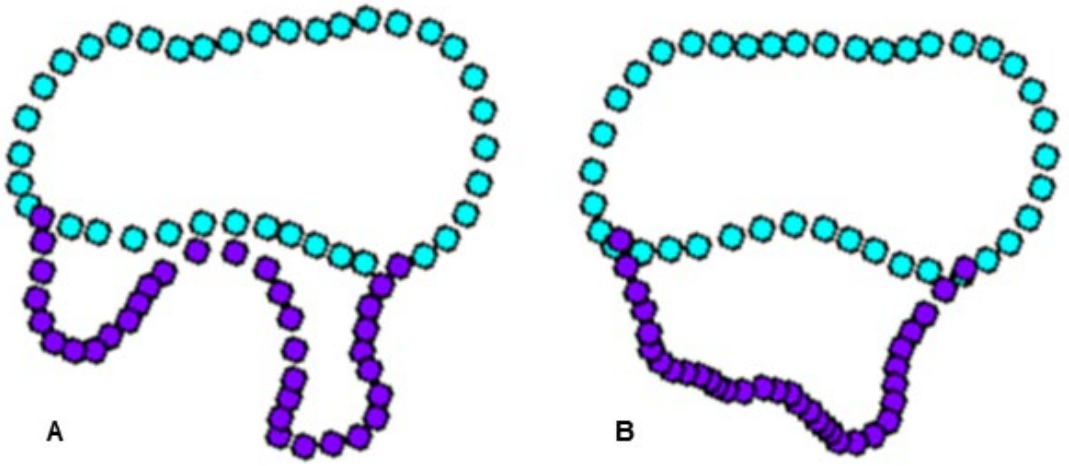


**Figure 12.** Hypotarsus landmark idealized shape deformations using the coefficients of the procD.lm model "shape ~ raptoriality". Hypotarsi are left sides. A) the independent effects of raptoriality on hypotarsus shape; B) non-raptorial hypotarsus shape.

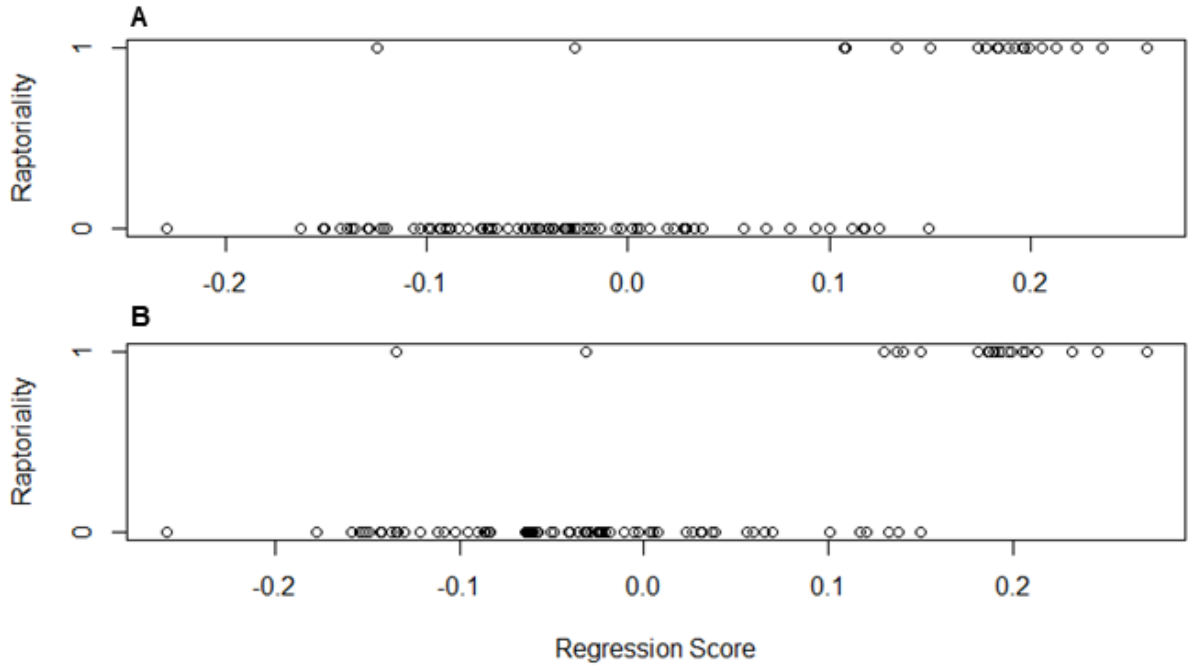


**Figure 13.** Raptorial foot use scores plotted against the regression scores from A) the procD.pgls model "shape ~ raptoriality"; B) the procD.lm model "shape ~ raptoriality".

### 2.3.3 Analysis of Fossil Taxa: Principal Components Analysis

A combined PCA of both fossil and extant taxa was performed in order to initially compare the potentially raptorial fossil taxa with known raptorial extant taxa (Figure 14). The fossil strigiforms overlap with the extant raptorial taxa in shape space, and even extend further into the positive PC2 and negative PC1 regions than extant taxa. The monosulcate fossil taxa generally overlap with the monosulcate extant taxa as well, including the fossil accipitrids and the falconiform *Thegornis musculosis*.

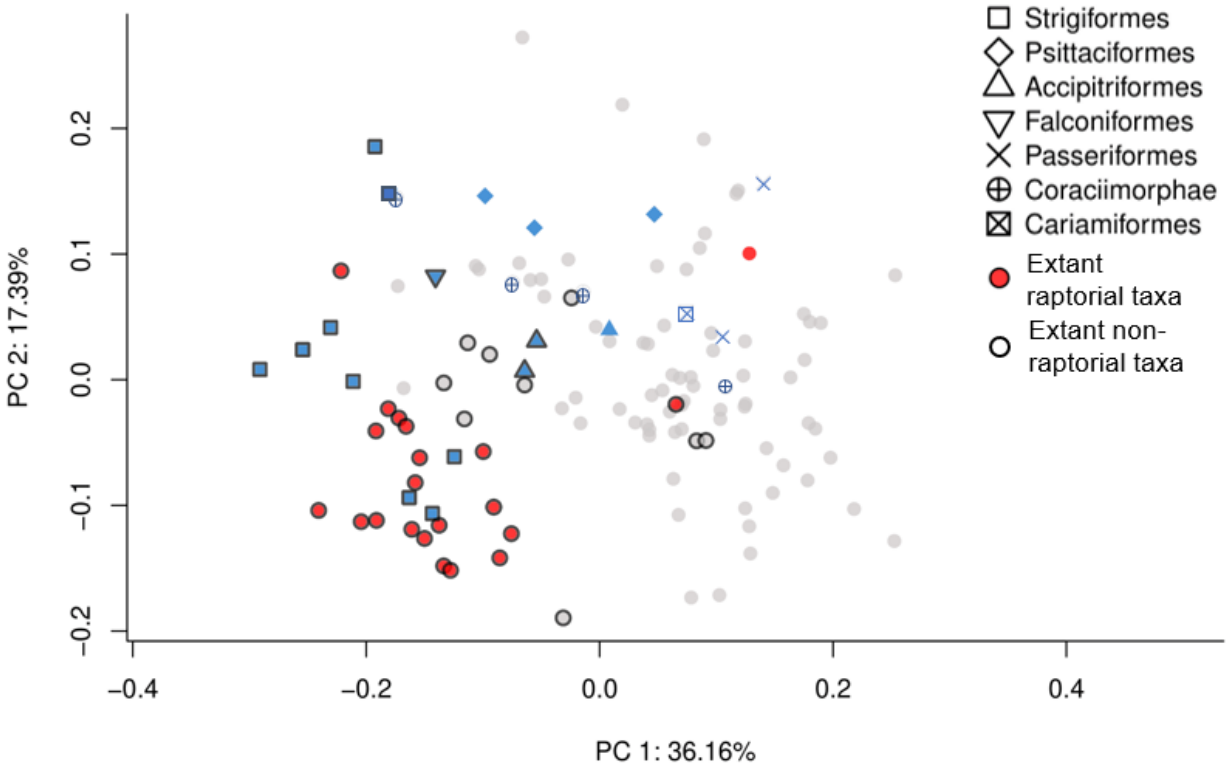


**Figure 14.** Principal components plot for both extant and fossil taxa (N = 125). Bolded outlines refer to monosulcate hypotarsus shape. Blue colouring refers to fossil taxa, red colouring refers to extant raptorial taxa.

### 2.3.4 Discriminant Function Analyses

The optimal Pagel's λ value for my data was determined to be zero, calculated using the optimal lambda value search function from Schmitz and Motani (2011; obtained from

supplemental materials in Choiniere et al. 2021). A λ value of zero describes the absence of phylogenetic signal in the relationship of hypotarsus shape data to raptorial foot use. This finding permits the use of ordinary (i.e. non-phylogenetic) forms of discriminant function analysis to infer the presence or absence of raptoriality in extinct species.

I performed four different discriminant function analyses: a linear discriminant analysis (LDA), a flexible discriminant analysis (FDA), a mixed discriminant analysis with multivariate adaptive regression splines (MARS MDA), and a phylogenetically informed flexible discriminant analysis (PhyFDA) both with λ=1 and λ=0. The value λ=0 is the optimal estimated value as inferred from my analyses (see above), and λ=1 was only used to illustrate the difference in results obtained when using this unsupported value that imposes strong phylogenetic signal on the relationship between hypotarsus shape and raptorial foot use. Whereas only 23 fossil taxa were used as the test set in the PhyFDA, 26 fossil taxa were used in all other discriminant analyses, as the uncertain phylogenetic affinities of *Paleopsittacus georgei*, *Horusornis vianeyliandae*, and Coraciiform sp.A (Lyon PQ1216) do not preclude these specimens from inclusion in non-phylogenetic test sets.

The results of my different modes of discriminant function analyses are largely overlapping, showing many similar predictions (Appendix Table C.2). Percent predictive accuracy of each analysis based on confusion matrices for species in the training set ranged from 88% to 100%. LDA has 99% accuracy for predicting raptoriality in specimens from the training set. However, it makes divergent predictions for two fossil specimens of the same species, *Berruornis orbisantiqui* (MNHN L3096, 1.00; MNHN R4155, 0.00), questioning some aspects of predictions from LDA for specimens outside the training set. The same lack of confidence arises from the FDA, the percent accuracy of which is 98% for specimens in the training set.

Nevertheless, both the FDA and the MARS MDA predict raptoriality for the non-monosulcate Coraciiform sp.A (Lyon PG1216; FDA posterior = 1.00; MARS MDA posterior = 0.90). Both of these outputs are also inconsistent with the other discriminant function analyses used. These are both unequivocal prediction posteriors, on specimens in either complete or only partly eroded preservational states.

Several fossil taxa, exclusively from Strigiformes, are predicted to be raptorial across a majority of the discriminant function analyses. These taxa are *Eostrix tsaganica* (PIN 3104-147; posteriors = 1.00), *Heterostrix tatsinensis* (PIN 3211-35; 0.99-1.00), *Necrobyas harpax* (MNHN QU15695; 1.00), *Selenornis steendorpensis* (IRSNB Av84a+b; 0.97-1.00) *Sophiornis quercynus* (Lyon PQ1202; 1.00), and *Tyto sanctialbani* (NHMUK A305; 1.00).

The MARS MDA, a discriminant analysis appropriate for regression modelling of high-dimensional data, had a percent predictive accuracy of 88%. In addition to the above fossil taxa, the analysis predicted *Berruornis orbisantiqui* (MNHN L3096; 0.96), and *Paleobyas cracrafti* (MNHN QU15746; 1.00) to be raptorial.

The PhyFDA set at the optimal value of $\lambda = 0$ (test set percent predictive accuracy = 100%) agreed with the MARS MDA results, apart from *B. orbisantiqui* (MNHN L3096; 0.99 non-raptorial) and *T. muscolosis* (MPM PV-3443; 0.97 non-raptorial), which were not predicted to be raptorial. This may be the result of eroded or broken preservational states. The old world vulture *Anchigyps voorhiesi* (UNSM 62877; 0.96) was also predicted to be raptorial by the PhyFDA.

### 2.3.5 Analysis of Soft Tissue

The total tendon areas were initially analysed as percentages of total “bone + tendon” cross-sectional area. Due to imaging limitations, no other surrounding soft-tissue was examined.

None of the six species' tendons made up more than 20% of total cross-sectional area of bone + tendon. The average percentage of total cross-sectional area for tendons is 10.5% for the image slice immediately proximal to hypotarsus (top image slice), and 14.5% for the image slice immediately distal to hypotarsus (bottom image slice). The only taxa for which the percentage of total bone + tendon cross-sectional area made up by tendons is above average are the American Kestrel (*Falco tinnunculus*) and the Tawny Owl (*Strix aluco*) for the top image slice, and the American Kestrel, Eurasian Sparrowhawk (*Accipiter nisus*), and Tawny Owl for the bottom image slice (Appendix Table C.3).

I performed a phylogenetic generalized least squares regression, using the function pgls (caper, version 1.0.1; Orme, 2018), to examine the relationships between the cross-sectional area measurements of the tendons, the bones, the body masses of the taxa, and raptoriality (Appendix Table C.4). There is a significant statistical relationship between total cross-sectional area for bottom image slice tendon and the average body mass of the species as recorded in Birds of the World (ed. Billerman, 2021) (model AICc = 0.72), which becomes redundant once raptoriality and total cross-section for bottom image slice bone are included (AICc = 7.28).

The model,

1. $$log_{10}(Total\ area\ for\ bottom\ slice\ tendon) \sim Raptoriality\ + log_{10}(Total\ area\ for\ bottom\ slice\ bone)$$

is significant and strong (AICc = -14.37; adj-$R^2$ = 0.993). The independent effects of raptoriality on total cross-sectional area of tendon immediately distal to the hypotarsus are low and positive; there is a slight increase in tendon cross-sectional area associated with raptorial foot use. The independent effects of total cross-sectional area of bone at the same position are slightly greater and positive; there is an increase in tendon cross-sectional area as bone cross-sectional area increases.

The same cannot be said of the cross-section immediately proximal to the hypotarsus, shown by the relationship,

$$2. \quad log_{10}(Total\ area\ for\ top\ slice\ tendon) \sim raptoriality + log_{10}(Total\ area\ of\ top\ slice\ bone)$$

for which none of the variables were found to be significant, and was weak overall (AICc = 14.61; adj-$R^2$ = 0.078). It appears that there are no significant independent effects of either raptoriality or total cross-sectional area of bone on the cross-sectional area of tendon immediately proximal to the hypotarsus.

The relationship of total cross-sectional area for the flexor digitorum longus (FDL) and the flexor hallucis longus (FHL) tendons with raptoriality and total cross-sectional area of bone was investigated with further models:

$$3. \quad log_{10}(Total\ area\ for\ bottom\ slice\ FDL) \sim raptoriality + log_{10}(Total\ area\ of\ top\ slice\ bone)$$

$$4. \quad log_{10}(Total\ area\ for\ bottom\ slice\ FHL) \sim raptoriality + log_{10}(Total\ area\ of\ top\ slice\ bone)$$

Neither of these models had significant coefficients; this means that across the six taxa included in the data, there is no particular bias for either tendon to increase in size relative to raptoriality and total cross-sectional area of bone for the bottom image slice. This agrees with the initial quantitative data which describes, even among the three raptors, no consistency in relative size of flexor tendons. This finding also agrees with the anatomical diversity of tendon arrangements, where the deep flexor tendons may branch apart from and/or interconnect with each other via a tendinous vinculum (Raikow, 1985), while still resulting in similar performance of motions of the foot across families.

## 2.4 Discussion

### 2.4.1 Raptoriality and Hypotarsus Shape in Extant Taxa

It was found that there is a strong, statistically significant relationship between raptoriality and hypotarsus shape (Appendix Table C.1), in which raptoriality tends to result in a deeply monosulcate hypotarsus (Figure 10a), and is strongly distinguishable and delineated in shape space from non-raptorial hypotarsus shapes (Figure 13). The relationship between raptoriality and hypotarsus shape is present and significant both when accounting for the potential effects of phylogenetic signal and when ignoring them. The optimal Pagel's λ for the relationship between hypotarsus shape and raptoriality was analytically determined to be zero; this suggests that hypotarsus morphology is a highly functionally constrained system, with essentially identical effects of raptoriality on hypotarsus shape, regardless of phylogenetic affinities (i.e. similar morphological effects across Accipitriformes, Strigiformes, and Falconiformes). The relationship between hypotarsus shape and raptorial foot use is therefore similar to the highly functionally constrained relationship between ocular performance and eye morphology resolved by Motani and Schmitz (2011), or between body mass and shaft circumference of mass-supporting limb bones by Benson et al. (2018; based on data from Campione and Evans, 2012).

### 2.4.2 Discriminant Analysis of Fossil Taxa

My analyses indicate an optimal λ value of zero in the relationship between raptoriality and hypotarsus shape, indicating that phylogenetic signal is essentially absent from that relationship. This allows for the use of non-phylogenetic forms of discriminant function analysis to predict the presence or absence of raptoriality in fossil taxa. Moreover, this means that fossil species can be classified as raptorial or non-raptorial independent of the accuracy of their

phylogenetic placement in my phylogenies. This is important because some of the studied fossil specimens do not have well-resolved phylogenetic affinities. For example, the majority of the fossil tarsometatarsi assigned to Strigiformes form a poorly-resolved cluster around the base of the strigiform stem. Nevertheless, these specimens provide strong evidence for an early origin of raptoriality in early stem-strigiforms. It is possible that the hypotarsi of Strigiformes have remained relatively unchanged, from a functional perspective, for approximately 60 million years.

For the 23 fossil taxa ultimately analysed, 11 are described in the literature as belonging to extant raptorial groups: nine are strigiforms, one is a falconiform, and one is an accipitrid. Two fossil taxa are accipitriform vultures (*Gymnogyps kofordi*, *Anchigyps voorhiesi*). Twelve fossil taxa possess a monosulcate hypotarsus, including all 11 taxa placed in raptorial groups, as well as *A. voorhiesi*, an Old World vulture (Figure 15).

Despite its placement within a colloquially raptorial group (assigned to the Old World vulture subfamily Gypaetinae by Zhang et al. (2012)), and its monosulcate hypotarsus, *A. voorhiesi* was only predicted to be raptorial by the LDA (posterior probability of raptoriality = 0.99) and the PhyFDA ($\lambda = 0$; posterior probability of raptoriality = 0.96). These results are accompanied by decisive posterior values, and a nearly entire preservation state; there is only some minor erosion to the end of the lateral hypotarsal crest. The unequivocal prediction of raptorial foot use for *A. voorhiesi* could indicate the potential of raptorial ancestry of the Old World vultures, a hypothesis that is consistent with the taxa's phylogenetic affinities. There is an extant delineation in non-raptorial accipitriforms between the asulcate Cathartidae (New World vultures), and the monosulcate Old World vultures, in addition to the consistent separation of the two groups by recent phylogenies (e.g. Mindell et al., 2018).

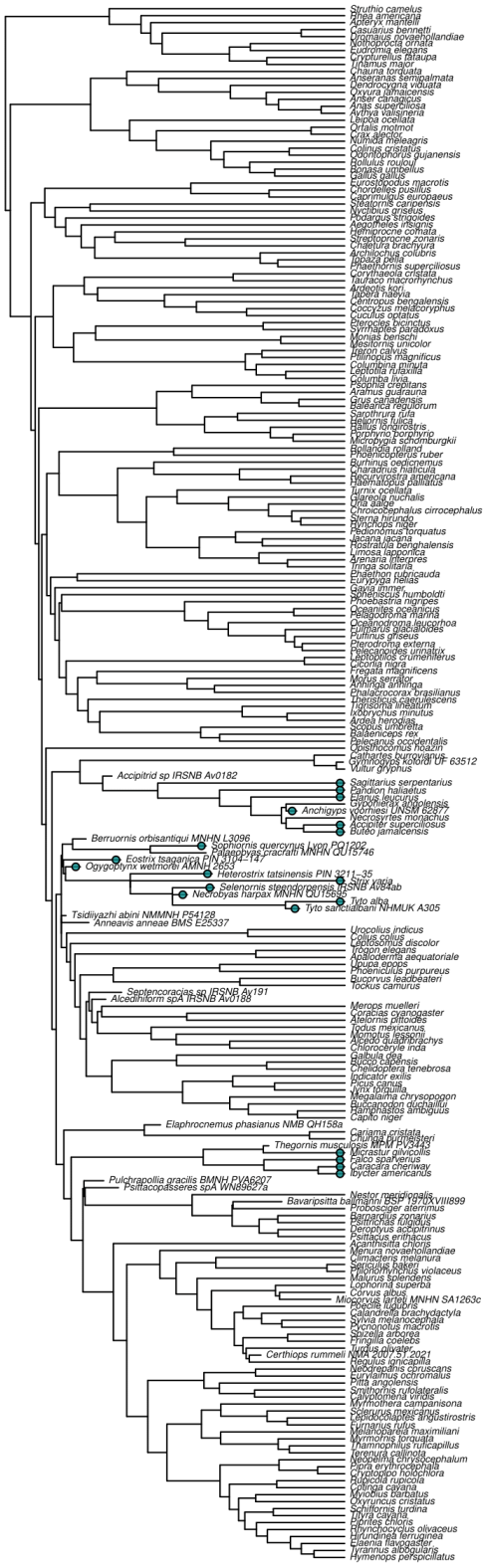
Struthio camelus
Rhea americana
Apteryx mantelli
Casuarius bennetti
Dromaius novaehollandiae
Nothoprocta ornata
Eudromia elegans
Crypturellus tataupa
Tinamus major
Chauna torquata
Anseranas semipalmata
Dendrocygna viduata
Oxyura jamaicensis
Anser canagicus
Anas superbiosa
Aythya valisineria
Lespa ocellata
Ortalis motmot
Crax alector
Numida meleagris
Colinus cristatus
Odontophorus gujanensis
Rollulus roulroul
Bonasa umbellus
Gallus gallus
Eurostopodus macrotis
Chordeiles pusillus
Caprimulgus europaeus
Steatornis caripensis
Nyctibius griseus
Podargus strigoides
Aegotheles insignis
Hemiprocne comata
Streptoprocne zonaris
Chaetura brachyura
Archilochus colubris
Ispidina picta
Phaethornis superciliosus
Corythaeola cristata
Taufaco macrorhynchus
Ardeotis kori
Otis tarda
Centropus bengalensis
Coccyzus melacoryphus
Cuculus optatus
Pteroptes bicinctus
Symhaptes paradoxus
Monias benschi
Mesitornis unicolor
Pterocnemia pennata
Rhinocrypta lanceolata
Taraba major
Thamnophilus punctatus
Melanopareia maximiliani
Formicarius colma
Grallaria varia
Conopophaga lineata
Scytalopus magellanicus
Rhinocrypta lanceolata
Pteroptochos megapodius
Hylactes tarnii
Eugralla paradoxa
Myiothlypis nigrocristata
Basileuterus culicivorus
Cardellina pusilla
Setophaga ruticilla
Geothlypis trichas
Cardellina rubrifrons
Myioborus miniatus
Setophaga pitiayumi
Setophaga citrina
Setophaga castanea
Setophaga fusca
Setophaga pensylvanica
Setophaga striata
Setophaga caerulescens
Setophaga virens
Setophaga dominica
Setophaga discolor
Setophaga palmarum
Setophaga pinus
Setophaga coronata
Setophaga graciae
Setophaga nigrescens
Setophaga townsendi
Setophaga occidentalis
Setophaga chrysoparia
Setophaga virens
Setophaga fusca
Setophaga castanea
Setophaga pensylvanica
Setophaga striata
Setophaga caerulescens
Setophaga dominica
Setophaga discolor
Setophaga palmarum
Setophaga pinus
Setophaga coronata
Setophaga graciae
Setophaga nigrescens
Setophaga townsendi
Setophaga occidentalis
Setophaga chrysoparia
Setophaga ruticilla
Geothlypis trichas
Cardellina rubrifrons
Myioborus miniatus
Setophaga pitiayumi
Setophaga citrina
Setophaga castanea
Setophaga fusca
Setophaga pensylvanica
Setophaga striata
Setophaga caerulescens
Setophaga vir

Originally, *Messelastur gratulator* Peters, 1994 was assigned to Accipitridae and has since been moved to stem group Psittaciformes within Pseudasturidae (Mayr, 2009b; 2010). It is sister to *Tynskya eocaena* within Messelasturidae, which was proposed by Mayr (2005) to be a stem group of Strigiformes, potentially forming a link between this clade and Falconiformes. Even when reassigned to stem group Psittaciformes (Mayr, 2009b), the messelasturids were still hypothesised to be raptorial based on their morphological similarities with extant raptors, one of which being the single, wide sulcus in the hypotarsus of *Tynskya* (Mayr, 2009b).

Although the extant genus *Nestor* consumes vertebrate material alongside a diet of fruits, nuts, and invertebrates, no extant parrots are raptorial (Winkler et al., 2020b). However, this doesn't rule out the possibility of raptoriality in messelasturids, or in other extinct psittaciform or stem-psittaciform groups. The hypotarsus of *M. gratulator* was landmarked but it was ultimately not included in the main results of my analyses due to its relatively poor preservational state. However, both the FDA and the MARS MDA predicted it to be raptorial (with definitive posterior values) even based on its uncertain morphology.

Similarly, I expect the posterior prediction of raptoriality or non-raptoriality based on fossil taxa with broken or eroded hypotarsal crests (e.g. *Thegornis musculosis*, *Ogygoptynx wetmorei*) would change upon the acquisition of entire and well-preserved specimens. As well, this tool of inference of raptoriality neither mathematically corrects for, nor quantifies intraspecific variation in either extant or extinct fossil specimens. However, limiting the scope of landmarking and shape analysis to solely the hypotarsus, and determining that centroid size and mean species body mass were non-significant explanatory variables for hypotarsus shape variation helps to control the potential effects of intraspecific variation in the data.

### 2.4.3 Foot Tendon Comparison

As an initial investigation into the functional morphology of the hypotarsus in raptors, with a dataset of six taxa and a basic evaluation of cross-sectional area, it appears that the hypotarsi of raptorial birds are likely deeply monosulcate due to the relative size of the flexor tendons. The size of the flexor tendons tends to be larger in raptorial birds and thus requires the hypotarsus to adjust.

Raikow (1985) suggested a number of classifications for tendon arrangements in parallel with digit arrangements, and commented on the possible functional inferences of such a scheme. Sustaita et al. (2013) confirmed that the functional significance of tendon classifications is unclear, yet for birds with enhanced grasping ability there is an increase in fibre pennation, and the number and attachment areas of digital flexor tendons. Backus et al. (2015) also suggested that the muscles and tendons involved with the hallux and distal portions of the foot generally tend to increase in cross-sectional area with evolutionary increases in foot uses such as carrying prey. These proposals form the basis for the hypothesis that raptoriality is likely correlated to the strength and spacing of tendons in the foot that control toe flexion; an increase in volume of the tendons associated with such activity would likely affect the morphology of the tarsometatarsal plantar surface and hypotarsal canal shape and/or presence in order to make room for strong and active soft tissue, and which is tested here. This activity would also have effects on the robustness and size of the phalanges (Ksepka & Clarke, 2012).

This may be analogous to hypotheses explaining the expansion of temporal fenestrae in early amniote skulls. These functional hypotheses range from reduction of cranium weight and thinning bone surface (Case, 1924; Frazzetta, 1968; Kuhn-Schnyder, 1980) to widening for increased muscle mass (Gregory and Adams, 1915; Romer and Price, 1940). The deeply

monosulcate condition of the hypotarsus in raptorial birds could similarly be due to a number of interrelated factors, but seems to primarily provide more space for increased tendon diameter. This analogy is only partially applicable, however, considering that the role of the temporal fenestra in tetrapods is as a muscle attachment site. The hypotarsus only acts as an attachment site for the gastrocnemius muscle, and is otherwise a channel through which flexor tendons pass. The monosulcate hypotarsus condition in raptorial birds may reflect these broader patterns of co-evolutionary interactions between skeletal structure and muscle mass in tetrapods, and/or may be a means of providing space to accommodate their comparatively larger flexor tendons.

Another anatomical comparison of the deep, wide hypotarsal sulcus of raptorial birds might be made to the avian triosseal canal; this structure is formed by the alignment of clavicle, coracoid and scapula bones at the coracoscapular joint, through which the supracoracoideus muscle is channeled in order to insert on the humerus (Raikow, 1985). It is commonly described as a "pulley" in the arrangement of the supracoracoideus muscle in the pectoral girdle, and acts similarly to the hypotarsus as a thoroughfare for soft tissue to travel. There has not been much comparative morphological research published on the coracoscapular joint, or on the potential ecomorphological relationship and variance between the supracoracoideus muscle, triosseal canal morphology, and wing use (e.g. Mayr, 2017; Mayr, 2021a), but perhaps with further investigation it could provide a compelling analogy to the hypotarsus and the flexor tendons it houses.

### 2.4.4 Implications for Telluravian Ancestry

The existence of a strong and highly-constrained form-function relationship between monosulcate hypotarsi and raptorial foot use suggests that multiple convergent origins of raptoriality in Telluraves is a more likely hypothesis than a raptorial common ancestor of

Telluraves. As a group of birds adapts raptorial foot use, the highly constrained system found here should result in a deeply monosulcate hypotarsus regardless of previous ecological ancestry, as shown by the optimal phylogenetic signal of zero of this form-function relationship.

I test the hypothesis of ancestral raptoriality using ancestral character estimation in Chapter 3 and reject the occurrence of raptorial foot use in the telluravian ancestor. Nevertheless, this does not refute the related hypothesis that the telluravian ancestor, or ancestors of many telluravian subclades may have been carnivorous, albeit lacking raptorial foot use. Moreover, the ancestrally carnivorous hypothesis is supported by molecular evidence: Wu et al. (2020) reported that Accipitriformes, Strigiformes, and Falconiformes possess enhanced digestion and absorption capabilities for fat and proteins, and inferred that the molecular markers for this were present in the common ancestor of Telluraves. Wu et al. (2020) proposed that these enhanced fat and protein digestion genes were under selection, and in conjunction with the hypothesis of ancestral telluravian raptoriality put forth by Prum et al. (2015), suggested a possible carnivorous ancestor for the group as a whole.

Further consistent with the presence of a carnivorous, but non-raptorial ancestor for Telluraves is that consumption of other vertebrates is widespread across extant Aves, and is not limited to the colloquially-defined raptors. Indeed, alongside the majority of waterbirds, Gruiformes, Otididae, Rheidae, Casuariidae, and many species of Phasianidae and Megapodidae, eight telluravian orders and 49 telluravian families (41 of which are in Passeriformes) have at least some species, if not all, which feed on vertebrates; usually lizards, small mammals, other birds, and frogs (Appendix Table A.2). This excludes those taxa which feed on insects and other invertebrates, which are also a source of proteins (but not necessarily fats). To propose that the

common ancestry of Telluraves is carnivorous is therefore plausible, given the prevalence of this diet throughout the group.

# Chapter 3:

## Convergent raptoriality in Telluraves based on ancestral character estimations

## 3.1 Introduction

There is much variation in morphology and ecology across the extant radiation of Aves, and the relationships that exist between these morphologies and ecologies are just as broad in range (e.g. Taylor and Thomas, 2014; Benson et al., 2017; Bright et al., 2019; Navalón et al, 2019; Lowi-Merri et al., 2021). It is possible to use these ecomorphological relationships to infer the ecologies of extinct birds known only from fossils using discriminant function analyses on shape data, to reconstruct the evolutionary history of bird groups. However, mapping the ecologies of both extant and fossil birds, with the intention of testing a hypothesis about the ancestral ecology of a group has rarely been done, particularly for Aves or Telluraves. For example, Field et al. (2018) investigated stem neornithine ecology to find ancestral arboreal lifestyles around the K-Pg boundary.

The relationship between monosulcate hypotarsus shape and raptoriality was found in Chapter 2 to be statistically significant, and an example of a strong, functionally constrained connection even with a negligible phylogenetic signal. This result suggests that a history of multiple ecologically convergent origins of raptoriality in Telluraves is more likely than that of a raptorial common ancestor of Telluraves; a morphology (monosulcate hypotarsus) determined to have essentially zero phylogenetic signal may be able to arise multiple times as long as the ecology (raptorial foot use) is adapted. The results of Chapter 2 also include inferences on raptorial foot use for 26 extinct taxa from across Telluraves, based on fossil hypotarsus morphologies.

I used ancestral character estimation (ACE) to evaluate the evolutionary history of foot uses among Telluraves, and test the hypothesis of ancestral raptoriality. I compare analysis of extant taxa with combined analysis of fossil and extant taxa to examine how the inclusion of

fossil taxa may affect the prediction of raptorial ancestry. Additionally, the histories of other foot uses present within Telluraves are investigated, in the case that they provide additional contextual information on the ancestral characterizations of the group as a whole.

Estimating or reconstructing ancestral ecological characters in a phylogenetic context is important to understanding the history of a group, and how its extant species have come to occupy specific ecological niches today. However, the assumption that the phylogenetic relationships between taxa are as accurate as possible is the basis of every reconstruction. Phylogenies with well-resolved internal nodes, as few polytomies as possible, and accurate branch lengths are able to provide important interspecific relational data that lays the groundwork for valid models of evolutionary comparison (Felsenstein, 1985; Purvis et al., 1994). I am using the phylogeny constructed by Prum et al. (2015) as it follows these conditions through the use of both genomic and fossil data.

Maximum likelihood methods in ACE provide a measure of statistical uncertainty and take into account prior ancestral probabilities and time available for change to occur (Schluter et al., 1997; Cunningham et al., 1998; Pagel, 1999). A phylogeny populated or partially populated with inferred ancestral states separates deep nodes with shorter branches, and may reflect ancestral ecology more faithfully than living species (Pagel, 1999). Thus, the inclusion of fossil material at or near decisive ancestral nodes of a phylogeny can result in significantly different ancestral character estimations.

The addition of fossil taxa at multiple nodes across a phylogeny can also "minimize the biases caused by directional trends" (Finarelli and Flynn, 2006, p. 310), and the information these fossil taxa provides helps to inform and constrain the value of estimates at those nodes

(Garland et al., 1999). Using ACE with relevant stem fossils of telluravian groups has the potential to constrain the timing and variation in foot uses in such telluravian clades.

In the case of Prum et al. (2015), their phylogeny is the most up-to-date understanding of extant avian relationships, based on analyses of genomic data from an extensive and well-represented taxon sample. It resolves uncertainties inherent to previous hypotheses of bird phylogenies, such as the placement of Tinamidae as sister to the cassowary and emu, the Aequorlitornithes as a comprehensive clade of waterbirds, and the hoatzin (*Opisthocomus hoazin*) as sister to all of Telluraves (Prum et al., 2015).

Falconiformes and Accipitriformes have had long and conjoined systematic histories, in which raptorial taxa were grouped together on the basis of anatomical similarity (e.g. Vieillot, 1820-30). However, there were hypotheses as early as the late 1800s that Falconiformes was actually a polyphyletic group, although there was little agreement on how its internal groups were truly related to the rest of Aves. Based on soft tissue comparisons, Garrod (1874) hypothesised that within the order Ciconiiformes (present day storks), both Cathartidae and "Accipitres" were separate "cohorts", and that within "Accipitres" were the families Falconidae and Strigidae. Gadow (1893) reordered the phylogeny so that Falconiformes were closely related to Ciconiiformes, with the cathartids as the link between the two orders. Jollie (1953) proposed that Cathartidae, Accipitridae, Falconidae, Pandionidae, and the individual *Sagittarius* were five discrete and unrelated groups within Falconiformes, and determined that these groups had quite disparate evolutionary relationships within Aves, from the cathartids as sister to Procellariformes and (the historically erroneous) Pelicaniformes, to Falconidae placed next to a combined "caprimulgiform-strigiform" order (p.370). Wetmore (1960) reintroduced the suborder Cathartae into Falconiformes, but separate from the other "superfamilies" Sagittarioidea (present day

Sagittaridae) and Falconoidea (hawks, falcons, and allies, including Old World vultures). With no thought to the rest of the family members, Cathartidae was moved back and forth between Ciconiiformes and Falconiformes a number of times (e.g. Ligon, 1967; Voous, 1972), until initial molecular studies (e.g. Wink et al., 1998) separated Falconidae, Accipitridae, Sagittaridae and Cathartidae out from their enigmatic Falconiformes grouping in maximum parsimony phylogenies. However, these families were still erroneously integrated among modern Ciconiiformes, Pelicaniformes, Phoenicopteriformes, and Gruiformes.

Hackett et al. (2008) split Falconiformes into its component families, placing these groups in the locations which have modern consensus. This research paved the way for subsequent genome-based phylogenies such as those constructed by Jarvis et al. (2014) and Prum et al. (2015), which allow for the evolutionary and ecomorphological hypotheses studied today.

## 3.2 Material and Methods

### 3.2.1 Terminology

Most anatomical nomenclature is used as per Baumel and Witmer (1993). Both Latin and English equivalents are used interchangeably for muscular and osteological structures. Terminology relating to geometric morphometrics and related statistical analyses is collated from multiple sources, namely Bookstein (1997), Zelditch et al. (2004), Webster and Sheets (2010), Grafen and Hails (2002), and Burnham and Anderson (2002). The Latin names used for extant bird species are in accordance with their information as currently listed in the online *Birds of the World* (ed. Billerman et al., 2021).

### 3.2.2 Data Collection

Tarsometatarsi of extant bird skeleton and spirit specimens were imaged using x-ray microcomputed tomography scans (CT scans). These CT scan images were processed using ImageJ software (Schneider et al., 2012), and segmented, visualized and turned into 3D models using Avizo Lite software (v.9.7.0). These models are stored on the open-access digital archive Morphosource (morphosource.org). 2D images of the proximal ends of 29 fossil specimens were collected from both the literature and from museum collections.

*Institutional abbreviations*—**AMNH**, American Museum of Natural History; **BSP**, Bayerische Staatssammlung für Paläontologie und Geologie, Munich; **BMS**, Buffalo Museum of Science, New York; **FMNH**, Field Museum of Natural History, Chicago; **IRSNB**, Royal Belgian Institute of Natural Sciences; **ML**, Musée des Confluences, Lyon; **MNHN**, Musée National d'Histoire Naturelle, Paris; **MPM**, Museo Regional Provincial Padre Molina, Santa Cruz; **NHMUK**, Natural History Museum of London; **NMB**, Naturhistorisches Museum Basel; **NMA**, Naturmusuem Augsberg; **NMMNH**, New Mexico Museum of Natural History; O**UMNH**, Oxford University Museum of Natural History; **PIN**, Paleontological Institute, Russian Academy of Sciences; **UF**, University of Florida Museum of Natural History; **UMMZ**, University of Michigan Museum of Zoology; **UMZC**, University Museum of Zoology, Cambridge; **UNSM**, University of Nebraska State Museum of Natural History; **YPM**, Yale Peabody Museum, Connecticut.

The complete list of extant and fossil taxa can be found in the Appendices (Appendix Data D.1, D.2).

### 3.2.3 Taxa and Character Scoring

A list of 200 extant taxa was used from Prum et al. (2015), as well as a list of 24 fossil taxa, for which I was able to estimate the presence or absence of raptorial foot use based on hypotarsus morphology (see Chapter 2). I included *Messelastur gratulator* among these extinct taxa, although the specimen of *M. gratulator* is taphonomically deformed (Mayr, 2011).

The ancestral reconstruction of 15 telluravian foot uses and ecologies were estimated for phylogenies of extant taxa: raptoriality, force grip foot use, digital manipulation, hanging/clinging, hold down foot use, scansoriality, anisodactyly, zygodactyly, pamprodactyly, heterodactyly, perching, documented walking ability, hopping, cursoriality, and terrestriality/arboreality.

The extant taxa were scored for these foot use and ecology characters using the scoring rubric in Chapter 1 (p. 23; Appendix Data D.1), and with ecological information gathered from Birds of the World (ed. Billerman, 2021). The fossil taxa were scored only for raptoriality, using the scores predicted in Chapter 2, from a phylogenetic flexible discriminant analysis (phyFDA; Motani and Schmitz, 2011) for which the phylogenetic signal $\lambda = 0$, which had a 100% predictive accuracy for the test data.

### 3.2.4 Phylogenetic Frameworks

An adapted version of the 'Avian Time Tree' recovered by Prum et al. (2015) was used in analyses solely on extant taxa, to which two Old World vultures (the Hooded vulture, *Necrosyrtes monachus* and the Palm-nut vulture, *Gypohierax angolensis*) were added. A second version of this tree was adapted to add the aforementioned extant taxa, as well as 23 of the fossil taxa in phylogenetic positions established in Chapter 2 (p. 125). A third version was adapted to include all aforementioned extant and fossil taxa, as well as *M. gratulator*.

In addition to the information in cited literature (i.e. new genus or species descriptions based on type or referred specimens), the ages of extinct taxa were taken from The Paleobiology Database (paleobiodb.org). These data were taken into account in the estimation of node ages in the adapted trees including all fossil taxa.

The placement of fossil specimens in the tree is as detailed in Chapter 2, with the addition of *M. gratulator* here, whose phylogenetic position is discussed in the next paragraph.

Messelasturidae shares traits with Accipitridae, Falconidae (as these two families were hypothesized to be within the order Falconiformes at the time), and Strigiformes (Mayr, 2005), such as a short and "raptor-like" beak (which here means deeply hooked), and a "tarsometatarsus with well-developed cristae hypotarsi bordering a wide sulcus" (p.636). After an initial assignation to Accipitridae (Peters, 1994), Mayr (2005) determined a sister-group relationship between Messelasturidae (which included both *M. gratulator* and *Tynskya eocaena*) and Strigiformes, and hypothesized that messelasturids were diurnal, arboreal birds, which potentially preyed on insects or small birds, with no mention of potential raptoriality related to foot morphology. Upon the description of the previously unknown hindlimb of *M. gratulator* by Mayr (2011), Messelasturidae was proposed as the sister-group to Halcyornithidae/'Pseudasturidae' rather than to Strigiformes, and *M. gratulator* is described as having a "more raptor-like" hindlimb morphology. Mayr (2011a) also proposes that *M. gratulator* had a carnivorous diet, based on similarities in beak and ungual phalanx shape to those of extant raptors. It is therefore conservative to include *M. gratulator* as a raptorial, early stem parrot, as it potentially increases the probability of inferring raptoriality among early Telluraves.

### 3.2.5 Ancestral Character Estimation

Ancestral character estimation was performed using the ace() function (ape, version 5.6-1; Paradis and Schliep, 2019). The use of maximum likelihood estimation with either the equal rates (ER) or the all rates different (ARD) matrix method is appropriate for the analysis of a discrete, binary variable (Schluter et al., 1997; Cunningham et al., 1998). Higher log-likelihoods and lower AICc (qpcr, version 1.4-1; Spiess, 2018) values were sought to determine which of the estimation methods is appropriate for each individual foot use reconstruction.

Fossil data was included only for the ancestral reconstruction of raptoriality in Telluraves; ancestral estimation of all other foot use characters were based solely on extant taxa.

## 3.3 Results

### 3.3.1 Raptoriality

Estimation of the presence/absence of raptoriality across the avian phylogeny suggests that raptoriality evolved convergently in Accipitriformes, Strigiformes, and Falconiformes for both the reconstruction which incorporates fossil information and the reconstruction with only extant taxa (Figure 2). The ER model reconstruction with fossils has a log-likelihood of -40.6 and AICc of 83.2, whereas the ARD model reconstruction has a log-likelihood of -64.3 and AICc of 132.5. I therefore interpret the results from the statistically stronger ER model reconstruction.

The “telluravian backbone”, or the nodes along the earliest stems of Telluraves which start at the branching off of *Opisthocomus hoazin* and lead down to Passeriformes, is consistently and definitively non-raptorial in its ancestral likelihoods (100% non-raptorial). This inference is not modified by the inclusion of the potentially raptorial stem psittaciform *Messelastur gratulator*.

The range of likelihoods of raptoriality for nodes within Falconiformes extends lower (12.6–100.0%) when non-raptorial fossil *Thegornis musculosis* is included at the base of the group, relative to the extant-only estimation (98.8–100.0%). *T. musculosis* possesses a partially broken hypotarsal crest. It was predicted to be non-raptorial by the phylogenetic discriminant function analysis (phyFDA; see Chapter 2), and its poor preservational state may introduce uncertainty to the ancestral state of raptoriality in Falconiformes.

Node percentages within Strigiformes are conclusively raptorial (97.4–100.0%) from *Eostrix* crownward, but the stem group sophiornithids (Berruornis, Sophiornis, Paleobyas; Figure 3) has a very low likelihood of raptoriality (0.3–1.9%). The inclusion of raptorial fossil taxa at the stem of Strigiformes pushes the node with a definitive likelihood of raptoriality in owls earlier in time (approx. 61mya) compared to the extant-only estimation (approx. 46 mya). *Ogygoptynx wetmorei* possesses eroded hypotarsal crests. It was predicted to be raptorial by the phyFDA (see Chapter 2), and its poor preservational state may introduce uncertainty to the ancestral state of raptoriality in Strigiformes.

There is no difference to the likelihood of raptoriality in Cathartidae between extant-only and with-fossil estimations (0.0%). At the node for Sagittarius + all other accipitriforms (Figure 1, 4), there is very little difference between extant and raptorial estimations (95.5% and 95.6%, respectively), as the fossil Accipitrid sp. (IRSNB Av0182) was placed outside of this group, closer to the stem. The Gypaetinae are more decisively estimated as raptorial (100%) with the inclusion of the fossil *Anchigyps* when compared to the extant estimation (85.3%). This suggests that raptorial foot use was ancestral to Old World vultures, and lost within the last 13.6 My.

An additional ancestral character estimation of raptoriality in Aves included the fossil *Messelastur gratulator* (Appendix Figure D.3), which was predicted to be raptorial by the

phyFDA when included (see Chapter 2). The addition of *M. gratulator* resulted in close to zero change in the ancestral likelihood of the tree as a whole, and did not affect the likelihood of raptoriality in stem parrots (0.0%). The node shared by Falconiformes and Psittacopasseres has a likelihood of raptoriality remaining at 0.0%. This suggests that raptoriality evolved independently and convergently in *M. gratulator*, and does not indicate that extant parrots were ancestrally raptorial.

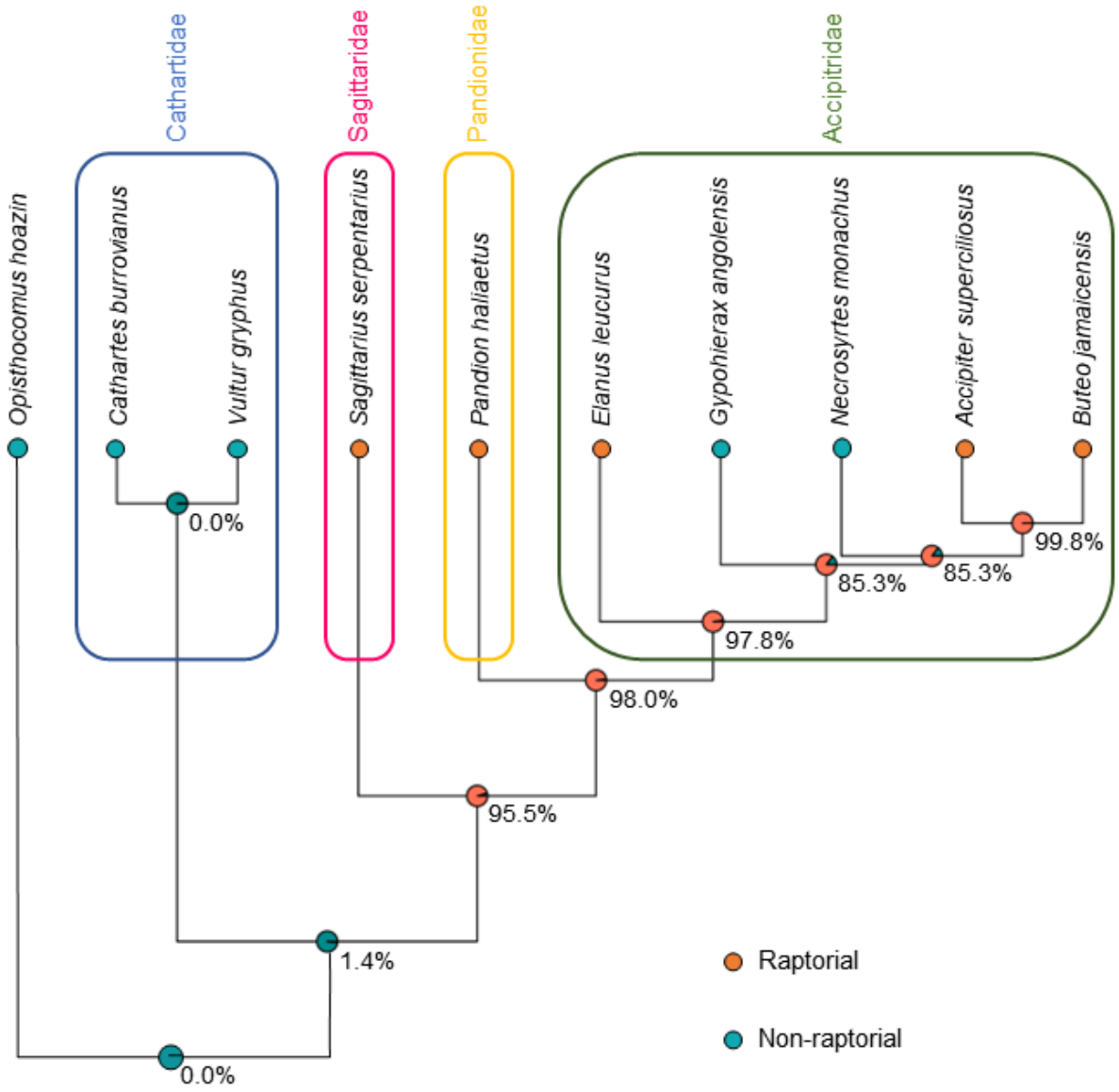


**Figure 1.** Phylogenetic tree of nine extant accipitriform taxa (outgroup: *Opisthocomus hoazin*) with ACE maximum likelihood estimates of raptoriality (ER model reconstruction) at each node.

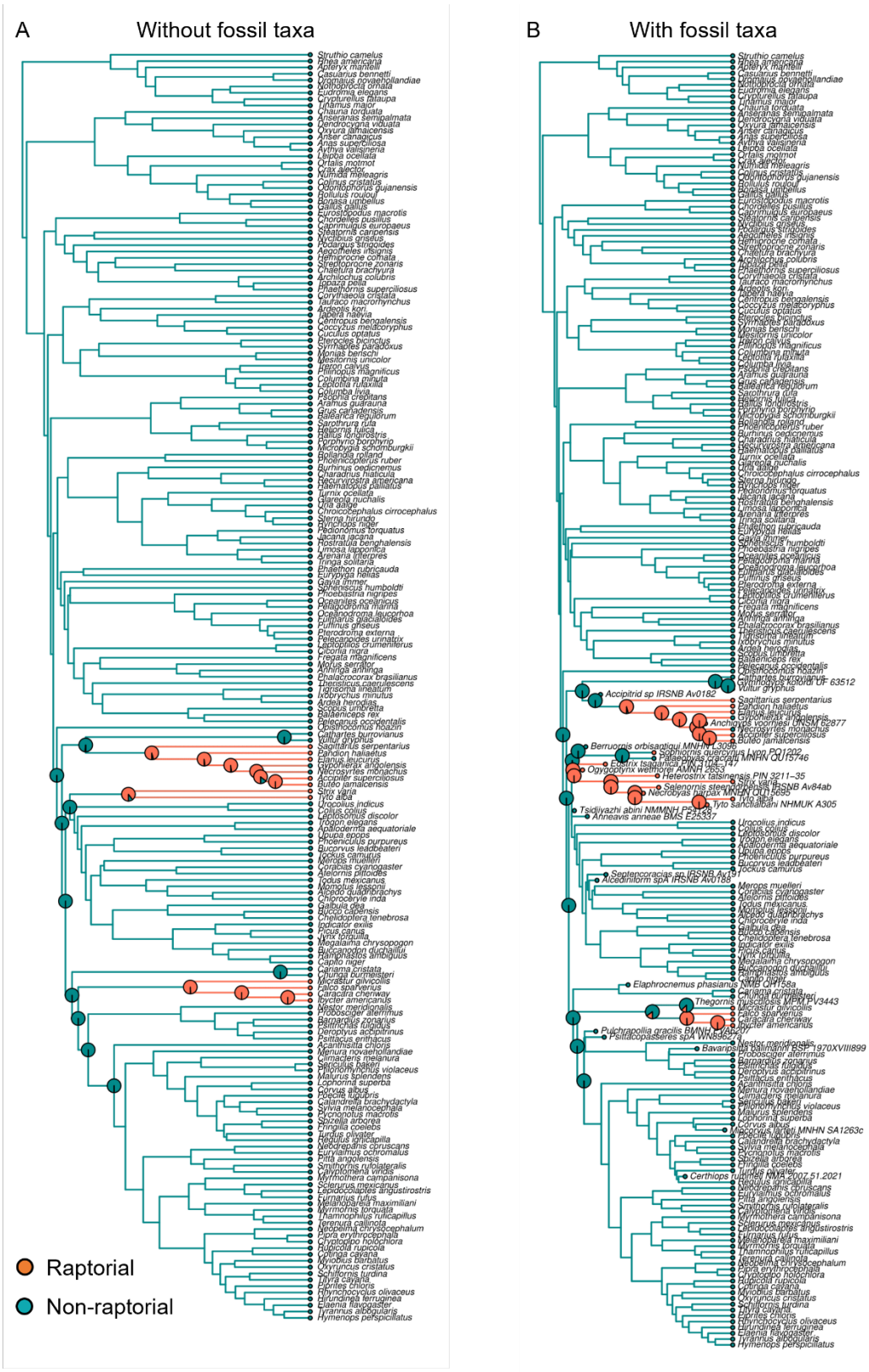


**Figure 2.** A) Phylogenetic tree of 200 extant avian taxa showing the ACE maximum likelihood estimates of raptoriality (ER model reconstruction) for key nodes along the telluravian backbone and raptorial

clades; B) Phylogenetic tree of 200 extant and 23 fossil Aves showing the ACE maximum likelihood estimates of raptoriality (ER model reconstruction) for key nodes along the telluravian backbone and raptorial clades.

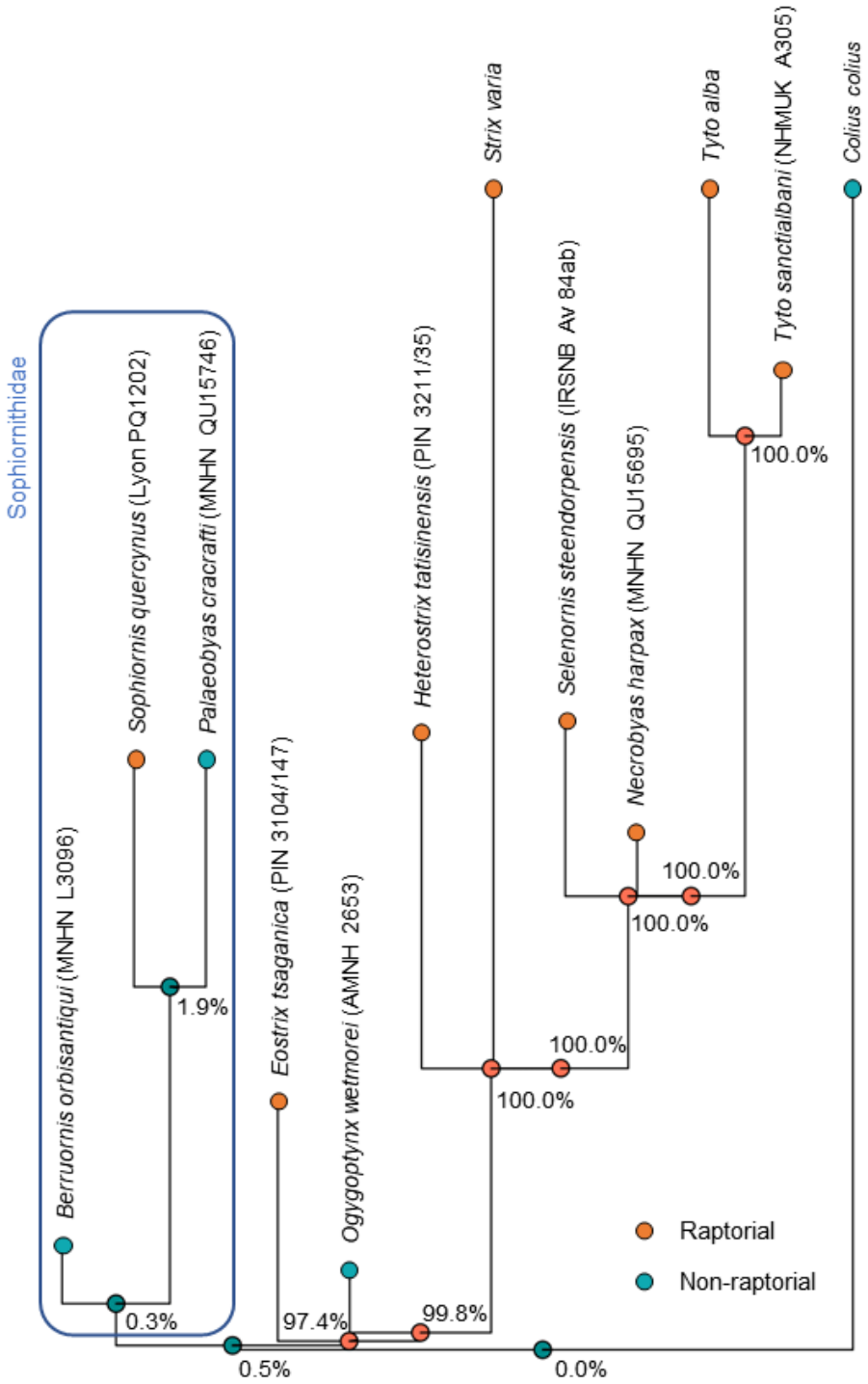


**Figure 3.** Phylogenetic tree of two extant and nine fossil strigiform taxa (outgroup: *Colius colius*) with ACE maximum likelihood estimates of raptoriality (ER model reconstruction) at each node.

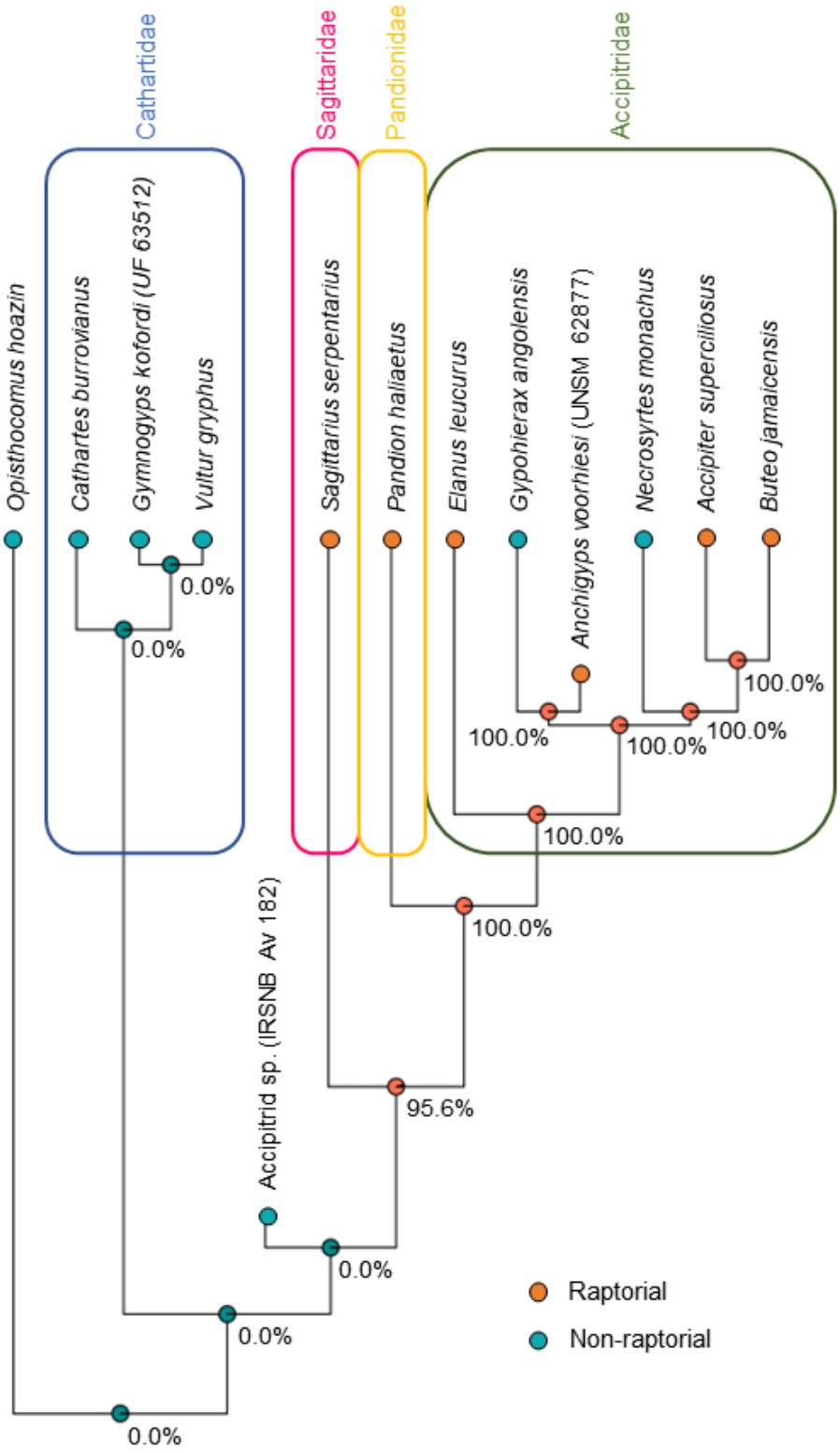


**Figure 4.** Phylogenetic tree of nine extant and three fossil accipitriform taxa (outgroup: *Opisthocomus hoazin*) with ACE maximum likelihood estimates of raptoriality (ER model reconstruction) at each node.

### 3.3.2 Force Grip

Force grip foot use appears to have arisen on Telluraves backbone at the node after Opisthocomidae has branched off, and so is ancestral to the extant groups which exhibit this foot use: Accipitriformes, Strigiformes, Falconiformes, and Psittaciformes (Figure 5). The ER model reconstruction has a log-likelihood of -30.2 and AICc of 62.4, and the ARD model reconstruction has a log-likelihood of -27.1 and AICc of 58.1. I therefore interpret the results from the statistically stronger ARD model reconstruction.

The nodes comprising the "telluravian backbone" all show a likelihood of the presence of force grip foot use of 100%, except at the node for which *O. hoazin* is sister to the rest of Telluraves (34.8% likelihood), and the node for the Passeriformes clade (17.3% likelihood). The likelihood of force grip foot use in Cathartidae is definitively 0.0%, whereas the nodes within the rest of Accipitriformes show a 99.6-100.0% likelihood of force grip foot use, even among Old World vultures (Figure 6).

The base of the Strigiformes + Coraciimorphae clade has a likelihood of force grip foot use of 99.7%, and Strigiformes has a likelihood of force grip foot use of 100.0%. The nodes throughout Coraciimorphae all have decreasingly low likelihoods of force grip foot use (24.5-1.6%), starting from the base node of Coliiformes, which has a likelihood of force grip foot use of 34.2%. This suggests a reversal to the absence of forceful gripping in coraciimorphs, from ancestors that possessed this capability.

All nodes within Falconiformes and Psittaciformes have a likelihood of force grip foot use of 100.0%. The node at the base of the Psittaciformes + Passeriformes clade has a slightly lower yet still definitive likelihood of force grip foot use of 99.8%. This suggests that the ability to forcefully grip was ancestral to, but subsequently lost in Passeriformes.

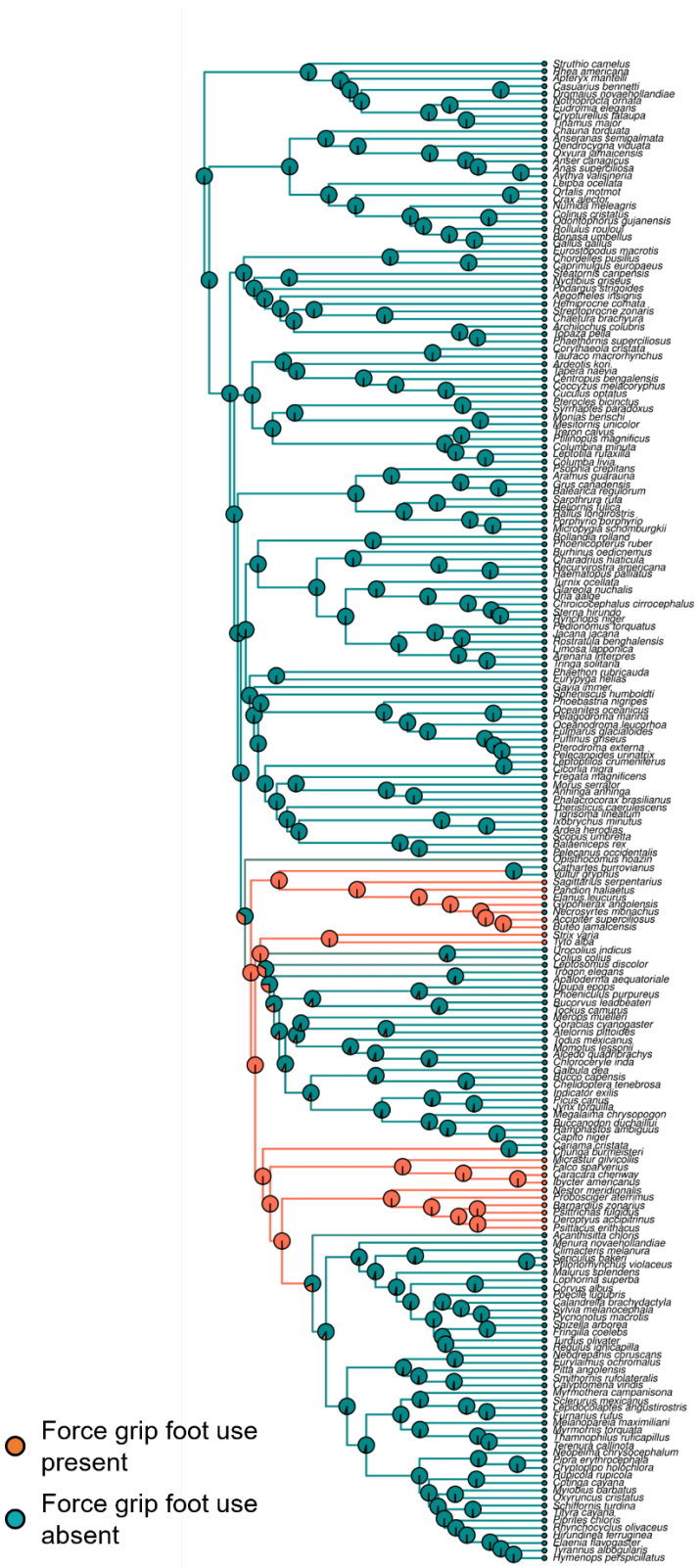


**Figure 5.** Phylogenetic tree of 200 extant avian taxa showing the ACE maximum likelihood estimates of force grip foot use (ARD model reconstruction) at each node.

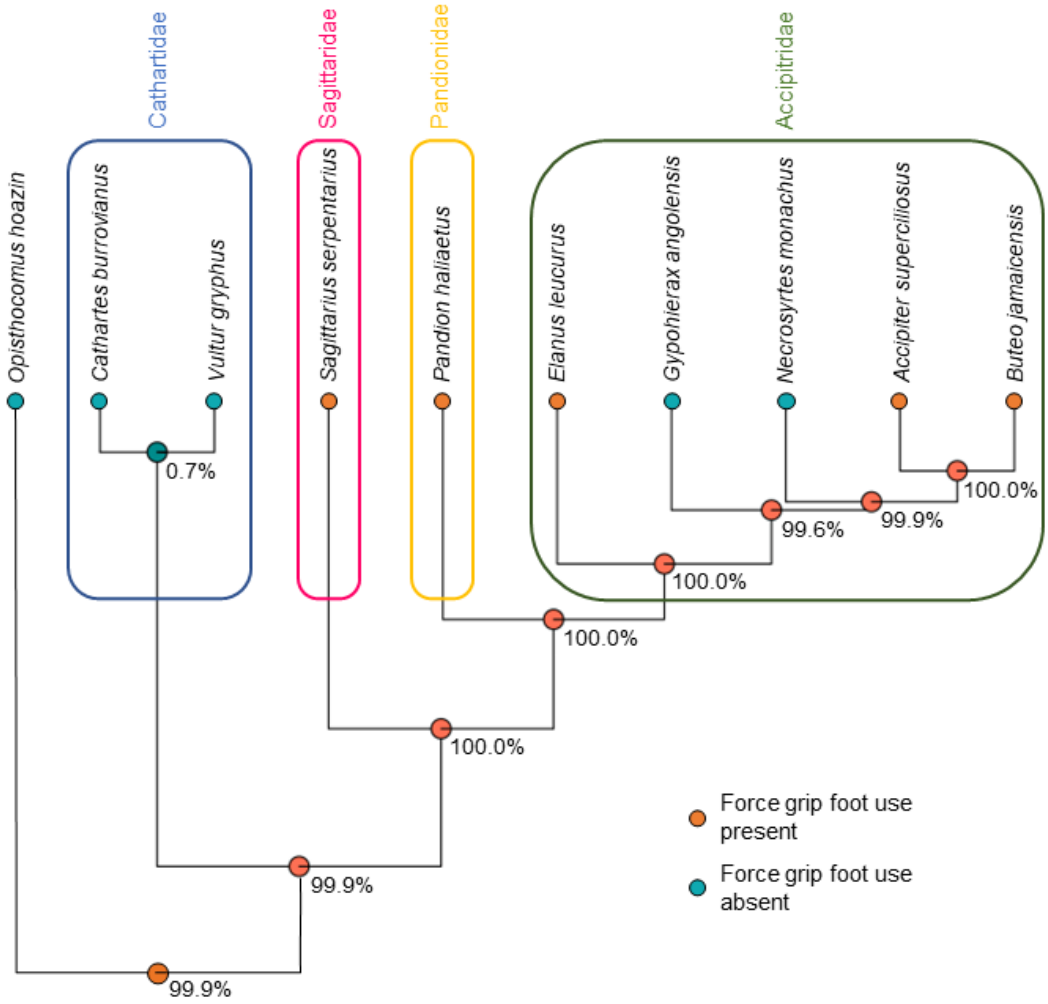


**Figure 6.** Phylogenetic tree of nine extant accipitriform taxa (outgroup: *Opisthocomus hoazin*) with ACE maximum likelihood estimates of force grip foot use (ARD model reconstruction) at each node.

### 3.3.3 Zygodactyly

Zygodactyl digit arrangement appears to have convergently evolved in Psittaciformes, Piciformes, Strigiformes, Coliiformes, Otidimorphae, Pandionidae and *Elanus* (Figure 7). The ER model reconstruction had a log-likelihood of -36.7 and AICc of 80.3, whereas the ARD model reconstruction had a log-likelihood of -40.0 and AICc of 85.3. I therefore interpret the results of the statistically stronger ER model reconstruction.

Whereas Pandionidae and *Elanus* have semi-zygodactyl digit orientation, the nodes for Pandionidae + Accipitridae, and *Elanus* + the rest of Accipitridae have maximum likelihoods of zygodactyl ancestry of 14.9% and 15.0% respectively. This suggests that the semi-zygodactyl digit orientation in *Pandion* and *Elanus* likely evolved independently.

The nodes comprising Psittaciformes have a 98.4–100% likelihood of zygodactyly. As well, the nodes comprising the Piciformes have a 94.7–100% likelihood. The node for Coliiformes has a likelihood of 98.5%, and that of Strigiformes is 83.9%, whereas the nodes along the stem of the clade comprising Strigiformes + Coraciimorphae have a likelihood of zygodactyly of 0.0%. This suggests that zygodactyly and semi-zygodactyly in these clades evolved convergently.

The ancestral node of Otidimorphae is equivocal in its maximum likelihood estimate of zygodactyly (42.0%). The Cuculiformes have a likelihood range of 98.5–100%, whereas the node for the clade comprising Otidiformes + Cuculiformes has a likelihood of 42.7%, likely accounting for the exceptional anisodactyly of the Otidiformes. The likelihood of zygodactyly at the node representing the stem of the Musophagiformes is 98.6%.

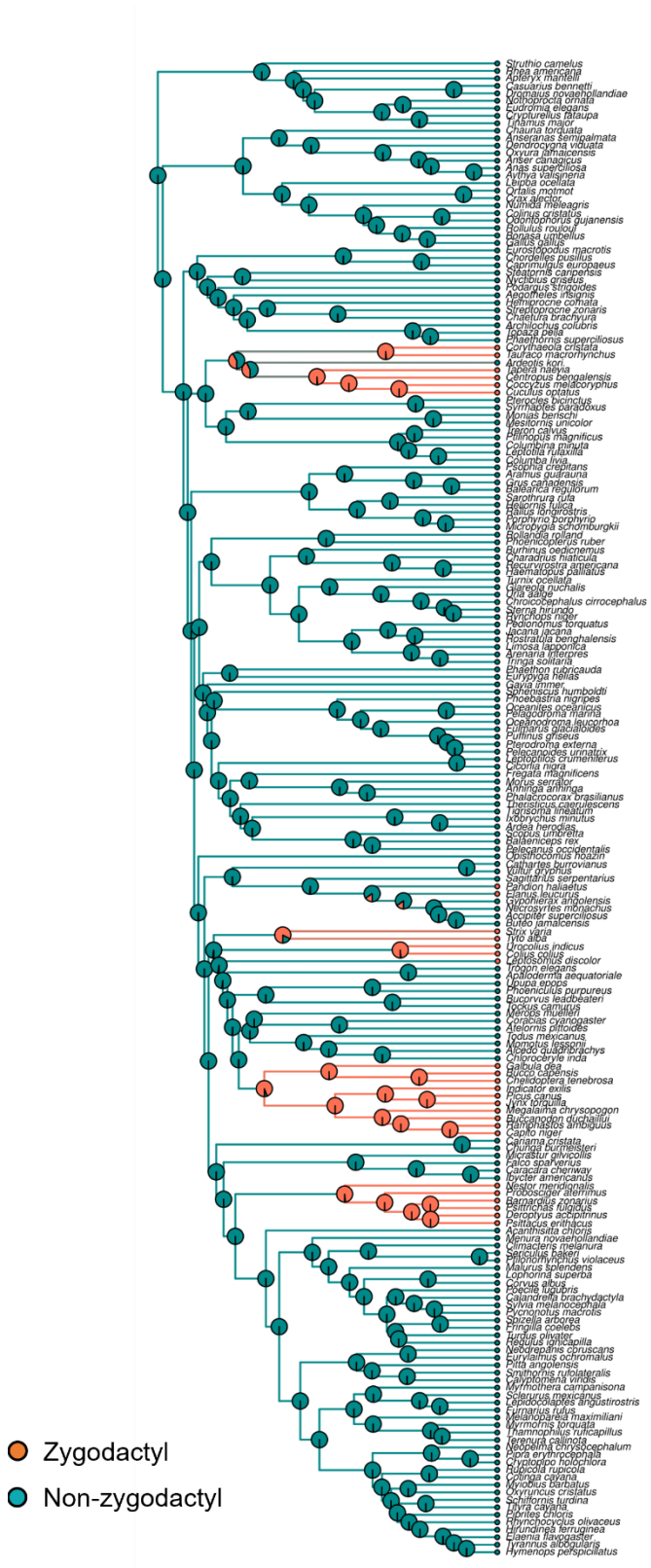


**Figure 7.** Phylogenetic tree of 200 extant avian taxa showing the ACE maximum likelihood estimates of zygodactyl digit orientation (ER model reconstruction) at each node.

### 3.3.4 Anisodactyly

Anisodactyl digit arrangement appears to have differing ancestral estimation between the ER model reconstruction and the ARD model reconstruction. Whereas the ER model had a log-likelihood of -42.7 and AICc of 87.4, the ARD model reconstruction had a log-likelihood of -40.3 and AICc of 84.6. The ARD reconstruction is a statistically stronger model, and describes the evolutionary history of anisodactyly as a convergent digit orientation across Aves (Figure 8B). However, due to the mutually inclusive binary character scoring of the taxa, such a reconstruction is comparing anisodactyl digit orientation to a general "non-anisodactyl" digit orientation, which encompasses multiple other digit orientations. As these are mutually inclusive characters, the presence of taxa with multiple digit orientations (i.e. semi-zygodactyly in Strigiformes) also complicate the reconstruction.

The ER model reconstruction (Figure 8A), despite its slightly statistically weaker strength, is a more convincing pattern of evolution in digit orientation. In this reconstruction, anisodactyly is ancestral to Aves and describes the majority of ancestral nodes throughout the phylogeny. Clades with only one "non-anisodactyl" digit orientation appear convergently within Telluraves, including the heterodactyl Trogoniformes, the zygodactyl Psittaciformes, the zygodactyl Galbuli, and zygodactyl Picides.

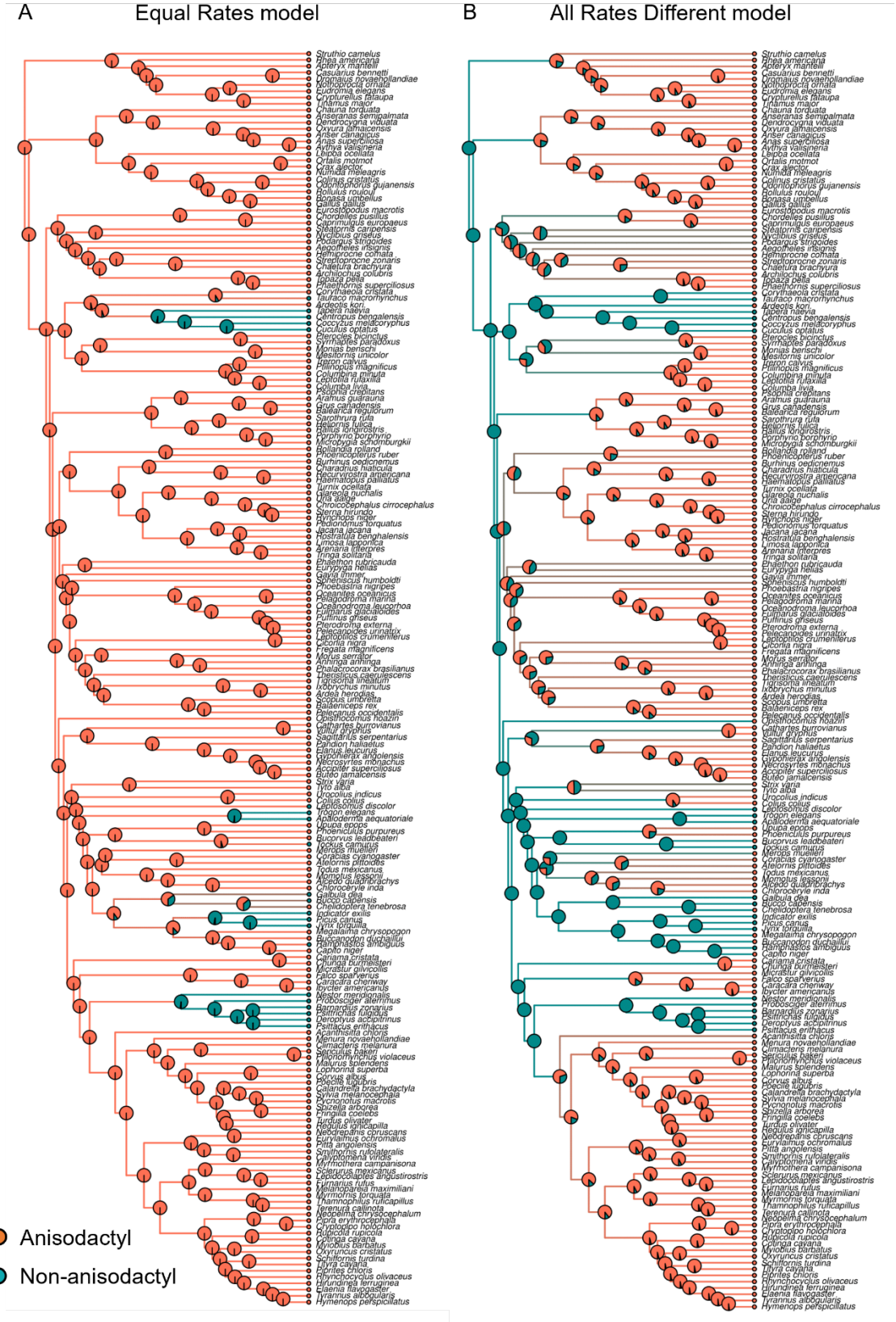


**Figure 8.** A) Phylogenetic tree of 200 extant avian taxa showing the ACE maximum likelihood estimates of anisodactyl digit orientation (ER model reconstruction) at each node; B) Phylogenetic tree of 200

extant avian taxa showing the ACE maximum likelihood estimates of anisodactyl digit orientation (ARD model reconstruction) at each node.

### 3.3.5 Heterodactyly

Heterodactyl digit arrangement appears to have evolved convergently in the two telluravian groups which exhibit it, the Trogoniformes and the digitally versatile Coliiformes (Winkler et al., 2020; Figure 9A). The ER model reconstruction had a log-likelihood of -10.8 and AICc of 23.6, whereas the ARD model reconstruction had a log-likelihood of -18.9 and AICc of 41.8.

### 3.3.6 Pamprodactyly

Pamprodactyl digit arrangement appears to have evolved convergently within Aves in both the Apodidae and the digitally versatile Coliiformes (Figure 9B). The ER model reconstruction had a log-likelihood of -11.7 and AICc of 25.5, whereas the ARD model reconstruction had a log-likelihood of -18.9 and AICc of 41.8.

**Figure 9.** A) Phylogenetic tree of 200 extant avian taxa showing the ACE maximum likelihood estimates of heterodactyl digit orientation (ER model reconstruction) at each node; B) Phylogenetic tree of 200

extant avian taxa showing the ACE maximum likelihood estimates of pamprodactyl digit orientation (ER model reconstruction) at each node.

### 3.3.7 Documented Walking Ability

The ancestral estimations for walking ability differ between the ER model reconstruction and the ARD model reconstruction. The ER model reconstruction had a log-likelihood of -31.6 and AICc of 65.3, whereas the ARD model reconstruction had a log-likelihood of -28.9 and AICc of 61.8. The ARD reconstruction is a statistically stronger model, and describes the evolutionary history of walking ability as a convergent trait across Aves, with multiple independent origins (Figure 10B).

The ER model reconstruction (Figure 10A), despite its slightly statistically weaker strength, is a more convincing pattern of evolution in walking ability. In this reconstruction, walking ability is ancestral to Aves and definitively describes the majority of ancestral nodes throughout the phylogeny. The single clade within Telluraves with a definitive lack of walking ability is Trogoniformes, with a 1.2% likelihood since at least the divergence between *Trogon* and *Apaloderma* (approx. 19 million years ago).

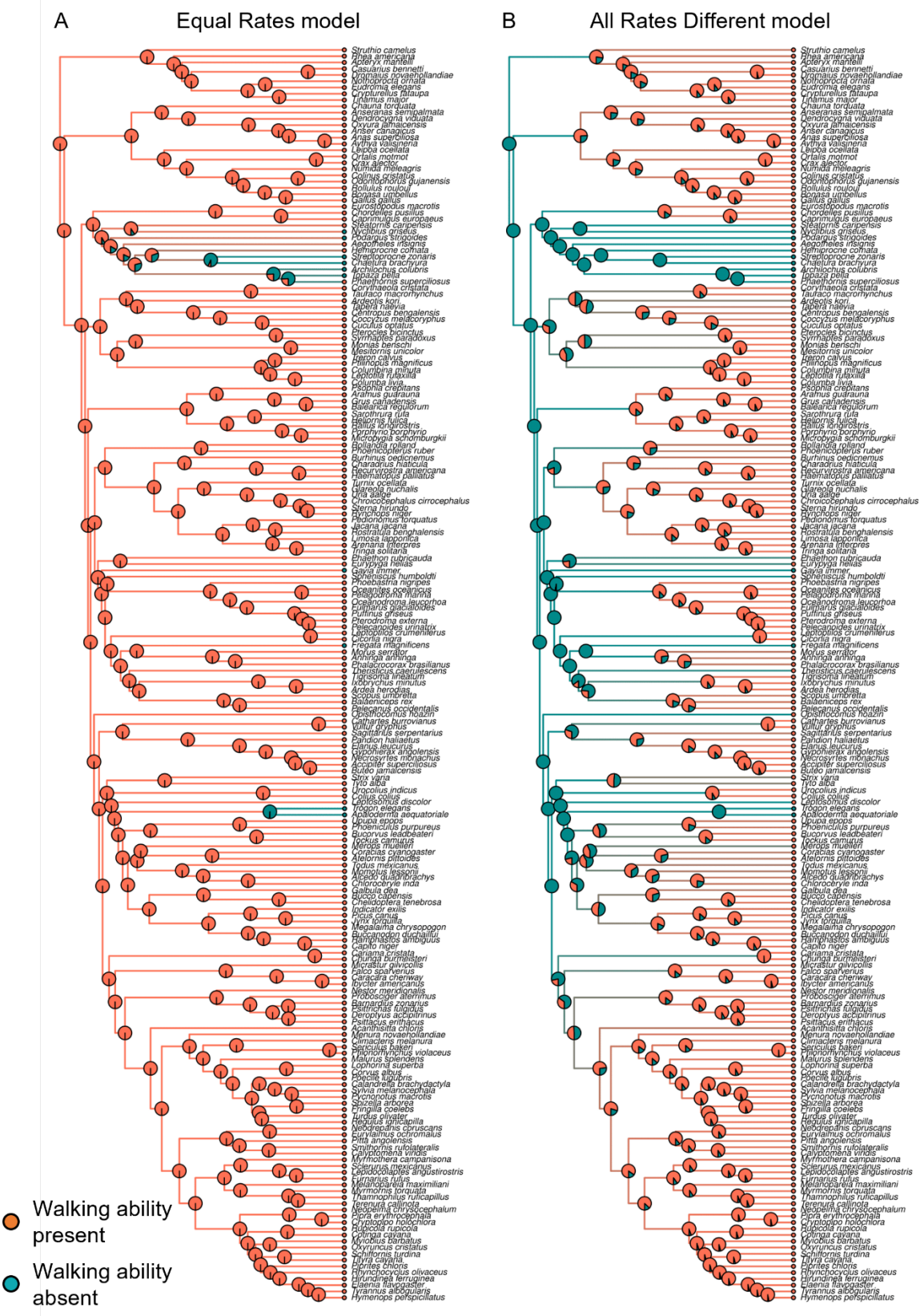


**Figure 10.** A) Phylogenetic tree of 200 extant avian taxa showing the ACE maximum likelihood estimates of walking ability (ER model reconstruction) at each node; B) Phylogenetic tree of 200 extant

avian taxa showing the ACE maximum likelihood estimates of walking ability (ARD model reconstruction) at each node.

### 3.3.8 Terrestrial vs. Arboreal

Mixed ecology (non-preference for terrestriality or arboreality) appears to be ancestral to Aves (91.1% likelihood), and there is equivocal likelihood for arboreal and mixed ecology to be ancestral to Telluraves (59.9% mixed; 40.1% arboreal; Figure 11). The ER model reconstruction had a log-likelihood of -127.9 and AICc of 257.7, whereas the ARD model reconstruction had a log-likelihood of -110.6 and AICc of 233.3. I therefore interpret the results of the statistically stronger ARD model reconstruction.

The likelihood of arboreal ancestry appears to become stronger moving along the "telluravian backbone", from a likelihood of 40.1% at the base of Telluraves, to 89.5% at the base of Passeriformes. There are some terrestrial taxa within Telluraves (e.g. Cariamiformes, *Menura novaehollandiae*, *Myrmornis torquata*) which have no close terrestrial sister groups, and appear to have evolved convergently.

The node within Cathartidae is equivocal in its likelihood of mixed and terrestrial ecology (45.4% terrestrial; 51.8% mixed), which differs greatly from the majority arboreal node likelihoods within the rest of Accipitriformes (66.9-91.0% arboreal). This suggests that Cathartidae have independently evolved to mixed and terrestrial lifestyles within an ancestrally arboreal clade.

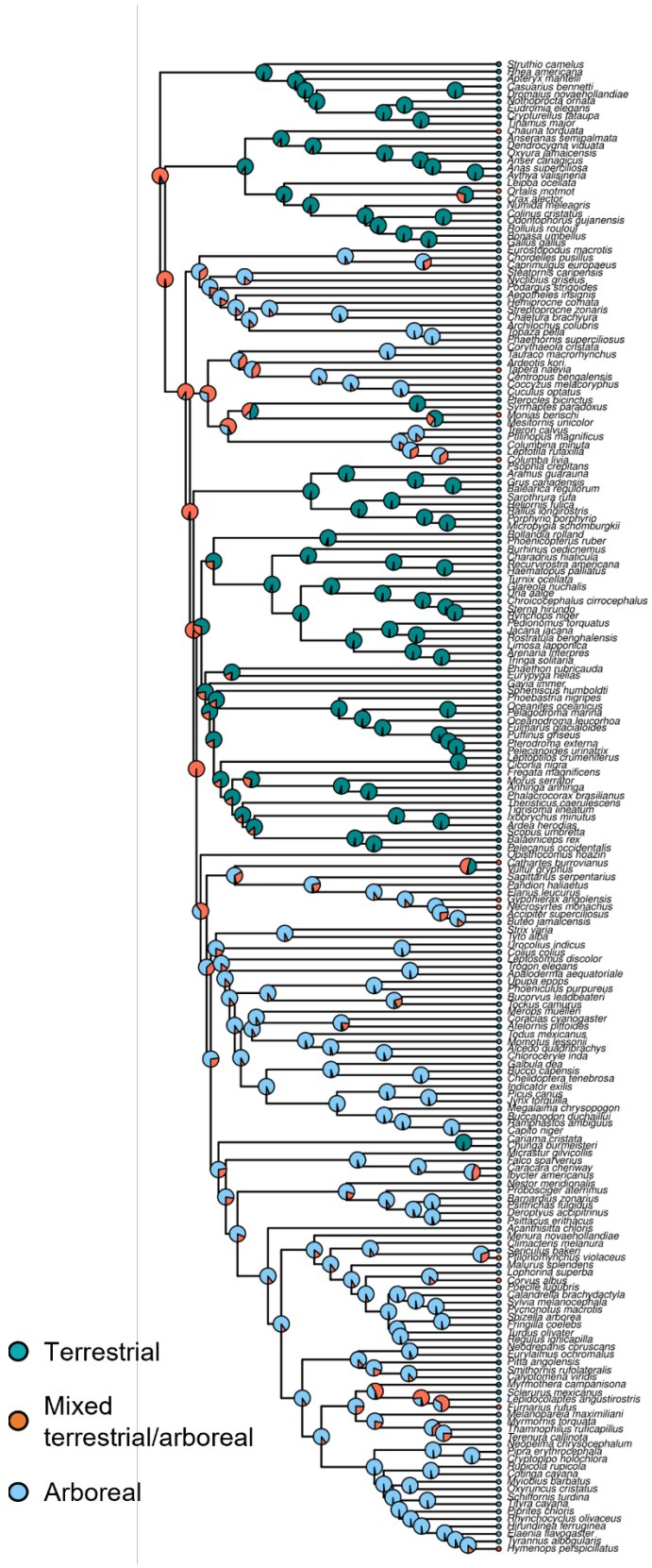


**Figure 11.** Phylogenetic tree of 200 extant avian taxa showing the ACE maximum likelihood estimates of terrestrial, arboreal, and mixed terrestrial/arboreal lifestyle (ARD model reconstruction) at each node.

### 3.3.9 Hanging and Clinging Behaviour

Hanging and clinging behaviour appears to have evolved multiple times throughout Aves (Figure 12). The ER model reconstruction had a log-likelihood of -63.1 and AICc of 128.2, whereas the ARD model reconstruction had a log-likelihood of -66.3 and AICc of 136.7. I therefore interpret the results of the statistically stronger ER model reconstruction.

The base node of Psittaciformes has a definitively high likelihood of hanging and clinging behaviour (96.6%), as well as the base node of Picides (94.8%) and Coliiformes (96.9%). Apart from these main clades, only a few other taxa within Telluraves exhibit hanging and clinging behaviour (e.g. *Oxyruncus cristatus*, *Upupa epops*) which appear to have evolved convergently. This suggests that hanging and clinging behaviour is likely a foot use that is easily evolved in a variety of digit orientations and ecologies.

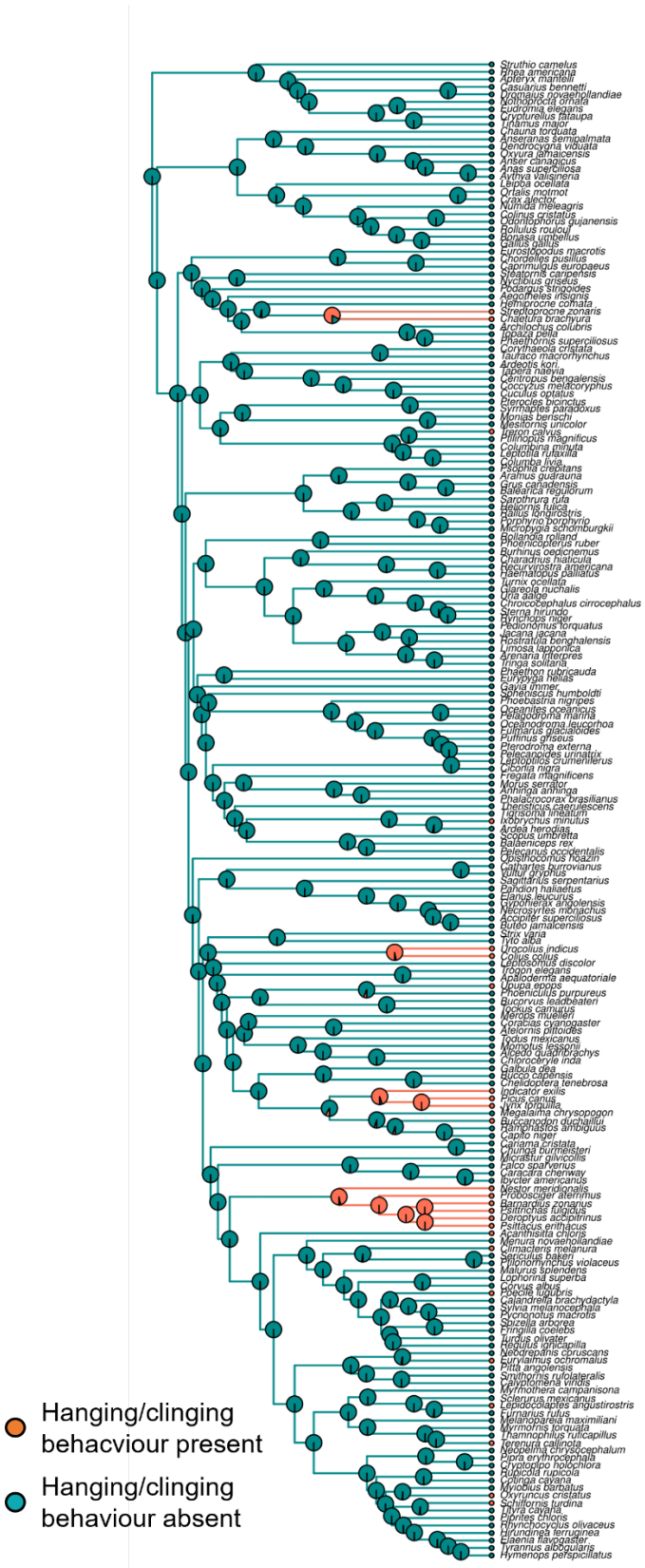


**Figure 12.** Phylogenetic tree of 200 extant avian taxa showing the ACE maximum likelihood estimates of hanging and clinging behaviour (ER model reconstruction) at each node.

### 3.3.10 Scansoriality

Scansoriality appears to have evolved multiple times throughout Telluraves (Figure 13). The ER model reconstruction had a log-likelihood of -21.9 and AICc of 45.9, whereas the ARD model reconstruction had a log-likelihood of -26.2 and AICc of 56.5. I therefore interpret the results of the statistically stronger ER model reconstruction.

Three of the six extant scansorial taxa are sufficiently widespread as to have negligible impact on the likelihood of scansoriality in their immediately ancestral nodes. The base and internal nodes of Picides are decisive in their high likelihood of ancestral scansoriality (98.7-100.0%).

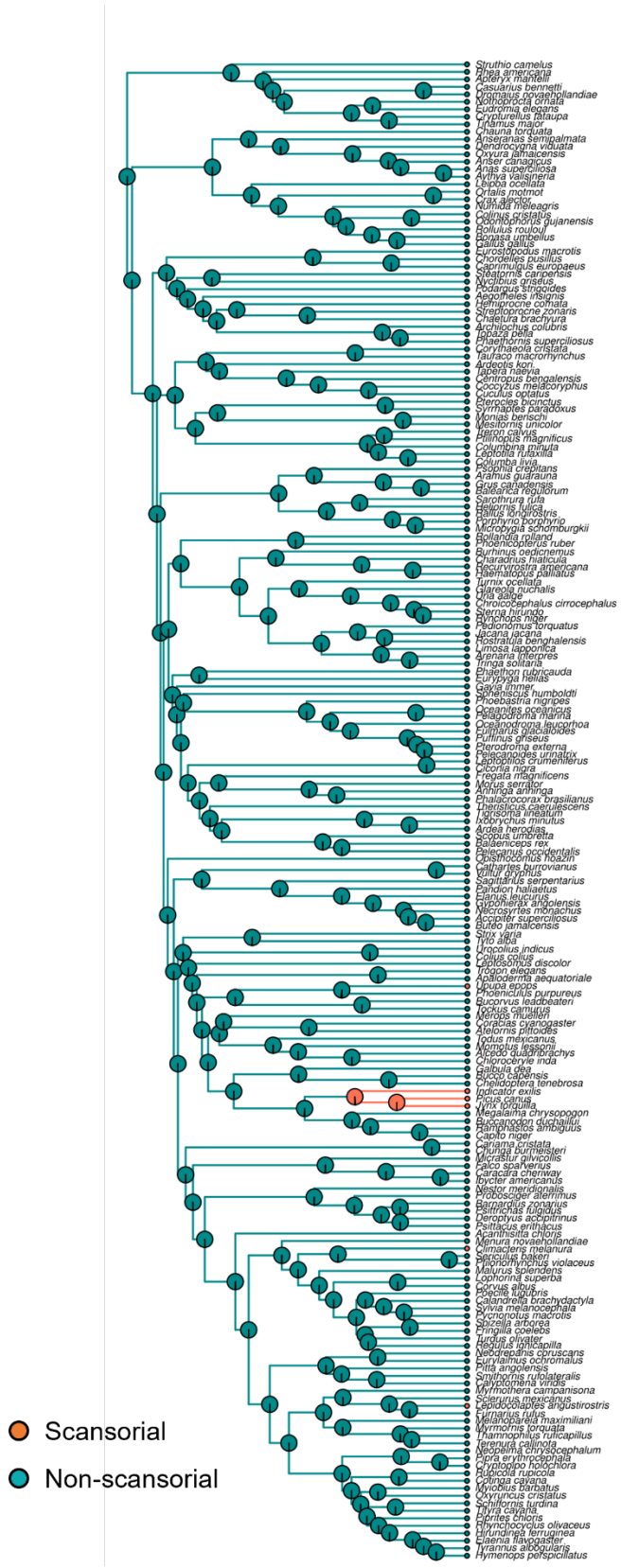


**Figure 13.** Phylogenetic tree of 200 extant avian taxa showing the ACE maximum likelihood estimates of scansoriality (ER model reconstruction) at each node.

### 3.3.11 Digital manipulation

Digital manipulation appears to have evolved multiple times throughout Telluraves (Figure 14). The ER model reconstruction had a log-likelihood of -35.2 and AICc of 72.4, whereas the ARD model reconstruction had a log-likelihood of -44.7 and AICc of 93.4. I therefore interpret the results of the statistically stronger ER model reconstruction.

There is very low likelihood of digital manipulation in Accipitriformes, as the taxa which exhibit this foot use are *Pandion*, *Elanus* and *Accipiter*; Pandionidae + Accipitridae (Figure 15) has only a 15.2% likelihood of the foot use, followed by 15.1% likelihood at *Elanus* + rest of Accipitriformes, and even more decisively low likelihoods closer to the tips. This suggests that digital manipulation may have evolved convergently in *Pandion*, *Elanus*, and *Accipiter* within Accipitriformes.

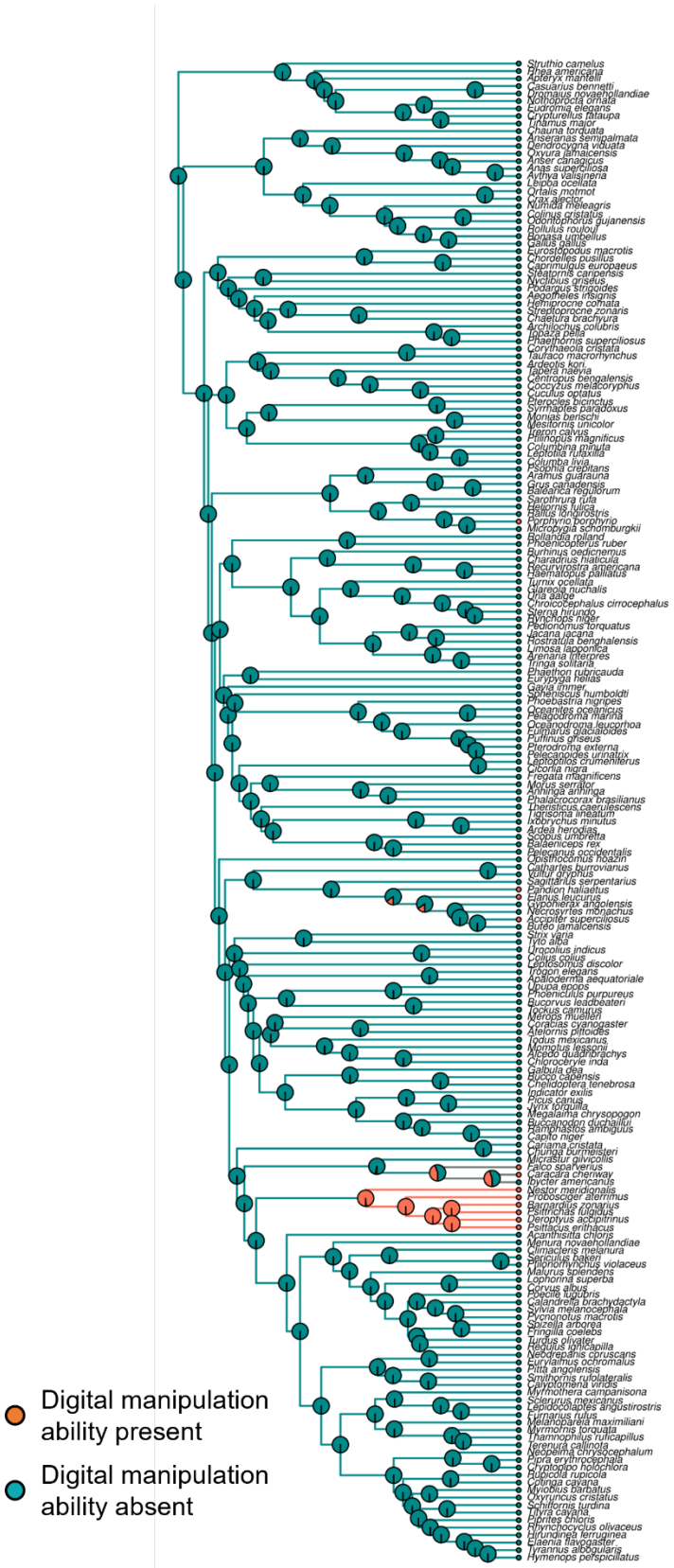


**Figure 14.** Phylogenetic tree of 200 extant avian taxa showing the ACE maximum likelihood estimates of digital manipulation ability (ER model reconstruction) at each node.

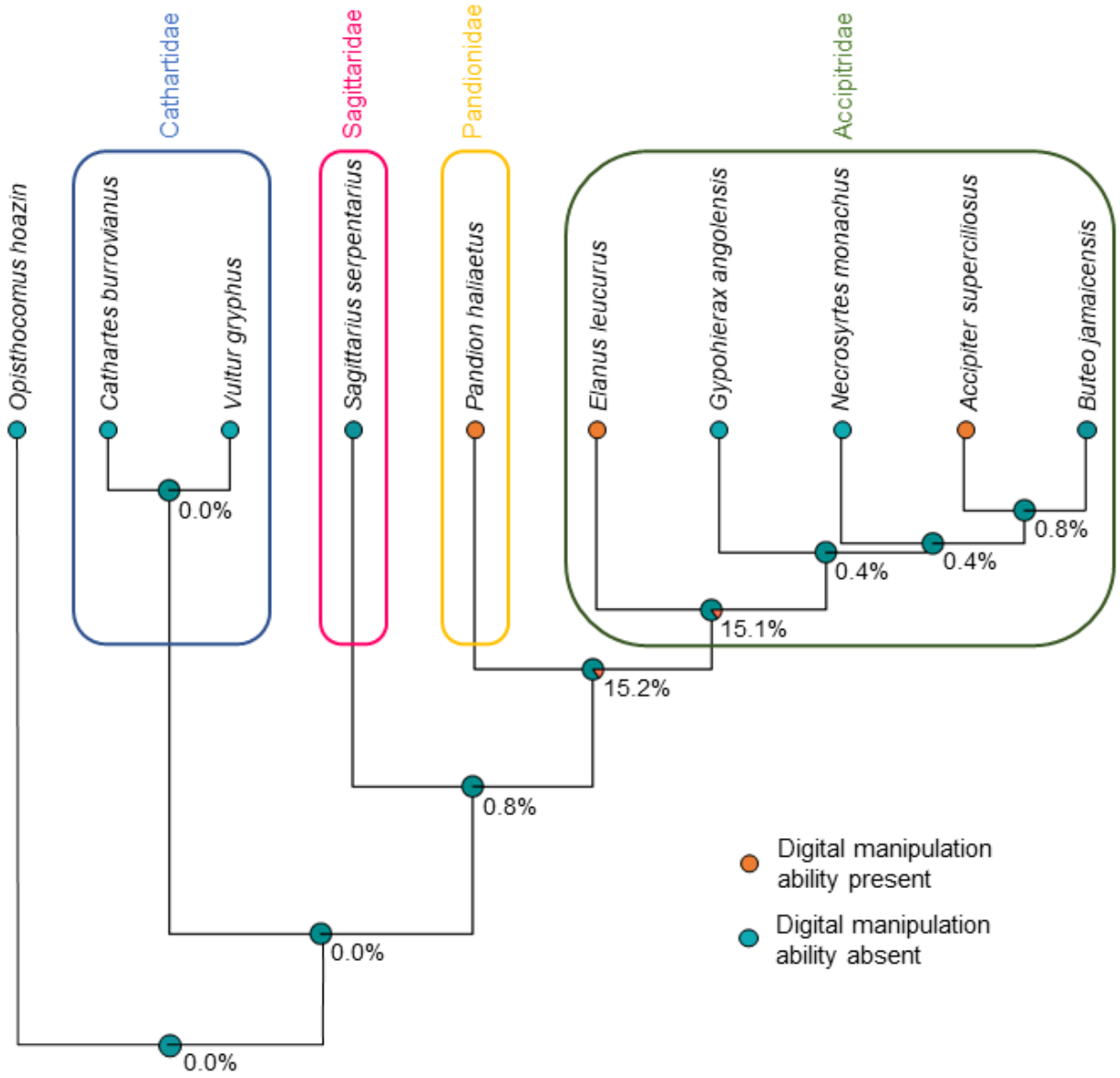


**Figure 15.** Phylogenetic tree of nine extant accipitriform taxa (outgroup: *Opisthocomus hoazin*) with ACE maximum likelihood estimates of digital manipulation ability (ER model reconstruction) at each node.

Falconiformes has an equivocal likelihood of digital manipulation in its internal nodes (44.7-44.8% likelihood of digital manipulation). Psittaciformes, however, has decisively high likelihood of digital manipulation from its stem upwards (98.6-100%). This suggests that Psittaciformes evolved the ability to manipulate objects with the toes at a much earlier point in

its evolutionary history, whereas there is an equivocal likelihood that the members of Falconiformes able to digitally manipulate objects (*Falco*, *Caracara*) evolved this trait convergently.

### 3.3.12 Ability to Hold Down Objects

The ability to hold down objects is not ancestral to Telluraves, although it does arise in the Accipitriformes, Strigiformes, Falconiformes and Psittaciformes from the base of each lineage (Figure 16). The ER model reconstruction had a log-likelihood of -35.9 and AICc of 73.7, whereas the ARD model reconstruction had a log-likelihood of -35.3 and AICc of 74.6. I therefore interpret the results of the statistically stronger ER model reconstruction.

The internal nodes within Accipitriformes are decisive in their high likelihood of ancestral ability to hold down objects, and the base node of the order has a likelihood of 85.4%. Strigiformes has a similar ancestral likelihood, of 85.6%.

The node that joins Falconiformes and Psittacopasseres has a likelihood of only 2.3%, but the base of Falconiformes (98.4%) and base of Psittaciformes (98.6%), as well as the nodes contained within each clade are decisively high in their likelihood of ability to hold down objects (Falconiformes: 98.4-100.0%; Psittaciformes: 98.6-100.0%). This suggests that the ability to hold down objects arose independently in Falconiformes and Psittaciformes, and is not ancestral to Passeriformes.

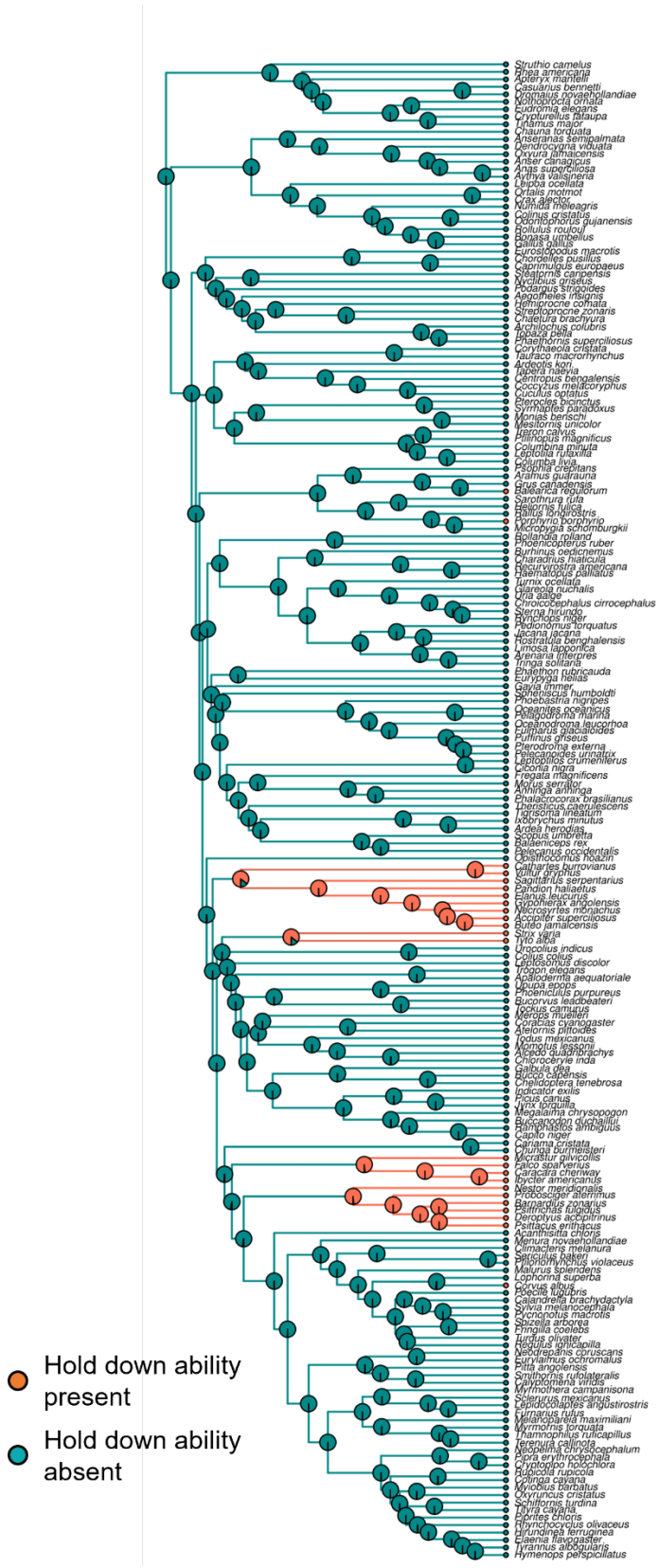


**Figure 16.** Phylogenetic tree of 200 extant avian taxa showing the ACE maximum likelihood estimates of hold down ability (ER model reconstruction) at each node.

### 3.3.13 General Perching Ability

Perching ability appears to be ancestral to a large portion of Telluraves (Figure 17), with equivocal likelihoods of perching ability at the telluravian base nodes (26.8-43.0%). The ER model reconstruction had a log-likelihood of -76.6 and AICc of 155.1, whereas the ARD model reconstruction had a log-likelihood of -71.1 and AICc of 146.3. I therefore interpret the results of the statistically stronger ARD model reconstruction.

The base node of Accipitriformes is low in its likelihood of perching ability (38.1%); this is likely due to the lack of perching ability in some members of Cathartidae, as the node ancestral to all non-New World vultures has a more decisively high likelihood (80.5%). This potentially suggests that perching ability has independent evolutionary origins in Accipitriformes. As perching ability is ubiquitous in the rest of Telluraves, the remainder of internal telluravian nodes are decisively high in likelihood of perching ability.

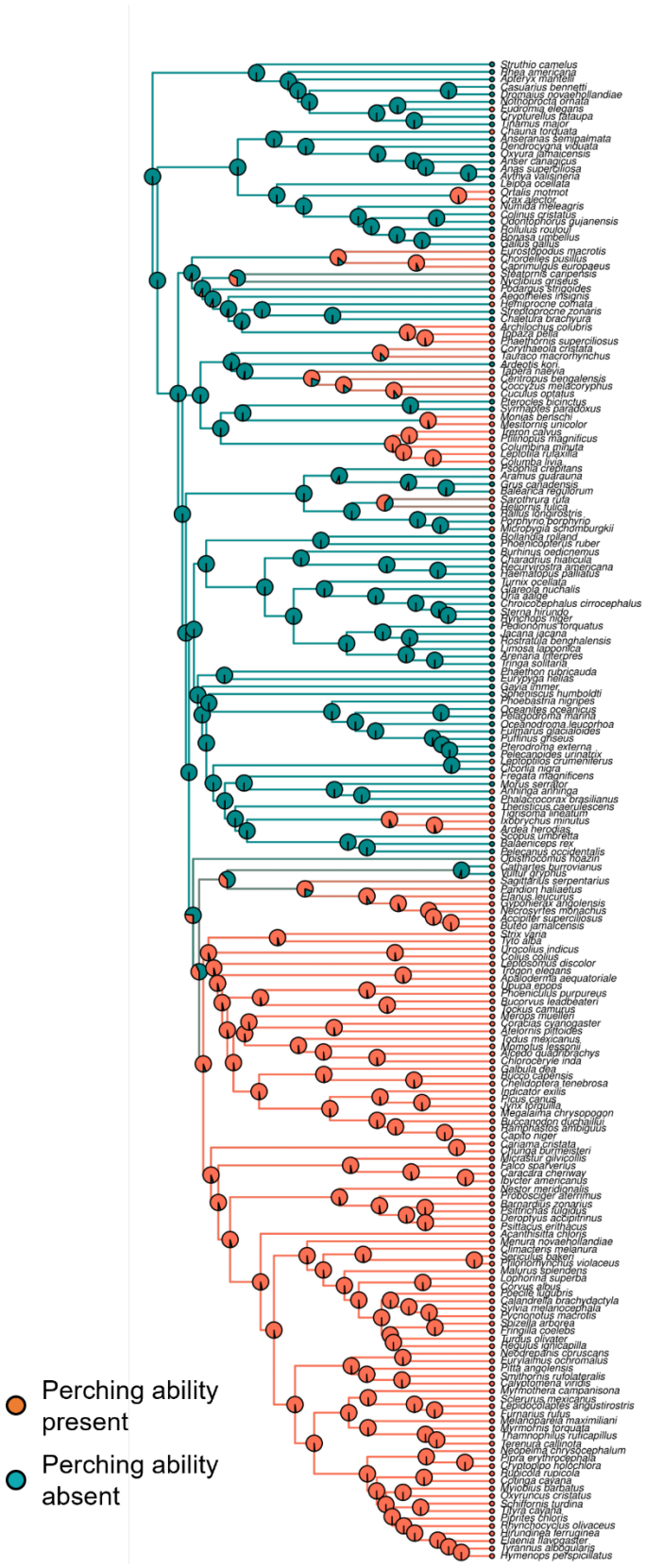


**Figure 17.** Phylogenetic tree of 200 extant avian taxa showing the ACE maximum likelihood estimates of perching ability (ARD model reconstruction) at each node.

### 3.3.14 Hopping Ability

Hopping ability appears to have differing ancestral estimation between the ER model reconstruction and the ARD model reconstruction. The ER model reconstruction had a log-likelihood of -63.3 and AICc of 128.6, whereas the ARD model reconstruction had a log-likelihood of -56.8 and AICc of 117.6. Similar to the ACE for anisodactyl digit orientation, hopping foot use may not be the sole mode of locomotion for many taxa, and is commonly present in birds which also exhibit walking ability. The ARD reconstruction is a statistically stronger model, and describes the evolutionary history of hopping locomotion as ancestral to Telluraves (Figure 18B). The ER reconstruction describes hopping locomotion as a convergent trait, arising much later and multiple times throughout Telluraves (Figure 18A). It is plausible that hopping locomotion is ancestral to Telluraves, as it does not preclude the ability to walk as categorized in these analyses.

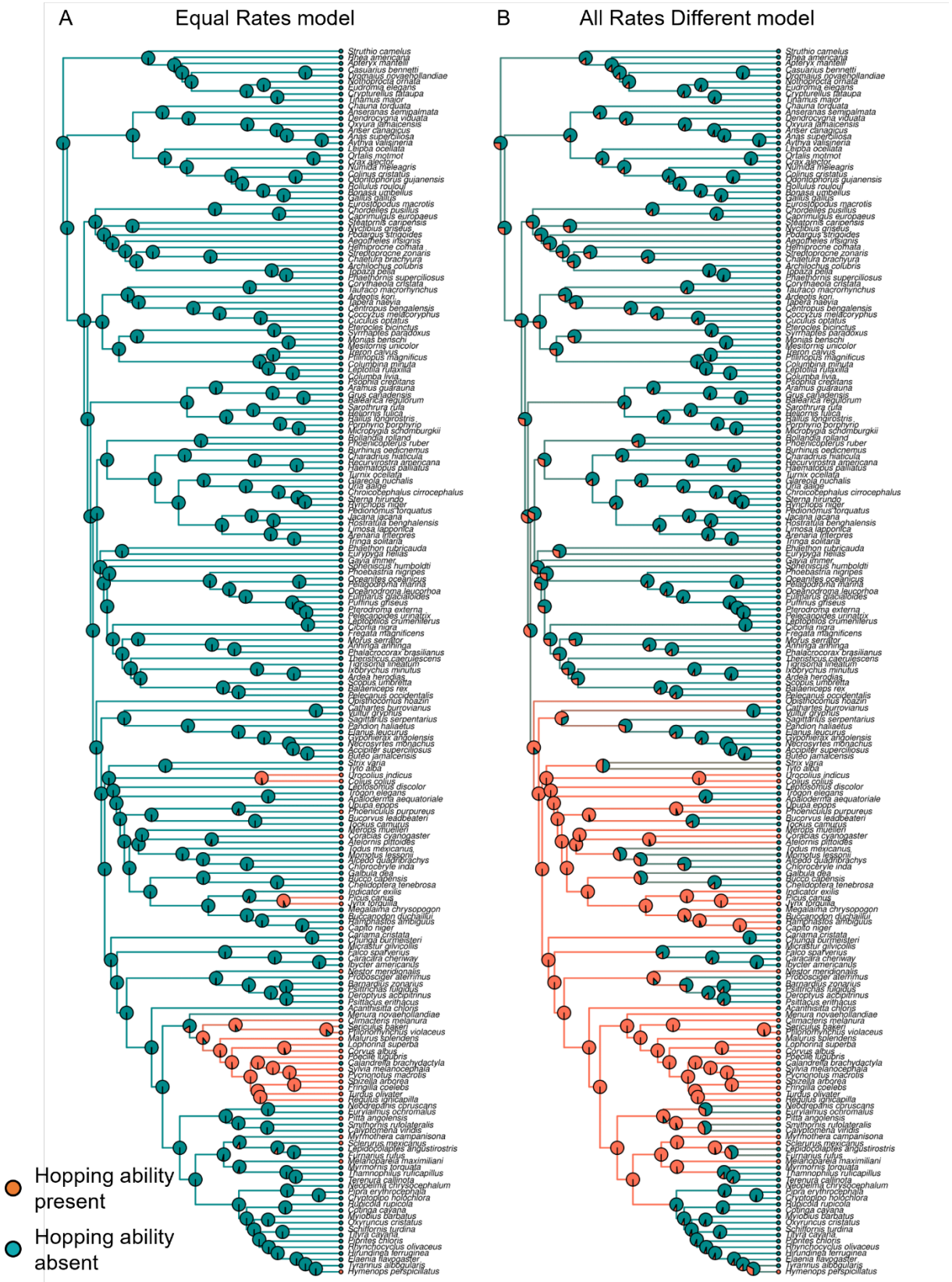


**Figure 18.** A) Phylogenetic tree of 200 extant avian taxa showing the ACE maximum likelihood estimates of hopping ability (ER model reconstruction) at each node; B) Phylogenetic tree of 200 extant

avian taxa showing the ACE maximum likelihood estimates of hopping ability (ARD model reconstruction) at each node.

### 3.3.14 Cursoriality

Cursoriality does not appear to be ancestral to Telluraves, and has equivocal likelihood of being ancestral to Aves (Figure 19). The ER model reconstruction had a log-likelihood of -63.1 and AICc of 128.3, whereas the ARD model reconstruction had a log-likelihood of -61.0 and AICc of 126.0. I therefore interpret the results of the statistically stronger ARD model reconstruction.

Only six taxa in Telluraves are cursorial, and apart from the two genera included in Cariamiformes, all of these taxa appear to have evolved their cursorial ecology convergently. Charadriiformes, Gruiformes, and Paleognathae appear to have evolved cursoriality separately, whereas the likelihood of cursoriality is equivocal at the Galloanseres node (50.8%), and at the two most ancestral nodes of Aves as a whole (54.0%; 48.5%).

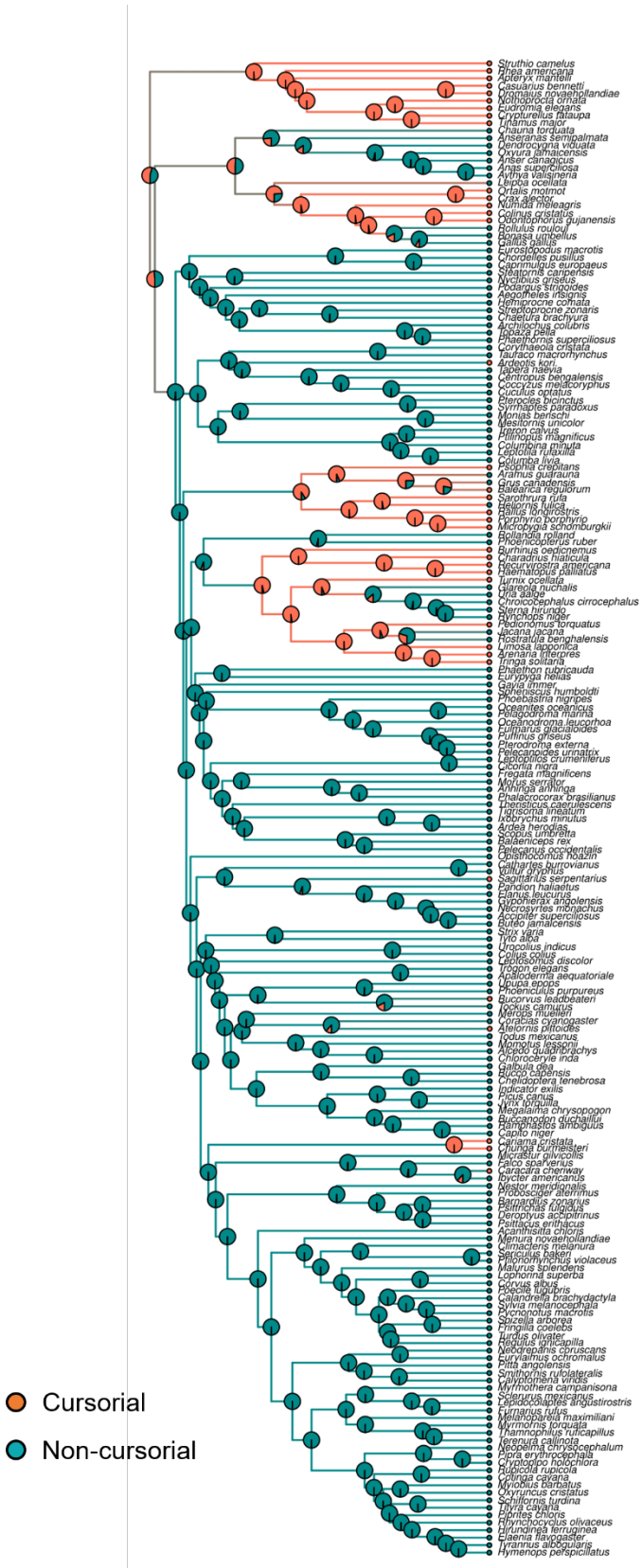


**Figure 19.** Phylogenetic tree of 200 extant avian taxa showing the ACE maximum likelihood estimates of cursoriality (ARD model reconstruction) at each node.

## 3.4 Discussion

A conservative estimate of ancestral character states reveals that raptorial foot use evolved convergently in Accipitriformes, Strigiformes, and Falconiformes. This disagrees with the hypothesis proposed by Jarvis et al. (2014) and Prum et al. (2015) of a raptorial ancestor of Telluraves, and is based on the ancestral character estimations I have reconstructed using the phylogeny of extant Aves by Prum et al. (2015) and the insertion of fossil taxa across multiple telluravian groups at ancestral nodes.

As found in Chapter 2, raptoriality is strongly linked to hypotarsus shape, so further estimates on the likelihoods of raptorial ancestry in Telluraves could be made upon the discovery of additional and relevant fossil material. Independent origins of raptorial foot use are inferred even when analysis is restricted only to extant taxa. Cathartidae are instrumental to this result, as the group does not possess monosulcate hypotarsi, is not raptorial, and is the sister to all other Accipitriformes. This implies that cathartids, unlike Old World vultures, evolved from an ancestor that did not have raptorial foot use, a conclusion that is supported by my ACE results.

The effects of raptoriality are relatively limited in both spread across the tree (within Telluraves) and in shape effect on the tarsometatarsus (monosulcate hypotarsus). It follows that since raptoriality is found to be a convergent adaptation despite resulting in significantly similar hypotarsus shapes across families, then the functional relationship present must be quite strong, and highly constrained (see Chapter 2).

Force grip foot use is exhibited by all extant raptorial taxa in these data (e.g. Figure 20), and reconstructing the ancestry of force grip foot use in Telluraves reveals that it is an ancestral trait of the group. The adaptations for force grip foot use were therefore already present for all independently evolved extant and fossil raptorial groups, prior to the evolution of raptoriality. As

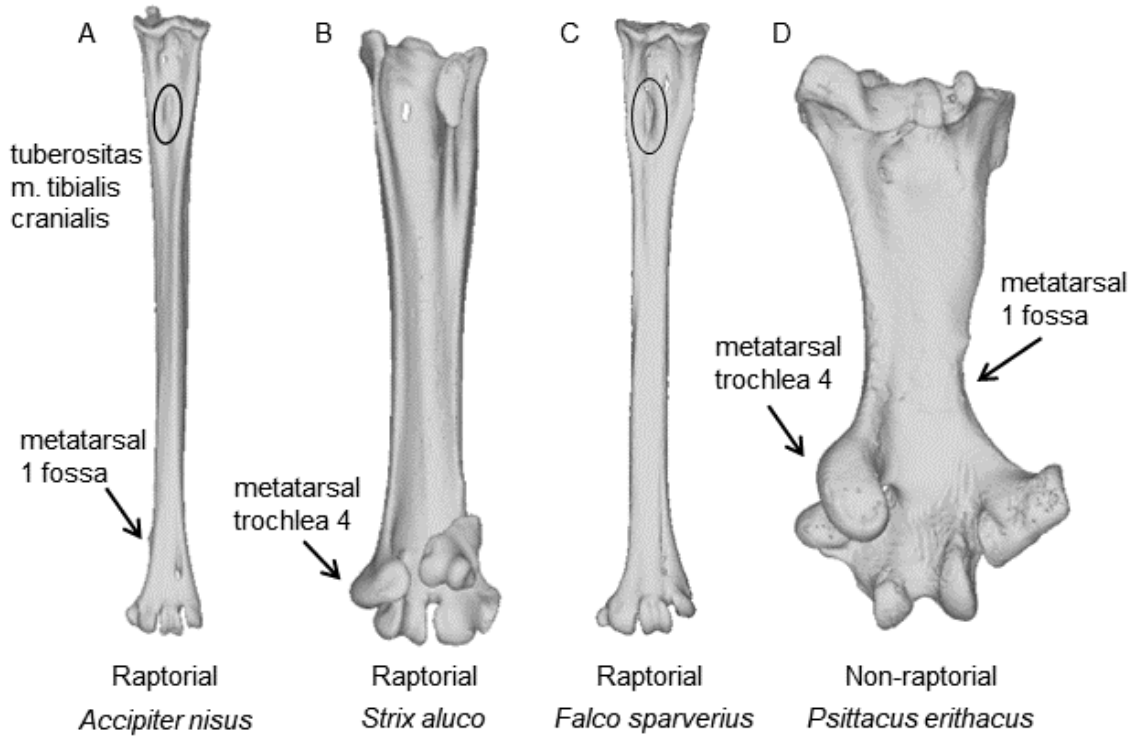


**Figure 20.** Entire left tarsometatarsi (3D models) showing the variation in morphology and force grip foot use across Telluraves; not to scale. A) Dorsal view of *Accipiter nisus* (Eurasian sparrowhawk, Accipitriformes; NHMUK S1982.149.1); B) Plantar view of *Strix aluco* (Tawny owl, Strigiformes; NHMUK S2001.38.1); C) Dorsal view of *Falco sparverius* (American kestrel, Falconiformes; UMMZ 154462); D) Plantar view of *Psittacus erithacus* (Grey parrot, Psittaciformes; NHMUK S1992.41.60).

found in Chapter 1, independent morphological effects of force grip foot use on the tarsometatarsus include a large metatarsal trochlea 4 that is anterioposteriorly flattened and rotated slightly laterally plantarward (Figure 21 A, B; Figure 23 B), a mediolaterally wider and more proximally positioned metatarsal 1 fossa (Figure 21 A; Figure 22 A, C, D, E; Figure 23 B), a more medially positioned m. tibialis cranialis tuberositas (Figure 21 A, B; Figure 22 B, D; Figure 23 A, C), and a less pronounced eminentia intercotylaris (Figure 22 D; Figure 23 A). Stem psittaciform taxa exhibit many of these characteristics (e.g. *Pulchrapollia gracilis* (BMNH PVA6207), *Messelastur gratulator* (SMF ME11348)), as well as some stem owls (e.g. *Berruornis orbisantiqui* (MNHN L3096), *Sophiornis quercynus* (Lyon PQ1202), *Eostrix*

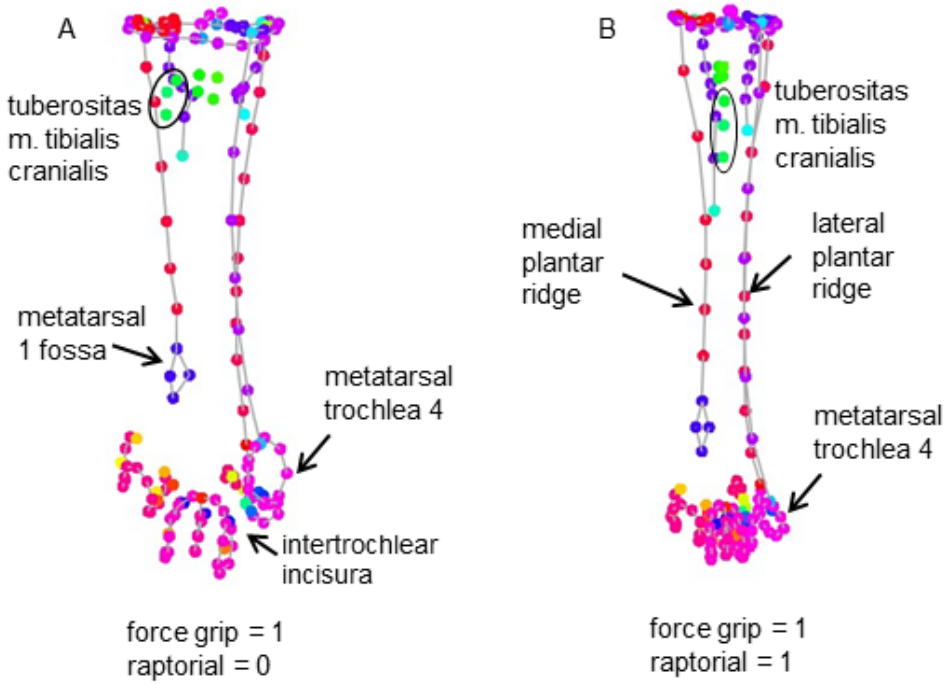


**Figure 21.** Shape deformations depicting the variation associated with force grip foot use and raptoriality from the model 'tarsometatarsus shape ~ centroid size + mean body mass + flightlessness + zygodactyly + raptoriality + force grip foot use', with centroid size set to mean value of 34 mm, mean body mass set to mean value of 1034 g, and all other foot use traits set to 0. A, B) Compared presence/absence (1/0) of force grip foot use and raptoriality.

*tsaganica* (PIN 3104/129)). Stem mousebirds (*Tsidiiyazhi abini* (NMMNH P54128) and *Anneavis anneae* (BMS E25337)) and stem coraciimorphs (*Septencoracias* sp. (IRSNB Av 191), Alcediniform sp. (IRSNB Av 190)) also exhibit the medial tuberositas m. tibialis cranialis, less pronounced eminentia intercotylaris, and more proximally positioned metatarsal 1 fossa. There is an even larger number of Paleocene and Eocene fossil taxa in this analysis which possess a flanged metatarsal trochlea 4, rather than a fully rotated one (Figure 27 B, C, D, F; Figure 28 A, C), which may indicate force grip foot use, capability of zygodactyl digit orientation, or some combination thereof. Given these qualitative observations of Paleocene and Eocene fossil taxa, an ACE of force grip foot use (or even of zygodactyl digit orientation) within Telluraves could result in an even more compelling ancestry if 3D landmarking of the entire tarsometatarsus (see

Chapter 1 methods) were able to be performed on the fossil specimens, and their foot uses statistically inferred.

The addition of fossil material to the phylogeny produces very little change in the estimation of ancestral raptoriality in Telluraves. However, the fossils were crucial to include, as they strengthened the estimations on a temporal basis (i.e. stem strigiforms have remained raptorial since the Eocene), and were particularly relevant to testing the hypothesis of raptorial ancestry in Telluraves.

*Messelastur gratulator* was also included in a set of ancestral estimations despite its deformed preservation state because of its potential raptoriality (Mayr, 2005; Mayr, 2011a). *Messelastur* was predicted to be raptorial by the flexible discriminant analysis (FDA), mixed discriminant analysis (MDA) and phyFDA (Chapter 2), and the effect of its inclusion in the phylogeny (alongside other fossil taxa) on the ancestry of Psittaciformes with respect to raptorial foot use was negligible. These results imply that some stem parrots, such as *Messelastur*, may have been raptorial, but these taxa represent independent evolutionary origins, and do not indicate that extant parrots were ancestrally raptorial.

Beyond the definition of raptoriality used in these analyses, foot uses in and adjacent to prey capture vary across raptorial clades. After stooping, ambushing, or otherwise striking their prey with their feet, raptors immobilise and dispatch their prey by asphyxiating pressure with the talons, successive strikes from the beak (Goslow, 1971; Sustaita, 2008), or utilising a combination of these techniques (Csermely et al., 1998; Hertel, 1995; Fowler et al., 2009). A convergent adaptation of morphology and raptoriality, combined with an ancestral adaptation for force grip foot use likely reflects the simultaneous scope of these individual differences as well as their functional similarities.

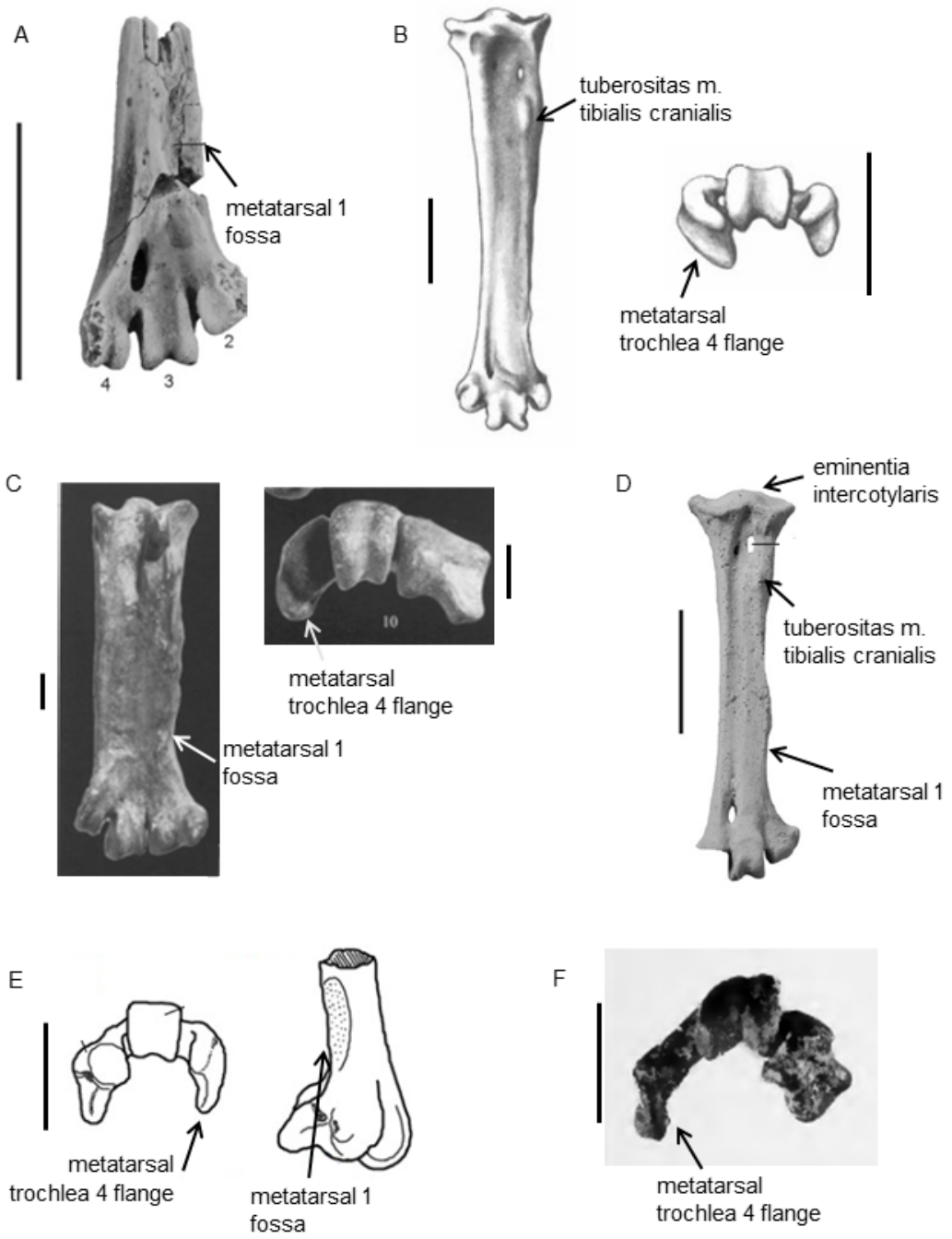


**Figure 22.** Original published images of fossil telluravian taxa; all scale bars = 5mm. A) Plantar view of Alcediniform sp. (IRSNB Av 190); B) Dorsal and distal views of *Anneavis anneae* (BMS E25337); C) Plantar and distal views of *Berrurornis orbisantiqui* (MNHN L3096); D) Plantar view of *Septencoracias* sp. (IRSNB Av 191); E) Distal and medial views of *Eostrix tsaganica* (PIN 3104/129); F) Distal view of *Ogygoptynx wetmorei* (AMNH 2653).

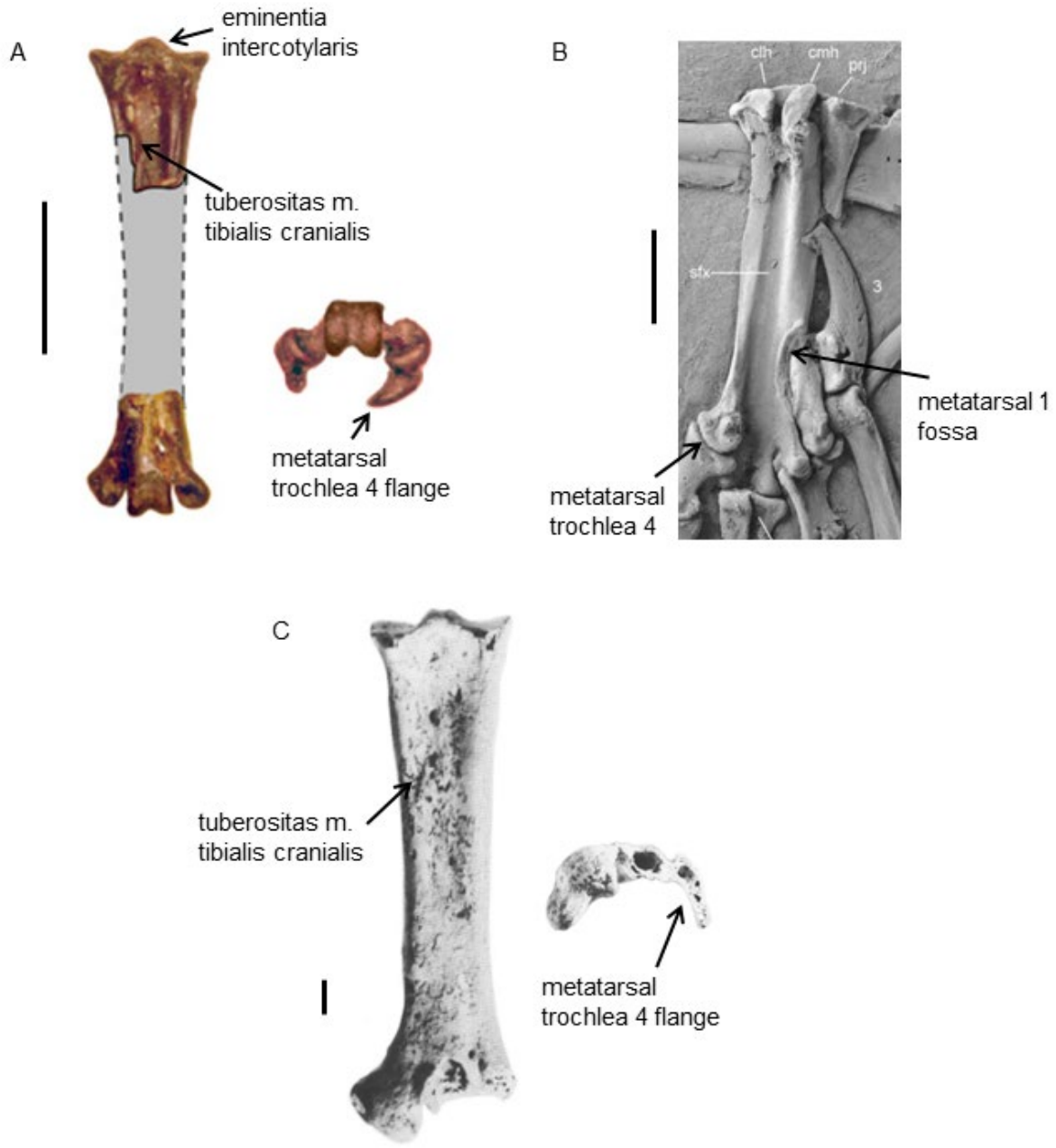


**Figure 23.** Original published images of fossil telluravian taxa; all scale bars = 5mm. A) Dorsal and distal views of *Tsidiiyazhi abini* (NMMNH P54128); B) Plantar view of *Messelastur gratulator* (SMF ME11348); C) Dorsal and distal views of *Sophiornis quercynus* (Lyon PQ1202).

### 3.4.1 Ancestral Foot Use of Telluraves

Cursoriality, ability to hold down objects, digital manipulation, scansoriality, and hanging and clinging behaviour appear to be convergent within Telluraves, in addition to raptorial foot use. The mutually inclusive nature of some of the foot uses result in confused ACE reconstructions (e.g. digit orientation characters, hopping locomotion) despite their statistically stronger models. Force grip foot use, perching ability, and potentially walking ability and anisodactyly appear to be ancestral to Telluraves.

These traits are inferred to have been widespread among ancestors of the telluravian backbone. Whereas walking ability and anisodactyly are widespread throughout Aves and are shared with the evolutionary relatives of Telluraves (e.g. Aequorlitornithes, Gruiformes), perching ability and force grip foot use are not. The telluravian backbone is also the beginning of a majority arboreal ecology, coinciding with ancestral perching ability, and contrasting with the majority terrestrial ecology of Aequorlitornithes and Gruiformes. This has intriguing implications for the ecology of their shared ancestor, as well as for the common ancestor of Telluraves, and may reflect a deep ecological split between Telluraves and its sister groups. Raptoriality evolved multiple times from a telluravian common ancestor which was arboreal and able to perch, with a foot capable of forceful gripping. These initial grasping conditions set the morphological and ecological stage for an entire radiation of birds with remarkably varied combinations of foot uses.

# Conclusion

## A. Summary

I investigated the relationship between morphology of the avian tarsometatarsus and avian foot uses and ecologies, particularly the hypotarsus and raptoriality. This significant and strong relationship provides a tool by which to infer raptoriality in extinct birds, and allowed for tests of the hypothesis of a raptorial telluravian ancestor.

In **Chapter 1**, I evaluated the ecological signal inherent to the structure of the bird tarsometatarsus. Using a combination of 3D shape data of extant taxa and foot use and ecology character scorings, I found that 26% of the variation in the overall shape of the tarsometatarsus is explained by size, body mass, raptoriality, force grip foot use, zygodactyl digit arrangement, and flightlessness. I used a phylogenetically-informed linear model to determine the statistically significant, independent effects of these foot uses and ecological aspects on tarsometatarsus shape.

In **Chapter 2**, I examined the relationship between the hypotarsus and raptoriality. Using a combination of 2D shape data of extant taxa and hypotarsus shape character scorings, I found that there is a strong, statistically significant relationship between raptoriality and hypotarsus shape, in which raptoriality tends to result in a deeply monosulcate hypotarsus. Raptoriality

explains approximately 16% of the variation in hypotarsus shape, using a linear model. This result is strongly distinguishable and delineated in shape space from non-raptorial hypotarsus shapes. I also found that the optimal value for phylogenetic signal (Pagel's λ) is 0; this suggests that hypotarsus morphology is a highly functionally constrained system, with essentially identical effects of raptoriality on hypotarsus shape, regardless of phylogenetic affinities. I inferred raptoriality in eight of 23 fossil telluravian taxa using the statistical relationship between raptoriality and extant hypotarsus shape, and 2D shape data of fossil taxa in a phylogenetic flexible discriminant analysis where $\lambda = 0$.

In **Chapter 3**, I evaluated the ancestral foot uses of Telluraves. Using the inferred raptoriality of fossil specimens in ancestral character estimations, I determined that raptoriality is convergent within Telluraves, not ancestral, as had been hypothesised. The incorporation of fossil taxa in the estimation of telluravian ancestral character state reinforces this conclusion, and increases the likelihood of an earlier evolution of raptoriality in Strigiformes than in estimations based solely on extant taxa. Force grip foot use, perching ability, arboreality and anisodactyl digit orientation were determined to be ancestral to Telluraves. Cursoriality, ability to hold down objects, digital manipulation, scansoriality, and hanging and clinging behaviour were determined to be convergent within Telluraves.

## **B.** Caveats

I was unable to incorporate fossils with uncertain phylogenetic affinities into both the phylogenetic discriminant function analyses and the ancestral character estimations, despite their relatively acceptable preservation quality (e.g. *Horusornis vianeyliaudae* (BFI 1958)). Tangentially, I am unable to use the results of my research into the relationship between

hypotarsus shape and raptoriality to assist in estimating those affinities; due to the highly constrained system with no phylogenetic signal ($\lambda = 0$), and the multiple convergent evolutions of raptoriality in Telluraves, taxa with deeply monosulcate hypotarsi can be predicted to be raptorial, but cannot be accurately assigned to well-resolved positions in the tree based on hypotarsus shape alone.

The regression analysis of digital flexor tendon cross-sectional area was performed on only six taxa, which means the results are only preliminary and should not be used for a source of reliable information. Ideally, a larger sample size of extant taxa across Telluraves would be analysed in further investigations.

The raptoriality of fossils that are poorly preserved (broken, eroded, etc) may not be accurately predicted because of the discriminant function analyses' basis on landmark shape comparison. This caveat corresponds with potential errors introduced by manual landmarking of both 2D and 3D shapes, and difficult landmarks to place, which would affect downstream analyses if gone unnoticed.

## C. Future Directions

The methods described in this research may be used in the near future for inferring raptoriality in other extinct avian taxa known only from fossils, as well as in fossil taxa from Ornithothoraces (encompassing both the group which includes modern birds and their closest ancestors, as well as Enantiornithes). Not only 2D shape analysis of the hypotarsus, but also 3D shape analysis of the tarsometatarsus may assist in making ecological inferences in fossil taxa; I believe my 3D landmarking scheme is both sufficiently thorough and informative to perform shape analysis on tarsometatarsi in future ecomorphological studies of any foot use.

It was found that there is a slight increase in digital flexor tendon cross-sectional area associated with raptorial foot use, as well as an increase in tendon cross-sectional area as bone cross-sectional area increases. A more robust investigation could be performed on this relationship between digital flexor tendon size and raptoriality with a larger sample of extant taxa across Telluraves. In addition to strengthening the statistical power of the analysis, a larger sample size would encompass a wider range of raptorial groups, and may allow for investigation of trends at the family level. There was found to be no particular bias for enlargement between the flexor digitorum longus (FDL) and the flexor hallucis longus (FHL) tendons in raptorial taxa, and this was provisionally explained by the wide variation in use of these tendons among raptorial taxa across families. This result may change if a sufficient number of specimens are added to the analysis so as to enable an examination of intra-family similarities (or dissimilarities).

Lastly, it may be elucidating to perform an investigation into the ancestry of force grip foot use using similar 3D tarsometatarsus shape analysis and discriminant function analyses as performed here. The additive relationship between ancestral force grip foot use and convergent raptoriality in Telluraves is an intriguing one, and the results of the ACE on force grip foot use may change or strengthen if similarly informative fossil material is added to the dataset. This would require initial research on the potential for inferring force grip foot use in fossil taxa of stem telluravian groups, as well as a wider fossil specimen sample.

## D. Synthesis

By first investigating the broader ecomorphological relationships between foot uses and tarsometatarsus shape, I was able to hone in on the hypotarsus as a particular anatomical region

for statistically inferring raptoriality in extant and extinct taxa. This new information in turn provided important data for estimating the evolutionary history of raptoriality in Telluraves.

This research adds to the knowledge of landbird evolution, particularly the ecomorphological relationships present in both extant and stem fossil taxa. Raptorial birds present a striking example of convergent evolution, and the hypotarsus provides a reliable tool for inferring raptoriality in extinct taxa known only from fossils. As well, the shared ancestry of force grip foot use, perching ability, and arboreality in Telluraves suggests that these traits may have also played a role in the convergent evolution of raptoriality.

# Appendices

# A. Supporting Charts for the Introduction

## *A.1 Tables*

**Table A.1.** Examples of raptorial terminology usage in literature from 1971 to the present, ordered chronologically.

| Author | Year | Title | Taxa |
|---|---|---|---|
| Goslow | 1971 | The Attack and Strike of Some North American Raptors | Accipitridae, Falconidae |
| Arredondo | 1976 | The Great Predatory Birds of the Pleistocene of Cuba | Vulturidae, Accipitridae, Strigidae, Tytonidae |
| Raikow | 1985 | Locomotor System | range |
| Burton | 1989 | Birds of Prey | range |
| Quinn and Baumel | 1990 | The digital tendon locking mechanism of the avian foot (Aves) | range |
| Hertel | 1995 | Ecomorphological Indicators of Feeding Behavior in Recent and Fossil Raptors | Accipitriformes, Falconidae |
| Csermely et al. | 1998 | Prey Killing by Eurasian Kestrels: The Role of the Foot and the Significance of Bill and Talons | Falco tinnunculus (Eurasian kestrel) |
| Mayr | 2000 | A new raptor-like bird from the Lower Eocene of North America and Europe | Tynskya eocaena |
| Middleton | 2001 | The morphological basis of hallucal orientation in extant birds | range |
| Ward et al. | 2002 | Functional Morphology of Raptor Hindlimbs: Impllications for Resource Partitioning | Accipitridae, Strigiformes, Falconidae |
| Zeffer and Norberg | 2003 | Leg morphology and locomotion in birds: requirements for force and speed during ankle flexion | range |
| Zeffer et al. | 2003 | Functional correlation between habitat use and leg morphology in birds (Aves) | range |
| Mayr | 2006 | A new raptorial bird from the Middle Eocene of Messel, Germany | Masillaraptor |
| Negro et al. | 2006 | Convergent Evolution of Elanus Kites and the Owls | Accipitridae, Strigiformes |
| Einoder and Richardson | 2007 | ASPECTS OF THE HINDLIMB MORPHOLOGY OF SOME AUSTRALIAN BIRDS OF PREY: A COMPARATIVE AND QUANTITATIVE STUDY | Accipitridae, Falconidae, Tytonidae, Strigidae |

| Author | Raptorial Reference | Uses "raptor"/"raptorial" | Definition of Raptorial |
|---|---|---|---|
| Goslow | "raptor", "raptorial", "birds of prey" | Yes | None |
| Arredondo | "raptorial birds", "predators", "diurnal raptors", "occupied the niches…usually filled by…carnivorous mammals", "carnivorous birds" | Yes | None |
| Raikow | "raptorial" | Yes | as a foot subtype under perching, "raptorial" or "prey-grasping" |
| Burton | "birds of prey", "raptor" | Yes | taxa which "capture prey large in proportion to their own size"; usually vertebrate prey; with "formidable" talons used to kill prey |
| Quinn and Baumel | "raptors" | Yes | in reference to perching and grasping |
| Hertel | "raptors", "birds of prey" | Yes | "diurnal birds of prey, including vultures", subdivided by diet |
| Csermely et al. | "birds of prey", "raptor" | Yes | None |
| Mayr | "raptor-like", "raptorial" | Yes | None |
| Middleton | "raptorial" | Yes | None |
| Ward et al. | "raptors" | Yes | "highly efficient predatory characteristics . . . largely dependent on their use of powerful hindlimbs to subdue prey." |
| Zeffer and Norberg | "birds of prey" | No | "mainly carry their prey close to the body with their claws during flight" |
| Zeffer et al. | "birds of prey" | No | "species that strike and carry prey with the feet" vultures not included |
| Mayr | "raptorial", "diurnal raptors" | Yes | Accipitriformes (incl. Cathartidae, Pandion and Sagittaridae), Falconiformes |
| Negro et al. | "diurnal raptors" | Yes | order Falconiformes (old def'n), owls separate |
| Einoder and Richardson | "bird of prey", "raptor", "predatory lifestyle" | Yes | rely heavily on feet and talons for feeding; use feet to catch, kill, and carry their prey; |

| Author | Year | Title | Taxa |
|---|---|---|---|
| Habib and Ruff | 2007 | The effects of locomotion on the structural characteristics of avian limb bones | range |
| Sustaita | 2008 | Musculoskeletal Underpinnings to Differences in Killing Behavior Between North American Accipiters (Falconiformes: Accipitridae) and Falcons (Falconidae | Accipitridae, Falconidae |
| Sustaita | 2008 | Musculoskeletal underpinnings to differences in killing behavior between North American accipiters (Falconiformes: Accipitridae) and falcons (Falconidae) | Accipitriformes, Falconiformes |
| Fowler et al. | 2009 | Predatory Functional Morphology in Raptors: Interdigital Variation in Talon Size Is Related to Prey Restraint and Immobilisation Technique | Accipitridae, Falconidae, Pandionidae, Strigiformes |
| Sustaita and Hertel | 2010 | In vivo bite and grip forces, morphology and prey-killing behavior of North American accipiters (Accipitridae) and falcons (Falconidae) | Accipitridae, Falconidae |
| Mayr et al. | 2013 | A Strigogyps-like bird from the middle Paleocene of China with an unusual grasping foot | Qianshanornis rapax |
| Sustaita et al. | 2013 | Getting a grip on tetrapod grasping: form, function, and evolution: Grasping in tetrapods | range |
| Jarvis et al. | 2014 | Whole-genome analyses resolve early branches in the tree of life of modern birds | range |
| Li et al. | 2014 | A new specimen of large-bodied basal enantiornithine Bohaiornis from the early Cretaceous of China and the inference of feeding ecology in Mesozoic birds | Bohaiornis, range |
| Backus et al. | 2015 | Mechanical analysis of avian feet: multiarticular muscles in grasping and perching | range |
| Heers and Dial | 2015 | Wings versus legs in the avian bauplan : Development and evolution of alternative locomotor strategies | range |

| Author | Raptorial Reference | Uses "raptor"/"raptorial" | Definition of Raptorial |
|---|---|---|---|
| Habib and Ruff | "raptor", "hypercarnivorous", "birds of prey" | Yes | None, but they mention that they don't place ravens with the other "raptors and owls" because ravens don't kill prey with the hindlimbs, and also don't exert enough force on their prey |
| Sustaita | "raptor" | Yes | Falconiformes (old group, including Accipitridae) |
| Sustaita | "raptors" | Yes | order Falconiformes (old def'n) |
| Fowler et al. | "raptor", "birds of prey" | Yes | None |
| Sustaita and Hertel | "raptors" | Yes | None (reference importance of grasping for subduing prey) |
| Mayr et al. | "raptor", "raptorial" | Yes | "used its feet to manipulate animal prey" |
| Sustaita et al. | "raptors", "predatory" | Yes | None ("Most raptors use their feet to seize and subdue their prey") |
| Jarvis et al. | "apex predator", "raptorial trait", Eocene taxa with "raptor-like feet" | Yes | None ("Seriema…could be considered to belong to a raptorial taxon because they kill vertebrate prey") |
| Li et al. | "raptorial", "predominantly carnivorous taxa" | Yes | "predominantly carnivorous taxa" "such as eagles, hawks and falcons, owls and vultures, with hooked bills and strong pedal unguals or [recurved] talons" |
| Backus et al. | "raptorial bird", "raptorial 'grasping' species" | Yes | hawks, falcons, owls; powerful manipulation with feet, as opposed to dexterous (parrots); 'grasping' spp carry prey with feet |
| Heers and Dial | "raptors", "predatory" | Yes | None |

| Author | Year | Title | Taxa |
|---|---|---|---|
| Hertel et al. | 2015 | Wing and hindlimb myology of vultures and raptors (Accipitriformes) in relation to locomotion and foraging | Accipitriformes (Accipitridae, Vulturidae) |
| Prum et al. | 2015 | A comprehensive phylogeny of birds (Aves) using targeted next-generation DNA sequencing | range |
| Mayr | 2016 | Variations in the hypotarsus morphology of birds and their evolutionary significance | range |
| Madan et al. | 2017 | Scaling and functional morphology in strigiform hind limbs | Strigiformes |
| Navalon et al. | 2017 | The evolutionary relationship among beak shape, mechanical advantage, and feeding ecology in modern birds | range |
| McClure et al. | 2019 | Commentary: Defining Raptors and Birds of Prey | definition |
| Sustaita et al. | 2019 | Behavioral correlates of semi-zygodactyly in Ospreys (Pandion haliaetus) based on analysis of internet images | Pandionidae |
| Tsang and McDonald | 2019 | A comparative study of avian pes morphotypes, and the functional implications of Australian raptor pedal flexibility | Accipitridae, Falconidae, Strigiformes |
| Mayr et al. | 2020 | Skeleton of a new owl from the early Eocene of North America (Aves, Strigiformes) with an Accipitrid-like foot morphology | Primoptynx poliotauros |
| Wu et al. | 2020 | Genomic bases underlying the adaptive radiation of core landbirds | range |

| Author | Raptorial Reference | Uses "raptor"/"raptorial" | Definition of Raptorial |
|---|---|---|---|
| Hertel et al. | "raptors", ("scavengers"), | Yes | "most raptors…seize and kill their prey with their feet" (but vultures rarely kill their prey) |
| Prum et al. | "raptorial" | Yes | indirect reference to owls, hawks, falcons and seriemas as "persistence of raptorial ecology" |
| Mayr | (no mention) | No | obliquely groups Accipitridae, Falconidae, and Strigiformes as taxa which capture prey with the feet |
| Madan et al. | "raptorial", "raptors" | Yes | None |
| Navalon et al. | "raptorial", "raptors" | Yes | (not about the feet) use beak for tearing to consume high % of vertebrates |
| McClure et al. | "raptor", "raptorial" | Yes | "all species within orders evolved from raptorial landbirds in which most species maintained raptorial lifestyles" so, Accipitriformes, Cathartiformes, Falconiformes, Strigiformes, also Cariamiformes |
| Sustaita et al. | "raptors", "birds of prey", "diurnal raptors" | Yes | None |
| Tsang and McDonald | "raptors", "birds of prey", "diurnal raptors" | Yes | birds that hunt animals and insects using their highly evolved senses (such as vision, hearing or smell), strongly curved beaks for tearing at prey and strong feet and sharp talons for holding and wounding prey. |
| Mayr et al. | "raptor", "raptorial" | Yes | None |
| Wu et al. | "raptorial", "birds of prey" | Yes | Accipitriformes, Strigiformes, Falconiformes |

**Table A.2.** Evidence of carnivorous diet in Telluraves, subsected by family. Consumption of vertebrates is bolded. All dietary information was gathered from *Birds of the World* (ed. Billerman et al., 2021).

| Carnivorous Telluravian Group | Family and Common Name | Carnivorous Diet |
|---|---|---|
| Order Accipitriformes | Cathartidae (New World Vultures) | **Vertebrates** (including carrion) |
| | Sagittaridae (Secretarybird) | **Vertebrates**, insects |
| | Pandionidae (Osprey) | **Vertebrates** |
| | Old World Vultures | **Vertebrates** (including carrion) |
| | Accipitridae (Hawks, Eagles, and Kites) | **Vertebrates**, insects (including larvae), crustaceans, snails, eggs, bone marrow |
| Order Strigiformes | Tytonidae (Barn-owls) | **Vertebrates**, insects |
| | Strigidae (Owls) | **Vertebrates**, insects |
| Order Leptosomiformes | Leptosomidae (Cuckoo-rollers) | **Vertebrates**, insects |
| Order Trogoniformes | Trogonidae (Trogons) | **Vertebrates**, insects |
| Order Bucerotiformes | Upupidae (Hoopoes) | Insects |
| | Phoeniculidae (Woodhoopoes and Scimitarbills) | Insects |
| | Bucorvidae (Ground-hornbills) | **Vertebrates**, insects |
| | Bucerotidae (Hornbills) | **Vertebrates**, insects |
| Order Coraciiformes | Todidae (Todies) | Insects |
| | Momotidae (Motmots) | Insects, **vertebrates**, crustaceans, annelids, snails |
| | Alcedinidae (Kingfishers) | **Vertebrates**, insects, annelids |
| | Meropidae (Bee-eaters) | Insects |
| | Coraciidae (Rollers) | Insects, **vertebrates** |
| | Brachypteraciidae (Ground-rollers) | Insects, crustaceans, **vertebrates**, snails |
| Order Galbuliformes | Bucconidae (Puffbirds) | **Vertebrates**, insects |
| | Galbulidae (Jacamars) | **Vertebrates**, insects |
| Order Piciformes | Lybiidae (African Barbets) | Insects |
| | Megalaimidae (Asian Barbets) | Insects, **vertebrates** |
| | Capitoniidae (New World Barbets) | Insects |
| | Semnornithidae (Toucan-Barbets) | Insects |
| | Ramphastidae (Toucans) | Insects, **vertebrates**, eggs |
| | Indicatoridae (Honeyguides) | Insects |
| | Picidae (Woodpeckers) | Insects |
| Order Cariamiformes | Cariamidae (Seriemas) | Insects, **vertebrates** |
| Order Falconiformes | Falconidae (Falcons and Caracaras) | **Vertebrates** (including carrion), insects (including larvae) |

| Carnivorous Telluravian Group | Family and Common Name | Carnivorous Diet |
|---|---|---|
| Order Psittaciformes | Strigopidae (New Zealand Parrots) | **Vertebrates** (including carrion), insects |
| | Cacatuidae (Cockatoos) | Insects |
| | Psittaculidae (Old World Parrots) | Insects |
| Order Passeriformes | Acanthisittidae (New Zealand Wrens) | Insects |
| | Calyptomenidae (African and Green Broadbills) | Insects |
| | Eurylaimidae (Asian and Grauer's Broadbills) | Insects, **vertebrates** |
| | Sapayoidae (Sapayoas) | Insects |
| | Philepittidae (Asities) | Insects |
| | Pittidae (Pittas) | Annelids, insects, **vertebrates**, snails |
| | Thamnophilidae (Typical Antbirds) | Insects, **vertebrates**, snails |
| | Melanopareiidae (Crescentchests) | Insects |
| | Conopophagidae (Gnateaters) | Insects, **vertebrates** |
| | Grallariidae (Antpittas) | Insects, annelids |
| | Rhinocryptidae (Tapaculos) | Insects |
| | Formicariidae (Antthrushes) | Insects, **vertebrates** |
| | Furnariidae (Ovenbirds and Woodcreepers) | Insects, **vertebrates**, crustaceans, molluscs |
| | Pipridae (Manakins) | Insects |
| | Cotingidae (Cotingas) | Insects, **vertebrates** |
| | Tityridae (Tityras and allies) | Insects, **vertebrates** |
| | Oxyruncidae (Sharpbill, Royal Flycatcher, and allies) | Insects |
| | Tyrannidae (Tyrant Flycatchers) | Insects, **vertebrates** |
| | Menuridae (Lyrebirds) | Insects, **vertebrates** |
| | Atrichornithidae (Scrub-birds) | Insects |
| | Ptilonorhynchidae (Bowerbirds) | Insects, **vertebrates** |
| | Climacteridae (Australasian Treecreepers) | Insects |
| | Maluridae (Fairywrens) | Insects |
| | Meliphagidae (Honeyeaters) | Insects |
| | Dasyornithidae (Bristlebirds) | Insects |
| | Pardalotidae (Pardalotes) | Insects |
| | Acanthizidae (Thornbills and allies) | Insects |
| | Pomatostomidae (Pseudo-babblers) | Insects |
| | Orthonychidae (Logrunners) | Insects |

| Carnivorous Telluravian Group | Family and Common Name | Carnivorous Diet |
|---|---|---|
| Order Passeriformes (cont'd) | Cinclosomatidae (Quail-thrushes and Jewel-babblers) | Insects |
| | Campephagidae (Cuckooshrikes) | Insects |
| | Mohouidae (Whiteheads) | Insects |
| | Neosittidae (Sittellas) | Insects (including larvae) |
| | Psophodidae (Whipbirds and Wedgebills) | Insects, snails |
| | Eulacestomatidae (Ploughbill) | Insects |
| | Oreoicidae (Australo-Papuan Bellbirds) | Insects, annelids |
| | Falcuculidae (Shrike-tit) | Insects |
| | Paramythiidae (Tit Berrypecker and Crested Berrypecker) | Insects |
| | Oriolidae (Old World Orioles) | Insects, **vertebrates** |
| | Macaerirhynchidae (Boatbills) | Insects |
| | Artamidae (Woodswallows, Bellmagpies, and allies) | Insects, **vertebrates**, eggs |
| | Rhagologidae (Mottled Berryhunter) | Insects |
| | Platysteiridae (Wattle-eyes and Batises) | Insects, **vertebrates** |
| | Vangidae (Vangas, Helmetshrikes, and allies) | Insects, **vertebrates** |
| | Pityriasidae (Bristlehead) | Insects, **vertebrates** |
| | Aegithinidae (Ioras) | Insects |
| | Malaconotidae (Bushshrikes and allies) | **Vertebrates**, insects |
| | Rhipiduridae (Fantails) | Insects, **vertebrates** |
| | Dicruridae (Drongos) | Insects |
| | Paradisaeidae (Birds-of-Paradise) | Insects |
| | Ifritidae (Ifrita) | Insects |
| | Monarchidae (Monarch Flycatchers) | Insects, **vertebrates** |
| | Corcoracidae (White-winged Chough and Apostlebird) | Insects, **vertebrates**, molluscs |
| | Melampittidae (Melampittas) | Insects, annelids, **vertebrates** |
| | Platylophidae (Crested Shrikejay) | Insects |
| | Laniidae (Shrikes) | Insects, **vertebrates** |
| | Corvidae (Crows, Jays, and Magpies) | **Vertebrates** (including carrion), insects, eggs, molluscs, annelids |
| | Cnemophilidae (Satinbirds) | Insects |
| | Melanocharitidae (Berrypeckers and Longbills) | Insects |

| Carnivorous Telluravian Group | Family and Common Name | Carnivorous Diet |
|---|---|---|
| Order Passeriformes (cont'd) | Callaeidae (Wattlebirds) | Insects |
| | Notiomystidae (Stitchbird) | Insects |
| | Petroicidae (Australasian Robins) | Insects, crustaceans, **vertebrates** |
| | Picathartidae (Rockfowl) | Insects, annelids, crustaceans, **vertebrates** |
| | Chaetopidae (Rockjumpers) | Insects, **vertebrates** |
| | Eupetidae (Rail-babbler) | Insects |
| | Hyliotidae (Hyliotas) | Insects |
| | Stenostiridae (Fairy Flycatchers) | Insects |
| | Paridae (Tits, Chickadees, and Titmice) | Insects |
| | Remizidae (Penduline-Tits) | Insects |
| | Alaudidae (Larks) | Insects |
| | Panuridae (Bearded Reedling) | Insects |
| | Nicatoridae (Nicators) | Insects, **vertebrates** |
| | Macrosphenidae (African Warblers) | Insects |
| | Cisticolidae (Cisticolas and allies) | Insects, **vertebrates** |
| | Acrocephalidae (Reed Warblers and allies) | Insects, **vertebrates** |
| | Locustellidae (Grassbirds and allies) | Insects, annelids, snails |
| | Donacobiidae (Donacobius) | Insects |
| | Bernieridae (Malagasy Warblers) | Insects, **vertebrates** |
| | Pnoepygidae (Cupwings) | Insects |
| | Hirundinidae (Swallows) | Insects |
| | Pycnonotidae (Bulbuls) | Insects, **vertebrates** (including carrion) |
| | Phylloscopidae (Leaf Warblers) | Insects |
| | Scotocercidae (Bush Warblers and allies) | Insects, snails |
| | Aegithalidae (Long-tailed Tits) | Insects |
| | Sylviidae (Sylviid Warblers, Parrotbills, and allies) | Insects |
| | Zosteropidae (White-eyes, Yuhinas, and allies) | Insects, snails |
| | Timaliidae (Tree-Babblers, Scimitar-Babblers, and allies) | Insects |
| | Pellorneidae (Ground Babblers and allies) | Insects, annelids, snails |
| | Leiothrichidae (Laughingthrushes and allies) | Insects, **vertebrates** |
| | Regulidae (Kinglets) | Insects (including larvae) |
| | Tichodromidae (Wallcreeper) | Insects, molluscs |

| Carnivorous Telluravian Group | Family and Common Name | Carnivorous Diet |
|---|---|---|
| | Sittidae (Nuthatches) | Insects |
| Order Passeriformes (cont'd) | Certhiidae (Treecreepers) | Insects |
| | Polioptilidae (Gnatcatchers) | Insects |
| | Troglodytidae (Wrens) | Insects, snails, **vertebrates** |
| | Elachuridae (Spotted Elachura) | Insects |
| | Cinclidae (Dippers) | Insects (including larvae), crustaceans, eggs |
| | Buphagidae (Oxpeckers) | Insects, blood |
| | Sturnidae (Starlings) | Insects, **vertebrates**, eggs |
| | Mimidae (Mockingbirds and Thrashers) | Insects, **vertebrates**, eggs |
| | Turdidae (Thrushes and allies) | Insects, annelids, **vertebrates** |
| | Muscicapidae (Old World Flycatchers) | Insects |
| | Bombycillidae (Waxwings) | Insects |
| | Mohoidae (Hawaiian Honeyeaters) | Insects |
| | Ptiliogonatidae (Silky-flycatchers) | Insects |
| | Dulidae (Palmchat) | Insects |
| | Hylocitreidae (Hylocitrea) | Insects |
| | Hypocoliidae (Hypocolius) | Insects |
| | Promeropidae (Sugarbirds) | Insects |
| | Modulatricidae (Dapple-throat and allies) | Insects |
| | Dicaeidae (Flowerpeckers) | Insects |
| | Nectariniidae (Sunbirds and Spiderhunters) | Insects |
| | Irenidae (Fairy-bluebirds) | Insects |
| | Chloropseidae (Leafbirds) | Insects |
| | Peucedramidae (Olive Warbler) | Insects |
| | Urocynchramidae (Przevalski's Pinktail) | Insects |
| | Ploceidae (Weavers and allies) | Insects, **vertebrates**, eggs |
| | Estrildidae (Waxbills and allies) | Insects, snails |
| | Viduidae (Indigobirds) | Insects |
| | Prunellidae (Accentors) | Insects |
| | Passeridae (Old World Sparrows) | Insects |
| | Motacillidae (Wagtails and Pipits) | Insects, annelids, crustaceans, snails, **vertebrates** |
| | Fringillidae (Finches, Euphonias, and allies) | Insects |

| Carnivorous Telluravian Group | Family and Common Name | Carnivorous Diet |
|---|---|---|
| Order Passeriformes (cont'd) | Calcariidae (Longspurs and Snow Buntings) | Insects |
| | Rhodinocichlidae (Thrush-Tanager) | Insects |
| | Emberizidae (Old World Buntings) | Insects |
| | Passerellidae (New World Sparrows) | Insects |
| | Calyptophilidae (Chat-Tanagers) | Insects |
| | Phaenicophilidae (Hispaniolan Tanagers) | Insects |
| | Nesospingidae (Puerto Rican Tanager) | Insects, snails, **vertebrates** |
| | Spindalidae (Spindalises) | Insects |
| | Zeledoniidae (Wrenthrush) | Insects |
| | Teretistridae (Cuban Warblers) | Insects |
| | Icteriidae (Yellow-breasted Chat) | Insects |
| | Icteridae (Troupials and allies) | Insects, **vertebrates** |
| | Mitrospingidae (Mitrospingid Tanagers) | Insects |
| | Cardinalidae (Cardinals and allies) | Insects |
| | Thraupidae (Tanagers and allies) | Insects |

# B. Supporting Charts for Chapter 1

*B.1 Tables*

**Table B.1.** ANOVA results (AIC value, AIC weight, AICc value, λ value, coefficient, standard variable error, t-value, and p-value) of PGLS models for variation in tarsometatarsus centroid size as explained by foot uses and mean species body mass. Significant p-values are bolded.

| Index | Model | AIC | AICc weight | AICc | Lambda | | Value | Std. Error | t-value | p-value |
|---|---|---|---|---|---|---|---|---|---|---|
| 1 | size ~ bmmean + terrestrial arboreal + webbed feet | -76.62878 | 0.840891265 | -76.86133 | 1.009173 | (Intercept) | 1.6301584 | 0.09210271 | 17.699353 | 0 |
| | | | | | | bmmean | 0.3333051 | 0.02340434 | 14.241166 | **0** |
| | | | | | | terr0arb1 | -0.0788768 | 0.02110013 | -3.738212 | **3.00E-04** |
| | | | | | | webbed | -0.1078094 | 0.02910597 | -3.704031 | **3.00E-04** |
| 2 | size ~ bmmean + webbed feet | -71.19235 | 0.055492447 | -71.33107 | 1.014787 | (Intercept) | 1.5052731 | 0.08919704 | 16.877712 | 0 |
| | | | | | | bmmean | 0.3647043 | 0.02264501 | 16.105284 | **0** |
| | | | | | | webbed | -0.1013715 | 0.03017004 | -3.360004 | **0.001** |
| 3 | size ~ bmmean + terrestrial arboreal | -70.69922 | 0.043366332 | -70.83795 | 1.011845 | (Intercept) | 1.6291761 | 0.09549118 | 17.061012 | 0 |
| | | | | | | bmmean | 0.3269059 | 0.02417013 | 13.525202 | **0** |
| | | | | | | terr0arb1 | -0.0740154 | 0.02182238 | -3.391718 | **9.00E-04** |
| 4 | size ~ bmmean + anisodactyly + webbed feet | -68.81916 | 0.016939575 | -69.05171 | 1.010105 | (Intercept) | 1.4339329 | 0.095405 | 15.029954 | 0 |
| | | | | | | bmmean | 0.3674645 | 0.02253455 | 16.305384 | **0** |
| | | | | | | anisodactyly | 0.1011288 | 0.05095093 | 1.984828 | **0.0487** |
| | | | | | | webbed | -0.1040584 | 0.02990528 | -3.479597 | **0.0006** |
| 5 | size ~ bmmean + anisodactyly + swimming | -68.39332 | 0.013690936 | -68.62588 | 0.856183 | (Intercept) | 1.3590367 | 0.12120683 | 11.212542 | 0 |
| | | | | | | bmmean | 0.3634388 | 0.02382272 | 15.255972 | **0** |
| | | | | | | anisodactyly | 0.1518542 | 0.06698248 | 2.267073 | **0.0246** |
| | | | | | | swimming | -0.0456767 | 0.02160674 | -2.114005 | **0.0359** |
| 6 | size ~ bmmean | -67.42828 | 0.008450388 | -67.49724 | 1.015125 | (Intercept) | 1.5113498 | 0.09176547 | 16.4697 | 0 |
| | | | | | | bmmean | 0.3568746 | 0.02317446 | 15.39948 | **0** |
| 7 | size ~ bmmean + terrestrial arboreal + anisodactyly | -66.69109 | 0.005845202 | -66.92365 | 1.006765 | (Intercept) | 1.5703669 | 0.10306725 | 15.236333 | 0 |
| | | | | | | bmmean | 0.3301307 | 0.02420461 | 13.639168 | **0** |
| | | | | | | terr0arb1 | -0.0710078 | 0.02185502 | -3.249037 | **0.0014** |
| | | | | | | anisodactyly | 0.0770707 | 0.05157102 | 1.4944457 | 0.1369 |
| 8 | size ~ bmmean + terrestrial arboreal + zygodactyly | -65.68555 | 0.003535489 | -65.91811 | 1.0101 | (Intercept) | 1.6363064 | 0.0955268 | 17.129292 | 0 |
| | | | | | | bmmean | 0.330539 | 0.02436647 | 13.565321 | **0** |
| | | | | | | terr0arb1 | -0.0679676 | 0.02244855 | -3.027705 | **0.0028** |
| | | | | | | zygodactyly | -0.0552052 | 0.04793077 | -1.151769 | 0.251 |
| 9 | size ~ bmmean + terrestrial arboreal + running | -65.28665 | 0.002896197 | -65.51921 | 1.011763 | (Intercept) | 1.6009739 | 0.09936779 | 16.111598 | 0 |
| | | | | | | bmmean | 0.3261843 | 0.02417692 | 13.491561 | **0** |
| | | | | | | terr0arb1 | -0.0665758 | 0.02299713 | -2.894963 | **0.0043** |
| | | | | | | running | 0.0460098 | 0.04489917 | 1.024735 | 0.3069 |

| Index | Model | AIC | AICc weight | AICc | Lambda | | Value | Std. Error | t-value | p-value |
|---|---|---|---|---|---|---|---|---|---|---|
| 10 | size ~ bmmean + running | -64.89008 | 0.002375273 | -65.0288 | 1.014517 | (Intercept) | 1.4803544 | 0.09229471 | 16.039429 | 0 |
| | | | | | | bmmean | 0.3498165 | 0.02324712 | 15.047734 | **0** |
| | | | | | | running | 0.0868999 | 0.04349719 | 1.997828 | **0.0473** |
| 11 | size ~ bmmean + zygodactyly | -64.57305 | 0.002027088 | -64.71178 | 1.013026 | (Intercept) | 1.538314 | 0.09213143 | 16.696952 | 0 |
| | | | | | | bmmean | 0.3587623 | 0.02304898 | 15.565211 | **0** |
| | | | | | | zygodactyly | -0.0890152 | 0.04750959 | -1.873626 | 0.0627 |
| 12 | size ~ bmmean + foot propelled swimming | -64.40404 | 0.001930137 | -64.54277 | 1.015171 | (Intercept) | 1.517176 | 0.09160609 | 16.561956 | 0 |
| | | | | | | bmmean | 0.3578466 | 0.02311995 | 15.477831 | **0** |
| | | | | | | footswim | -0.1296691 | 0.09219791 | -1.406421 | 0.1614 |
| 13 | size ~ bmmean + anisodactyly | -64.33792 | 0.001802244 | -64.47664 | 1.01245 | (Intercept) | 1.4467083 | 0.09839269 | 14.703412 | 0 |
| | | | | | | bmmean | 0.35925 | 0.02310099 | 15.551282 | **0** |
| | | | | | | anisodactyly | 0.0919988 | 0.05236034 | 1.757031 | 0.0807 |
| 14 | size ~ bmmean + webbed feet + swimming | -63.85256 | 0.001413906 | -64.08512 | 1.014194 | (Intercept) | 1.5068592 | 0.08928637 | 16.8767 | 0 |
| | | | | | | bmmean | 0.363799 | 0.02269992 | 16.026448 | **0** |
| | | | | | | webbed | -0.0926479 | 0.0322036 | -2.876942 | **0.0045** |
| | | | | | | swimming | -0.0166712 | 0.0214107 | -0.778636 | 0.4373 |
| 15 | size ~ bmmean + swimming | -62.857 | 0.000859482 | -62.99573 | 1.012889 | (Intercept) | 1.5140395 | 0.09105044 | 16.628581 | 0 |
| | | | | | | bmmean | 0.03562863 | 0.02302602 | 15.473203 | **0** |
| | | | | | | swimming | -0.0382179 | 0.02049157 | -1.865056 | 0.0639 |
| 16 | size ~ bmmean + running + anisodactyly | -61.39693 | 0.000414178 | -61.62949 | 1.011845 | (Intercept) | 1.4217742 | 0.09851963 | 14.43138 | 0 |
| | | | | | | bmmean | 0.3523897 | 0.02321106 | 15.181974 | **0** |
| | | | | | | running | 0.0824213 | 0.04337331 | 1.900276 | 0.0591 |
| | | | | | | anisodactyly | 0.085785 | 0.05211699 | 1.646009 | 0.1016 |

**Table B.2.** ANOVA results (adjusted-$R^2$, degrees of freedom, sum of squares, $R^2$, F-value, and p-value) of PGLS models for variation in tarsometatarsus shape as explained by foot uses, centroid size and mean species body mass. Significant p-values are bolded.

| Index | Model | Adj-$R^2$ | ANOVA: | df | SS | $R^2$ | F-value | p-value |
|---|---|---|---|---|---|---|---|---|
| 1 | shape ~ size + bmmean + digital manipulate + raptorial + force grip + zygodactyly + flightless | 0.26826 | size | 1 | 0.007383 | 0.19438 | 46.7527 | **0.001** |
| | | | bmmean | 1 | 0.004461 | 0.11745 | 28.2485 | **0.001** |
| | | | manipulate | 1 | 0.000399 | 0.0105 | 2.5259 | 0.51 |
| | | | raptorial | 1 | 0.000494 | 0.01302 | 3.1314 | **0.014** |
| | | | force grip | 1 | 0.000646 | 0.01701 | 4.0924 | **0.007** |
| | | | zygodactyly | 1 | 0.00046 | 0.01212 | 2.9152 | **0.021** |
| | | | flightless | 1 | 0.000554 | 0.0146 | 3.5105 | **0.015** |
| | | | residuals | 169 | 0.026687 | 0.70264 | | |
| | | | total | 176 | 0.037981 | | | |
| 2 | shape ~ size + bmmean + flightless + raptorial + force grip + zygodactyly | 0.26168 | size | 1 | 0.007361 | 0.1938 | 46.198 | **0.001** |
| | | | bmmean | 1 | 0.00444 | 0.1169 | 27.8661 | **0.001** |
| | | | flightless | 1 | 0.000712 | 0.01874 | 4.4663 | **0.002** |
| | | | raptorial | 1 | 0.000435 | 0.01146 | 2.7318 | **0.027** |
| | | | force grip | 1 | 0.000541 | 0.01424 | 3.3955 | **0.023** |
| | | | zygodactyly | 1 | 0.000456 | 0.01201 | 2.8623 | **0.023** |
| | | | residuals | 170 | 0.027086 | 0.71314 | | |
| | | | total | 176 | 0.037981 | | | |
| 3 | shape ~ size + bmmean + digital manipulate + raptorial + force grip + zygodactyly | 0.25743 | size | 1 | 0.008067 | 0.21239 | 50.3416 | **0.001** |
| | | | bmmean | 1 | 0.005344 | 0.14071 | 33.3507 | **0.001** |
| | | | manipulate | 1 | 0.000556 | 0.01464 | 3.4705 | **0.033** |
| | | | raptorial | 1 | 0.000426 | 0.01122 | 2.6598 | **0.037** |
| | | | force grip | 1 | 0.000588 | 0.01548 | 3.6694 | **0.016** |
| | | | zygodactyly | 1 | 0.000457 | 0.01204 | 2.8545 | **0.02** |
| | | | residuals | 170 | 0.027242 | 0.71724 | | |
| | | | total | 176 | 0.037981 | | | |
| 4 | shape ~ size + bmmean + flightless + raptorial + force grip | 0.25364 | size | 1 | 0.007335 | 0.19311 | 45.5383 | **0.001** |
| | | | bmmean | 1 | 0.004406 | 0.11601 | 27.3563 | **0.001** |
| | | | flightless | 1 | 0.000711 | 0.01871 | 4.4126 | **0.003** |
| | | | raptorial | 1 | 0.000437 | 0.0115 | 2.7115 | **0.027** |
| | | | force grip | 1 | 0.00059 | 0.01553 | 3.6629 | **0.018** |
| | | | residuals | 171 | 0.027542 | 0.72515 | | |
| | | | total | 176 | 0.037981 | | | |

| Index | Model | Adj-$R^2$ | ANOVA: | df | SS | $R^2$ | F-value | p-value |
|---|---|---|---|---|---|---|---|---|
| 5 | shape ~ size + bmmean + flightless + zygodactyly | 0.25206 | size | 1 | 0.007766 | 0.20446 | 48.1131 | **0.001** |
| | | | bmmean | 1 | 0.004726 | 0.12443 | 29.2805 | **0.001** |
| | | | flightless | 1 | 0.000664 | 0.01747 | 4.1114 | **0.005** |
| | | | zygodactyly | 1 | 0.000534 | 0.01405 | 3.3067 | **0.011** |
| | | | residuals | 172 | 0.027762 | 0.73094 | | |
| | | | total | 176 | 0.037981 | | | |
| 6 | shape ~ size + bmmean + flightless + anisodactyly | 0.02501 | size | 1 | 0.007777 | 0.20476 | 48.0582 | **0.001** |
| | | | bmmean | 1 | 0.004736 | 0.12469 | 19.2654 | **0.001** |
| | | | flightless | 1 | 0.000666 | 0.01753 | 4.1139 | **0.005** |
| | | | anisodactyly | 1 | 0.000462 | 0.01217 | 2.8569 | **0.026** |
| | | | residuals | 172 | 0.027834 | 0.73282 | | |
| | | | total | 176 | 0.037981 | | | |
| 7 | shape ~ size + bmmean + digital manipulate + raptorial + force grip | 0.24939 | size | 1 | 0.00805 | 0.21194 | 49.6946 | **0.001** |
| | | | bmmean | 1 | 0.005314 | 0.1399 | 32.8041 | **0.001** |
| | | | manipulate | 1 | 0.000554 | 0.01458 | 3.4192 | **0.034** |
| | | | raptorial | 1 | 0.000426 | 0.01122 | 2.6305 | **0.039** |
| | | | force grip | 1 | 0.000624 | 0.01644 | 3.855 | **0.01** |
| | | | residuals | 171 | 0.027699 | 0.72928 | | |
| | | | total | 176 | 0.037981 | | | |
| 8 | shape ~ size + bmmean + terrestrial arboreal + flightless | 0.02463 | size | 1 | 0.006855 | 0.18049 | 42.1475 | **0.001** |
| | | | bmmean | 1 | 0.004786 | 0.126 | 29.425 | **0.001** |
| | | | terrarb | 1 | 0.000321 | 0.00845 | 1.973 | 0.075 |
| | | | flightless | 1 | 0.000673 | 0.01771 | 4.1362 | **0.004** |
| | | | residuals | 172 | 0.027975 | 0.73654 | | |
| | | | total | 176 | 0.037981 | | | |
| 9 | shape ~ size + bmmean + digital manipulate + zygodactyly | 0.24605 | size | 1 | 0.008176 | 0.21526 | 50.2495 | **0.001** |
| | | | bmmean | 1 | 0.005314 | 0.13991 | 32.6606 | **0.001** |
| | | | manipulate | 1 | 0.000441 | 0.0116 | 2.7083 | **0.048** |
| | | | zygodactyly | 1 | 0.000523 | 0.01377 | 3.215 | **0.014** |
| | | | residuals | 172 | 0.027985 | 0.73681 | | |
| | | | total | 176 | 0.037981 | 0.20052 | | |

| Index | Model | Adj-$R^2$ | ANOVA: | df | SS | $R^2$ | F-value | p-value |
|---|---|---|---|---|---|---|---|---|
| 10 | shape ~ size + bmmean + surface swimming + flightless | 0.24538 | size | 1 | 0.007842 | 0.20646 | 48.1524 | **0.001** |
| | | | bmmean | 1 | 0.004757 | 0.12523 | 29.2085 | **0.001** |
| | | | surfswim | 1 | 0.000286 | 0.00753 | 1.7557 | 0.097 |
| | | | flightless | 1 | 0.000663 | 0.01744 | 4.0683 | **0.005** |
| | | | residuals | 172 | 0.02801 | 0.73747 | | |
| | | | total | 176 | 0.037981 | | | |
| 11 | shape ~ size + bmmean + digital manipulate + flightless | 0.24531 | size | 1 | 0.007616 | 0.20052 | 46.8021 | **0.001** |
| | | | bmmean | 1 | 0.004551 | 0.11982 | 27.9656 | **0.001** |
| | | | manipulate | 1 | 0.000307 | 0.00807 | 1.8843 | 0.106 |
| | | | flightless | 1 | 0.000519 | 0.01366 | 3.1891 | **0.019** |
| | | | residuals | 172 | 0.027989 | 0.73692 | | |
| | | | total | 176 | 0.037981 | | | |
| 12 | shape ~ size + bmmean + digital manipulate + anisodactyly | 0.24414 | size | 1 | 0.008174 | 0.21521 | 50.1117 | **0.001** |
| | | | bmmean | 1 | 0.005314 | 0.13991 | 32.5768 | **0.001** |
| | | | manipulate | 1 | 0.000443 | 0.01167 | 2.7166 | 0.052 |
| | | | anisodactyly | 1 | 0.00452 | 0.0119 | 2.7713 | **0.028** |
| | | | residuals | 172 | 0.028056 | 0.73868 | | |
| | | | total | 176 | 0.037981 | | | |
| 13 | shape ~ size + bmmean + flightless + foot propelled swimming | 0.02434 | size | 1 | 0.007788 | 0.20505 | 47.7031 | **0.001** |
| | | | bmmean | 1 | 0.00476 | 0.12533 | 29.1556 | **0.001** |
| | | | flightless | 1 | 0.000673 | 0.01772 | 4.1233 | **0.005** |
| | | | footswim | 1 | 0.000214 | 0.00564 | 1.3124 | 0.205 |
| | | | residuals | 172 | 0.028082 | 0.73935 | | |
| | | | total | 176 | 0.037981 | | | |
| 14 | shape ~ size + bmmean + digital manipulate + force grip | 0.24228 | size | 1 | 0.00818 | 0.21536 | 50.0231 | **0.001** |
| | | | bmmean | 1 | 0.005311 | 0.13983 | 32.4791 | **0.001** |
| | | | manipulate | 1 | 0.000522 | 0.01375 | 3.194 | **0.035** |
| | | | force grip | 1 | 0.000383 | 0.01009 | 2.3427 | 0.051 |
| | | | residuals | 172 | 0.028125 | 0.7405 | | |
| | | | total | 176 | 0.037981 | | | |

| Index | Model | Adj-$R^2$ | ANOVA: | df | SS | $R^2$ | F-value | p-value |
|---|---|---|---|---|---|---|---|---|
| 15 | shape ~ size + bmmean + flightless | 0.24208 | size | 1 | 0.007815 | 0.20577 | 47.7828 | **0.001** |
| | | | bmmean | 1 | 0.004752 | 0.12512 | 29.0551 | **0.001** |
| | | | flightless | 1 | 0.000668 | 0.0176 | 4.0865 | **0.005** |
| | | | residuals | 173 | 0.028296 | 0.74499 | | |
| | | | total | 176 | 0.037981 | | | |
| 16 | shape ~ size + bmmean + terrestrial arboreal + anisodactyly | 0.24069 | size | 1 | 0.007785 | 0.20496 | 47.5081 | **0.001** |
| | | | bmmean | 1 | 0.006045 | 0.15916 | 36.8917 | **0.001** |
| | | | terrarb | 1 | 0.000315 | 0.0083 | 1.9238 | 0.085 |
| | | | anisodactyly | 1 | 0.000464 | 0.01221 | 2.8295 | **0.026** |
| | | | residuals | 172 | 0.028184 | 0.74205 | | |
| | | | total | 176 | 0.037981 | | | |
| 17 | shape ~ size + bmmean + terrestrial arboreal + digital manipulate | 0.24047 | size | 1 | 0.007287 | 0.19186 | 44.4604 | **0.001** |
| | | | bmmean | 1 | 0.005349 | 0.14083 | 32.635 | **0.001** |
| | | | terrarb | 1 | 0.000317 | 0.00833 | 1.9312 | 0.078 |
| | | | manipulate | 1 | 0.000456 | 0.01201 | 2.7822 | **0.044** |
| | | | residuals | 172 | 0.028192 | 0.74225 | | |
| | | | total | 176 | 0.037981 | | | |
| 18 | shape ~ size + bmmean + surface swimming + anisodactyly | 0.24001 | size | 1 | 0.008736 | 0.23001 | 53.2664 | **0.001** |
| | | | bmmean | 1 | 0.005986 | 0.15759 | 36.4968 | **0.001** |
| | | | surfswim | 1 | 0.00029 | 0.00765 | 1.7709 | 0.099 |
| | | | anisodactyly | 1 | 0.000464 | 0.01221 | 2.8269 | **0.021** |
| | | | residuals | 172 | 0.028209 | 0.7427 | | |
| | | | total | 176 | 0.037981 | | | |
| 19 | shape ~ size + bmmean + anisodactyly + zygodactyly | 0.23974 | size | 1 | 0.008699 | 0.22903 | 53.0216 | **0.001** |
| | | | bmmean | 1 | 0.005982 | 0.15749 | 36.4594 | **0.001** |
| | | | anisodactyly | 1 | 0.000207 | 0.00545 | 1.2607 | 0.25 |
| | | | zygodactyly | 1 | 0.00028 | 0.00738 | 1.7089 | 0.138 |
| | | | residuals | 172 | 0.028219 | 0.74297 | | |
| | | | total | 176 | 0.037981 | | | |

| Index | Model | Adj-$R^2$ | ANOVA: | df | SS | $R^2$ | F-value | p-value |
|---|---|---|---|---|---|---|---|---|
| 20 | shape ~ size + bmmean + raptorial + force grip | 0.23883 | size | 1 | 0.008405 | 0.22129 | 51.1675 | **0.001** |
| | | | bmmean | 1 | 0.005809 | 0.15294 | 35.3647 | **0.001** |
| | | | raptorial | 1 | 0.000395 | 0.01039 | 2.4018 | **0.045** |
| | | | force grip | 1 | 0.000543 | 0.0143 | 3.3061 | **0.027** |
| | | | residuals | 172 | 0.028253 | 0.74386 | | |
| | | | total | 176 | 0.037981 | | | |
| 21 | shape ~ size + bmmean + zygodactyly | 0.2386 | size | 1 | 0.008702 | 0.22912 | 52.9615 | **0.001** |
| | | | bmmean | 1 | 0.005983 | 0.15751 | 36.4105 | **0.001** |
| | | | zygodactyly | 1 | 0.000539 | 0.01418 | 3.2774 | **0.013** |
| | | | residuals | 173 | 0.028426 | 0.74841 | | |
| | | | total | 176 | 0.037981 | | | |
| 22 | shape ~ size + bmmean + anisodactyly | 0.23664 | size | 1 | 0.008705 | 0.22919 | 52.843 | **0.001** |
| | | | bmmean | 1 | 0.005985 | 0.15758 | 36.331 | **0.001** |
| | | | anisodactyly | 1 | 0.000465 | 0.01224 | 2.8225 | **0.029** |
| | | | residuals | 173 | 0.028499 | 0.75035 | | |
| | | | total | 176 | 0.037981 | | | |
| 23 | shape ~ size + bmmean + digital manipulate | 0.2364 | size | 1 | 0.008174 | 0.21521 | 49.6034 | **0.001** |
| | | | bmmean | 1 | 0.0053 | 0.13954 | 32.162 | **0.001** |
| | | | manipulate | 1 | 0.000456 | 0.01201 | 2.7675 | 0.047 |
| | | | residuals | 173 | 0.028508 | 0.75058 | | |
| | | | total | 176 | 0.037981 | | | |
| 24 | shape ~ size + bmmean + digital manipulate + hold down | 0.23463 | size | 1 | 0.008173 | 0.21519 | 49.4841 | **0.001** |
| | | | bmmean | 1 | 0.005202 | 0.13697 | 31.4982 | **0.001** |
| | | | manipulate | 1 | 0.000292 | 0.00768 | 1.7652 | 0.104 |
| | | | hold down | 1 | 0.0001 | 0.00262 | 0.6027 | 0.704 |
| | | | residuals | 172 | 0.028409 | 0.74796 | | |
| | | | total | 176 | 0.037981 | | | |
| 25 | shape ~ size + bmmean + force grip | 0.23268 | size | 1 | 0.008739 | 0.2301 | 52.7769 | **0.001** |
| | | | bmmean | 1 | 0.005944 | 0.1565 | 35.8956 | **0.001** |
| | | | force grip | 1 | 0.000317 | 0.00834 | 1.9135 | 0.094 |
| | | | residuals | 173 | 0.028647 | 0.75425 | | |
| | | | total | 176 | 0.037981 | | | |

| Index | Model | Adj-$R^2$ | ANOVA: | df | SS | $R^2$ | F-value | p-value |
|---|---|---|---|---|---|---|---|---|
| 26 | shape ~ size + bmmean + terrestrial arboreal | 0.23265 | size | 1 | 0.007775 | 0.2047 | 46.9521 | **0.001** |
| | | | bmmean | 1 | 0.006054 | 0.15939 | 36.5578 | **0.001** |
| | | | terrarb | 1 | 0.000317 | 0.00833 | 1.9117 | 0.077 |
| | | | residuals | 173 | 0.028648 | 0.75426 | | |
| | | | total | 176 | 0.037981 | | | |
| 27 | shape ~ size + bmmean + surface swimming | 0.23198 | size | 1 | 0.008769 | 0.23089 | 52.9118 | **0.001** |
| | | | bmmean | 1 | 0.006 | 0.15798 | 36.2047 | **0.001** |
| | | | surfswim | 1 | 0.000292 | 0.00768 | 1.7605 | 0.098 |
| | | | residuals | 173 | 0.028673 | 0.75491 | | |
| | | | total | 176 | 0.037981 | | | |
| 28 | shape ~ size + bmmean + hold down | 0.23126 | size | 1 | 0.008474 | 0.2231 | 51.078 | **0.001** |
| | | | bmmean | 1 | 0.005363 | 0.14121 | 32.3282 | **0.001** |
| | | | hold down | 1 | 0.000264 | 0.00695 | 1.5916 | 0.15 |
| | | | residuals | 173 | 0.0287 | 0.75564 | | |
| | | | total | 176 | 0.037981 | | | |
| 29 | shape ~ size + bm + heterodactyly | 0.23072 | size | 1 | 0.008807 | 0.23187 | 53.0497 | **0.001** |
| | | | bmmean | 1 | 0.005984 | 0.15754 | 36.0435 | **0.001** |
| | | | heterodactyly | 1 | 0.000245 | 0.00644 | 1.4742 | 0.194 |
| | | | residuals | 173 | 0.02872 | 0.75615 | | |
| | | | total | 176 | 0.037981 | | | |
| 30 | shape ~ size + bmmean + webbed feet | 0.23013 | size | 1 | 0.008072 | 0.21252 | 48.5858 | **0.001** |
| | | | bmmean | 1 | 0.005413 | 0.1425 | 35.5783 | **0.001** |
| | | | webbed feet | 1 | 0.000222 | 0.00585 | 1.3385 | 0.226 |
| | | | residuals | 173 | 0.028742 | 0.75674 | | |
| | | | total | 176 | 0.037981 | | | |
| 31 | shape ~ size + bmmean + swimming | 0.22992 | size | 1 | 0.008577 | 0.22581 | 51.6091 | **0.001** |
| | | | bmmean | 1 | 0.005945 | 0.15653 | 35.7753 | **0.001** |
| | | | swimming | 1 | 0.000215 | 0.75694 | 1.2922 | 0.217 |
| | | | residuals | 173 | 0.02875 | | | |
| | | | total | 176 | 0.037981 | | | |

| Index | Model | Adj-$R^2$ | ANOVA: | df | SS | $R^2$ | F-value | p-value |
|---|---|---|---|---|---|---|---|---|
| 32 | shape ~ size + bmmean + foot propelled swimming | 0.22978 | size | 1 | 0.00869 | 0.22881 | 52.2852 | **0.001** |
| | | | bmmean | 1 | 0.005996 | 0.15786 | 36.0734 | **0.001** |
| | | | footswim | 1 | 0.000209 | 0.00551 | 1.2602 | 0.228 |
| | | | residuals | 173 | 0.028755 | 0.75708 | | |
| | | | total | 176 | 0.037981 | | | |
| 33 | shape ~ size + bm + running | 0.22922 | size | 1 | 0.008685 | 0.22866 | 52.2143 | **0.001** |
| | | | bmmean | 1 | 0.00601 | 0.15823 | 36.1318 | **0.001** |
| | | | running | 1 | 0.000189 | 0.00497 | 1.1343 | 0.295 |
| | | | residuals | 173 | 0.028776 | 0.75762 | | |
| | | | total | 176 | 0.037981 | | | |
| 34 | shape ~ size + bmmean + scansorial | 0.22922 | size | 1 | 0.00873 | 0.22986 | 52.4875 | **0.001** |
| | | | bmmean | 1 | 0.006005 | 0.15809 | 36.0997 | **0.001** |
| | | | scansorial | 1 | 0.000189 | 0.00496 | 1.1336 | 0.292 |
| | | | residuals | 173 | 0.028776 | 0.7563 | | |
| | | | total | 176 | 0.037981 | | | |
| 35 | shape ~ size + bmmean + nesting substrate | 0.22919 | size | 1 | 0.00875 | 0.23039 | 52.6044 | **0.001** |
| | | | bmmean | 1 | 0.006011 | 0.15827 | 36.1384 | **0.001** |
| | | | nesting | 1 | 0.000187 | 0.00492 | 1.1234 | 0.306 |
| | | | residuals | 173 | 0.028777 | 0.75767 | | |
| | | | total | 176 | 0.037981 | | | |
| 36 | shape ~ size + bmmean + perching | 0.22897 | size | 1 | 0.008701 | 0.22909 | 52.2943 | **0.001** |
| | | | bmmean | 1 | 0.00599 | 0.1577 | 35.998 | **0.001** |
| | | | perch | 1 | 0.000179 | 0.00472 | 1.0764 | 0.336 |
| | | | residuals | 173 | 0.028785 | 0.75788 | | |
| | | | total | 176 | 0.037981 | | | |
| 37 | shape ~ size + bmmean + hanging clinging | 0.22895 | size | 1 | 0.008743 | 0.23019 | 52.5441 | **0.001** |
| | | | bmmean | 1 | 0.006047 | 0.1592 | 36.3406 | **0.001** |
| | | | hangcling | 1 | 0.000179 | 0.00471 | 1.0743 | 0.351 |
| | | | residuals | 173 | 0.028786 | 0.75788 | | |
| | | | total | 176 | 0.037981 | | | |

| Index | Model | Adj-$R^2$ | ANOVA: | df | SS | $R^2$ | F-value | p-value |
|---|---|---|---|---|---|---|---|---|
| 38 | shape ~ size + bmmean + submerged swimming | 0.22882 | size | 1 | 0.008816 | 0.23212 | 52.9752 | **0.001** |
| | | | bmmean | 1 | 0.005916 | 0.15577 | 35.5499 | **0.001** |
| | | | subswim | 1 | 0.000173 | 0.00455 | 1.0385 | 0.331 |
| | | | residuals | 173 | 0.028791 | 0.75804 | | |
| | | | total | 176 | 0.037981 | | | |
| 39 | shape ~ size + bmmean | 0.22864 | size | 1 | 0.008741 | 0.23015 | 52.513 | **0.001** |
| | | | bmmean | 1 | 0.006004 | 0.15809 | 36.07 | **0.001** |
| | | | residuals | 174 | 0.028964 | 0.76259 | | |
| | | | total | 176 | 0.037981 | | | |
| 40 | shape ~ size + bmmean + walking | 0.22796 | size | 1 | 0.008345 | 0.21972 | 50.0885 | **0.001** |
| | | | bmmean | 1 | 0.006029 | 0.15873 | 36.1862 | **0.001** |
| | | | walking | 1 | 0.000141 | 0.00371 | 0.8457 | 0.499 |
| | | | residuals | 173 | 0.028823 | 0.75888 | | |
| | | | total | 176 | 0.037981 | | | |
| 41 | shape ~ size + bmmean + hopping | 0.22622 | size | 1 | 0.008746 | 0.23026 | 52.3745 | **0.001** |
| | | | bmmean | 1 | 0.005983 | 0.15752 | 35.8302 | **0.001** |
| | | | hopping | 1 | 0.000077 | 0.00202 | 0.4594 | 0.891 |
| | | | residuals | 173 | 0.028888 | 0.76057 | | |
| | | | total | 176 | 0.037981 | | | |
| 42 | shape ~ size + bmmean + raptorial | 0.22386 | size | 1 | 0.008677 | 0.22845 | 52.1294 | **0.001** |
| | | | bmmean | 1 | 0.006004 | 0.15807 | 36.0695 | **0.001** |
| | | | raptorial | 1 | 0.000168 | 0.00443 | 1.0113 | 0.379 |
| | | | residuals | 173 | 0.028796 | 0.75816 | | |
| | | | total | 176 | 0.037981 | | | |
| 43 | shape ~ size | 0.07404 | size | 1 | 0.003013 | 0.07932 | 15.078 | **0.001** |
| | | | residuals | 175 | 0.034969 | 0.92068 | | |
| | | | total | 176 | 0.037981 | | | |
| 44 | shape ~ flightless | 0.04073 | flightless | 1 | 0.001755 | 0.04619 | 8.4754 | **0.001** |
| | | | residuals | 175 | 0.036227 | 0.95381 | | |
| | | | total | 176 | 0.037981 | | | |

| Index | Model | Adj-$R^2$ | ANOVA: | df | SS | $R^2$ | F-value | p-value |
|---|---|---|---|---|---|---|---|---|
| 45 | shape ~ bmmean + terrestrial arboreal | 0.02999 | bmmean | 1 | 0.000617 | 0.01624 | 2.9461 | **0.025** |
| | | | terrarb | 1 | 0.001283 | 0.03378 | 6.1288 | **0.001** |
| | | | residuals | 174 | 0.036423 | 0.95896 | | |
| | | | total | 176 | 0.037981 | | | |
| 46 | shape ~ digital manipulate | 0.02447 | manipulate | 1 | 0.001141 | 0.03003 | 5.4177 | **0.008** |
| | | | residuals | 175 | 0.036841 | 0.96997 | | |
| | | | total | 176 | 0.037981 | | | |
| 47 | shape ~ webbed feet | 0.01981 | webbed feet | 1 | 0.000964 | 0.02539 | 4.5585 | **0.003** |
| | | | residuals | 175 | 0.037017 | 0.97461 | | |
| | | | total | 176 | 0.037981 | | | |
| 48 | shape ~ terrestrial arboreal | 0.01923 | terrarb | 1 | 0.000942 | 0.0248 | 4.4508 | **0.002** |
| | | | residuals | 175 | 0.037039 | 0.9752 | | |
| | | | total | 176 | 0.037981 | | | |
| 49 | shape ~ hold down | 0.01174 | hold down | 1 | 0.000659 | 0.01736 | 3.0919 | **0.026** |
| | | | residuals | 175 | 0.037322 | 0.98264 | | |
| | | | total | 176 | 0.037981 | | | |
| 50 | shape ~ zygodactyly | 0.00988 | zygodactyly | 1 | 0.000589 | 0.01551 | 2.7572 | **0.035** |
| | | | residuals | 175 | 0.037392 | 0.98449 | | |
| | | | total | 176 | 0.037981 | | | |
| 51 | shape ~ anisodactyly | 0.00787 | anisodactyly | 1 | 0.000513 | 0.01351 | 2.396 | 0.062 |
| | | | residuals | 175 | 0.037468 | 0.98649 | | |
| | | | total | 176 | 0.037981 | | | |
| 52 | shape ~ walking ability | 0.00578 | walking | 1 | 0.000435 | 0.01145 | 2.0265 | 0.09 |
| | | | residuals | 175 | 0.037547 | 0.98855 | | |
| | | | total | 176 | 0.037981 | | | |
| 53 | shape ~ swimming | 0.00427 | swim | 1 | 0.000378 | 0.00994 | 1.7576 | 0.11 |
| | | | residuals | 175 | 0.037604 | 0.99006 | | |
| | | | total | 176 | 0.037981 | | | |
| 54 | shape ~ force grip | 0.00306 | force grip | 1 | 0.000331 | 0.00872 | 1.5398 | 0.174 |
| | | | residuals | 175 | 0.3765 | 0.99128 | | |
| | | | total | 176 | 0.037981 | | | |

| Index | Model | Adj-$R^2$ | ANOVA: | df | SS | $R^2$ | F-value | p-value |
|---|---|---|---|---|---|---|---|---|
| 55 | shape ~ bmmean | 0.00156 | bmmean | 1 | 0.000276 | 0.00726 | 1.2801 | 0.239 |
| | | | residuals | 175 | 0.037706 | 0.99274 | | |
| | | | total | 176 | 0.037981 | | | |
| 56 | shape ~ surface swimming | 0.00146 | surface swim | 1 | 0.000272 | 0.00716 | 1.2622 | 0.242 |
| | | | residuals | 175 | 0.03771 | 0.99284 | | |
| | | | total | 176 | 0.037981 | | | |
| 57 | shape ~ raptorial | 0.00001 | raptorial | 1 | 0.000219 | 0.00578 | 1.017 | 0.352 |
| | | | residuals | 175 | 0.037762 | 0.99422 | | |
| | | | total | 176 | 0.037981 | | | |

*B.2 Data*

All data and code used to produce the final results are archived at https://doi.org/10.5281/zenodo.7031733. All computations were processed in an R statistical environment (R Core Team 2022).

**Data B.1** Spreadsheet of foot use character scoring and mean species body masses for all extant taxa.

**Data B.2** Process to retrieve 3D landmark data from Avizo files provided by R. Benson.

**Data B.3** Generalised Procrustes analysis of 3D tarsometatarsus landmark data.

**Data B.4** Phylogenetic generalised least squares for variation in tarsometatarsus shape as explained by foot uses, centroid size and mean species body mass.

**Data B.5** Phylogenetic generalised least squares for variation in tarsometatarsus centroid size as explained by foot uses and mean species body mass.

# C. Supporting Charts for Chapter 2

*C.1 Figures*

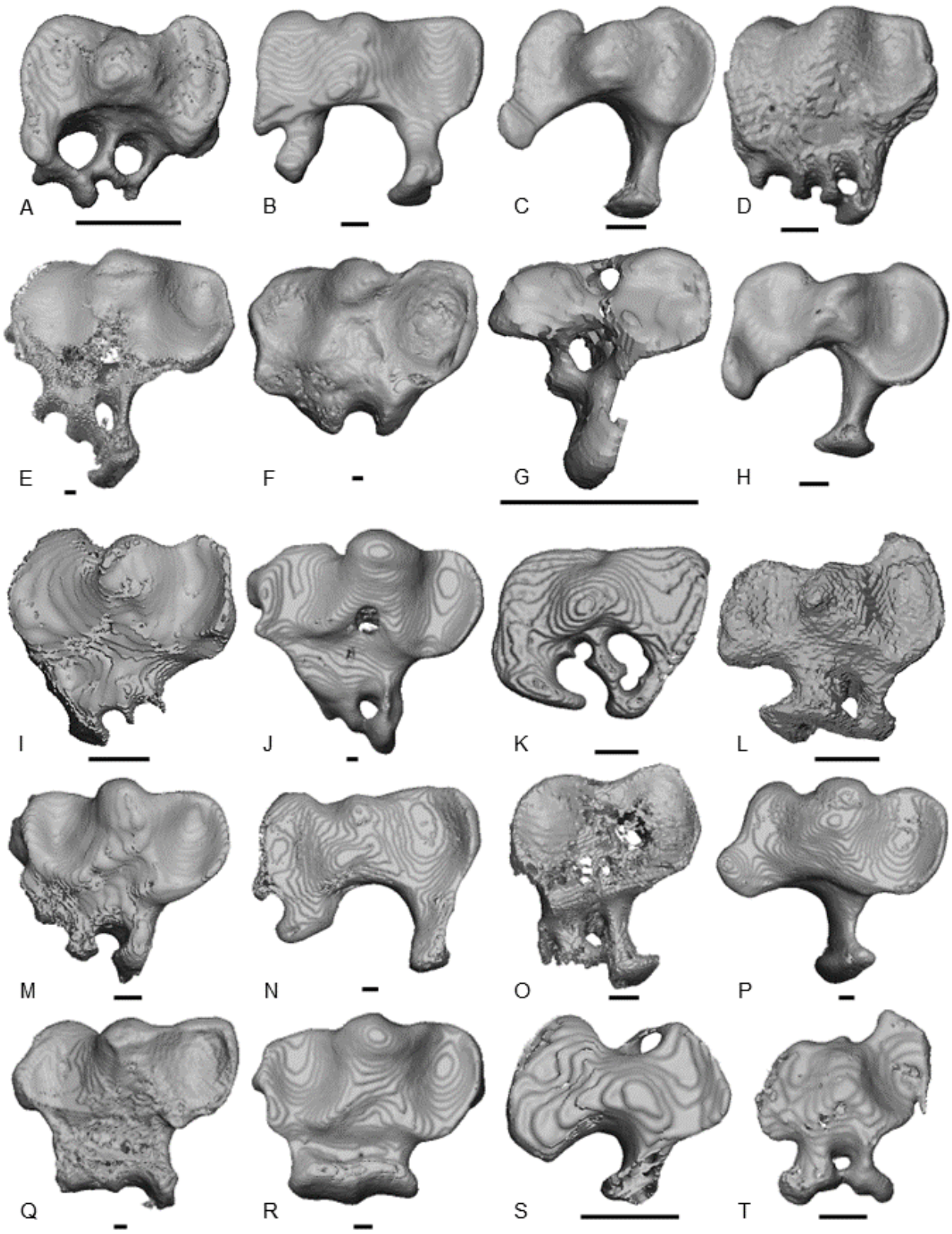
A
B
C
D
E
F
G
H
I
J
K
L
M
N
O
P
Q
R
S
T

**Figure C.1.** Proximal views of extant hypotarsi 3D models analysed herein. Scale bar for each specimen is 1mm, all mirrored to left sides. A) *Acanthisitta chloris* (YPM 125219); B) *Accipiter nisus* (NHMUK S.1982.149.1); C) *Aegolius acadicus* (FMNH 465196); D) *Anas discors* (NHMUK S.2001.2.5); E) *Anseranas semipalmata* (NHMUK 1852.7.22.1); F) *Apteryx australis* (FMNH 391011); G) *Archilochus colubris* (FMNH 484738); H) *Athene noctua* (NHMUK S.1996.11.1); I) *Atlantisia rogersi* (NHMUK 1924.1.2.2); J) *Balearica pavonina* (NHMUK 1859.10.26); K) *Barnardius zonarius* (NHMUK S.1983.5.1); L) *Bucco capensis* (FMNH 330305); M) *Burhinus senegalensis* (FMNH 313704); N) *Buteo rufofuscus* (NHMUK 1862.1.18.1); O) *Caprimulgus macrurus* (FMNH 392245); P) *Caracara cheriway* (UMMZ 133664); Q) *Cariama cristata* (FMNH 105653); R) *Cathartes burrovianus* (UMMZ 227466); S) *Chaetura brachyura* (UMMZ 157689); T) *Chloroceryle amazona* (UMMZ 209261).

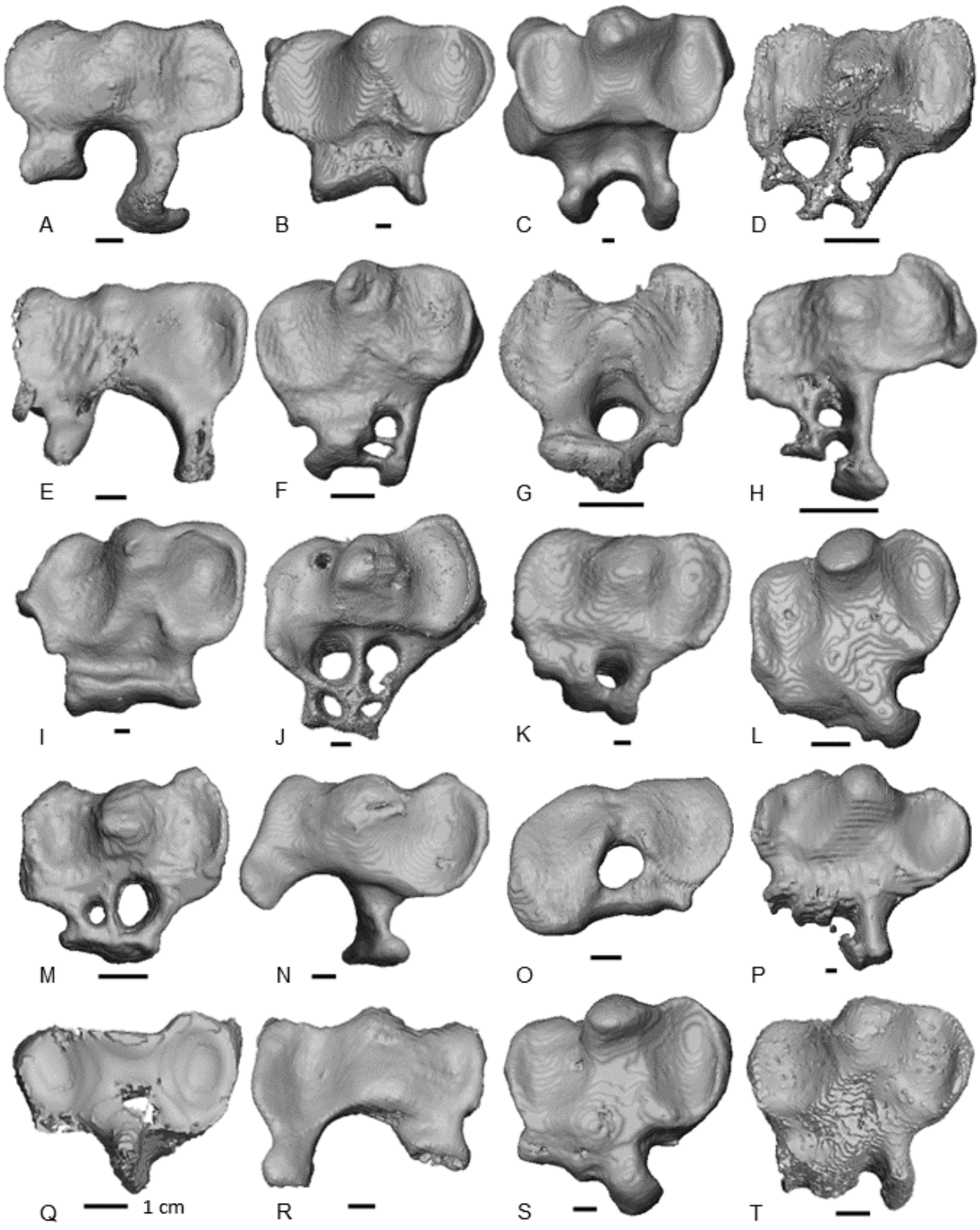
A
B
C
D
E
F
G
H
I
J
K
L
M
N
O
P
Q
1 cm
R
S
T

**Figure C.2.** Proximal views of extant hypotarsi 3D models analysed herein. Scale bar for each specimen is 1mm except where otherwise specified, all mirrored to left sides. A) *Chondrohierax uncinatus* (UMMZ 133635); B) *Chunga burmeisteri* (FMNH 106731); C) *Ciconia ciconia* (NHMUK 2007.107.1); D) *Cinclus cinclus* (NHMUK S.1988.33.1); E) *Circus macrourus* (UMZC 504MB); F) *Colinus virginianus* (FMNH 105065); G) *Colius striatus* (FMNH 384817); H) *Columbina minuta* (FMNH 289160); I) *Coragyps atratus* (UMMZ 71891); J) *Corvus albus* (NHMUK 1866.8.6.13); K) *Corythaeola cristata* (FMNH 313066); L) *Crypturellus tataupa* (UMMZ 201948); M) *Cuculus fugax* (FMNH 357420); N) *Daptrius ater* (UMMZ 157622); O) *Deroptyus accipitrinus* (NHMUK 2002.14.2); P) *Diomedea irrorata* (NHMUK S1963.28.4); Q) *Dromaius novaehollandiae* (NHMUK 1897.12.30.1), scale bar is 1cm; R) *Elanus caeruleus* (NHMUK 1850.8.15.159); S) *Eudromia elegans* (UMMZ 156966); T) *Eurypyga helias* (FMNH 317341).

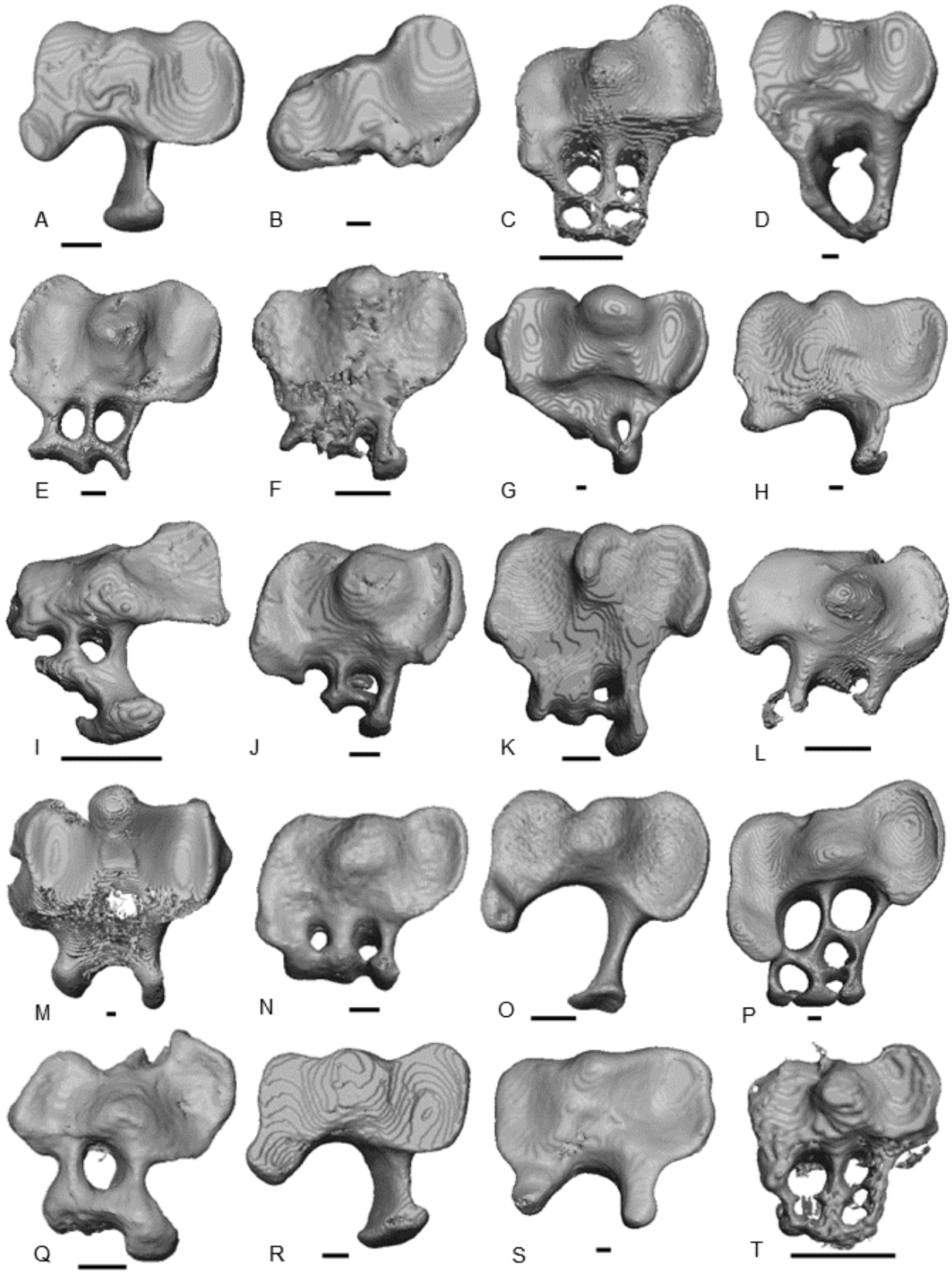
A
B
C
D
E
F
G
H
I
J
K
L
M
N
O
P
Q
R
S
T

**Figure C.3.** Proximal views of extant hypotarsi 3D models analysed herein. Scale bar for each specimen is 1mm, all mirrored to left sides. A) *Falco sparverius* (UMMZ 154452); B) *Fregata aquila* (NHMUK 1890.11.3.3); C) *Fringilla coelebs* (OUMNH 24647); D) *Gavia stellata* (NHMUK 1891.7.2.132); E) *Geococcyx californianus* (UMMZ 227059); F) *Glareola pratincola* (FMNH 368875); G) *Grus leucogeranus* (UMZC 344D); H) *Gypohierax angolensis* (UMMZ 235897); I) *Hemiprocne comata* (UMMZ 158224); J) *Ixobrychus minutus* (NHMUK S2007.61.1); K) *Jacana jacana* (NHMUK S.1990.2.5); L) *Jynx torquilla* (NHMUK S.1986.36.10); M) *Leptoptilos crumeniferus* (NHMUK S.1952.3.182); N) *Leptosomus discolor* (NHMUK 1968.30.38); O) *Megascops kennicottii* (NHMUK S.1998.103.4); P) *Menura novaehollandiae* (FMNH 336751); Q) *Merops orientalis* (UMMZ 216577); R) *Micrastur ruficollis* (FMNH330226); S) *Necrosyrtes monachus* (UMMZ 158168); T) *Neodrepanis coruscans* (FMNH 363807).

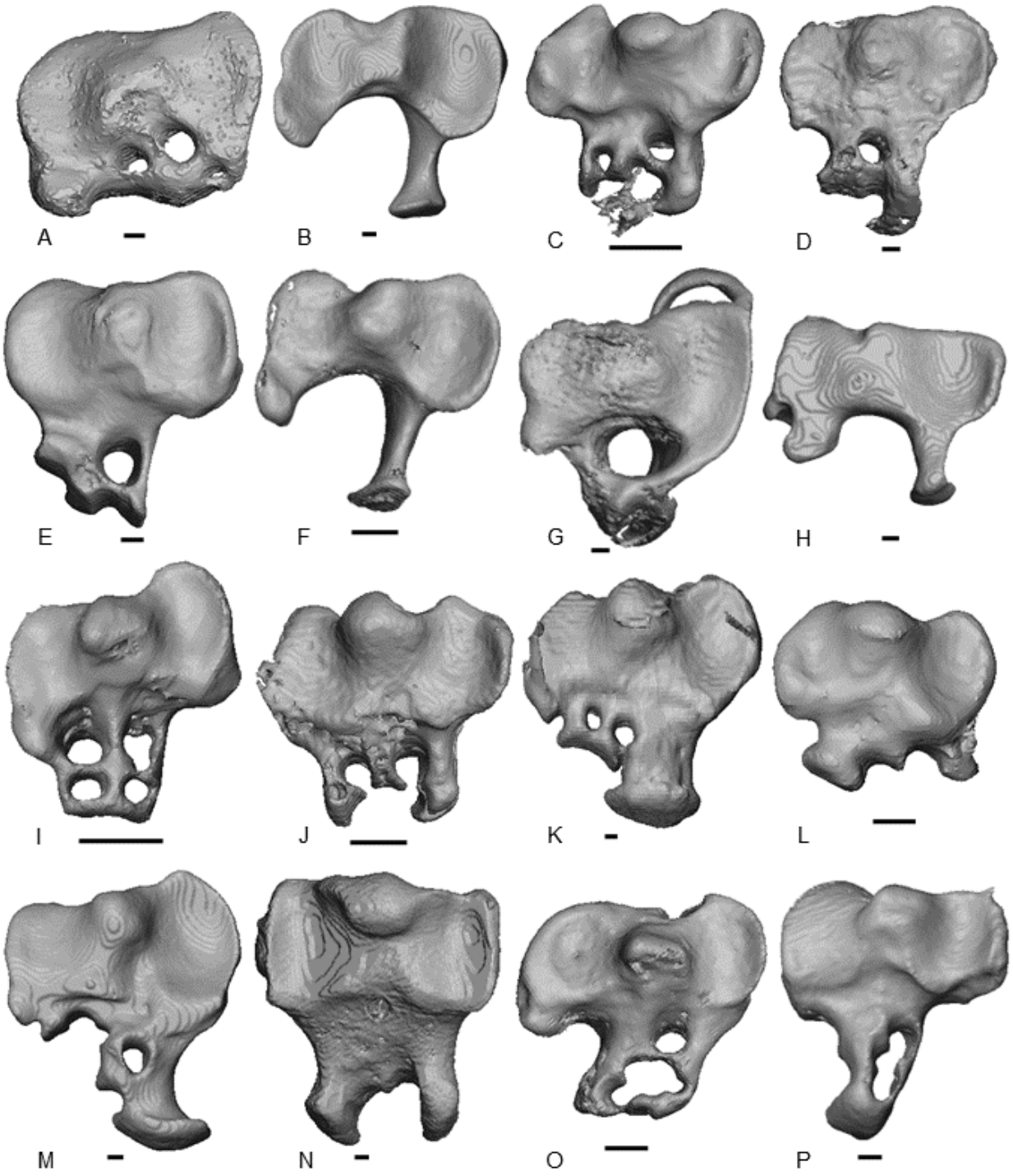
A
B
C
D
E
F
G
H
I
J
K
L
M
N
O
P

**Figure C.4.** Proximal views of extant hypotarsi 3D models analysed herein. Scale bar for each specimen is 1mm, all mirrored to left sides. A) *Nestor notabilis* (FMNH 23530); B) *Nyctea scandiaca* (NHMUK S.1998.5.1); C) *Oceanodroma leucorhoa* (NHMUK S.1953.2.10); D) *Opisthocomus hoazin* (NHMUK S.1961.6.2); E) *Ortalis ruficauda* (UMMZ 155489); F) *Otus spilocephalus* (NHMUK S1974.25.42); G) *Pandion haliaetus* (FMNH 437336); H) *Parabuteo unicinctus* (NHMUK 1899.6.12.3); I) *Passer domesticus* (NHMUK S.1977.70.3); J*) Pelecanoides urinatrix* (NHMUK S.2006.1.14); K) *Pelecanus occidentalis* (NHMUK S.1973.66.16); L) *Phaethon lepturus* (NHMUK 1876.3.16.3); M) *Phalacrocorax albiventer* (NHMUK S.2012.2.1); N) *Phoenicopterus roseus* (UMZC 346B); O) *Picus viridis* (NHMUK S.1982.2.1); P) *Podica senegalensis* (UMZC 209A).

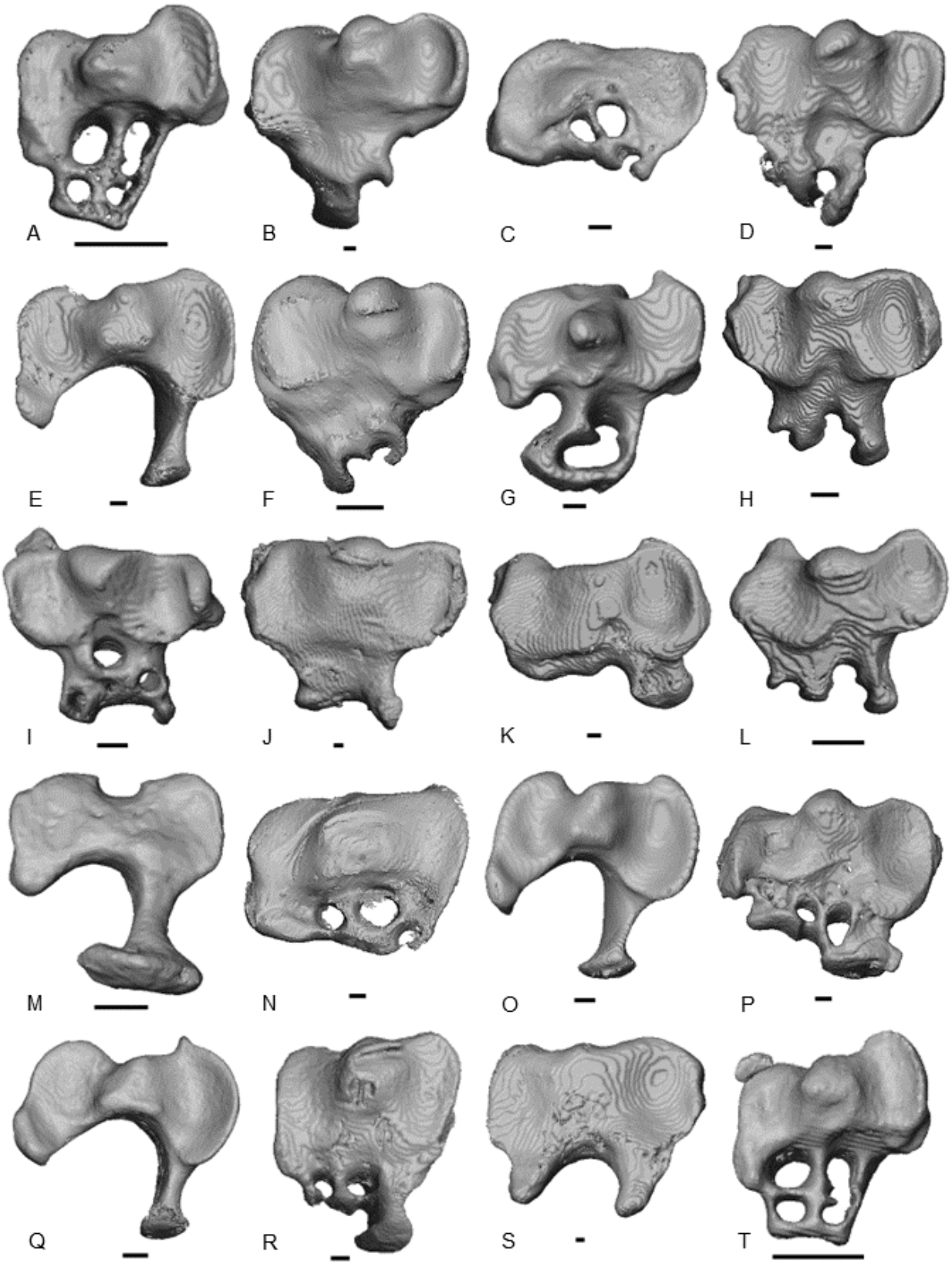
A
B
C
D
E
F
G
H
I
J
K
L
M
N
O
P
Q
R
S
T

**Figure C.5.** Proximal views of extant hypotarsi 3D models analysed herein. Scale bar for each specimen is 1mm, all mirrored to left sides. A) *Poecile atricapillis* (FMNH 504323); B) *Porphyrio hochstetteri* (NHMUK S.1961.17.1); C) *Psittacus erithacus* (NHMUK S.1992.41.60); D) *Psophia crepitans* (FMNH 105783); E) *Pulsatrix perspicillata* (NHMUK 1872.10.25.6); F) *Rallus limicola* (FMNH 501812); G) *Ramphastos ambiguous* (NHMUK S.2002.21.2); H) *Recurvirostra avosetta* (NHMUK S.1962.10.1); I) *Rollandia rolland* (UMMZ 156975); J) *Sagittarius serpentarius* (NHMUK 1898.5.7); K) *Spheniscus humboldti* (NHMUK S.2000.7.1); L) *Sterna hirundo* (NHMUK 1975.65.4); M) *Streptoprocne zonaris* (FMNH 85767); N) *Strigops habroptilus* (NHMUK 1881.1.17.71); O) *Strix aluco* (NHMUK S.2001.38.1); P) *Sula dactylatra* (NHMUK 1890.11.3.10); Q) *Surnia ulula* (NHMUK 1899.2.16.38); R) *Tigrisoma lineatum* (FMNH 105528); S) *Torgos tracheliotus* (NHMUK 1963.23.2); T) *Troglodytes troglodytes* (NHMUK 1963.23.2).

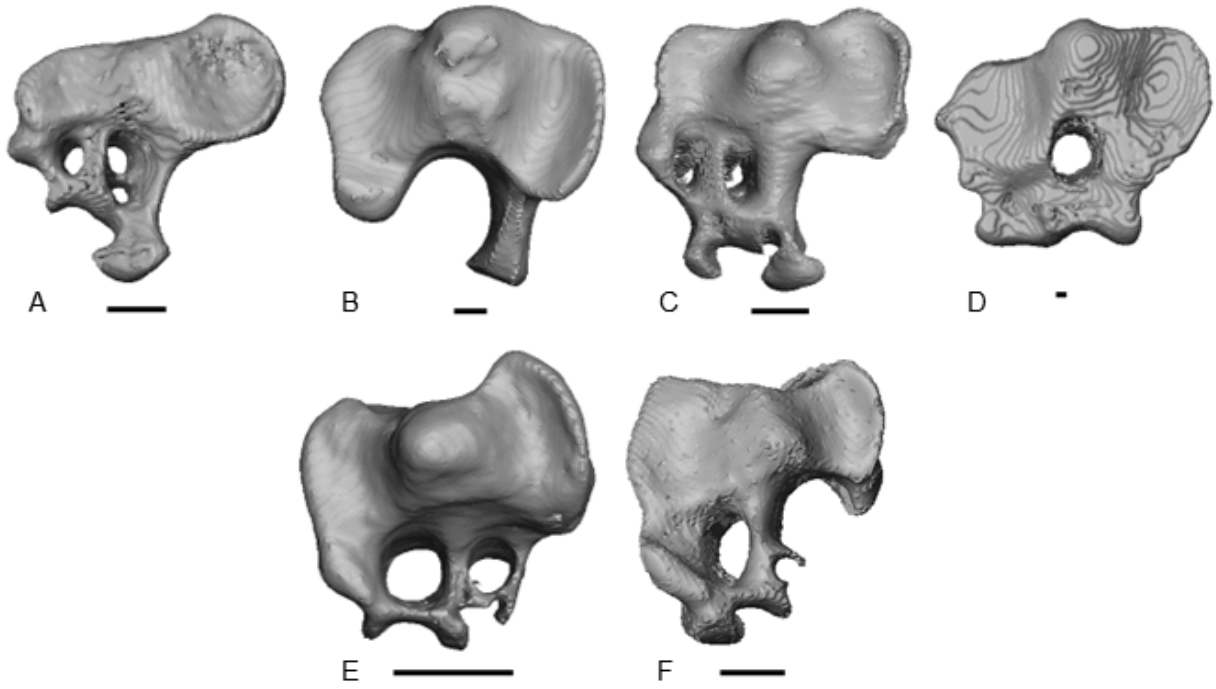


**Figure C.6.** Proximal views of extant hypotarsi 3D models analysed herein. Scale bar for each specimen is 1mm, all mirrored to left sides. A) *Trogon melanurus* (FMNH 290496); B) *Tyto alba* (NHMUK S.1989.22.1); C) *Upupa epops* (FMNH 352821); D) *Vultur gryphus* (NHMUK S.1955.5.11); E) *Xenicus gilviventris* (NHMUK 1940.12.8.145); F*) Xiphocolaptes promeropirhynchus* (YPM 121550).

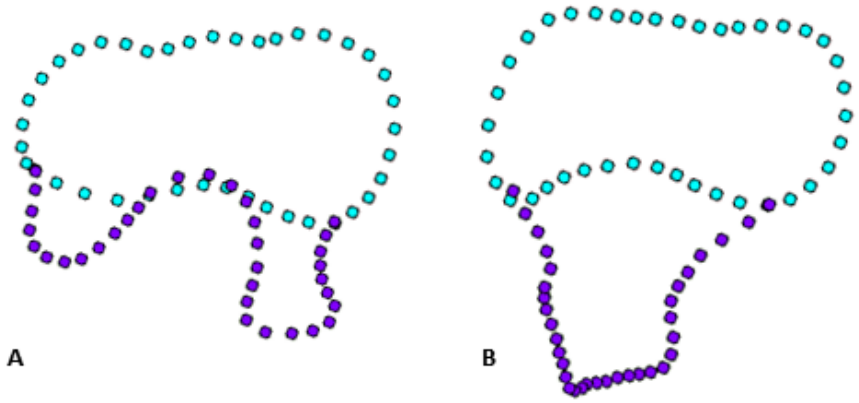


**Figure C.7.** Visualisation of hypotarsi representing the A) minimum, and B) maximum values of Principal Component 1.

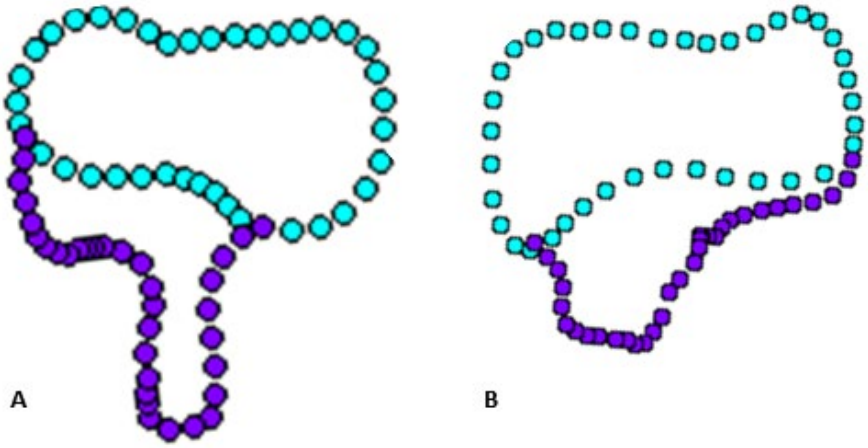


**Figure C.8.** Visualisation of hypotarsi representing the A) minimum, and B) maximum values of Principal Component 2.

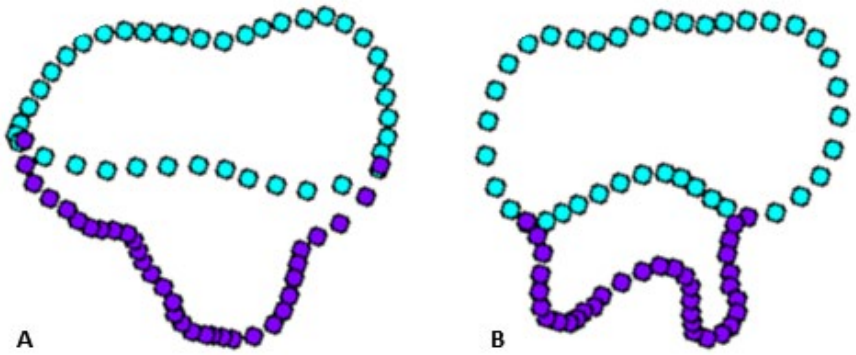


**Figure C.9.** Visualisation of hypotarsi representing the A) minimum, and B) maximum values of Principal Component 3.

*C.2 Tables*

**Table C.1.** ANOVA results (adjusted-$R^2$, degrees of freedom, sum of squares, $R^2$, F-value, and p-value) of PGLS and non-phylogenetic linear models for variation in hypotarsus shape as explained by raptoriality, centroid size, and mean species body mass. Significant p-values are bolded.

| Index | Model | Adj-$R^2$ | ANOVA: | df | SS | $R^2$ | F-value | p-value |
|---|---|---|---|---|---|---|---|---|
| 1 | (LM) shape ~ raptoriality | 0.16119 | raptoriality | 1 | 0.7339 | 0.1695 | 20.409 | **0.001** |
| | | | residuals | 100 | 3.5959 | 0.8305 | | |
| | | | total | 101 | 4.3298 | | | |
| 2 | (PGLS) shape ~ raptoriality | 0.02405 | raptoriality | 1 | 0.001614 | 0.03371 | 3.4891 | **0.002** |
| | | | residuals | 100 | 0.46264 | 0.96629 | | |
| | | | total | 101 | 0.047878 | | | |
| 3 | (PGLS) shape ~ size + raptoriality | 0.02322 | size | 1 | 0.000423 | 0.00885 | 0.9146 | 0.448 |
| | | | raptoriality | 1 | 0.001707 | 0.03566 | 3.6876 | **0.001** |
| | | | residuals | 99 | 0.4584 | 0.95744 | | |
| | | | total | 101 | 0.047878 | | | |
| 4 | (PGLS) shape ~ size + mean body mass + raptoriality | 0.02178 | size | 1 | 0.000476 | 0.00994 | 1.0263 | 0.359 |
| | | | bmmean | 1 | 0.000397 | 0.00828 | 0.8552 | 0.502 |
| | | | raptoriality | 1 | 0.001764 | 0.03684 | 3.8034 | **0.001** |
| | | | residuals | 98 | 0.045444 | 0.94916 | | |
| | | | total | 101 | 0.047878 | | | |
| 5 | (PGLS) shape ~ mean body mass + raptoriality | 0.02154 | bmmean | 1 | 0.000344 | 0.00719 | 0.742 | 0.641 |
| | | | raptoriality | 1 | 0.001631 | 0.03407 | 3.517 | **0.002** |
| | | | residuals | 99 | 0.045919 | 0.9591 | | |
| | | | total | 101 | 0.047878 | | | |
| 6 | (PGLS) shape ~ size*mean body mass + raptoriality | 0.02009 | size | 1 | 0.000415 | 0.00868 | 0.8942 | 0.471 |
| | | | bmmean | 1 | 0.000387 | 0.00808 | 0.8325 | 0.528 |
| | | | raptoriality | 1 | 0.001783 | 0.03724 | 3.8379 | **0.001** |
| | | | size:bmmean | 1 | 0.000386 | 0.00805 | 0.83 | 0.528 |
| | | | residuals | 97 | 0.045058 | 0.9411 | | |
| | | | total | 101 | 0.047878 | | | |

**Table C.2.** Preservation, age, taxonomic association, and hypotarsus shape of fossil specimens, as well as the posterior prediction results of the linear discriminant analysis, flexible discriminant analysis, mixed discriminant analysis with multivariate adaptive regression splines (MARS), phylogenetic flexible discriminant analysis with $\lambda = 0$, and phylogenetic flexible discriminant analysis with $\lambda = 1$. Discriminant function analysis results are predicted on non-raptorial/raptorial (0/1) binary.

| Taxon | Shape | Taxonomic Association | Preservation |
|---|---|---|---|
| Accipitrid species (IRSNB Av0182) | monosulcate | Accipitriformes | possibly eroded/broken hypotarsal crests |
| Alcediniform species A (IRSNB Av0188) | multisulcate | Coraciimorphae | possibly eroded/broken hypotarsal crests |
| *Anchigyps voorhiesi* (UNSM 62877) | monosulcate | Accipitriformes | entire |
| *Anneavis anneae* (BMS E25337) | multicanaliculate | Coraciimorphae | presumed entire |
| *Bavarpsitta ballmanni* (BSP 1970XVIII899) | multicanaliculate | Psittaciformes | minor erosion |
| *Berruornis orbisantiqui* (MNHN L3096) | monosulcate | Strigiformes | entire |
| *Berruornis orbisantiqui* (MNHN R4155) | monosulcate | Strigiformes | entire |
| *Certhiops rummeli* (NMA 2007.51.2021) | multicanaliculate | Passeriformes | presumed entire |
| Coraciiform species A (Lyon PQ1216) | multisulcate | Coraciimorphae | entire |
| *Elaphrocnemus phasianus* (NMB QH158a) | multisulcate | Cariamiformes | possibly eroded/broken hypotarsal crests |
| *Eostrix tsaganica* (PIN 3104/147) | monosulcate | Strigiformes | entire |
| *Gymnogyps kofordi* (UF 63512) | asulcate | Accipitriformes | entire |
| *Heterostrix tatsinensis* (PIN 3211/35) | monosulcate | Strigiformes | entire |
| *Horusornis vianeyliaudae* (Montpellier BFI1958) | monosulcate | Accipitriformes | possibly eroded/broken hypotarsal crests |
| *Messelastur gratulator* (SMF ME11348) | monosulcate | Psittaciformes | deformed/broken |
| *Miocorvus larteti* (MNHN SA1263c) | multisulcate | Passeriformes | entire |
| *Necrobyas harpax* (MNHN QU15695) | monosulcate | Strigiformes | entire |
| *Ogygoptynx wetmorei* (AMNH 2653) | monosulcate | Strigiformes | possibly eroded/broken hypotarsal crests |
| *Palaeobyas cracrafti* (MNHN QU15746) | monosulcate | Strigiformes | possibly eroded/broken hypotarsal crests |
| *Palaeopsittacus georgei* (WN91682) | multicanaliculate | Psittaciformes | entire |
| Psittacopasseres species A (WN89627A) | multisulcate | Psittacopasseres | entire |
| *Pulchrapollia gracilis* (BMNH PVA6207) | multisulcate | Psittaciformes | possibly eroded/broken hypotarsal crests |
| *Pulchrapollia* species (SMF Av628) | multisulcate | Psittaciformes | entire |
| *Selenornis steendorpensis* (IRSNB Av84ab) | monosulcate | Strigiformes | entire |
| *Septencoracias* species (IRSNB Av191) | multisulcate | Coraciimorphae | entire |
| *Sophiornis quercynus* (Lyon PQ1202) | monosulcate | Strigiformes | entire |
| *Thegornis musculosis* (MPM PV-3443) | monosulcate | Falconiformes | broken medial hypotarsal crest |
| *Tsidiiyazhi abini* (NMMNH P54128) | multisulcate | Coraciimorphae | possibly eroded/broken hypotarsal crests |
| *Tyto sanctialbani* (NHMUK A305) | monosulcate | Strigiformes | entire |

| Taxon | Age | LDA | FDA | MDA MARS | PhyFDA λ=0 | PhyFDA λ=1 |
|---|---|---|---|---|---|---|
| Accipitrid species (IRSNB Av0182) | Early Eocene | 0 | **1** | 0 | 0 | 0 |
| Alcediniform species A (IRSNB Av0188) | Early Eocene | 0 | 0 | 0 | 0 | **1** |
| *Anchigyps voorhiesi* (UNSM 62877) | Late Miocene | **1** | **1** | 0 | **1** | 0 |
| *Anneavis anneae* (BMS E25337) | Early Eocene | 0 | 0 | 0 | 0 | 0 |
| *Bavarpsitta ballmanni* (BSP 1970XVIII899) | Middle Miocene | 0 | 0 | 0 | 0 | 0 |
| *Berruornis orbisantiqui* (MNHN L3096) | Late Paleocene | 0 | 0 | **1** | 0 | 0 |
| *Berruornis orbisantiqui* (MNHN R4155) | Late Paleocene | **1** | 0 | **1** | | |
| *Certhiops rummeli* (NMA 2007.51.2021) | Early Miocene | 0 | 0 | 0 | 0 | 0 |
| Coraciiform species A (Lyon PQ1216) | Paleogene | 0 | **1** | **1** | | |
| *Elaphrocnemus phasianus* (NMB QH158a) | Late Eocene to Early Oligocene | 0 | 0 | 0 | 0 | 0 |
| *Eostrix tsaganica* (PIN 3104/147) | Early Eocene | **1** | 0 | **1** | **1** | **1** |
| *Gymnogyps kofordi* (UF 63512) | Early Pleistocene | 0 | 0 | 0 | 0 | 0 |
| *Heterostrix tatsinensis* (PIN 3211/35) | Early Oligocene | **1** | **1** | **1** | **1** | 0 |
| *Horusornis vianeyliaudae* (Montpellier BFI1958) | Late Eocene | 0 | 0 | 0 | | |
| *Messelastur gratulator* (SMF ME11348) | Middle Eocene | 0 | **1** | **1** | | |
| *Miocorvus larteti* (MNHN SA1263c) | Middle Miocene | 0 | 0 | 0 | 0 | 0 |
| *Necrobyas harpax* (MNHN QU15695) | Early Oligocene | **1** | **1** | **1** | **1** | **1** |
| *Ogygoptynx wetmorei* (AMNH 2653) | Middle Paleocene | 0 | **1** | 0 | **1** | 0 |
| *Palaeobyas cracrafti* (MNHN QU15746) | Eocene to Oligocene | 0 | 0 | **1** | 0 | 0 |
| *Palaeopsittacus georgei* (WN91682) | Early Eocene | 0 | 0 | 0 | | |
| Psittacopasseres species A (WN89627A) | Early Eocene | 0 | 0 | 0 | 0 | 0 |
| *Pulchrapollia gracilis* (BMNH PVA6207) | Early Eocene | 0 | 0 | 0 | 0 | 0 |
| *Pulchrapollia* species (SMF Av628) | Early Eocene | **1** | **1** | 0 | | |
| *Selenornis steendorpensis* (IRSNB Av84ab) | Early Oligocene | 0 | **1** | **1** | **1** | 0 |
| *Septencoracias* species (IRSNB Av191) | Early Eocene | 0 | 0 | 0 | 0 | 0 |
| *Sophiornis quercynus* (Lyon PQ1202) | Eocene to Oligocene | 0 | 0 | **1** | **1** | 0 |
| *Thegornis musculosis* (MPM PV-3443) | Miocene | 0 | 0 | 0 | 0 | 0 |
| *Tsidiiyazhi abini* (NMMNH P54128) | Early Paleocene | 0 | 0 | 0 | 0 | **1** |
| *Tyto sanctialbani* (NHMUK A305) | Middle Miocene | **1** | **1** | **1** | **1** | 0 |

**Table C.3.** Tendon and bone cross-sectional areas for frozen extant taxa, as well as specimen total body mass, genus average body mass, and raptorial foot use scoring. Cross-sectional areas for the flexor digitorum longus (FDL) and flexor hallucis longus (FHL) are also included.

| Taxon | Raptorial | Top slice total tendon area ($mm^2$) | Bottom slice total tendon area ($mm^2$) | Top slice FDL area ($mm^2$) | Bottom slice FDL area ($mm^2$) |
|---|---|---|---|---|---|
| *Falco tinnunculus* (Eurasian Kestrel) | 1 | 1.991 | 1.3789 | 1.4183 | 0.78795 |
| *Lorius garrulus* (Chattering Lory) | 0 | 1.2729 | 1.2199 | 0.15906 | 0.31812 |
| *Corvus corone* (Carrion Crow) | 0 | 2.8138 | 2.5973 | 0.7214 | 0.7214 |
| *Accipiter nisus* (Eurasian Sparrowhawk) | 1 | 1.190297 | 2.05889 | 0.28953 | 0.45038 |
| *Strix aluco* (Tawny Owl) | 1 | 4.0354 | 4.6435 | 1.82423 | 1.60311 |
| *Picus viridis* (Eurasian Green Woodpecker) | 0 | 0.77904 | 0.77904 | 0.25041 | 0.111292 |

| Taxon | Raptorial | Top slice FHL area ($mm^2$) | Bottom slice FHL area ($mm^2$) | Top slice total bone area ($mm^2$) | Bottom slice total bone area ($mm^2$) |
|---|---|---|---|---|---|
| *Falco tinnunculus* (Eurasian Kestrel) | 1 | 0.1576 | 0.4334 | 12.580623 | 7.2815 |
| *Lorius garrulus* (Chattering Lory) | 0 | 0.15906 | 0.34463 | 11.26675 | 9.64964 |
| *Corvus corone* (Carrion Crow) | 0 | 1.1544 | 0.6493 | 35.78144 | 16.88076 |
| *Accipiter nisus* (Eurasian Sparrowhawk) | 1 | 0.6434 | 1.12596 | 19.14115 | 10.10138 |
| *Strix aluco* (Tawny Owl) | 1 | 0.60808 | 0.60808 | 16.52872 | 20.73 |
| *Picus viridis* (Eurasian Green Woodpecker) | 0 | 0.22258 | 0.16694 | 11.71348 | 5.981945 |

| Taxon | Raptorial | Specimen body mass (g) | Average genus body mass (g) |
|---|---|---|---|
| *Falco tinnunculus* (Eurasian Kestrel) | 1 | 195 | 225 |
| *Lorius garrulus* (Chattering Lory) | 0 | 162 | 161 |
| *Corvus corone* (Carrion Crow) | 0 | 443 | 499 |
| *Accipiter nisus* (Eurasian Sparrowhawk) | 1 | 256 | 228 |
| *Strix aluco* (Tawny Owl) | 1 | 258 | 497 |
| *Picus viridis* (Eurasian Green Woodpecker) | 0 | 96 | 194 |

**Table C.4.** ANOVA results (adjusted-$R^2$, AICc value, coefficient, standard variable error, and p-value) of PGLS models for variation in tendon cross-sectional area as explained by raptoriality, body mass, and bone cross-sectional area. Significant p-values are bolded.

| Index | Model | Adj-$R^2$ | AICc | Variable | Estimate | Standar Error | Pr (>\|t\|) |
|---|---|---|---|---|---|---|---|
| 1 | total bottom tendon ~ raptorial + total bottom bone | 0.9931 | -14.36929 | raptorial | 0.166662 | 0.050892 | **0.0031189** |
| | | | | total bot bone | 1.163223 | 0.018996 | **0.0001669** |
| | | | | intercept | -1.02742 | 0.049305 | **0.0002657** |
| 2 | total bottom tendon ~ average body mass | 0.6632 | 0.719231 | avgbm | 1.08536 | 0.32958 | **0.03012** |
| | | | | intercept | -2.38593 | 0.80465 | **0.04134** |
| 3 | total bottom tendon ~ average body mass + raptorial + total bottom bone | 0.9974 | 7.282866 | avgbm | 0.14063 | 0.05722 | 0.133253 |
| | | | | raptorial | 0.164648 | 0.011632 | **0.004954** |
| | | | | total bot bone | 1.03863 | 0.058966 | **0.003208** |
| | | | | intercept | -1.24045 | 0.092084 | **0.005466** |
| 4 | total top tendon ~ raptorial + total top bone | 0.07832 | 14.61078 | raptorial | 0.20559 | 0.20993 | 0.3996 |
| | | | | total top bone | 0.74634 | 0.58495 | 0.2918 |
| | | | | intercept | -0.77709 | 0.73275 | 0.3667 |
| 5 | bottom FDL ~ total bottom bone + raptorial | 0.7531 | 11.58971 | total bot bone | 1.30188 | 0.42892 | 0.05608 |
| | | | | raptorial | 0.37565 | 0.16525 | 0.10761 |
| | | | | intercept | -1.84073 | 0.44273 | **0.0253** |
| 6 | bottom FHL ~ total bottom bone + raptorial | 0.3441 | 13.23957 | total bot bone | 0.70775 | 0.49214 | 0.246 |
| | | | | raptorial | 0.25187 | 0.18961 | 0.2761 |
| | | | | intercept | -1.17843 | 0.50798 | 0.1031 |
| 7 | total bottom tendon ~ total bottom bone | 0.8628 | -4.670756 | total bot bone | 1.2373 | 0.2172 | **0.004692** |
| | | | | intercept | -1.017 | 0.2275 | **0.011071** |
| 8 | total bottom tendon ~ raptorial | 0.04021 | 7.00243 | raptorial | 0.24344 | 0.22136 | 0.3332 |
| | | | | intercept | 0.12762 | 0.16437 | 0.4808 |
| 9 | total bottom tendon ~ average body mass + total bottom bone | 0.8273 | 4.983755 | avgbm | 0.19767 | 0.16876 | 0.7017 |
| | | | | total bot bone | 1.06095 | 0.4841 | 0.1161 |
| | | | | intercept | -1.31662 | 0.75496 | 0.1795 |
| 10 | total bottom tendon ~ average body mass + raptorial | 0.7336 | 7.586816 | avgbm | 1.00713 | 0.29816 | **0.04316** |
| | | | | raptorial | 0.17013 | 0.11863 | 0.24702 |
| | | | | intercept | -2.28398 | 0.71919 | 0.05026 |

*C.3 Data*

All data and code used to produce the final results are archived at https://doi.org/10.5281/zenodo.7031733. All computations were processed in an R statistical environment (R Core Team 2022).

**Data C.1** Phylogenetic tree (Newick format) of 102 extant avian taxa and 23 fossil taxa based on the Hackett et al. (2008) backbone.

**Data C.2** Phylogenetic tree (Newick format) of six extant telluravian taxa.

**Data C.3** Generalised Procrustes analysis of 2D extant hypotarsus landmark data.

**Data C.4** Generalised Procrustes analysis of 2D fossil hypotarsus landmark data.

**Data C.5** Phylogenetic generalised least squares models for variation in hypotarsus shape as explained by raptoriality, centroid size and mean species body mass.

**Data C.6** Generalised Procrustes analysis of fossil and extant hypotarsus shape data; discriminant function analyses of fossil and extant hypotarsus shape data.

**Data C.7** Phylogenetic flexible discriminant analysis by Motani and Schmitz (2011).

**Data C.8** Phylogenetic generalised least squares models for variation in tendon cross-sectional area as explained by raptoriality, bone cross-sectional area, and mean genus body mass.

# D. Supporting Charts for Chapter 3

*D.1 Figures*

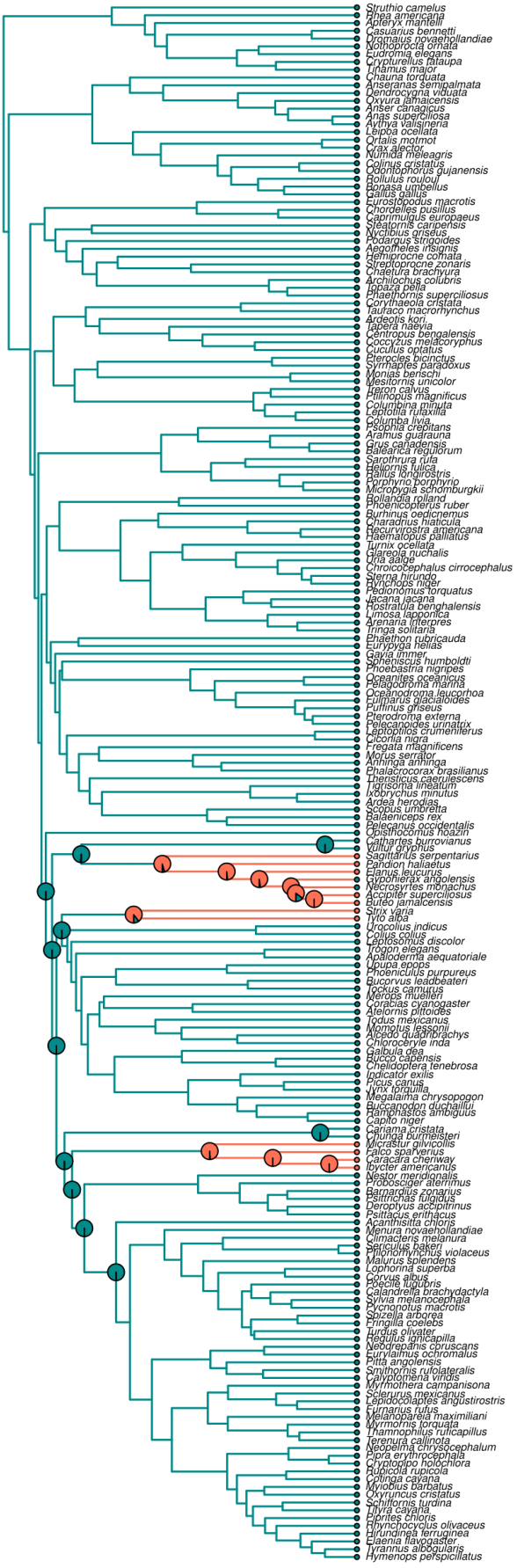
Struthio camelus
Rhea americana
Apteryx mantelli
Casuarius bennetti
Dromaius novaehollandiae
Nothoprocta ornata
Eudromia elegans
Crypturellus tataupa
Tinamus major
Chauna torquata
Anseranas semipalmata
Dendrocygna viduata
Oxyura jamaicensis
Anser canagicus
Anas superciliosa
Aythya valisineria
Leipoa ocellata
Ortalis motmot
Crax alector
Numida meleagris
Colinus cristatus
Odontophorus gujanensis
Rollulus rouloul
Bonasa umbellus
Gallus gallus
Eurostopodus macrotis
Chordeiles pusillus
Caprimulgus europaeus
Steatornis caripensis
Nyctibius griseus
Podargus strigoides
Aegotheles insignis
Hemiprocne comata
Streptoprocne zonaris
Chaetura brachyura
Archilochus colubris
Topaza pella
Phaethornis superciliosus
Corythaeola cristata
Tauraco macrorhynchus
Ardeotis kori
Tapera naevia
Centropus bengalensis
Coccyzus melacoryphus
Cuculus optatus
Eurocles bicinctus
Syrmaptes paradoxus
Monias benschi
Mesitornis unicolor
Ireron calvus
Pitiliopus magnificus
Columbina minuta
Leptotila rufaxilla
Columba livia
Psophia crepitans
Aramus guarauna
Grus canadensis
Balearica regulorum
Sarothrura rufa
Heliornis fulica
Rallus longirostris
Porphyrio porphyrio
Micropygia schomburgkii
Rollandia rolland
Phoenicopterus ruber
Burhinus oedicnemus
Charadrius hiaticula
Recurvirostra americana
Haematopus palliatus
Turnix ocellata
Glareola nuchalis
Vria aalge
Chroicocephalus cirrocephalus
Sterna hirundo
Rynchops niger
Pedionomus torquatus
Jacana jacana
Rostratula benghalensis
Limosa lapponica
Arenaria interpres
Tringa solitaria
Phaethon rubricauda
Eurypyga helias
Gavia immer
Spheniscus humboldti
Phoebastria nigripes
Oceanites oceanicus
Pelagodroma marina
Oceanodroma leucorhoa
Fulmarus glacialoides
Puffinus griseus
Pterodroma externa
Pelecanoides urinatrix
Leptoptilos crumeniferus
Ciconia nigra
Fregata magnificens
Morus serrator
Anhinga anhinga
Phalacrocorax brasilianus
Theristicus caerulescens
Tigrisoma lineatum
Ixobrychus minutus
Ardea herodias
Scopus umbretta
Balaeniceps rex
Pelecanus occidentalis
Opisthocomus hoazin
Calhartes burrovianus
Vultur gryphus
Sagittarius serpentarius
Pandion haliaetus
Elanus leucurus
Gypohierax angolensis
Necrosyrtes monachus
Accipiter superciliosus
Buteo jamaicensis
Strix varia
Tyto alba
Urocolius indicus
Colius colius
Leptosomus discolor
Trogon elegans
Aplodermis aequatoriale
Upupa epops
Phoeniculus purpureus
Bucorvus leadbeateri
Tockus camurus
Merops muelleri
Coracias cyanogaster
Afelornis plitoides
Todus mexicanus
Momotus lessonii
Alcedo quadribrachys
Chloroceryle inda
Galbula dea
Bucco capensis
Cheloptera tenebrosa
Indicator exilis
Picus canus
Jynx torquilla
Megalaima chrysopogon
Bucanodon duchaillui
Ramphastos ambiguus
Capito niger
Cariama cristata
Chunga burmeisteri
Micrastur gilvicollis
Falco sparverius
Caracara cheriway
Ibycter americanus
Nestor meridionalis
Probosciger aterrimus
Barnardius zonarius
Psittrichas fulgidus
Deroptyus accipitrinus
Psittacus erithacus
Acanthisitta chloris
Menura novaehollandiae
Climacteris melanura
Sericulus bakeri
Philonorhynchus violaceus
Malurus splendens
Lophorina superba
Corvus albus
Poecile hudsonica
Calandrella brachydactyla
Sylvia melanocephala
Pycnonotus macrotis
Spizella arborea
Fringilla coelebs
Turdus olivater
Regulus ignicapilla
Nebrephanis cruscans
Eurylaimus ochromalus
Pitta angolensis
Smithornis rufolateralis
Calyptomena viridis
Myrmotherа campanisona
Sclerurus mexicanus
Lepidocolaptes angustirostris
Furnarius rufus
Melanopareia maximiliani
Myrmorнis torquata
Thamnophilus ruficapillus
Terenura callinota
Neopelma chrysocephalum
Pipra erythrocephala
Chiroxiphia holochlora
Rupicola rupicola
Cotinga cayana
Mionobius barbatus
Oxyruncus cristatus
Schiffornis turdina
Tityra cayana
Pipрites chloris
Rhynchocyclus olivaceus
Hirundinea ferruginea
Elaenia flavogaster
Tyrannus albogularis
Hymenops perspicillatus

**Figure D.1.** Phylogenetic tree of 200 extant avian taxa showing the ACE maximum likelihood estimates of raptoriality (Equal Rates model reconstruction) at key nodes along the telluravian backbone and extant raptorial clades. Orange denotes percentage likelihood of raptoriality.

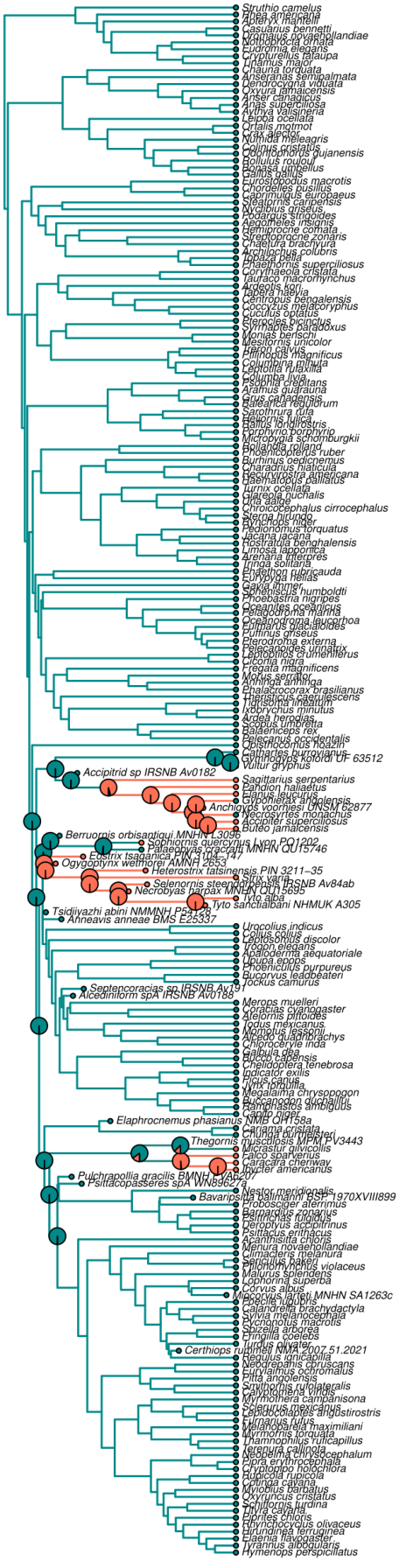
Struthio camelus
Rhea americana
Apteryx mantelli
Casuarius bennetti
Dromaius novaehollandiae
Mothocrocia ornata
Eudromia elegans
Cryptturellus tataupa
Tinamus major
Chauna torquata
Anseranas semipalmata
Dendrocygna viduata
Oxyura jamaicensis
Anser canadicus
Anas superciliosa
Aythya valisineria
Lerwa lerwa
Crax alberti
Numida meleagris
Colinus cristatus
Odontophorus gujanensis
Rollulus rouloul
Bonasa umbellus
Gallus gallus
Eurostopodus macrotis
Chordeiles pusillus
Caprimulgus europaeus
Steatornis caripensis
Nyctibius griseus
Podargus strigoides
Aegotheles insignis
Hemiprocne comata
Streptoprocne zonaris
Chaetura brachyura
Archilochus colubris
Tobalaza peltata
Phaethornis superciliosus
Corythaeola cristata
Taurco macrorhynchus
Ardeotis kori
Tapera naevia
Centropus bengalensis
Coccyzus melacoryphus
Cuculus optatus
Pteroclles bicinctus
Syrrhaptes paradoxus
Monias benschi
Mesitornis unicolor
Heron calvus
Phimopus magnificus
Columbina minuta
Leptotila rufaxilla
Columba livia
Psophia crepitans
Aramus guarauna
Grus carladensis
Balearica regulorum
Sarothrura rufa
Heliornis fulica
Ramus longirostris
Porphyrio porphyrio
Micropygia schomburgkii
Rallina rallina
Phoenicopterus ruber
Burhinus oedicnemus
Charadrius hiaticula
Recurvirostra americana
Haematopus palliatus
Turnix ocellata
Glareola nuchalis
Uria aalge
Chroicocephalus cirrocephalus
Sterna hirundo
Rynchops niger
Pedionomus torquatus
Jacana jacana
Nostramus benghalensis
Limosa lapponica
Arenaria interpres
Tringa solitaria
Phaethon rubricauda
Eurypyga helias
Cakile rumex
Nycteibius humboldti
Phoebastria nigripes
Oceanites oceanicus
Pelagodroma marina
Oceanodroma leucorhoa
Fulmarus glacialoides
Puffinus griseus
Pterodroma externa
Pelecanoides urinatrix
Leptoptilos dumerilerius
Ciconia nigra
Fregata magnificens
Morus serrator
Anhinga anhinga
Phalacrocorax brasilianus
Threskiornis aethiopicus
Platalea leucorodia
Ixobrychus minutus
Ardea herodias
Scopus umbretta
Balaeniceps rex
Pelecanus occidentalis
Cathartes burrovianus
Gymnogyps kofordi UF 63512
Vultur gryphus
Accipitrid sp IRSNB Av0182
Sagittarius serpentarius
Pandion haliaetus
Elanus leucurus
Circhelax africanus
Anchiornis voorhiesi UNSM 62877
Necrosyrtes monachus
Accipiter superciliosus
Buteo jamaicensis
Berruornis orbisantiqui MNHN 1.3006
Sophiornis quarcyrius Lyon PO1202
Palaeoglaux artacta MNHN QU15746
Eostrix isaacnica MNHN QU15747
Ogygoptynx wetmorei AMNH 2653
Heterostrix tatsinensis PIN 3211–35
Strix varia
Selenornis steenbalkensis IRSNB Av84ab
Necrobyas barpax MNHN QU15695
Tyto alba
Tyto sanctialbani NHMUK A305
Tsidiiyazhi abini NMMNH P27158
Anneavis anneae BMS E25337
Urocolius indicus
Colius colius
Leptosomus discolor
Trogon elegans
Apaloderma aequatoriale
Upupa epops
Phoeniculus purpureus
Bucorvus leadbeateri
Tockus camurus
Septencoracias sp IRSNB Av1191
Alcediniform spA IRSNB Av0188
Merops muelleri
Coracias cyanogaster
Atelornis pittoides
Todus mexicanus
Momotus lessonii
Alcedo quadribrachys
Chloroceryle inda
Galbula dea
Bucco capensis
Chelidoptera tenebrosa
Indicator exilis
Picus canus
Jynx torquilla
Megalaima chrysopogon
Buccanodon duchaillui
Pteroglossus aracari
Capito niger
Elaphrocnemus phasianus MNB OR158a
Cariama cristata
Chunga burmeisteri
Thegornis musculosis MPM PV3443
Micrastur ruficollis
Falco sparverius
Caracara cheriway
Polyborus americanus
Pulchrapollia gracilis BMNH 1.AB207
Psittacopasseres spA WN86627a
Nestor meridionalis
Bavaripsitta talainani BSP 1970XVIII899
Proboscigeri aterrimus
Barnardius zonarius
Psittrichas fulgidus
Deroptyus accipitrinus
Psittacus erithacus
Acanthisitta chloris
Menura novaehollandiae
Climacteris melanurus
Setopsius bakeri
Chlamydera nuchalis violaceus
Malurus splendens
Lophorina superba
Corvus albus
Miocorvus larteti MNHN SA1263c
Cracticus nigrus
Calandrella brachydactyla
Sylvia melanocephala
Pycnonotus macrotis
Spizella arborea
Fringilla coelebs
Turdus pilaris
Certhiops rubiginosa MNA V2007.51.2021
Hedulus tyniscapia
Mendegobis obruscans
Furnariamus ochromalus
Pitta angolensis
Smithornis rufolateralis
Calyptomena viridis
Myrmotherea campanisona
Sclerurus mexicanus
Lepidocolaptes angustirostris
Furnarius rufus
Melanopareia maximiliani
Myrmornis torquata
Thamnophilus ruficapillus
Terenura callinota
Neopelma chrysocephalum
Pipra erythrocephala
Cryptopipo holochlora
Rupicola rupicola
Cotinga cayana
Myiobius barbatus
Oxyruncus cristatus
Schiffornis turdina
Tityra cayana
Pachyrhynchus olivaceus
Hirundinea ferruginea
Elaenia flavogaster
Tyrannus albogularis
Hymenops perspicillatus

**Figure D.2.** Phylogenetic tree of 200 extant and 23 fossil avian taxa showing the ACE maximum likelihood estimates of raptoriality (Equal Rates model reconstruction) for key nodes along the telluravian backbone and raptorial clades. Orange denotes percentage likelihood of raptorialitiy.

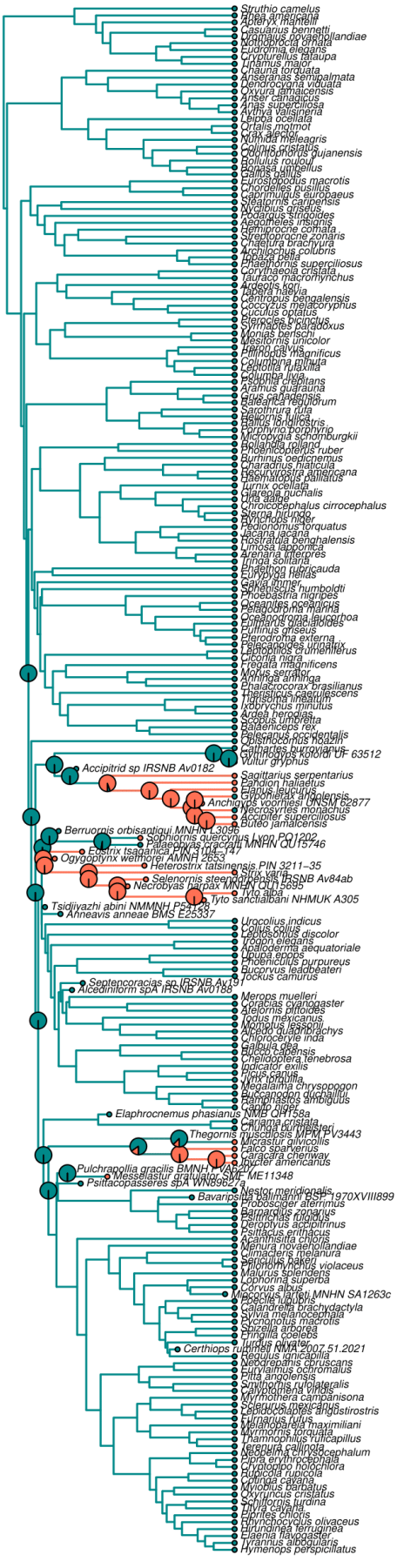
Struthio camelus
Tinamus major
Eudromia elegans
Cryptoprocta ferox
Eurypyga helias
Phoenicopterus ruber
Podiceps cristatus
Phaethon aethereus
Gavia stellata
Fregata magnificens
Sula dactylatra
Pelecanus occidentalis
Phalacrocorax brasilianus
Anhinga anhinga
Ardea herodias
Cathartes burrovianus
Gypaetus barbatus
Haliaeetus albicilla
Pandion haliaetus
Elanus leucurus
Accipitrid sp IRSNB Av0182
Sagittarius serpentarius
Anchiornis huxleyi IVPP V22877
Necrosyrtes monachus
Accipiter superciliosus
Buteo jamaicensis
Berruornis orbisantiqui MNHN 1.3096
Falco tinnunculus
Falco peregrinus
Psittacopasserines sp IRSNB Av0187
Merops muelleri
Coracias cyanogaster
Todus mexicanus
Momotus lessonii
Alcedo quadribrachys
Chloroceryle inda
Galbula dea
Bucco capensis
Cheloptera tenebrosa
Indicator exilis
Trogon elegans
Upupa epops
Phoeniculus purpureus
Bucorvus leadbeateri
Tockus camurus
Septencoracias sp IRSNB Av0191
Alcediniform spA IRSNB Av0188
Elaphrocnemus phasianus NMB OHT58a
Cariama cristata
Chunga burmeisteri
Thegornis musculosus MPM PV3443
Micrastur gilvicollis
Falco sparverius
Caracara cheriway
Vireo altiloquus
Pulchragolla gracilis BMNH 1A1907
Messelastur gratulator SMF ME11348
Psittacopasseres spA WN89627a
Nestor meridionalis
Bavarispina baumanni BSP 1970XVIII899
Proboscicer aterrimus
Barnardius zonarius
Platycercus elegans
Deroptyus accipitrinus
Psittacus erithacus
Acanthisitta chloris
Menura novaehollandiae
Climacteris melanura
Sericulus bakeri
Ptilonorhynchus violaceus
Malurus splendens
Lophorina superba
Corvus albus
Melocryus larteti MNHN SA1263c
Pomarea nigra
Calandrella brachydactyla
Sylvia melanocephala
Pycnonotus macrotis
Spizella arborea
Fringilla coelebs
Turdus olivater
Certhiops rufinella NMA 2007.51.2021
Regulus ignicapilla
Nectarophila cruciger
Eurylaimus ochromalus
Pitta angolensis
Smithornis rufolateralis
Calyptomena viridis
Myrmotherula campanisona
Sclerurus mexicanus
Lepidocolaptes angustirostris
Furnarius rufus
Melanopareia maximiliani
Myrmoborus lugubris
Thamnophilus ruficapillus
Tersina viridis
Tersina cf viridis
Pipra erythrocephala
Cryptopipo holochlora
Rupicola rupicola
Cotinga cayana
Myiobius barbatus
Oxyruncus cristatus
Schiffornis turdina
Tityra cayana
Piprites chloris
Rhynchocyclus olivaceus
Hirundinea ferruginea
Elaenia flavogaster
Tyrannus albogularis
Hymenops perspicillatus

**Figure D.3.** Phylogenetic tree of 200 extant and 24 fossil avian taxa showing the ACE maximum likelihood estimates of raptoriality (Equal Rates model reconstruction) at key nodes along the telluravian backbone, raptorial clades, and stem-Psittaciformes. Orange denotes the percentage likelihood of raptoriality.

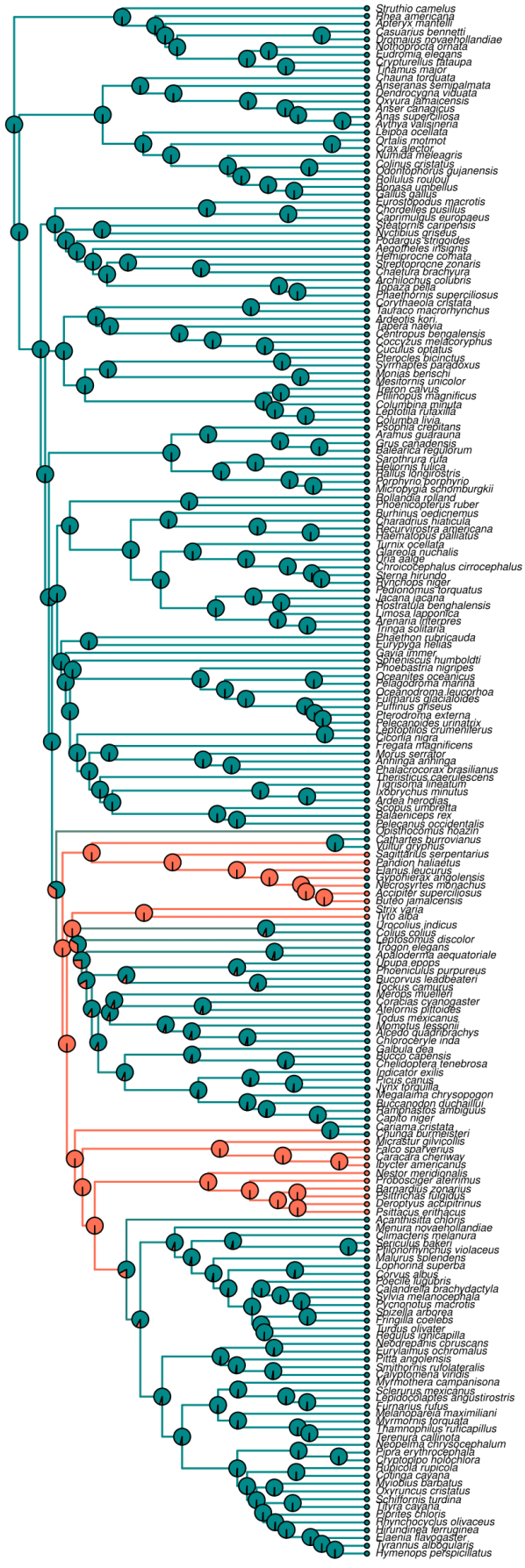
Struthio camelus
Rhea americana
Apteryx mantelli
Casuarius bennetti
Dromaius novaehollandiae
Nothoprocta ornata
Eudromia elegans
Crypturellus tataupa
Tinamus major
Chauna torquata
Anseranas semipalmata
Dendrocygna viduata
Oxyura jamaicensis
Anser canagicus
Anas superciliosa
Aythya valisineria
Leipoa ocellata
Ortalis motmot
Crax alector
Numida meleagris
Colinus cristatus
Odontophorus gujanensis
Rollulus rouloul
Bonasa umbellus
Gallus gallus
Eurostopodus macrotis
Chordeiles pusillus
Caprimulgus europaeus
Steatornis caripensis
Nyctibius griseus
Podargus strigoides
Aegotheles insignis
Hemiprocne comata
Streptoprocne zonaris
Chaetura brachyura
Archilochus colubris
Topaza pella
Phaethornis superciliosus
Corythaeola cristata
Taufaco macrorhynchus
Ardeotis kori
Tapera naevia
Centropus bengalensis
Coccyzus melacoryphus
Cuculus optatus
Pterocles bicinctus
Syrrhaptes paradoxus
Monias benschi
Mesitornis unicolor
Ireron calvus
Pitiliopus magnificus
Columbina minuta
Leptotila rufaxilla
Columba livia
Psophia crepitans
Aramus guarauna
Grus canadensis
Balearica regulorum
Sarothrura rufa
Heliornis fulica
Rallus longirostris
Porphyrio porphyrio
Microhydra schdmburgkii
Rollandia rolland
Phoenicopterus ruber
Burhinus oedicnemus
Charadrius hiaticula
Recurvirostra americana
Haematopus palliatus
Turnix ocellata
Glareola nuchalis
Uria aalge
Chroicocephalus cirrocephalus
Sterna hirundo
Rynchops niger
Pedionomus torquatus
Jacana jacana
Rostratula benghalensis
Limosa lapponica
Arenaria interpres
Tringa solitaria
Phaethon rubricauda
Eurypyga helias
Gavia immer
Spheniscus humboldti
Phoebastria nigripes
Oceanites oceanicus
Pelagodroma marina
Oceanodroma leucorhoa
Fulmarus glacialoides
Puffinus griseus
Pterodroma externa
Pelecanoides urinatrix
Leptoptilos crumeniferus
Ciconia nigra
Fregata magnificens
Morus serrator
Anhinga anhinga
Phalacrocorax brasilianus
Theristicus caerulescens
Tigrisoma lineatum
Ixobrychus minutus
Ardea herodias
Scopus umbretta
Balaeniceps rex
Pelecanus occidentalis
Opisthocomus hoazin
Calhartes burrovianus
Vultur gryphus
Sagittarius serpentarius
Pandion haliaetus
Elanus leucurus
Circhinera angolensis
Necrosyrtes monachus
Accipiter superciliosus
Buteo jamaicensis
Strix varia
Tyto alba
Urocolius indicus
Colius colius
Leptosomus discolor
Trogon elegans
Aplodermis aequatoriale
Upupa epops
Phoeniculus purpureus
Bucorvus leadbeateri
Tockus camurus
Merops muelleri
Coracias cyanogaster
Afelornis pitloides
Todus mexicanus
Momotus lessonii
Alcedo quadribrachys
Chloroceryle inda
Galbula dea
Bucco capensis
Chelidoptera tenebrosa
Indicator exilis
Picus canus
Jynx torquilla
Megalaima chrysopogon
Bucanodon duchaillui
Ramphastos ambiguus
Capito niger
Cariama cristata
Chunga burmeisteri
Micrastur gilvicollis
Falco sparverius
Caracara cheriway
Ibycter americanus
Nestor meridionalis
Proboscier aterrimus
Barnardius zonarius
Psittrichas fulgidus
Deroptyus accipitrinus
Psittacus erithacus
Acanthisitta chloris
Menura novaehollandiae
Climacteris melanura
Sericulus bakeri
Philonorhynchus violaceus
Malurus splendens
Lophorina superba
Corvus albus
Poecile hudsonica
Calandrella brachydactyla
Sylvia melanocephala
Pycnonotus macrotis
Spizella arborea
Fringilla coelebs
Turdus olivater
Hedulus ignicapilla
Nebrephanis obruscans
Eurylaimus ochromalus
Pitta angolensis
Smithornis rufolateralis
Calyptomena viridis
Myrmotherа campanisona
Sclerurus mexicanus
Lepidocolaptes angustirostris
Furnarius rufus
Melanopareia maximiliani
Myrmorнis torquata
Thamnophilus ruficapillus
Terenura callinota
Neopelma chrysocephalum
Pipra erythrocephala
Chytodipo holochlora
Rupicola rupicola
Cotinga cayana
Mynobius barbatus
Oxyruncus cristatus
Schiffornis turdina
Tityra cayana
Piprites chloris
Rhynchocyclus olivaceus
Hirundinea ferruginea
Elaenia flavogaster
Tyrannus albogularis
Hymenops perspicillatus

**Figure D.4.** Phylogenetic tree of 200 extant avian taxa showing the ACE maximum likelihood estimates of force grip foot use (All Rates Different model reconstruction) at each node. Orange denotes percentage likelihood of the presence of force grip foot use.

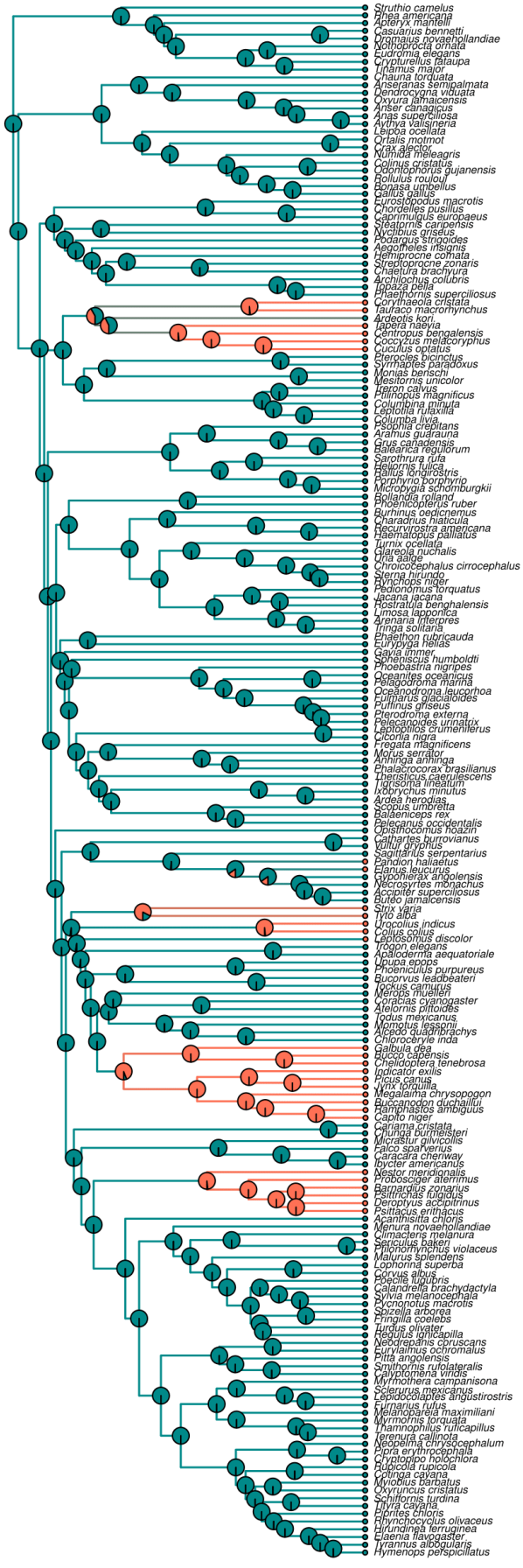
Struthio camelus
Rhea americana
Apteryx mantelli
Casuarius bennetti
Dromaius novaehollandiae
Nothoprocta ornata
Eudromia elegans
Crypturellus tataupa
Tinamus major
Chauna torquata
Anseranas semipalmata
Dendrocygna viduata
Oxyura jamaicensis
Anser canagicus
Anas superciliosa
Aythya valisineria
Lagopa ocellata
Ortalis motmot
Crax alector
Numida meleagris
Colinus cristatus
Odontophorus gujanensis
Rollulus rouloul
Bonasa umbellus
Gallus gallus
Eurostopodus macrotis
Chordeiles pusillus
Caprimulgus europaeus
Steatornis caripensis
Nyctibius griseus
Podargus strigoides
Aegotheles insignis
Hemiprocne comata
Streptoprocne zonaris
Chaetura brachyura
Archilochus colubris
Tapaza pella
Phaethornis superciliosus
Corythaeola cristata
Tauraco macrorhynchus
Ardeotis kori
Tapera naevia
Centropus bengalensis
Coccyzus melacoryphus
Cuculus optatus
Pterocles bicinctus
Syrrhaptes paradoxus
Monias benschi
Mesitornis unicolor
Treron calvus
Ptilinopus magnificus
Columbina minuta
Leptotila rufaxilla
Columba livia
Hesperia creditans
Aramus guarauna
Grus canadensis
Balearica regulorum
Sarothrura rufa
Heliornis fulica
Rallus longirostris
Porphyrio porphyrio
Micropygia schomburgkii
Rollandia rolland
Phoenicopterus ruber
Burhinus oedicnemus
Charadrius hiaticula
Recurvirostra americana
Haematopus palliatus
Turnix ocellata
Glareola nuchalis
Uria aalge
Chroicocephalus cirrocephalus
Sterna hirundo
Rynchops niger
Pedionomus torquatus
Jacana jacana
Rostratula benghalensis
Limosa lapponica
Arenaria interpres
Tringa solitaria
Phaethon rubricauda
Eurypyga helias
Gavia immer
Spheniscus humboldti
Phoebastria nigripes
Oceanites oceanicus
Pelagodroma marina
Oceanodroma leucorhoa
Fulmarus glacialoides
Puffinus griseus
Pterodroma externa
Pelecanoides urinatrix
Leptodirus cruminiferus
Ciconia nigra
Fregata magnificens
Morus serrator
Anhinga anhinga
Phalacrocorax brasilianus
Theristicus caerulescens
Tigrisoma lineatum
Ixobrychus minutus
Ardea herodias
Scopus umbretta
Balaeniceps rex
Pelecanus occidentalis
Opisthocomus hoazin
Cathartes burrovianus
Vultur gryphus
Sagittarius serpentarius
Pandion haliaetus
Elanus leucurus
Gypohierax angolensis
Necrosyrtes monachus
Accipiter superciliosus
Buteo jamaicensis
Strix varia
Tyto alba
Urocolius indicus
Colius colius
Leptosomus discolor
Trogon elegans
Apaloderma aequatoriale
Upupa epops
Phoeniculus purpureus
Bucorvus leadbeateri
Tockus camurus
Merops muelleri
Corabias cyanogaster
Atelornis pittoides
Todus mexicanus
Momotus lessonii
Alcedo quadribrachys
Chloroceryle inda
Galbula dea
Bucco capensis
Chelidoptera tenebrosa
Indicator exilis
Picus canus
Jynx torquilla
Megalaima chrysopogon
Buccanodon duchaillui
Ramphastos ambiguus
Capito niger
Cariama cristata
Chunga burmeisteri
Micrastur gilvicollis
Falco sparverius
Caracara cheriway
Ibycter americanus
Nestor meridionalis
Probosciger aterrimus
Barnardius zonarius
Psittrichas fulgidus
Deroptyus accipitrinus
Psittacus erithacus
Acanthisitta chloris
Menura novaehollandiae
Climacteris melanura
Ptilonorhynchus violaceus
Maluridae splendens
Lophorina superba
Corvus albus
Poecile lugubris
Calandrella brachydactyla
Sylvia melanocephala
Pycnonotus macrotis
Spizella arborea
Fringilla coelebs
Turdus olivater
Regulus ignicapilla
Nebrephdris cruscans
Eurylaimus ochromalus
Pitta angolensis
Smithornis rufolateralis
Calyptomena viridis
Myrmotherea campanisona
Sclerurus mexicanus
Lepidocolaptes angustirostris
Furnarius rufus
Melanopareia maximiliani
Myrmornis torquata
Thamnophilus ruficapillus
Terenura callinota
Neopelma chrysocephalum
Pipra erythrocephala
Cryptolopo holochlora
Rupicola rupicola
Cotinga cayana
Myiobius barbatus
Oxyruncus cristatus
Schiffornis turdina
Tityra cayana
Pipites chloris
Rhynchocyclus olivaceus
Hirundinea ferruginea
Elaenia flavogaster
Tyrannus albogularis
Hymenops perspicillatus

**Figure D.5.** Phylogenetic tree of 200 extant avian taxa showing the ACE maximum likelihood estimates of zygodactyl digit orientation (Equal Rates model reconstruction) at each node. Orange denotes the percentage likelihood of zygodactyl digit orientation.

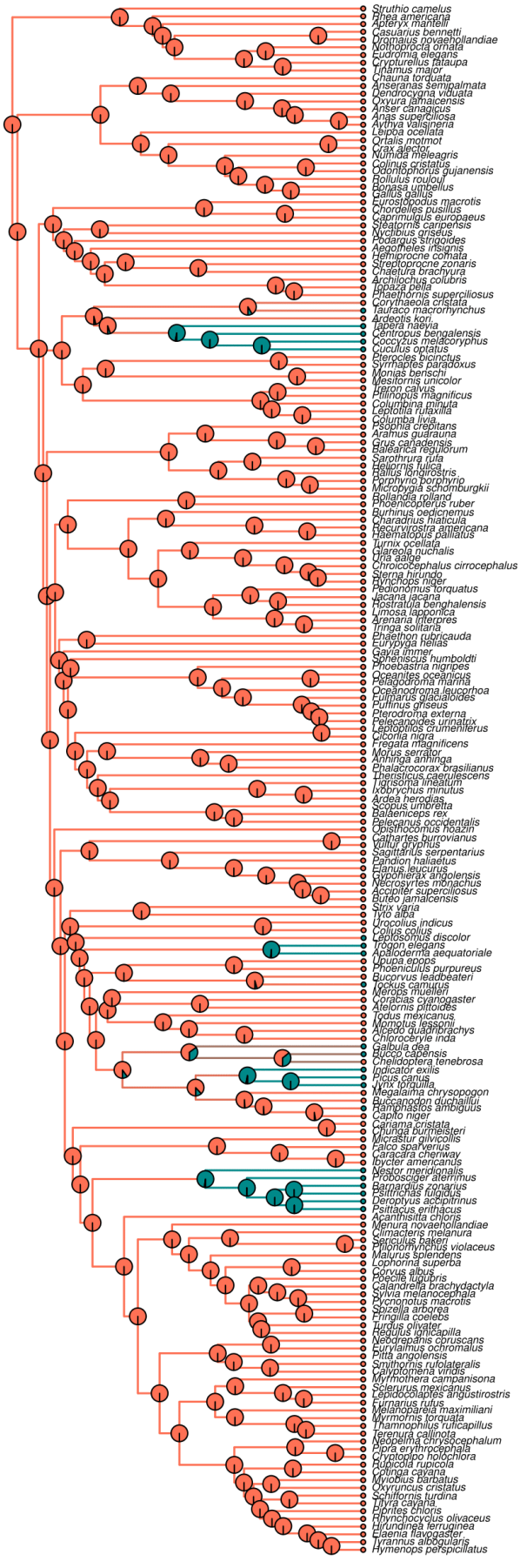
Struthio camelus
Rhea americana
Apteryx mantelli
Casuarius bennetti
Dromaius novaehollandiae
Nothoprocta ornata
Eudromia elegans
Crypturellus fataupa
Tinamus major
Chauna torquata
Anseranas semipalmata
Dendrocygna viduata
Oxyura jamaicensis
Anser canagicus
Anas superciliosa
Aythya valisineria
Limpkin ocellata
Ortalis motmot
Crax alector
Numida meleagris
Colinus cristatus
Odontophorus gujanensis
Rollulus rouloul
Bonasa umbellus
Gallus gallus
Eurostopodus macrotis
Chordeiles pusillus
Caprimulgus europaeus
Steatornis caripensis
Nyctibius griseus
Podargus strigoides
Aegotheles insignis
Hemiprocne comata
Streptoprocne zonaris
Chaetura brachyura
Archilochus colubris
Tobaza pelia
Phaethornis superciliosus
Corythaeola cristata
Tauraco macrorhynchus
Ardeotis kori
Tapera naevia
Centropus bengalensis
Coccyzus melacoryphus
Cuculus optatus
Pteroctes bicinctus
Syrrhaptes paradoxus
Monias benschi
Mesitornis unicolor
Heron calvus
Pelinopus magnificus
Columbina minuta
Leptotila rufaxilla
Columba livia
Psophia crepitans
Aramus guarauna
Grus canadensis
Balearica regulorum
Sarothrura rufa
Heliornis fulica
Rallus longirostris
Porphyrio porphyrio
Micropygia schomburgkii
Rollandia rolland
Phoenicopterus ruber
Burhinus oedicnemus
Charadrius hiaticula
Recurvirostra americana
Haematopus palliatus
Turnix ocellata
Glareola nuchalis
Uria aalge
Chroicocephalus cirrocephalus
Sterna hirundo
Rynchops niger
Pedionomus torquatus
Jacana jacana
Rostratula benghalensis
Limosa lapponica
Arenaria interpres
Tringa solitaria
Phaethon rubricauda
Eurypyga helias
Gavia immer
Spheniscus humboldti
Phoebastria nigripes
Oceanites oceanicus
Pelagodroma marina
Oceanodroma leucorhoa
Fulmarus glacialoides
Puffinus griseus
Pterodroma externa
Pelecanoides urinatrix
Leptoptilos crumeniferus
Ciconia nigra
Fregata magnificens
Morus serrator
Anhinga anhinga
Phalacrocorax brasilianus
Threskiornis caerulescens
Tigrisoma lineatum
Ixobrychus minutus
Ardea herodias
Scopus umbretta
Balaeniceps rex
Pelecanus occidentalis
Opisthocomus hoazin
Cathartes burrovianus
Gyps rueppellii
Sagittarius serpentarius
Pandion haliaetus
Elanus leucurus
Gypohierax angolensis
Necrosyrtes monachus
Accipiter superciliosus
Buteo jamaicensis
Strix varia
Tyto alba
Urocolius indicus
Colius colius
Leptosomus discolor
Trogon elegans
Apaloderma aequatoriale
Upupa epops
Phoeniculus purpureus
Bucorvus leadbeateri
Tockus camurus
Merops muelleri
Coracias cyanogaster
Ateleornis pittoides
Todus mexicanus
Momotus lessonii
Alcedo quadribrachys
Chloroceryle inda
Galbula dea
Bucco capensis
Chelidoptera tenebrosa
Indicator exilis
Picus canus
Jynx torquilla
Megalaima chrysopogon
Buccanodon duchaillui
Ramphastos ambiguus
Capito niger
Cariama cristata
Chunga burmeisteri
Micrastur gilvicollis
Falco sparverius
Caracara cheriway
Ibycter americanus
Nestor meridionalis
Probosciger aterrimus
Barnardius zonarius
Psittrichas fulgidus
Deroptyus accipitrinus
Psittacus erithacus
Acanthisitta chloris
Menura novaehollandiae
Climacteris melanura
Sericulus bakeri
Ptilonorhynchus violaceus
Malurus splendens
Lophorina superba
Corvus albus
Hoeniza fuliginis
Calandrella brachydactyla
Sylvia melanocephala
Pycnonotus macrotis
Spizella arborea
Fringilla coelebs
Turdus olivater
Regulus ignicapilla
Nebrephanis obruscans
Eurylaimus ochromalus
Pitta angolensis
Smithornis rufolateralis
Calyptomena viridis
Myrmothera campanisona
Sclerurus mexicanus
Lepidocolaptes angustirostris
Furnarius rufus
Melanopareia maximiliani
Myrmornis torquata
Thamnophilus ruficapillus
Terenura callinota
Neopelma chrysocephalum
Pipra erythrocephala
Cryptopipo holochlora
Rupicola rupicola
Cotinga cayana
Myiobius barbatus
Oxyruncus cristatus
Schiffornis turdina
Tityra cayana
Pipites chloris
Rhynchocyclus olivaceus
Hirundinea ferruginea
Elaenia flavogaster
Tyrannus albogularis
Hymenops perspicillatus

**Figure D.6.** Phylogenetic tree of 200 extant avian taxa showing the ACE maximum likelihood estimates of anisodactyl digit orientation (Equal Rates model reconstruction) at each node. Orange denotes the percentage likelihood of anisodactyl digit orientation.

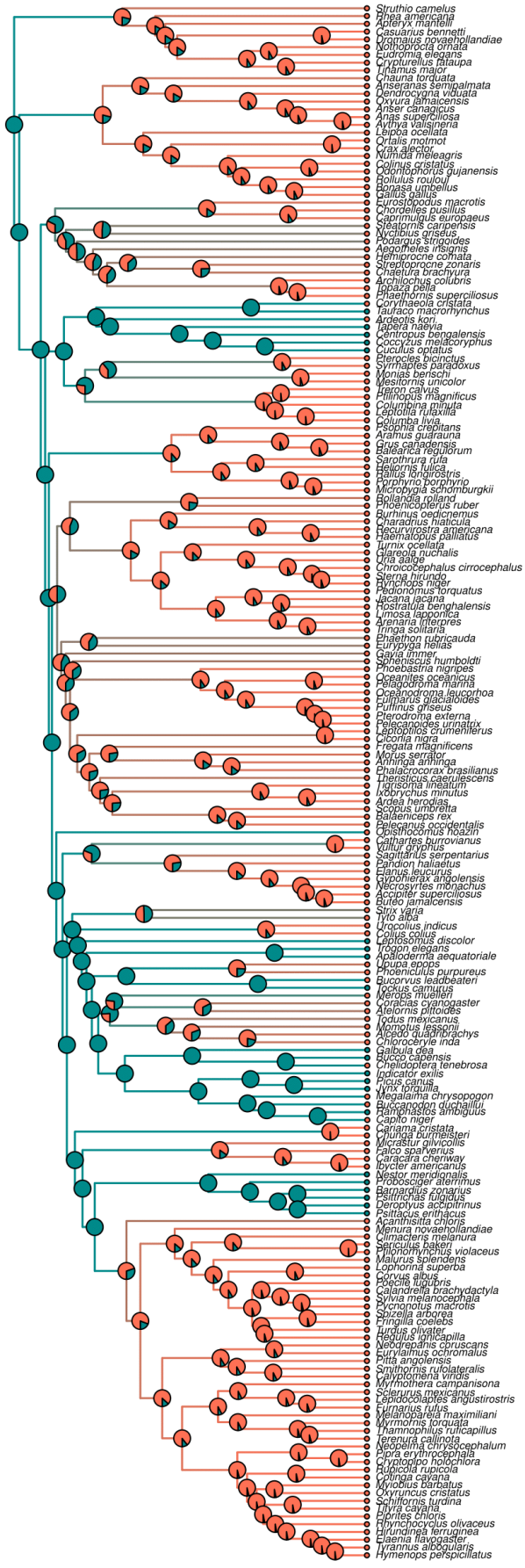
Struthio camelus
Rhea americana
Apteryx mantelli
Casuarius bennetti
Dromaius novaehollandiae
Nothoprocta ornata
Eudromia elegans
Crypturellus tataupa
Tinamus major
Chauna torquata
Anseranas semipalmata
Dendrocygna viduata
Oxyura jamaicensis
Anser canagicus
Anas superciliosa
Aythya valisineria
Leipoa ocellata
Ortalis motmot
Crax alector
Numida meleagris
Colinus cristatus
Odontophorus gujanensis
Rollulus roulroul
Bonasa umbellus
Gallus gallus
Eurostopodus macrotis
Chordeiles pusillus
Caprimulgus europaeus
Steatornis caripensis
Nyctibius griseus
Podargus strigoides
Aegotheles insignis
Hemiprocne comata
Streptoprocne zonaris
Chaetura brachyura
Archilochus colubris
Topaza pella
Phaethornis superciliosus
Corythaeola cristata
Taufaco macrorhynchus
Ardeotis kori
Tapera naevia
Centropus bengalensis
Coccyzus melacoryphus
Cuculus optatus
Pterocles bicinctus
Syrrhaptes paradoxus
Monias benschi
Mesitornis unicolor
Irrisor calvus
Phlilopus magnificus
Columbina minuta
Leptotila rufaxilla
Columba livia
Psophia crepitans
Aramus guarauna
Grus canadensis
Balearica regulorum
Sarothrura rufa
Heliornis fulica
Rallus longirostris
Porphyrio porphyrio
Microhydra schdmburgkii
Hollandia rolland
Phoenicopterus ruber
Burhinus oedicnemus
Charadrius hiaticula
Recurvirostra americana
Haematopus palliatus
Turnix ocellata
Glareola nuchalis
Uria aalge
Chroicocephalus cirrocephalus
Sterna hirundo
Rynchops niger
Pedionomus torquatus
Jacana jacana
Rostratula benghalensis
Limosa lapponica
Arenaria interpres
Tringa solitaria
Phaethon rubricauda
Eurypyga helias
Gavia immer
Spheniscus humboldti
Phoebastria nigripes
Oceanites oceanicus
Pelagodroma marina
Oceanodroma leucorhoa
Fulmarus glacialoides
Puffinus griseus
Pterodroma externa
Pelecanoides urinatrix
Leptoptilos crumeniferus
Ciconia nigra
Fregata magnificens
Morus serrator
Anhinga anhinga
Phalacrocorax brasilianus
Theristicus caerulescens
Tigrisoma lineatum
Ixobrychus minutus
Ardea herodias
Scopus umbretta
Balaeniceps rex
Pelecanus occidentalis
Opisthocomus hoazin
Calhartes burrovianus
Vultur gryphus
Sagittarius serpentarius
Pandion haliaetus
Elanus leucurus
Falco rusticolus
Necrosyrtes monachus
Accipiter superciliosus
Buteo jamaicensis
Strix varia
Tyto alba
Urocolius indicus
Colius colius
Leptosomus discolor
Trogon elegans
Aplodermis aequatoriale
Upupa epops
Phoeniculus purpureus
Bucorvus leadbeateri
Tockus camurus
Merops muelleri
Coracias cyanogaster
Afelornis pittoides
Todus mexicanus
Momotus lessonii
Alcedo quadribrachys
Chloroceryle inda
Galbula dea
Bucco capensis
Chelidoptera tenebrosa
Indicator exilis
Picus canus
Jynx torquilla
Megalaima chrysopogon
Buccanodon duchaillui
Ramphastos ambiguus
Capito niger
Cariama cristata
Chunga burmeisteri
Micrastur gilvicollis
Falco sparverius
Caracara cheriway
Ibycter americanus
Nestor meridionalis
Probosciger aterrimus
Barnardius zonarius
Psittrichas fulgidus
Deroptyus accipitrinus
Psittacus erithacus
Acanthisitta chloris
Menura novaehollandiae
Climacteris melanura
Sericulus bakeri
Philonornynchus violaceus
Malurus splendens
Lophorina superba
Corvus albus
Poecile hudsonicus
Calandrella brachydactyla
Sylvia melanocephala
Pycnonotus macrotis
Spizella arborea
Fringilla coelebs
Turdus olivater
Hedulus ignicapilla
Nebrephanis obruscans
Eurylaimus ochromalus
Pitta angolensis
Smithornis rufolateralis
Calyptomena viridis
Myrmotherа campanisona
Sclerurus mexicanus
Lepidocolaptes angustirostris
Furnarius rufus
Melanopareia maximiliani
Myrmorнis torquata
Thamnophilus ruficapillus
Terenura callinota
Neopelma chrysocephalum
Pipra erythrocephala
Chytodipo holochlora
Rupicola rupicola
Cotinga cayana
Mynobius barbatus
Oxyruncus cristatus
Schiffornis turdina
Tityra cayana
Pipnites chloris
Rhynchocyclus olivaceus
Hirundinea ferruginea
Elaenia flavogaster
Tyrannus albogularis
Hymenops perspicillatus

**Figure D.7.** Phylogenetic tree of 200 extant avian taxa showing the ACE maximum likelihood estimates of anisodactyl digit orientation (All Rates Different model reconstruction) at each node. Orange denotes the percentage likelihood of anisodactyl digit orientation.

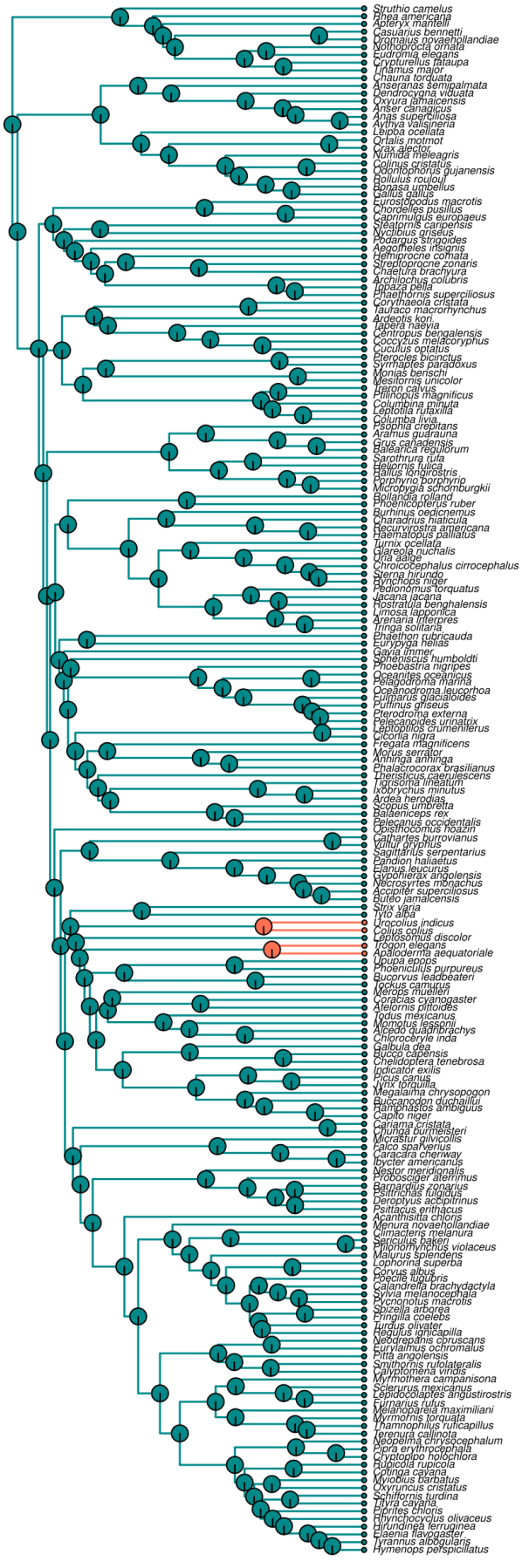
Struthio camelus
Rhea americana
Apteryx mantelli
Casuarius bennetti
Dromaius novaehollandiae
Nothoprocta ornata
Eudromia elegans
Crypturellus tataupa
Tinamus major
Chauna torquata
Anseranas semipalmata
Dendrocygna viduata
Oxyura jamaicensis
Anser canagicus
Anas superciliosa
Aythya valisineria
Leipoa ocellata
Ortalis motmot
Crax alector
Numida meleagris
Colinus cristatus
Odontophorus gujanensis
Rollulus roulroul
Bonasa umbellus
Gallus gallus
Eurostopodus macrotis
Chordeiles pusillus
Caprimulgus europaeus
Steatornis caripensis
Nyctibius griseus
Podargus strigoides
Aegotheles insignis
Hemiprocne comata
Streptoprocne zonaris
Chaetura brachyura
Archilochus colubris
Ispidina picta
Phaethornis superciliosus
Corythaeola cristata
Tauraco macrorhynchus
Ardeotis kori
Tapera naevia
Centropus bengalensis
Coccyzus melacoryphus
Cuculus optatus
Pterocles bicinctus
Syrrhaptes paradoxus
Monias benschi
Mesitornis unicolor
Treron calvus
Ptilinopus magnificus
Columbina minuta
Leptotila rufaxilla
Columba livia
Hesperiphona vespertina
Aramus guarauna
Grus canadensis
Balearica regulorum
Sarothrura rufa
Heliornis fulica
Rallus longirostris
Porphyrio porphyrio
Micropygia schomburgkii
Rollandia rolland
Phoenicopterus ruber
Burhinus oedicnemus
Charadrius hiaticula
Recurvirostra americana
Haematopus palliatus
Turnix ocellata
Glareola nuchalis
Uria aalge
Chroicocephalus cirrocephalus
Sterna hirundo
Rynchops niger
Pedionomus torquatus
Jacana jacana
Rostratula benghalensis
Limosa lapponica
Arenaria interpres
Tringa solitaria
Phaethon rubricauda
Eurypyga helias
Gavia immer
Spheniscus humboldti
Phoebastria nigripes
Oceanites oceanicus
Pelagodroma marina
Oceanodroma leucorhoa
Fulmarus glacialoides
Puffinus griseus
Pterodroma externa
Pelecanoides urinatrix
Leptoptilos crumeniferus
Ciconia nigra
Fregata magnificens
Morus serrator
Anhinga anhinga
Phalacrocorax brasilianus
Theristicus caerulescens
Tigrisoma lineatum
Ixobrychus minutus
Ardea herodias
Scopus umbretta
Balaeniceps rex
Pelecanus occidentalis
Opisthocomus hoazin
Cathartes burrovianus
Vultur gryphus
Sagittarius serpentarius
Pandion haliaetus
Elanus leucurus
Gypohierax angolensis
Necrosyrtes monachus
Accipiter superciliosus
Buteo jamaicensis
Strix varia
Tyto alba
Urocolius indicus
Colius colius
Leptosomus discolor
Trogon elegans
Apaloderma aequatoriale
Upupa epops
Phoeniculus purpureus
Bucorvus leadbeateri
Tockus camurus
Merops muelleri
Corabias cyanogaster
Atelornis pittoides
Todus mexicanus
Momotus lessonii
Alcedo quadribrachys
Chloroceryle inda
Galbula dea
Bucco capensis
Chelidoptera tenebrosa
Indicator exilis
Picus canus
Jynx torquilla
Megalaima chrysopogon
Buccanodon duchaillui
Ramphastos ambiguus
Capito niger
Cariama cristata
Chunga burmeisteri
Micrastur gilvicollis
Falco sparverius
Caracara cheriway
Ibycter americanus
Nestor meridionalis
Probosciger aterrimus
Barnardius zonarius
Psittrichas fulgidus
Deroptyus accipitrinus
Psittacus erithacus
Acanthisitta chloris
Menura novaehollandiae
Climacteris melanura
Sericulus bakeri
Ptilonorhynchus violaceus
Malurus splendens
Lophorina superba
Corvus albus
Poecile lugubris
Calandrella brachydactyla
Sylvia melanocephala
Pycnonotus macrotis
Spizella arborea
Fringilla coelebs
Turdus olivater
Regulus ignicapilla
Nedrepadnis coruscans
Eurylaimus ochromalus
Pitta angolensis
Smithornis rufolateralis
Calyptomena viridis
Myrmotherа campanisona
Sclerurus mexicanus
Lepidocolaptes angustirostris
Furnarius rufus
Melanopareia maximiliani
Myrmornis torquata
Thamnophilus ruficapillus
Terenura callinota
Neopelma chrysocephalum
Pipra erythrocephala
Cryptolopo holochlora
Rupicola rupicola
Optinga cayana
Myiobius barbatus
Oxyruncus cristatus
Schiffornis turdina
Tityra cayana
Pitohui dichrous
Rhynchocyclus olivaceus
Hirundinea ferruginea
Elaenia flavogaster
Tyrannus albogularis
Hymenops perspicillatus

**Figure D.8.** Phylogenetic tree of 200 extant avian taxa showing the ACE maximum likelihood estimates of heterodactyl digit orientation (Equal Rates model reconstruction) at each node. Orange denotes the percentage likelihood of heterodactyl digit orientation.

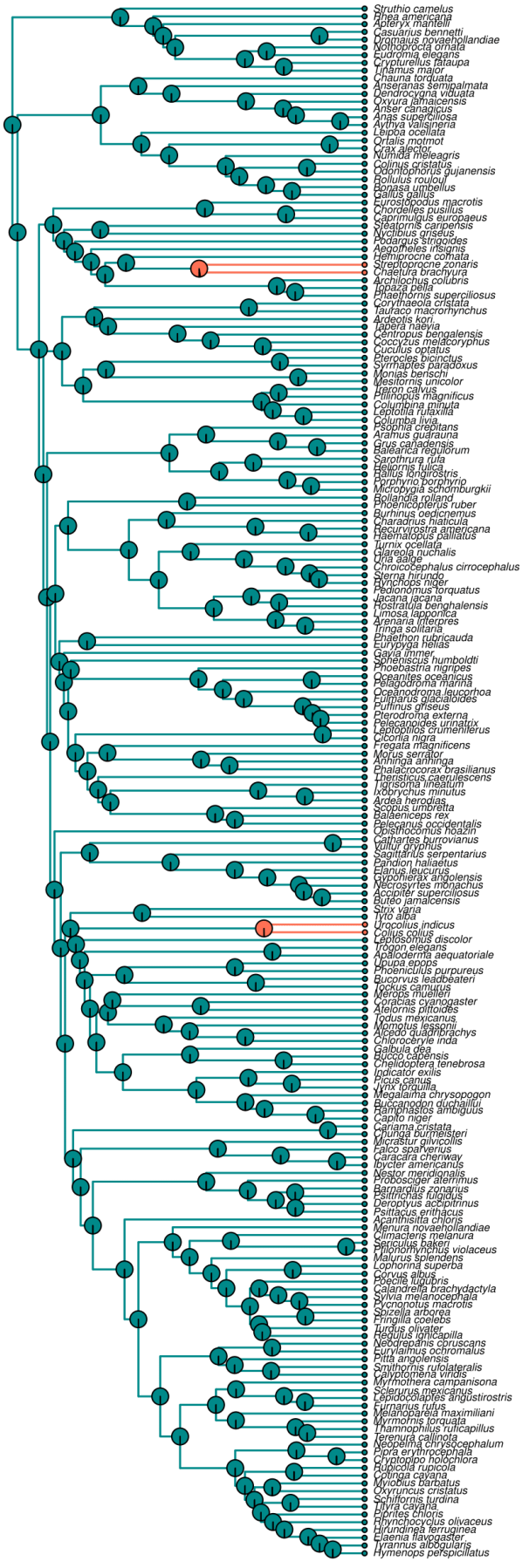
Struthio camelus
Rhea americana
Apteryx mantelli
Casuarius bennetti
Dromaius novaehollandiae
Nothoprocta ornata
Eudromia elegans
Crypturellus tataupa
Tinamus major
Chauna torquata
Anseranas semipalmata
Dendrocygna viduata
Oxyura jamaicensis
Anser canagicus
Anas superciliosa
Aythya valisineria
Lerwa lerwa
Ortalis motmot
Crax alector
Numida meleagris
Colinus cristatus
Odontophorus gujanensis
Rollulus rouloul
Bonasa umbellus
Gallus gallus
Eurostopodus macrotis
Chordeiles pusillus
Caprimulgus europaeus
Steatornis caripensis
Nyctibius griseus
Podargus strigoides
Aegotheles insignis
Hemiprocne comata
Streptoprocne zonaris
Chaetura brachyura
Archilochus colubris
Tobias pella
Phaethornis superciliosus
Corythaeola cristata
Tauraco macrorhynchus
Ardeotis kori
Tapera naevia
Centropus bengalensis
Coccyzus melacoryphus
Cuculus optatus
Pteroces bicinctus
Syrrhaptes paradoxus
Monias benschi
Mesitornis unicolor
Heron calvus
Pitilopus magnificus
Columbina minuta
Leptotila rufaxilla
Columba livia
Psophia crepitans
Aramus guarauna
Grus canadensis
Balearica regulorum
Sarothrura rufa
Heliornis fulica
Rallus longirostris
Porphyrio porphyrio
Micropygia schomburgkii
Rollandia rolland
Phoenicopterus ruber
Burhinus oedicnemus
Charadrius hiaticula
Recurvirostra americana
Haematopus palliatus
Turnix ocellata
Glareola nuchalis
Uria aalge
Chroicocephalus cirrocephalus
Sterna hirundo
Rynchops niger
Pedionomus torquatus
Jacana jacana
Rostratula benghalensis
Limosa lapponica
Arenaria interpres
Tringa solitaria
Phaethon rubricauda
Eurypyga helias
Gavia immer
Spheniscus humboldti
Phoebastria nigripes
Oceanites oceanicus
Pelagodroma marina
Oceanodroma leucorhoa
Fulmarus glacialoides
Puffinus griseus
Pterodroma externa
Pelecanoides urinatrix
Leptoptilos crumeniferus
Ciconia nigra
Fregata magnificens
Morus serrator
Anhinga anhinga
Phalacrocorax brasilianus
Theristicus caerulescens
Tigrisoma lineatum
Ixobrychus minutus
Ardea herodias
Scopus umbretta
Balaeniceps rex
Pelecanus occidentalis
Opisthocomus hoazin
Cathartes burrovianus
Gypaetus barbatus
Gypohierax angolensis
Necrosyrtes monachus
Accipiter superciliosus
Buteo jamaicensis
Strix varia
Tyto alba
Urocolius indicus
Colius colius
Leptosomus discolor
Trogon elegans
Apaloderma aequatoriale
Upupa epops
Phoeniculus purpureus
Bucorvus leadbeateri
Tockus camurus
Merops muelleri
Coracias cyanogaster
Eurystomus glaucurus
Todus mexicanus
Momotus lessonii
Alcedo quadribrachys
Chloroceryle inda
Galbula dea
Bucco capensis
Chelidoptera tenebrosa
Indicator exilis
Picus canus
Jynx torquilla
Megalaima chrysopogon
Buccanodon duchaillui
Ramphastos ambiguus
Capito niger
Cariama cristata
Chunga burmeisteri
Micrastur gilvicollis
Falco sparverius
Caracara cheriway
Ibycter americanus
Nestor meridionalis
Probosciger aterrimus
Barnardius zonarius
Psittrichas fulgidus
Deroptyus accipitrinus
Psittacus erithacus
Acanthisitta chloris
Menura novaehollandiae
Climacteris melanura
Sericulus bakeri
Philonorrhynchus violaceus
Malurus splendens
Lophorina superba
Corvus albus
Hoeyella fuliginosa
Calandrella brachydactyla
Sylvia melanocephala
Pycnonotus macrotis
Spizella arborea
Fringilla coelebs
Turdus olivater
Regulus ignicapilla
Nebrephanis obruscans
Eurylaimus ochromalus
Pitta angolensis
Smithornis rufolateralis
Calyptomena viridis
Myrmothera campanisona
Sclerurus mexicanus
Lepidocolaptes angustirostris
Furnarius rufus
Melanopareia maximiliani
Myrmornis torquata
Thamnophilus ruficapillus
Terenura callinota
Neopelma chrysocephalum
Pipra erythrocephala
Cryptopipo holochlora
Rupicola rupicola
Cotinga cayana
Myiobius barbatus
Oxyruncus cristatus
Schiffornis turdina
Tityra cayana
Pipites chloris
Rhynchocyclus olivaceus
Hirundinea ferruginea
Elaenia flavogaster
Tyrannus albogularis
Hymenops perspicillatus

**Figure D.9.** Phylogenetic tree of 200 extant avian taxa showing the ACE maximum likelihood estimates of pamprodactyl digit orientation (Equal Rates model reconstruction) at each node. Orange denotes the percentage likelihood of pamprodactyl digit orientation.

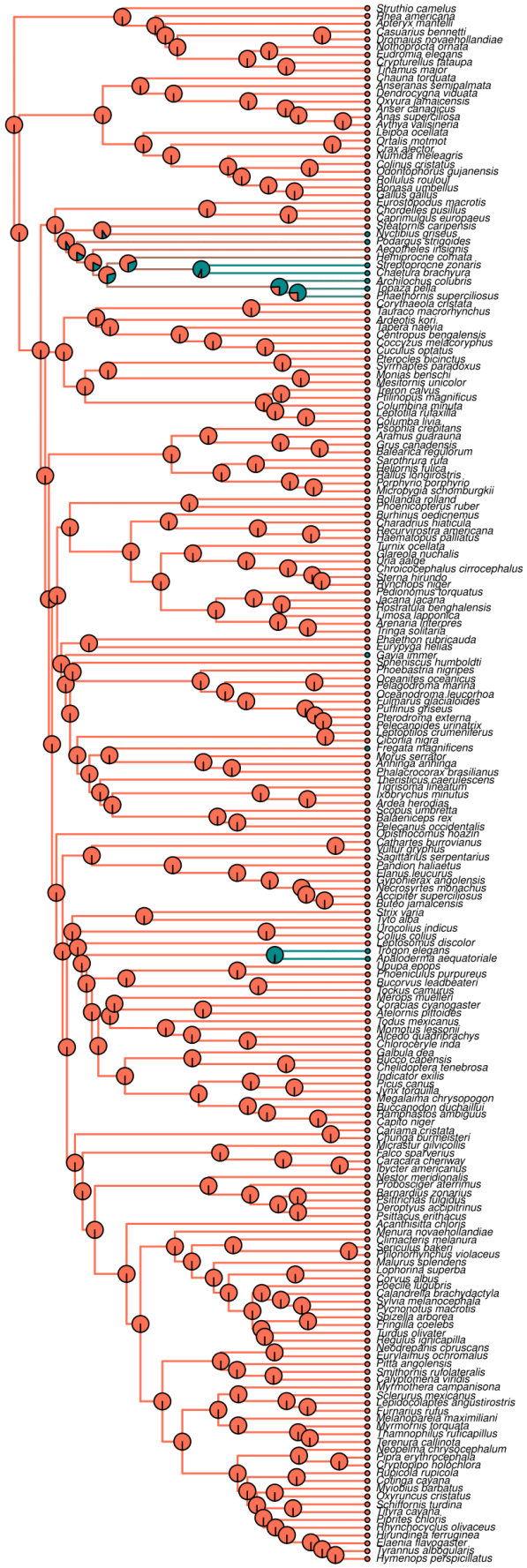
Struthio camelus
Rhea americana
Apteryx mantelli
Casuarius bennetti
Dromaius novaehollandiae
Nothoprocta ornata
Eudromia elegans
Crypturellus tataupa
Tinamus major
Chauna torquata
Anseranas semipalmata
Dendrocygna viduata
Oxyura jamaicensis
Anser canagicus
Anas superciliosa
Aythya valisineria
Leipoa ocellata
Ortalis motmot
Crax alector
Numida meleagris
Colinus cristatus
Odontophorus gujanensis
Rollulus rouloul
Bonasa umbellus
Gallus gallus
Eurostopodus macrotis
Chordeiles pusillus
Caprimulgus europaeus
Steatornis caripensis
Nyctibius griseus
Podargus strigoides
Aegotheles insignis
Hemiprocne comata
Streptoprocne zonaris
Chaetura brachyura
Archilochus colubris
Topaza pella
Phaethornis superciliosus
Corythaeola cristata
Taufaco macrorhynchus
Ardeotis kori
Tapera naevia
Centropus bengalensis
Coccyzus melidocryphus
Cuculus optatus
Pterocles bicinctus
Syrrhaptes paradoxus
Monias benschi
Mesitornis unicolor
Irrisor calvus
Phlilopsis magnificus
Columbina minuta
Leptotila rufaxilla
Columba livia
Psophia crepitans
Aramus guarauna
Grus canadensis
Balearica regulorum
Sarothrura rufa
Heliornis fulica
Rallus longirostris
Porphyrio porphyrio
Microbygia schomburgkii
Rollandia rolland
Phoenicopterus ruber
Burhinus oedicnemus
Charadrius hiaticula
Recurvirostra americana
Haematopus palliatus
Turnix ocellata
Glareola nuchalis
Ora aalge
Chroicocephalus cirrocephalus
Sterna hirundo
Rynchops niger
Pedionomus torquatus
Jacana jacana
Rostratula benghalensis
Limosa lapponica
Arenaria interpres
Tringa solitaria
Phaethon rubricauda
Eurypyga helias
Gavia immer
Spheniscus humboldti
Phoebastria nigripes
Oceanites oceanicus
Pelagodroma marina
Oceanodroma leucorhoa
Fulmarus glacialoides
Puffinus griseus
Pterodroma externa
Pelecanoides urinatrix
Leptopilos crumeniferus
Ciconia nigra
Fregata magnificens
Morus serrator
Anhinga anhinga
Phalacrocorax brasilianus
Theristicus caerulescens
Tigrisoma lineatum
Ixobrychus minutus
Ardea herodias
Scopus umbretta
Balaeniceps rex
Pelecanus occidentalis
Opisthocomus hoazin
Cathartes burrovianus
Vultur gryphus
Sagittarius serpentarius
Pandion haliaetus
Elanus leucurus
Gypohierax angolensis
Necrosyrtes monachus
Accipiter superciliosus
Buteo jamaicensis
Strix varia
Tyto alba
Urocolius indicus
Colius colius
Leptosomus discolor
Trogon elegans
Aplodermia aequatoriale
Upupa epops
Phoeniculus purpureus
Bucorvus leadbeateri
Tockus camurus
Merops mueller
Coracias cyanogaster
Atelornis pittoides
Todus mexicanus
Momotus lessonii
Alcedo quadribrachys
Chloroceryle inda
Galbula dea
Bucco capensis
Chelidoptera tenebrosa
Indicator exilis
Picus canus
Jynx torquilla
Megalaima chrysopogon
Buccanodon duchaillui
Ramphastos ambiguus
Capito niger
Cariama cristata
Chunga burmeisteri
Micrastur gilvicollis
Falco sparverius
Caracara cheriway
Ibycter americanus
Nestor meridionalis
Probosciger aterrimus
Barnardius zonarius
Psittrichas fulgidus
Deroptyus accipitrinus
Psittacus erithacus
Acanthisitta chloris
Menura novaeholandiae
Climacteris melanura
Sericulus bakeri
Ptilonorhynchus violaceus
Malurus splendens
Lophorina superba
Corvus albus
Poecile lugubris
Calandrella brachydactyla
Sylvia melanocephala
Pycnonotus macrotis
Spizella arborea
Fringilla coelebs
Turdus olivater
Regulus ignicapilla
Neodrepanis coruscans
Eurylaimus ochromalus
Pitta angolensis
Smithornis rufolateralis
Calyptomena viridis
Myiothera campanisona
Selerurus mexicanus
Lepidocolaptes angustirostris
Furnarius rufus
Melanopareia maximiliani
Myrmornis torquata
Thamnophilus ruficapillus
Terenura callinota
Neopelma chrysocephalum
Pipra erythrocephala
Cryptopipo holochlora
Rupicola rupicola
Cotinga cayana
Myiobius barbatus
Oxyruncus cristatus
Schiffornis turdina
Tityra cayana
Pipirites chloris
Rhynchocyclus olivaceus
Hirundinea ferruginea
Elaenia flavogaster
Tyrannus albogularis
Hymenops perspicillatus

**Figure D.10.** Phylogenetic tree of 200 extant avian taxa showing the ACE maximum likelihood estimates of walking ability (Equal Ratesq model reconstruction) at each node. Orange denotes the percentage likelihood of walking ability.

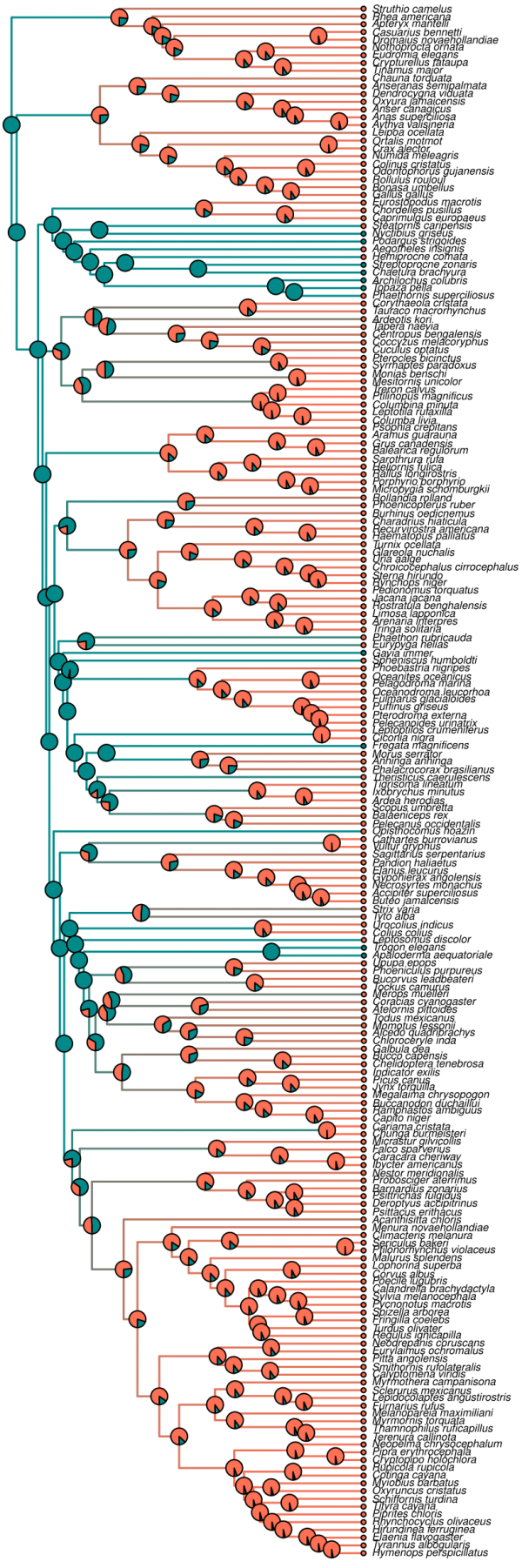
Struthio camelus
Rhea americana
Apteryx mantelli
Casuarius bennetti
Dromaius novaehollandiae
Nothoprocta ornata
Eudromia elegans
Crypturellus tataupa
Tinamus major
Chauna torquata
Anseranas semipalmata
Dendrocygna viduata
Oxyura jamaicensis
Anser canagicus
Anas superciliosa
Aythya valisineria
Laysan ocellata
Ortalis motmot
Crax alector
Numida meleagris
Colinus cristatus
Odontophorus gujanensis
Rollulus roulroul
Bonasa umbellus
Gallus gallus
Eurostopodus macrotis
Chordeiles pusillus
Caprimulgus europaeus
Steatornis caripensis
Nyctibius griseus
Podargus strigoides
Aegotheles insignis
Hemiprocne comata
Streptoprocne zonaris
Chaetura brachyura
Archilochus colubris
Topaza pella
Phaethornis superciliosus
Corythaeola cristata
Tauraco macrorhynchus
Ardeotis kori
Tapera naevia
Centropus bengalensis
Coccyzus melacoryphus
Cuculus optatus
Pterocles bicinctus
Syrrhaptes paradoxus
Monias benschi
Mesitornis unicolor
Heron calvus
Pilherodius pileatus
Columbina minuta
Leptotila rufaxilla
Columba livia
Psophia crepitans
Aramus guarauna
Grus canadensis
Balearica regulorum
Sarothrura rufa
Heliornis fulica
Rallus longirostris
Porphyrio porphyrio
Microbygia schomburgkii
Bollandia bolland
Phoenicopterus ruber
Burhinus oedicnemus
Charadrius hiaticula
Recurvirostra americana
Haematopus palliatus
Turnix olivii
Glareola nuchalis
Uria aalge
Chroicocephalus cirrocephalus
Sterna hirundo
Rynchops niger
Pedionomus torquatus
Jacana jacana
Rostratula benghalensis
Limosa lapponica
Arenaria interpres
Tringa solitaria
Phaethon rubricauda
Eurypyga helias
Gavia immer
Spheniscus humboldti
Phoebastria nigripes
Oceanites oceanicus
Pelagodroma marina
Oceanodroma leucorhoa
Fulmarus glacialoides
Puffinus griseus
Pterodroma externa
Pelecanoides urinatrix
Leptoptilos crumeniferus
Ciconia nigra
Fregata magnificens
Morus serrator
Anhinga anhinga
Phalacrocorax brasilianus
Theristicus caerulescens
Tigrisoma lineatum
Ixobrychus minutus
Ardea herodias
Scopus umbretta
Balaeniceps rex
Pelecanus occidentalis
Opisthocomus hoazin
Cathartes burrovianus
Vultur gryphus
Sagittarius serpentarius
Pandion haliaetus
Elanus leucurus
Gypohierax angolensis
Necrosyrtes monachus
Accipiter superciliosus
Buteo jamaicensis
Strix varia
Tyto alba
Urocolius indicus
Colius colius
Leptosomus discolor
Trogon elegans
Apaloderma aequatoriale
Upupa epops
Phoeniculus purpureus
Bucorvus leadbeateri
Tockus camurus
Merops mulleri
Coracias cyanogaster
Aleiornis pittoides
Todus mexicanus
Momotus lessonii
Alcedo quadribrachys
Chloroceryle inda
Galbula dea
Bucco capensis
Chelidoptera tenebrosa
Indicator exilis
Picus canus
Jynx torquilla
Megalaima chrysopogon
Buccanodon duchaillui
Ramphastos ambiguus
Capito niger
Cariama cristata
Chunga burmeisteri
Micrastur gilvicollis
Falco sparverius
Caracara cheriway
Ibycter americanus
Nestor meridionalis
Probosciger aterrimus
Barnardius zonarius
Psittrichas fulgidus
Deroptyus accipitrinus
Psittacus erithacus
Acanthisitta chloris
Menura novaehollandiae
Climacteris melanura
Sericulus bakeri
Ptilonorhynchus violaceus
Malurus splendens
Lophorina superba
Corvus albus
Poecile lugubris
Calandrella brachydactyla
Sylvia melanocephala
Pycnonotus macrotis
Spizella arborea
Fringilla coelebs
Turdus olivater
Mequitus ignicapilla
Nebrephus obscuratus
Eurylaimus ochromalus
Pitta angolensis
Smithornis rufolateralis
Calyptomena viridis
Myrmotherula campanisona
Sclerurus mexicanus
Lepidocolaptes angustirostris
Furnarius rufus
Melanopareia maximiliani
Myrmornis torquata
Thamnophilus ruficapillus
Terenura callinota
Neopelma chrysocephalum
Pipra erythrocephala
Cryptopipo holochlora
Rupicola rupicola
Cotinga cayana
Mynobius barbatus
Oxyruncus cristatus
Schiffornis turdina
Tityra cayana
Pipirites chloris
Hylnchocyclus olivaceus
Hirundinea ferruginea
Elaenia flavogaster
Tyrannus albogularis
Hymenops perspicillatus

**Figure D.11.** Phylogenetic tree of 200 extant avian taxa showing the ACE maximum likelihood estimates of walking ability (All Rates Different model reconstruction) at each node. Orange denotes the percentage likelihood of walking ability.

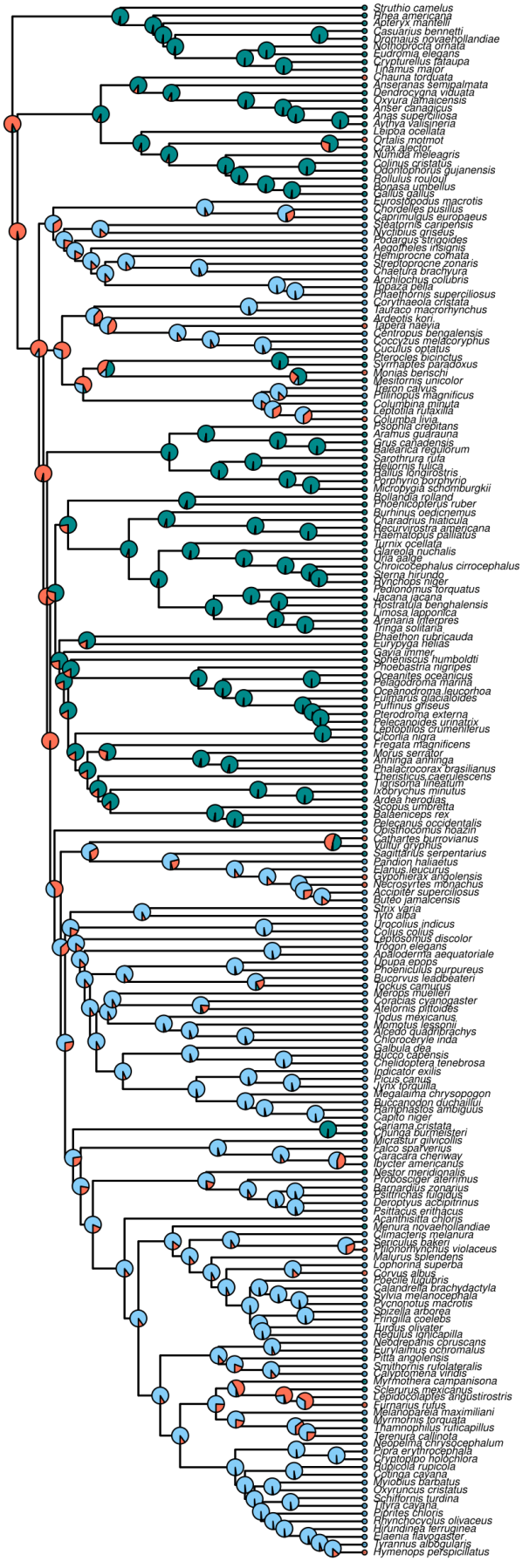
Struthio camelus
Rhea americana
Apteryx mantelli
Casuarius bennetti
Dromaius novaehollandiae
Nothoprocta ornata
Eudromia elegans
Crypturellus tataupa
Tinamus major
Chauna torquata
Anseranas semipalmata
Dendrocygna viduata
Oxyura jamaicensis
Anser canagicus
Anas superciliosa
Aythya valisineria
Leipoa ocellata
Ortalis motmot
Crax alector
Numida meleagris
Colinus cristatus
Odontophorus gujanensis
Rollulus rouloul
Bonasa umbellus
Gallus gallus
Eurostopodus macrotis
Chordeiles pusillus
Caprimulgus europaeus
Steatornis caripensis
Nyctibius griseus
Podargus strigoides
Aegotheles insignis
Hemiprocne comata
Streptoprocne zonaris
Chaetura brachyura
Archilochus colubris
Apaxa pelia
Phaethornis superciliosus
Corythaeola cristata
Tauraco macrorhynchus
Ardeotis kori
Tapera naevia
Centropus bengalensis
Coccyzus melacoryphus
Cuculus optatus
Pterocles bicinctus
Syrrhaptes paradoxus
Monias benschi
Mesitornis unicolor
Turnix calvus
Pitilopus magnificus
Columbina minuta
Leptotila rufaxilla
Columba livia
Hesperia creditans
Aramus guarauna
Grus canadensis
Balearica regulorum
Sarothrura rufa
Heliornis fulica
Rallus longirostris
Porphyrio porphyrio
Micropygia schomburgkii
Rollandia rolland
Phoenicopterus ruber
Burhinus oedicnemus
Charadrius hiaticula
Recurvirostra americana
Haematopus palliatus
Turnix ocellata
Glareola nuchalis
Uria aalge
Chroicocephalus cirrocephalus
Sterna hirundo
Rynchops niger
Pedionomus torquatus
Jacana jacana
Rostratula benghalensis
Limosa lapponica
Arenaria interpres
Tringa solitaria
Phaethon rubricauda
Eurypyga helias
Gavia immer
Spheniscus humboldti
Phoebastria nigripes
Oceanites oceanicus
Hydrobates marinus
Oceanodroma leucorhoa
Fulmarus glacialoides
Puffinus griseus
Pterodroma externa
Pelecanoides urinatrix
Leptoptilos crumeniferus
Ciconia nigra
Fregata magnificens
Morus serrator
Anhinga anhinga
Phalacrocorax brasilianus
Theristicus caerulescens
Tigrisoma lineatum
Ixobrychus minutus
Ardea herodias
Scopus umbretta
Balaeniceps rex
Pelecanus occidentalis
Opisthocomus hoazin
Cathartes burrovianus
Vultur gryphus
Sagittarius serpentarius
Pandion haliaetus
Elanus leucurus
Gypohierax angolensis
Necrosyrtes monachus
Accipiter superciliosus
Buteo jamaicensis
Strix varia
Tyto alba
Urocolius indicus
Colius colius
Leptosomus discolor
Trogon elegans
Apaloderma aequatoriale
Upupa epops
Phoeniculus purpureus
Bucorvus leadbeateri
Tockus camurus
Merops muelleri
Coracias cyanogaster
Ateleornis pittoides
Todus mexicanus
Momotus lessonii
Alcedo quadribrachys
Chloroceryle inda
Galbula dea
Bucco capensis
Chelidoptera tenebrosa
Indicator exilis
Picus canus
Jynx torquilla
Megalaima chrysopogon
Buccanodon duchaillui
Ramphastos ambiguus
Capito niger
Cariama cristata
Chunga burmeisteri
Micrastur gilvicollis
Falco sparverius
Caracara cheriway
Ibycter americanus
Nestor meridionalis
Probosciger aterrimus
Barnardius zonarius
Psittrichas fulgidus
Deroptyus accipitrinus
Psittacus erithacus
Acanthisitta chloris
Menura novaehollandiae
Climacteris melanura
Sarcoglaux baileri
Philonomynchus violaceus
Malurus splendens
Lophorina superba
Corvus albus
Poecile lugubris
Calandrella brachydactyla
Sylvia melanocephala
Pycnonotus macrotis
Spizella arborea
Fringilla coelebs
Turdus olivater
Regulus ignicapilla
Nebrephanis obruscans
Eurylaimus ochromalus
Pitta angolensis
Smithornis rufolateralis
Calyptomena viridis
Myrmotherga campanisona
Sclerurus mexicanus
Lepidocolaptes angustirostris
Furnarius rufus
Melanopareia maximiliani
Myrmornis torquata
Thamnophilus ruficapillus
Terenura callinota
Neopelma chrysocephalum
Pipra erythrocephala
Cryptolipo holochlora
Rupicola rupicola
Cotinga cayana
Myiobius barbatus
Oxyruncus cristatus
Schiffornis turdina
Tityra cayana
Pipites chloris
Rhynchocyclus olivaceus
Hirundinea ferruginea
Elaenia flavogaster
Tyrannus albogularis
Hymenops perspicillatus

**Figure D.12.** Phylogenetic tree of 200 extant avian taxa showing the ACE maximum likelihood estimates of terrestrial, arboreal, and mixed terrestrial/arboreal lifestyle (All Rates Different model reconstruction) at each node. Green denotes percentage likelihood of terrestrial lifestyle, orange denotes percentage likelihood of mixed terrestrial/arboreal lifestyle, and blue denotes percentage likelihood of arboreal lifestyle.

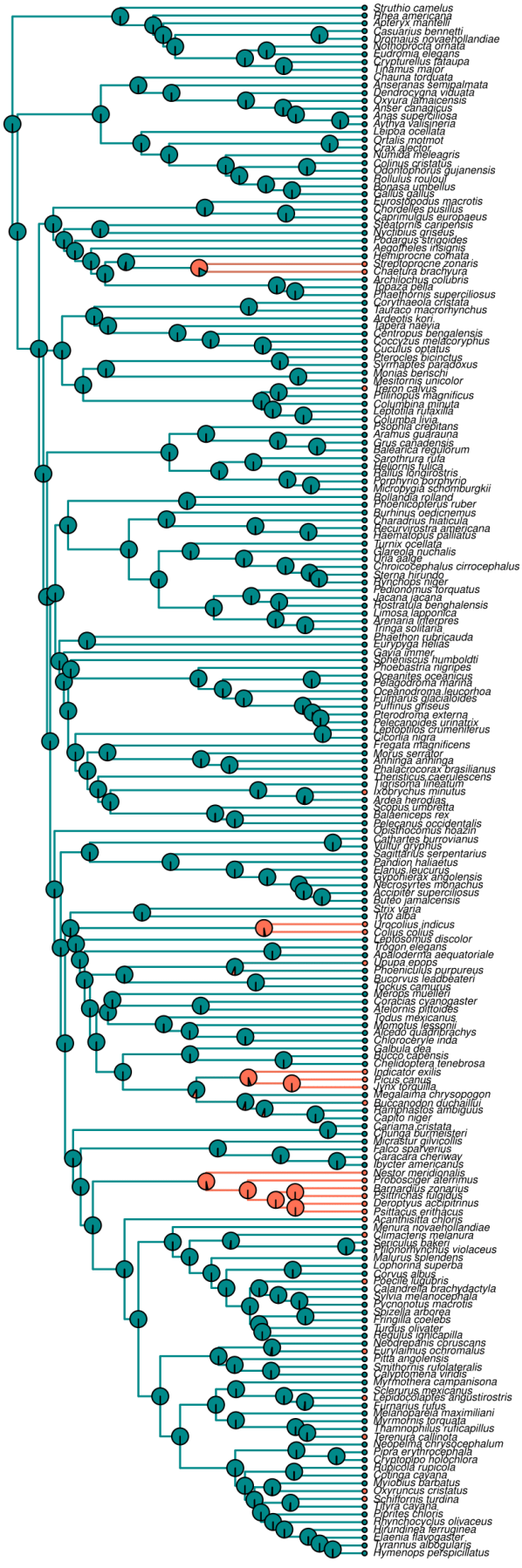
Struthio camelus
Rhea americana
Apteryx mantelli
Casuarius bennetti
Dromaius novaehollandiae
Nothoprocta ornata
Eudromia elegans
Crypturellus tataupa
Tinamus major
Chauna torquata
Anseranas semipalmata
Dendrocygna viduata
Oxyura jamaicensis
Anser canagicus
Anas superciliosa
Aythya valisineria
Leipoa ocellata
Ortalis motmot
Crax alector
Numida meleagris
Colinus cristatus
Odontophorus gujanensis
Rollulus rouloul
Bonasa umbellus
Gallus gallus
Eurostopodus macrotis
Chordeiles pusillus
Caprimulgus europaeus
Steatornis caripensis
Nyctibius griseus
Podargus strigoides
Aegotheles insignis
Hemiprocne comata
Streptoprocne zonaris
Chaetura brachyura
Archilochus colubris
Tapaza pella
Phaethornis superciliosus
Corythaeola cristata
Tauraco macrorhynchus
Ardeotis kori
Tapera naevia
Centropus bengalensis
Coccyzus melacoryphus
Cuculus optatus
Pterocles bicinctus
Syrrhaptes paradoxus
Monias benschi
Mesitornis unicolor
Treron calvus
Ptilinopus magnificus
Columbina minuta
Leptotila rufaxilla
Columba livia
Hesperia creditans
Aramus guarauna
Grus canadensis
Balearica regulorum
Sarothrura rufa
Heliornis fulica
Rallus longirostris
Porphyrio porphyrio
Micropygia schomburgkii
Rollandia rolland
Phoenicopterus ruber
Burhinus oedicnemus
Charadrius hiaticula
Recurvirostra americana
Haematopus palliatus
Turnix ocellata
Glareola nuchalis
Uria aalge
Chroicocephalus cirrocephalus
Sterna hirundo
Rynchops niger
Pedionomus torquatus
Jacana jacana
Rostratula benghalensis
Limosa lapponica
Arenaria interpres
Tringa solitaria
Phaethon rubricauda
Eurypyga helias
Gavia immer
Spheniscus humboldti
Phoebastria nigripes
Oceanites oceanicus
Pelagodroma marina
Oceanodroma leucorhoa
Fulmarus glacialoides
Puffinus griseus
Pterodroma externa
Pelecanoides urinatrix
Leptoptilos crumeniferus
Ciconia nigra
Fregata magnificens
Morus serrator
Anhinga anhinga
Phalacrocorax brasilianus
Theristicus caerulescens
Tigrisoma lineatum
Ixobrychus minutus
Ardea herodias
Scopus umbretta
Balaeniceps rex
Pelecanus occidentalis
Opisthocomus hoazin
Cathartes burrovianus
Vultur gryphus
Sagittarius serpentarius
Pandion haliaetus
Elanus leucurus
Gypohierax angolensis
Necrosyrtes monachus
Accipiter superciliosus
Buteo jamaicensis
Strix varia
Tyto alba
Urocolius indicus
Colius colius
Leptosomus discolor
Trogon elegans
Apaloderma aequatoriale
Upupa epops
Phoeniculus purpureus
Bucorvus leadbeateri
Tockus camurus
Merops muelleri
Coracias cyanogaster
Ateleornis pittoides
Todus mexicanus
Momotus lessonii
Alcedo quadribrachys
Chloroceryle inda
Galbula dea
Bucco capensis
Chelidoptera tenebrosa
Indicator exilis
Picus canus
Jynx torquilla
Megalaima chrysopogon
Buccanodon duchaillui
Ramphastos ambiguus
Capito niger
Cariama cristata
Chunga burmeisteri
Micrastur gilvicollis
Falco sparverius
Caracara cheriway
Ibycter americanus
Nestor meridionalis
Probosciger aterrimus
Barnardius zonarius
Psittrichas fulgidus
Deroptyus accipitrinus
Psittacus erithacus
Acanthisitta chloris
Menura novaehollandiae
Climacteris melanura
Sericulus bakeri
Ptilonorhynchus violaceus
Malurus splendens
Lophorina superba
Corvus albus
Paecilia rufiventris
Calandrella brachydactyla
Sylvia melanocephala
Pycnonotus macrotis
Spizella arborea
Fringilla coelebs
Turdus olivater
Regulus ignicapilla
Nebrephanis cruscans
Eurylaimus ochromalus
Pitta angolensis
Smithornis rufolateralis
Calyptomena viridis
Myrmothera campanisona
Sclerurus mexicanus
Lepidocolaptes angustirostris
Furnarius rufus
Melanopareia maximiliani
Myrmornis torquata
Thamnophilus ruficapillus
Terenura callinota
Neopelma chrysocephalum
Pipra erythrocephala
Cryptopipo holochlora
Rupicola rupicola
Cotinga cayana
Myiobius barbatus
Oxyruncus cristatus
Schiffornis turdina
Tityra cayana
Pipites chloris
Rhynchocyclus olivaceus
Hirundinea ferruginea
Elaenia flavogaster
Tyrannus albogularis
Hymenops perspicillatus

**Figure D.13.** Phylogenetic tree of 200 extant avian taxa showing the ACE maximum likelihood estimates of hanging and clinging behaviour (Equal Rates model reconstruction) at each node. Orange denotes percentage likelihood of hanging and clinging behaviour.

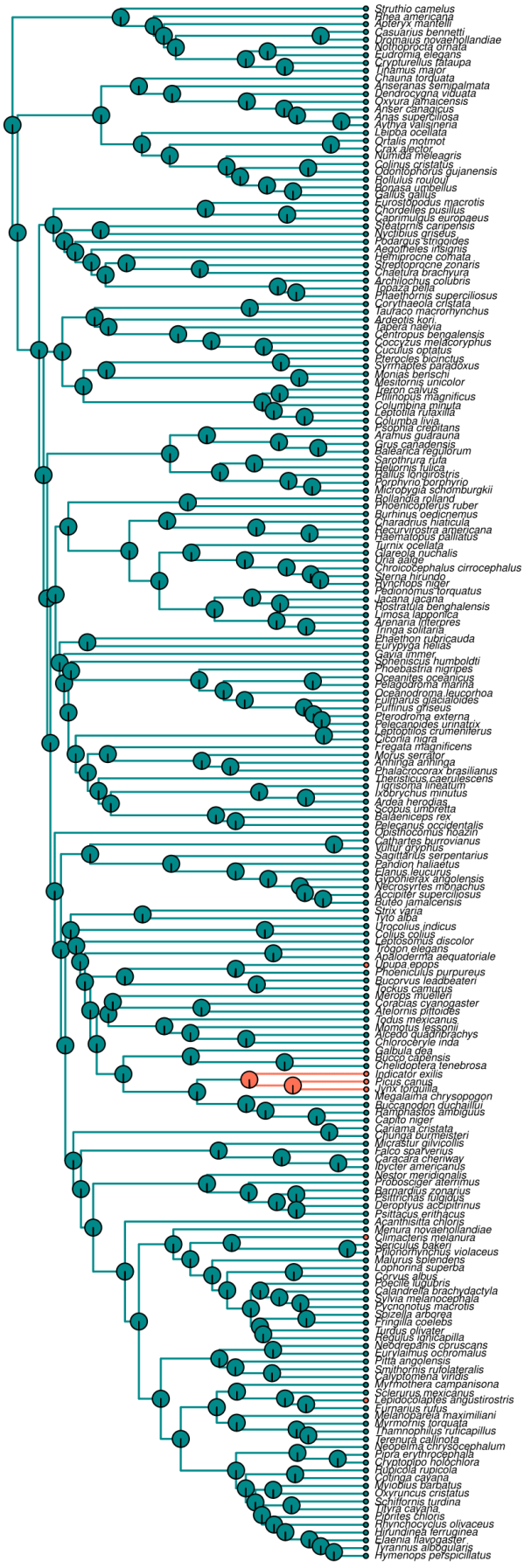
Struthio camelus
Rhea americana
Apteryx mantelli
Casuarius bennetti
Dromaius novaehollandiae
Nothoprocta ornata
Eudromia elegans
Crypturellus tataupa
Tinamus major
Chauna torquata
Anseranas semipalmata
Dendrocygna viduata
Oxyura jamaicensis
Anser canagicus
Anas superciliosa
Aythya valisineria
Limpkin ocellata
Ortalis motmot
Crax alector
Numida meleagris
Colinus cristatus
Odontophorus gujanensis
Rollulus rouloul
Bonasa umbellus
Gallus gallus
Eurostopodus macrotis
Chordeiles pusillus
Caprimulgus europaeus
Steatornis caripensis
Nyctibius griseus
Podargus strigoides
Aegotheles insignis
Hemiprocne comata
Streptoprocne zonaris
Chaetura brachyura
Archilochus colubris
Ispidina picta
Phaethornis superciliosus
Corythaeola cristata
Tauraco macrorhynchus
Ardeotis kori
Tapera naevia
Centropus bengalensis
Coccyzus melacoryphus
Cuculus optatus
Pteroglossus bicinctus
Syrrhaptes paradoxus
Monias benschi
Mesitornis unicolor
Treron calvus
Ptilinopus magnificus
Columbina minuta
Leptotila rufaxilla
Columba livia
Psophia crepitans
Aramus guarauna
Grus canadensis
Balearica regulorum
Sarothrura rufa
Heliornis fulica
Rallus longirostris
Porphyrio porphyrio
Micropygia schomburgkii
Rollandia rolland
Phoenicopterus ruber
Burhinus oedicnemus
Charadrius hiaticula
Recurvirostra americana
Haematopus palliatus
Turnix ocellata
Glareola nuchalis
Uria aalge
Chroicocephalus cirrocephalus
Sterna hirundo
Rynchops niger
Pedionomus torquatus
Jacana jacana
Rostratula benghalensis
Limosa lapponica
Arenaria interpres
Tringa solitaria
Phaethon rubricauda
Eurypyga helias
Gavia immer
Spheniscus humboldti
Phoebastria nigripes
Oceanites oceanicus
Pelagodroma marina
Oceanodroma leucorhoa
Fulmarus glacialoides
Puffinus griseus
Pterodroma externa
Pelecanoides urinatrix
Lantonilos cruminerus
Ciconia nigra
Fregata magnificens
Morus serrator
Anhinga anhinga
Phalacrocorax brasilianus
Theristicus caerulescens
Tigrisoma lineatum
Ixobrychus minutus
Ardea herodias
Scopus umbretta
Balaeniceps rex
Pelecanus occidentalis
Opisthocomus hoazin
Cathartes burrovianus
Vultur gryphus
Sagittarius serpentarius
Pandion haliaetus
Elanus leucurus
Gypohierax angolensis
Necrosyrtes monachus
Accipiter superciliosus
Buteo jamaicensis
Strix varia
Tyto alba
Urocolius indicus
Colius colius
Leptosomus discolor
Trogon elegans
Apaloderma aequatoriale
Upupa epops
Phoeniculus purpureus
Bucorvus leadbeateri
Tockus camurus
Merops muelleri
Coracias cyanogaster
Atelornis pittoides
Todus mexicanus
Momotus lessonii
Alcedo quadribrachys
Chloroceryle inda
Galbula dea
Bucco capensis
Chelidoptera tenebrosa
Indicator exilis
Picus canus
Jynx torquilla
Megalaima chrysopogon
Buccanodon duchaillui
Hanghastes ambiguus
Capito niger
Cariama cristata
Chunga burmeisteri
Micrastur gilvicollis
Falco sparverius
Caracara cheriway
Ibycter americanus
Nestor meridionalis
Probosciger aterrimus
Barnardius zonarius
Psittrichas fulgidus
Deroptyus accipitrinus
Psittacus erithacus
Acanthisitta chloris
Menura novaehollandiae
Climacteris melanura
Serpculus bakeri
Philonorrhynchus violaceus
Malurus splendens
Lophorina superba
Corvus albus
Poecile lugubris
Calandrella brachydactyla
Sylvia melanocephala
Pycnonotus macrotis
Spizella arborea
Fringilla coelebs
Turdus olivater
Regulus ignicapilla
Nesodrepanis obruscans
Eurylaimus ochromalus
Pitta angolensis
Smithornis rufolateralis
Calyptomena viridis
Myrmothera campanisona
Sclerurus mexicanus
Lepidocolaptes angustirostris
Furnarius rufus
Melanopareia maximiliani
Myrmornis torquata
Thamnophilus ruficapillus
Terenura callinota
Neopelma chrysocephalum
Pipra erythrocephala
Cryptolipo holochlora
Rupicola rupicola
Cotinga cayana
Myiobius barbatus
Oxyruncus cristatus
Schiffornis turdina
Tityra cayana
Pipites chloris
Rhynchocyclus olivaceus
Hirundinea ferruginea
Elaenia flavogaster
Tyrannus albogularis
Hymenops perspicillatus

**Figure D.14.** Phylogenetic tree of 200 extant avian taxa showing the ACE maximum likelihood estimates of scansoriality (Equal Rates model reconstruction) at each node. Orange denotes percentage likelihood of scansoriality.

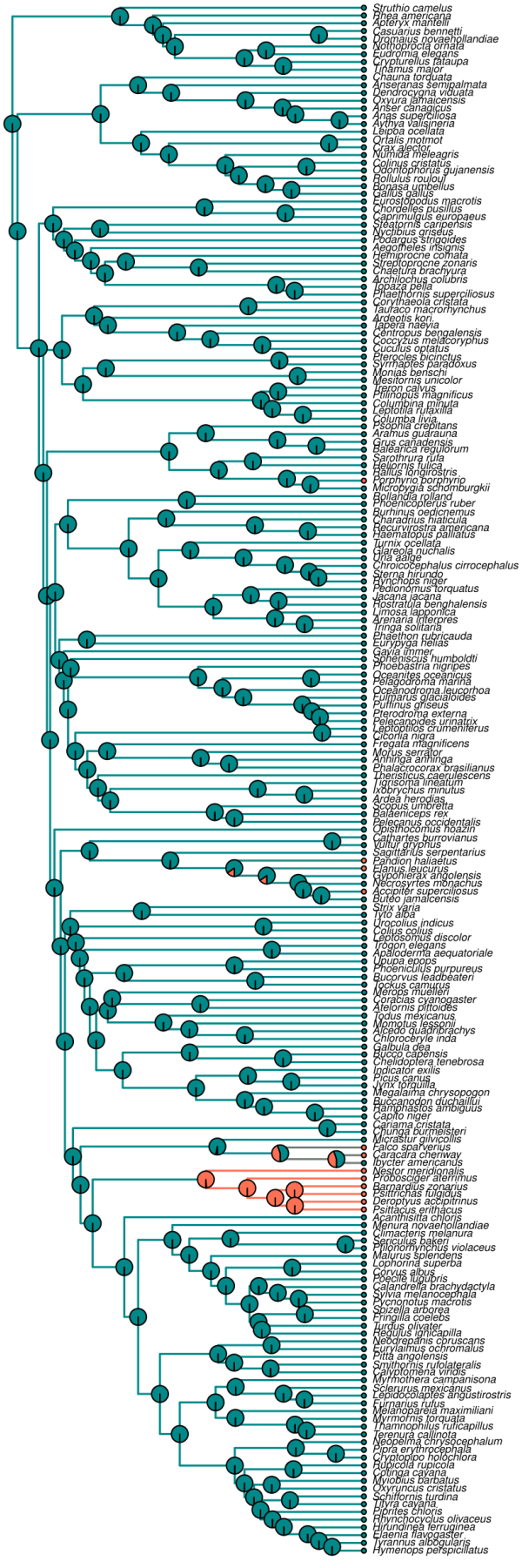
Struthio camelus
Rhea americana
Apteryx mantelli
Casuarius bennetti
Dromaius novaehollandiae
Nothoprocta ornata
Eudromia elegans
Crypturellus tataupa
Tinamus major
Chauna torquata
Anseranas semipalmata
Dendrocygna viduata
Oxyura jamaicensis
Anser canagicus
Anas superciliosa
Aythya valisineria
Lagopus ocellata
Ortalis motmot
Crax alector
Numida meleagris
Colinus cristatus
Odontophorus gujanensis
Rollulus rouloul
Bonasa umbellus
Gallus gallus
Eurostopodus macrotis
Chordeiles pusillus
Caprimulgus europaeus
Steatornis caripensis
Nyctibius griseus
Podargus strigoides
Aegotheles insignis
Hemiprocne comata
Streptoprocne zonaris
Chaetura brachyura
Archilochus colubris
Topaza pella
Phaethornis superciliosus
Corythaeola cristata
Tauraco macrorhynchus
Ardeotis kori
Tapera naevia
Centropus bengalensis
Coccyzus melacoryphus
Cuculus optatus
Pterocles bicinctus
Syrmaptes paradoxus
Monias benschi
Mesitornis unicolor
Heron calvus
Pulinopus magnificus
Columbina minuta
Leptotila rufaxilla
Columba livia
Psophia crepitans
Aramus guarauna
Grus canadensis
Balearica regulorum
Sarothrura rufa
Heliornis fulica
Rallus longirostris
Porphyrio porphyrio
Micropygia schomburgkii
Rollandia rolland
Phoenicopterus ruber
Burhinus oedicnemus
Charadrius hiaticula
Recurvirostra americana
Haematopus palliatus
Turnix ocellata
Glareola nuchalis
Uria aalge
Chroicocephalus cirrocephalus
Sterna hirundo
Rynchops niger
Pedionomus torquatus
Jacana jacana
Nostrattula benghalensis
Limosa lapponica
Arenaria interpres
Tringa solitaria
Phaethon rubricauda
Eurypyga helias
Gavia immer
Sphenisciss humboldti
Phoebastria nigripes
Oceanites oceanicus
Pelagodroma marina
Oceanodroma leucorhoa
Fulmarus glacialoides
Puffinus griseus
Pterodroma externa
Pelecanoides urinatrix
Laptoptilos crumeniferus
Ciconia nigra
Fregata magnificens
Morus serrator
Anhinga anhinga
Phalacrocorax brasilianus
Theristicus caerulescens
Tigrisoma lineatum
Ixobrychus minutus
Ardea herodias
Scopus umbretta
Balaeniceps rex
Pelecanus occidentalis
Opisthocomus hoazin
Cathartes burrovianus
Gultur gryphus
Sagittarius serpentarius
Pandion haliaetus
Elanus leucurus
Gypohierax angolensis
Necrosyrtes monachus
Accipiter superciliosus
Buteo jamaicensis
Strix varia
Tyto alba
Urocolius indicus
Colius colius
Leptosomus discolor
Trogon elegans
Apaloderma aequatoriale
Upupa epops
Phoeniculus purpureus
Bucorvus leadbeateri
Tockus camurus
Merops muelleri
Corabias cyanogaster
Ateleornis pittoides
Todus mexicanus
Momotus lessonii
Alcedo quadribrachys
Chloroceryle inda
Galbula dea
Bucco capensis
Chelidoptera tenebrosa
Indicator exilis
Ficus canus
Jynx torquilla
Megalaima chrysopogon
Buccanodon duchaillui
Hamphastos ambiguus
Capito niger
Cariama cristata
Chunga burmeisteri
Micrastur gilvicollis
Falco sparverius
Caracara cheriway
Ibycter americanus
Nestor meridionalis
Probosciger aterrimus
Barnardius zonarius
Psittrichas fulgidus
Deroptyus accipitrinus
Psittacus erithacus
Acanthisitta chloris
Menura novaehollandiae
Climacteris melanura
Sarcoptilus bakeri
Ptilonorhynchus violaceus
Malurus splendens
Lophorina superba
Corvus albus
Poecile hudsonica
Calandrella brachydactyla
Sylvia melanocephala
Pycnonotus macrotis
Spizella arborea
Fringilla coelebs
Turdus olivater
Regulus ignicapilla
Nebrepanis cruscans
Eurylaimus ochromalus
Pitta angolensis
Smithornis rufolateralis
Calyptomena viridis
Myrmotherа campanisona
Sclerurus mexicanus
Lepidocolaptes angustirostris
Furnarius rufus
Melanopareia maximiliani
Myrmornis torquata
Thamnophilus ruficapillus
Terenura callinota
Neopelma chrysocephalum
Pipra erythrocephala
Chiroxiphia pareola
Rupicola rupicola
Cotinga cayana
Myiobius barbatus
Oxyruncus cristatus
Schiffornis turdina
Tityra cayana
Pipites chloris
Rhynchocyclus olivaceus
Hirundinea ferruginea
Elaenia flavogaster
Tyrannus albogularis
Hymenops perspicillatus

**Figure D.15.** Phylogenetic tree of 200 extant avian taxa showing the ACE maximum likelihood estimates of digital manipulation ability (Equal Rates model reconstruction) at each node. Orange denotes percentage likelihood of digital manipulation ability.

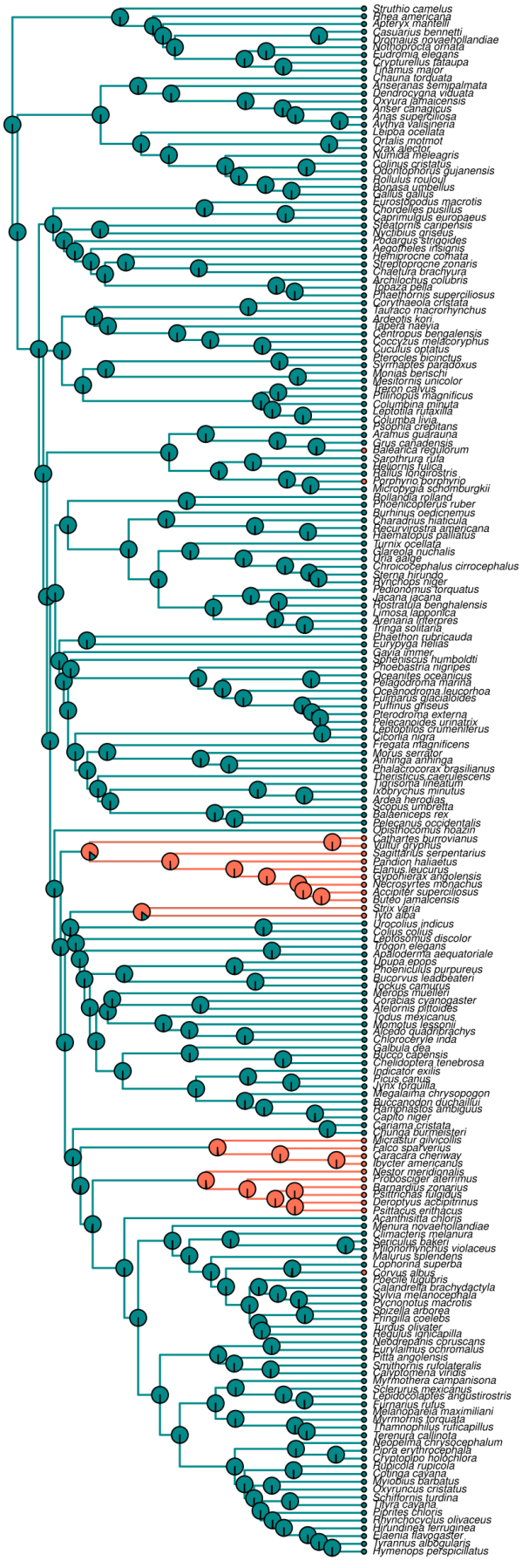
Struthio camelus
Rhea americana
Apteryx mantelli
Casuarius bennetti
Dromaius novaehollandiae
Nothoprocta ornata
Eudromia elegans
Crypturellus tataupa
Tinamus major
Chauna torquata
Anseranas semipalmata
Dendrocygna viduata
Oxyura jamaicensis
Anser canagicus
Anas superciliosa
Aythya valisineria
Leipoa ocellata
Ortalis motmot
Crax alector
Numida meleagris
Colinus cristatus
Odontophorus gujanensis
Rollulus rouloul
Bonasa umbellus
Gallus gallus
Eurostopodus macrotis
Chordeiles pusillus
Caprimulgus europaeus
Steatornis caripensis
Nyctibius griseus
Podargus strigoides
Aegotheles insignis
Hemiprocne comata
Streptoprocne zonaris
Chaetura brachyura
Archilochus colubris
Tapaza pella
Phaethornis superciliosus
Corythaeola cristata
Tauraco macrorhynchus
Ardeotis kori
Tapera naevia
Centropus bengalensis
Coccyzus melacoryphus
Cuculus optatus
Pterocles bicinctus
Syrrhaptes paradoxus
Monias benschi
Mesitornis unicolor
Treron calvus
Ptilinopus magnificus
Columbina minuta
Leptotila rufaxilla
Columba livia
Psophia crepitans
Aramus guarauna
Grus canadensis
Balearica regulorum
Sarothrura rufa
Heliornis fulica
Rallus longirostris
Porphyrio porphyrio
Micropygia schomburgkii
Rollandia rolland
Phoenicopterus ruber
Burhinus oedicnemus
Charadrius hiaticula
Recurvirostra americana
Haematopus palliatus
Turnix ocellata
Glareola nuchalis
Uria aalge
Chroicocephalus cirrocephalus
Sterna hirundo
Rynchops niger
Pedionomus torquatus
Jacana jacana
Rostratula benghalensis
Limosa lapponica
Arenaria interpres
Tringa solitaria
Phaethon rubricauda
Eurypyga helias
Gavia immer
Spheniscus humboldti
Phoebastria nigripes
Oceanites oceanicus
Pelagodroma marina
Oceanodroma leucorhoa
Fulmarus glacialoides
Puffinus griseus
Pterodroma externa
Pelecanoides urinatrix
Leptoptilos crumeniferus
Ciconia nigra
Fregata magnificens
Morus serrator
Anhinga anhinga
Phalacrocorax brasilianus
Theristicus caerulescens
Tigrisoma lineatum
Ixobrychus minutus
Ardea herodias
Scopus umbretta
Balaeniceps rex
Pelecanus occidentalis
Opisthocomus hoazin
Cathartes burrovianus
Vultur gryphus
Sagittarius serpentarius
Pandion haliaetus
Elanus leucurus
Gypohierax angolensis
Necrosyrtes monachus
Accipiter superciliosus
Buteo jamaicensis
Strix varia
Tyto alba
Urocolius indicus
Colius colius
Leptosomus discolor
Trogon elegans
Apaloderma aequatoriale
Upupa epops
Phoeniculus purpureus
Bucorvus leadbeateri
Tockus camurus
Merops muelleri
Coracias cyanogaster
Aleiornis pittoides
Todus mexicanus
Momotus lessonii
Alcedo quadribrachys
Chloroceryle inda
Galbula dea
Bucco capensis
Chelidoptera tenebrosa
Indicator exilis
Picus canus
Jynx torquilla
Megalaima chrysopogon
Buccanodon duchaillui
Hamphastos ambiguus
Capito niger
Cariama cristata
Chunga burmeisteri
Micrastur gilvicollis
Falco sparverius
Caracara cheriway
Ibycter americanus
Nestor meridionalis
Probosciger aterrimus
Barnardius zonarius
Psittrichas fulgidus
Deroptyus accipitrinus
Psittacus erithacus
Acanthisitta chloris
Menura novaehollandiae
Climacteris melanura
Sericulus bakeri
Ptilonorhynchus violaceus
Malurus splendens
Lophorina superba
Corvus albus
Poecile lugubris
Calandrella brachydactyla
Sylvia melanocephala
Pycnonotus macrotis
Spizella arborea
Fringilla coelebs
Turdus olivater
Regulus ignicapilla
Nebrephdnis cruscans
Eurylaimus ochromalus
Pitta angolensis
Smithornis rufolateralis
Calyptomena viridis
Myrmothera campanisona
Sclerurus mexicanus
Lepidocolaptes angustirostris
Furnarius rufus
Melanopareia maximiliani
Myrmornis torquata
Thamnophilus ruficapillus
Terenura callinota
Neopelma chrysocephalum
Pipra erythrocephala
Cryptopipo holochlora
Rupicola rupicola
Cotinga cayana
Myiobius barbatus
Oxyruncus cristatus
Schiffornis turdina
Tityra cayana
Pipirites chloris
Rhynchocyclus olivaceus
Hirundinea ferruginea
Elaenia flavogaster
Tyrannus albogularis
Hymenops perspicillatus

**Figure D.16.** Phylogenetic tree of 200 extant avian taxa showing the ACE maximum likelihood estimates of hold down ability (Equal Rates model reconstruction) at each node. Orange denotes percentage likelihood of hold down ability.

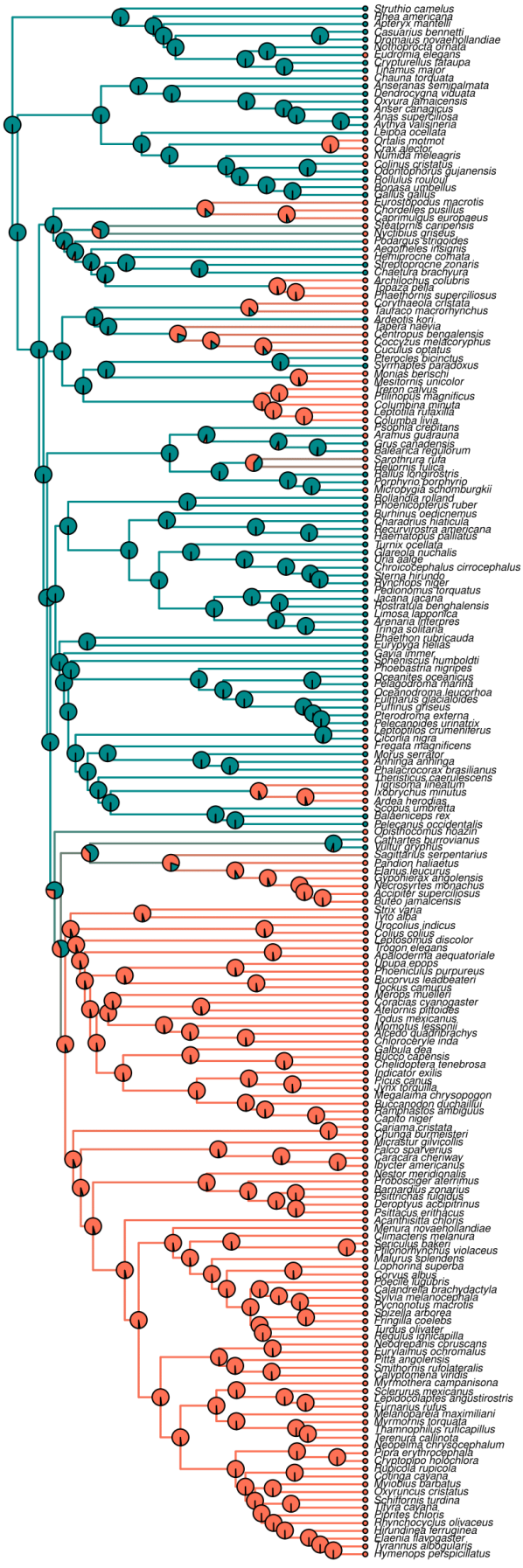
Struthio camelus
Rhea americana
Apteryx mantelli
Casuarius bennetti
Dromaius novaehollandiae
Nothoprocta ornata
Eudromia elegans
Crypturellus tataupa
Tinamus major
Chauna torquata
Anseranas semipalmata
Dendrocygna viduata
Oxyura jamaicensis
Anser canagicus
Anas superciliosa
Aythya valisineria
Leipoa ocellata
Ortalis motmot
Crax alector
Numida meleagris
Colinus cristatus
Odontophorus gujanensis
Rollulus rouloul
Bonasa umbellus
Gallus gallus
Eurostopodus macrotis
Chordeiles pusillus
Caprimulgus europaeus
Steatornis caripensis
Nyctibius griseus
Podargus strigoides
Aegotheles insignis
Hemiprocne comata
Streptoprocne zonaris
Chaetura brachyura
Archilochus colubris
Tapaza pella
Phaethornis superciliosus
Corythaeola cristata
Tauraco macrorhynchus
Ardeotis kori
Tapera naevia
Centropus bengalensis
Coccyzus melacoryphus
Cuculus optatus
Pteroclesbicinctus
Syrrhaptes paradoxus
Monias benschi
Mesitornis unicolor
Treron calvus
Ptilinopus magnificus
Columbina minuta
Leptotila rufaxilla
Columba livia
Hesperia creditans
Aramus guarauna
Grus canadensis
Balearica regulorum
Sarothrura rufa
Heliornis fulica
Rallus longirostris
Porphyrio porphyrio
Micropygia schomburgkii
Rollandia rolland
Phoenicopterus ruber
Burhinus oedicnemus
Charadrius hiaticula
Recurvirostra americana
Haematopus palliatus
Turnix ocellata
Glareola nuchalis
Uria aalge
Chroicocephalus cirrocephalus
Sterna hirundo
Rynchops niger
Pedionomus torquatus
Jacana jacana
Rostratula benghalensis
Limosa lapponica
Arenaria interpres
Tringa solitaria
Phaethon rubricauda
Eurypyga helias
Gavia immer
Spheniscus humboldti
Phoebastria nigripes
Oceanites oceanicus
Pelagodroma marina
Oceanodroma leucorhoa
Fulmarus glacialoides
Puffinus griseus
Pterodroma externa
Pelecanoides urinatrix
Leptoptilos crumeniferus
Ciconia nigra
Fregata magnificens
Morus serrator
Anhinga anhinga
Phalacrocorax brasilianus
Theristicus caerulescens
Tigrisoma lineatum
Ixobrychus minutus
Ardea herodias
Scopus umbretta
Balaeniceps rex
Pelecanus occidentalis
Opisthocomus hoazin
Cathartes burrovianus
Vultur gryphus
Sagittarius serpentarius
Pandion haliaetus
Elanus leucurus
Gypohierax angolensis
Necrosyrtes monachus
Accipiter superciliosus
Buteo jamaicensis
Strix varia
Tyto alba
Urocolius indicus
Colius colius
Leptosomus discolor
Trogon elegans
Apaloderma aequatoriale
Upupa epops
Phoeniculus purpureus
Bucorvus leadbeateri
Tockus camurus
Merops muelleri
Coracias cyanogaster
Ateleornis pittoides
Todus mexicanus
Momotus lessonii
Alcedo quadribrachys
Chloroceryle inda
Galbula dea
Bucco capensis
Chelidoptera tenebrosa
Indicator exilis
Picus canus
Jynx torquilla
Megalaima chrysopogon
Buccanodon duchaillui
Ramphastos ambiguus
Capito niger
Cariama cristata
Chunga burmeisteri
Micrastur gilvicollis
Falco sparverius
Caracara cheriway
Ibycter americanus
Nestor meridionalis
Probosciger aterrimus
Barnardius zonarius
Psitrichas fulgidus
Deroptyus accipitrinus
Psittacus erithacus
Acanthisitta chloris
Menura novaehollandiae
Climacteris melanura
Sericulus bakeri
Ptilonorhynchus violaceus
Malurus splendens
Lophorina superba
Corvus albus
Poecile lugubris
Calandrella brachydactyla
Sylvia melanocephala
Pycnonotus macrotis
Spizella arborea
Fringilla coelebs
Turdus olivater
Regulus ignicapilla
Nebrephdnis cruscans
Eurylaimus ochromalus
Pitta angolensis
Smithornis rufolateralis
Calyptomena viridis
Myrmothera campanisona
Sclerurus mexicanus
Lepidocolaptes angustirostris
Furnarius rufus
Melanopareia maximiliani
Myrmornis torquata
Thamnophilus ruficapillus
Terenura callinota
Neopelma chrysocephalum
Pipra erythrocephala
Cryptolipo holochlora
Rupicola rupicola
Cotinga cayana
Myiobius barbatus
Oxyruncus cristatus
Schiffornis turdina
Tityra cayana
Florites chloris
Rhynchocyclus olivaceus
Hirundinea ferruginea
Elaenia flavogaster
Tyrannus albogularis
Hymenops perspicillatus

**Figure D.17.** Phylogenetic tree of 200 extant avian taxa showing the ACE maximum likelihood estimates of perching ability (All Rates Different model reconstruction) at each node. Orange denotes percentage likelihood of perching ability.

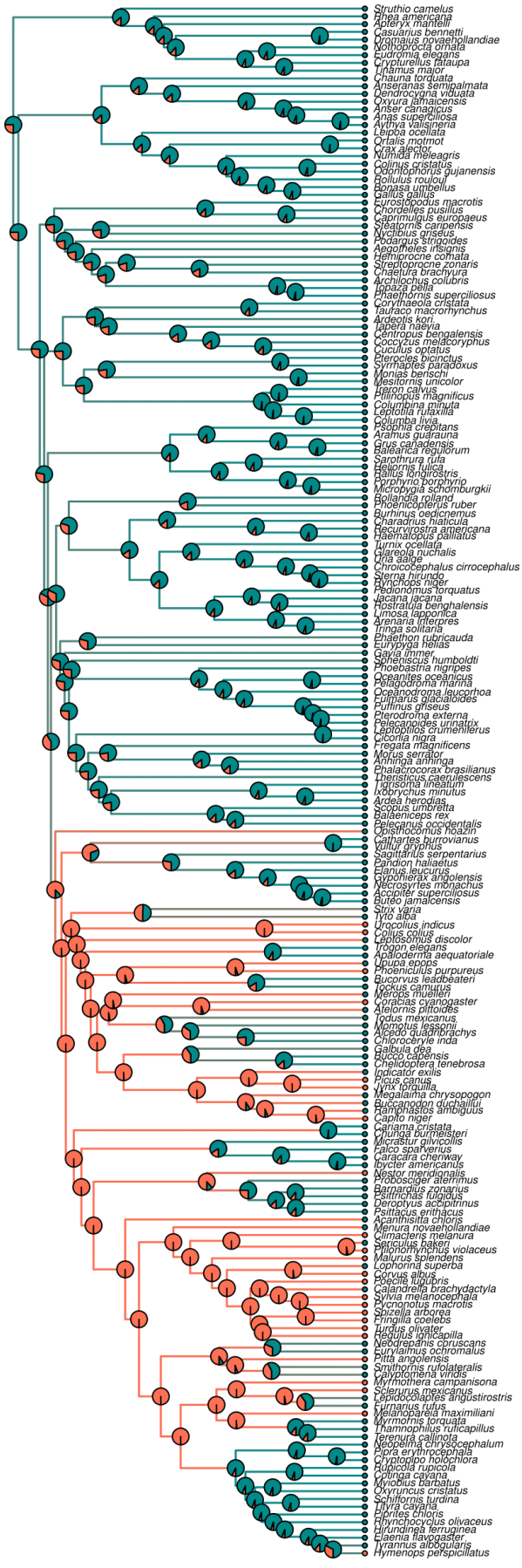
Struthio camelus
Rhea americana
Apteryx mantelli
Casuarius bennetti
Dromaius novaehollandiae
Nothoprocta ornata
Eudromia elegans
Crypturellus tataupa
Tinamus major
Chauna torquata
Anseranas semipalmata
Dendrocygna viduata
Oxyura jamaicensis
Anser canagicus
Anas superciliosa
Aythya valisineria
Lerwa lerwa
Ortalis motmot
Crax alector
Numida meleagris
Colinus cristatus
Odontophorus gujanensis
Rollulus rouloul
Bonasa umbellus
Gallus gallus
Eurostopodus macrotis
Chordeiles pusillus
Caprimulgus europaeus
Steatornis caripensis
Nyctibius griseus
Podargus strigoides
Aegotheles insignis
Hemiprocne comata
Streptoprocne zonaris
Chaetura brachyura
Archilochus colubris
Tobaza pelia
Phaethornis superciliosus
Corythaeola cristata
Tauraco macrorhynchus
Ardeotis kori
Tapera naevia
Centropus bengalensis
Coccyzus melacoryphus
Cuculus optatus
Pteroclesbicinctus
Syrrhaptes paradoxus
Monias benschi
Mesitornis unicolor
Heron calvus
Pelinopus magnificus
Columbina minuta
Leptotila rufaxilla
Columba livia
Psophia crepitans
Aramus guarauna
Grus canadensis
Balearica regulorum
Sarothrura rufa
Heliornis fulica
Rallus longirostris
Porphyrio porphyrio
Micropygia schomburgkii
Rollandia rolland
Phoenicopterus ruber
Burhinus oedicnemus
Charadrius hiaticula
Recurvirostra americana
Haematopus palliatus
Turnix ocellata
Glareola nuchalis
Uria aalge
Chroicocephalus cirrocephalus
Sterna hirundo
Rynchops niger
Pedionomus torquatus
Jacana jacana
Rostratula benghalensis
Limosa lapponica
Arenaria interpres
Tringa solitaria
Phaethon rubricauda
Eurypyga helias
Gavia immer
Spheniscus humboldti
Phoebastria nigripes
Oceanites oceanicus
Pelagodroma marina
Oceanodroma leucorhoa
Fulmarus glacialoides
Puffinus griseus
Pterodroma externa
Pelecanoides urinatrix
Leptoptilos crumeniferus
Ciconia nigra
Fregata magnificens
Morus serrator
Anhinga anhinga
Phalacrocorax brasilianus
Theristicus caerulescens
Tigrisoma lineatum
Ixobrychus minutus
Ardea herodias
Scopus umbretta
Balaeniceps rex
Pelecanus occidentalis
Opisthocomus hoazin
Cathartes burrovianus
Gypaetus barbatus
Gyps fulvus
Sagittarius serpentarius
Pandion haliaetus
Elanus leucurus
Gypohierax angolensis
Necrosyrtes monachus
Accipiter superciliosus
Buteo jamaicensis
Strix varia
Tyto alba
Urocolius indicus
Colius colius
Leptosomus discolor
Trogon elegans
Apaloderma aequatoriale
Upupa epops
Phoeniculus purpureus
Bucorvus leadbeateri
Tockus camurus
Merops muelleri
Coracias cyanogaster
Eurystomus glaucurus
Todus mexicanus
Momotus lessonii
Alcedo quadribrachys
Chloroceryle inda
Galbula dea
Bucco capensis
Chelidoptera tenebrosa
Indicator exilis
Picus canus
Jynx torquilla
Megalaima chrysopogon
Buccanodon duchaillui
Ramphastos ambiguus
Capito niger
Cariama cristata
Chunga burmeisteri
Micrastur gilvicollis
Falco sparverius
Caracara cheriway
Ibycter americanus
Nestor meridionalis
Proboscigerus aterrimus
Barnardius zonarius
Psittrichas fulgidus
Deroptyus accipitrinus
Psittacus erithacus
Acanthisitta chloris
Menura novaehollandiae
Climacteris melanura
Sericulus bakeri
Ptilonorhynchus violaceus
Malurus splendens
Lophorina superba
Corvus albus
Hoeyella fuliginosa
Calandrella brachydactyla
Sylvia melanocephala
Pycnonotus macrotis
Spizella arborea
Fringilla coelebs
Turdus olivater
Regulus ignicapilla
Nebrephanis obruscans
Eurylaimus ochromalus
Pitta angolensis
Smithornis rufolateralis
Calyptomena viridis
Myrmothera campanisona
Sclerurus mexicanus
Lepidocolaptes angustirostris
Furnarius rufus
Melanopareia maximiliani
Myrmornis torquata
Thamnophilus ruficapillus
Terenura callinota
Neopelma chrysocephalum
Pipra erythrocephala
Cryptopipo holochlora
Rupicola rupicola
Cotinga cayana
Myiobius barbatus
Oxyruncus cristatus
Schiffornis turdina
Tityra cayana
Pipites chloris
Rhynchocyclus olivaceus
Hirundinea ferruginea
Elaenia flavogaster
Tyrannus albogularis
Hymenops perspicillatus

**Figure D.18.** Phylogenetic tree of 200 extant avian taxa showing the ACE maximum likelihood estimates of hopping ability (All Rates Different model reconstruction) at each node. Orange denotes percentage likelihood of hopping ability.

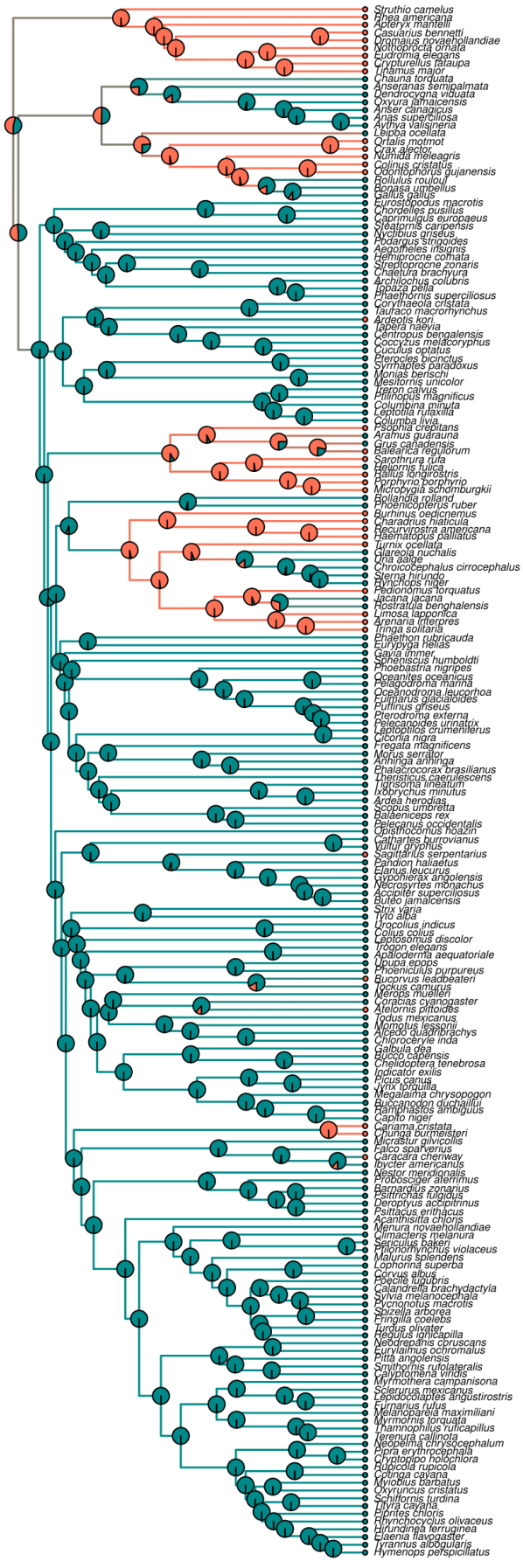
Struthio camelus
Rhea americana
Apteryx mantelli
Casuarius bennetti
Dromaius novaehollandiae
Nothoprocta ornata
Eudromia elegans
Crypturellus tataupa
Tinamus major
Chauna torquata
Anseranas semipalmata
Dendrocygna viduata
Oxyura jamaicensis
Anser canagicus
Anas superciliosa
Aythya valisineria
Limpkin pictata
Ortalis motmot
Crax alector
Numida meleagris
Colinus cristatus
Odontophorus gujanensis
Rollulus rouloul
Bonasa umbellus
Gallus gallus
Eurostopodus macrotis
Chordeiles pusillus
Caprimulgus europaeus
Steatornis caripensis
Nyctibius griseus
Podargus strigoides
Aegotheles insignis
Hemiprocne comata
Streptoprocne zonaris
Chaetura brachyura
Archilochus colubris
Tijazia petia
Phaethornis superciliosus
Corythaeola cristata
Tauraco macrorhynchus
Ardeotis kori
Tapera naevia
Centropus bengalensis
Coccyzus melacoryphus
Cuculus optatus
Pterocles bicinctus
Syrrhaptes paradoxus
Monias benschi
Mesitornis unicolor
Treron calvus
Ptilinopus magnificus
Columbina minuta
Leptotila rufaxilla
Columba livia
Hesperia creditans
Aramus guarauna
Grus canadensis
Balearica regulorum
Sarothrura rufa
Heliornis fulica
Rallus longirostris
Porphyrio porphyrio
Micropygia schomburgkii
Rollandia rolland
Phoenicopterus ruber
Burhinus oedicnemus
Charadrius hiaticula
Recurvirostra americana
Haematopus palliatus
Turnix ocellata
Glareola nuchalis
Uria aalge
Chroicocephalus cirrocephalus
Sterna hirundo
Rynchops niger
Pedionomus torquatus
Jacana jacana
Rostratula benghalensis
Limosa lapponica
Arenaria interpres
Tringa solitaria
Phaethon rubricauda
Eurypyga helias
Gavia immer
Spheniscus humboldti
Phoebastria nigripes
Oceanites oceanicus
Pelagodroma marina
Oceanodroma leucorhoa
Fulmarus glacialoides
Puffinus griseus
Pterodroma externa
Pelecanoides urinatrix
Leptoptilos crumeniferus
Ciconia nigra
Fregata magnificens
Morus serrator
Anhinga anhinga
Phalacrocorax brasilianus
Theristicus caerulescens
Tigrisoma lineatum
Ixobrychus minutus
Ardea herodias
Scopus umbretta
Balaeniceps rex
Pelecanus occidentalis
Opisthocomus hoazin
Cathartes burrovianus
Vultur gryphus
Sagittarius serpentarius
Pandion haliaetus
Elanus leucurus
Gypohierax angolensis
Necrosyrtes monachus
Accipiter superciliosus
Buteo jamaicensis
Strix varia
Tyto alba
Urocolius indicus
Colius colius
Leptosomus discolor
Trogon elegans
Apaloderma aequatoriale
Upupa epops
Phoeniculus purpureus
Bucorvus leadbeateri
Tockus camurus
Merops muelleri
Corabias cyanogaster
Atelornis pittoides
Todus mexicanus
Momotus lessonii
Alcedo quadribrachys
Chloroceryle inda
Galbula dea
Bucco capensis
Chelidoptera tenebrosa
Indicator exilis
Picus canus
Jynx torquilla
Megalaima chrysopogon
Buccanodon duchaillui
Ramphastos ambiguus
Capito niger
Cariama cristata
Chunga burmeisteri
Micrastur gilvicollis
Falco sparverius
Caracara cheriway
Ibycter americanus
Nestor meridionalis
Probosciger aterrimus
Barnardius zonarius
Psittrichas fulgidus
Deroptyus accipitrinus
Psittacus erithacus
Acanthisitta chloris
Menura novaehollandiae
Climacteris melanura
Sericulus bakeri
Ptilonorhynchus violaceus
Malurus splendens
Lophorina superba
Corvus albus
Poecile lugubris
Calandrella brachydactyla
Sylvia melanocephala
Pycnonotus macrotis
Spizella arborea
Fringilla coelebs
Turdus olivater
Regulus ignicapilla
Nelodrepanis coruscans
Eurylaimus ochromalus
Pitta angolensis
Smithornis rufolateralis
Calyptomena viridis
Myrmotherea campanisona
Sclerurus mexicanus
Lepidocolaptes angustirostris
Furnarius rufus
Melanopareia maximiliani
Myrmornis torquata
Thamnophilus ruficapillus
Terenura callinota
Neopelma chrysocephalum
Pipra erythrocephala
Cryptopipo holochlora
Rupicola rupicola
Cotinga cayana
Myiobius barbatus
Oxyruncus cristatus
Schiffornis turdina
Tityra cayana
Piprites chloris
Rhynchocyclus olivaceus
Hirundinea ferruginea
Elaenia flavogaster
Tyrannus albogularis
Hymenops perspicillatus

**Figure D.19.** Phylogenetic tree of 200 extant avian taxa showing the ACE maximum likelihood estimates of cursoriality (All Rates Different model reconstruction) at each node. Orange denotes percentage likelihood of cursoriality.

*D.2 Tables*

**Table D.1.** Rates, log-likelihood estimates, and AICc values for the ACE models, grouped by foot use character.

| Ancestral Character Estimation Model | AICc | log-likelihood | rates |
|---|---|---|---|
| Raptoriality with fossils - Equal Rates (ER) | 83.2 | -40.602 | 0.001 |
| Raptoriality with fossils - All Rates Different (ARD) | 132.5 | -64.265 | 1.398, 0.13 |
| Raptoriality with fossils and Messelastur gratulator - ER | 91.5 | -44.763 | 0.001 |
| Raptoriality with fossils and Messelastur gratulator - ARD | 137.4 | -66.704 | 1.365, 0.134 |
| Raptoriality without fossils - ER | 54.8 | -26.406 | 0.001 |
| Raptoriality without fossils - ARD | 87.8 | -41.903 | 1.696, 0.099 |
| Force grip foot use - ER | 62.4 | -30.223 | 0.001 |
| Force grip foot use - ARD | 58.1 | -27.059 | 0.011, 0.0002 |
| Zygodactyly - ER | 80.3 | -36.677 | 0.0003 |
| Zygodactyly - ARD | 85.3 | -39.986 | 0.019, 0.0 |
| Anisodactyly - ER | 87.4 | -42.686 | 0.002 |
| Anisodactyly - ARD | 84.6 | -40.279 | 0.0, 0.027 |
| Heterodactyly - ER | 23.6 | -10.81 | 0.0003 |
| Heterodactyly - ARD | 41.8 | -18.914 | 4.912, 0.100 |
| Pamprodactyly - ER | 25.5 | -11.728 | 0.0003 |
| Pamprodactyly - ARD | 41.8 | -18.915 | 4.912, 0.100 |
| Documented walking ability - ER | 65.3 | -31.649 | 0.001 |
| Documented walking ability - ARD | 61.8 | -28.888 | 0.0, 0.036 |
| Terrestrial/Arboreal - ER | 257.7 | -127.859 | 0.0004 |
| Terrestrial/Arboreal - ARD | 233.3 | -110.649 | 0.063, 0.0003, 0.003, 0.011, 0.0, 0.074 |
| Hanging and clinging behaviour - ER | 128.2 | -63.1 | 0.003 |
| Hanging and clinging behaviour - ARD | 136.7 | -66.341 | 0.039, 0.002 |
| Scansoriality - ER | 45.9 | -21.938 | 0.0006 |
| Scansoriality - ARD | 56.5 | -26.255 | 3.241, 0.100 |
| Digital manipulation - ER | 72.4 | -35.207 | 0.001 |
| Digital manipulation - ARD | 93.4 | -44.7 | 1.541, 0.098 |
| Ability to hold down objects - ER | 73.7 | -35.855 | 0.001 |
| Ability to hold down objects - ARD | 74.6 | -35.318 | 0.000, 0.001 |
| Perching ability - ER | 155.1 | -76.567 | 0.004 |
| Perching ability - ARD | 146.3 | -71.141 | 0.0002, 0.012 |
| Hopping ability - ER | 128.6 | -63.323 | 0.003 |
| Hopping ability - ARD | 117.6 | -56.805 | 0.029, 0.0008 |
| Cursoriality - ER | 128.4 | -63.186 | 0.003 |
| Cursoriality - ARD | 126.04 | -61.02 | 0.009, 0.002 |

*D.3 Data*

All data and code used to produce the final results are archived at https://doi.org/10.5281/zenodo.7031733. All computations were processed in an R statistical environment (R Core Team 2022).

**Data D.1** Spreadsheet of taxa included in the phylogeny by Prum et al. (2015), with two extant and 23 fossil taxa added, scored for raptoriality and other foot uses.

**Data D.2** Spreadsheet of taxa included in the phylogeny by Prum et al. (2015), with two extant and 24 fossil taxa added (includes *Messelastur gratulator*), scored for raptoriality and other foot uses.

**Data D.3** Phylogenetic tree (Newick format) by Prum et al. (2015), with two extant and 23 fossil taxa added.

**Data D.4** Phylogenetic tree (Newick format) by Prum et al. (2015), with two extant and 24 fossil taxa added (includes *Messelastur gratulator*)

**Data D.5** Ancestral Character Estimations of foot uses in extant and fossil taxa in Aves.

# References


Abel, P., Werneburg, I., 2021. Morphology of the temporal skull region in tetrapods: reserach history, functional explanations, and a new comprehensive classification scheme. Biological Reviews 96 (5), 2229-2257. doi: 10.1111/brv.12751

Adams, D.C., 2014. A method for assessing phylogenetic least squares models for shape and other high-dimensional multivariate data: PGLS for high-dimensional data. Evolution 68, 2675–2688. https://doi.org/10.1111/evo.12463

Adams, D.C., Collyer, M.L. and Kaliontzopoulou, A., 2020. Geomorph: Software for geometric morphometric analyses. R package version 3.2.1. https://cran.r-project.org/package=geomorph.

Alcover, J.A., Pieper, H., Pereira, F., Rando, J.C., 2015. Five new extinct species of rails (Aves: Gruiformes: Rallidae) from the Macaronesian Islands (North Atlantic Ocean). Zootaxa 4057 (2), 151-190. http://dx.doi.org/10.11646/zootaxa.4057.2.1

Arredondo O., 1976. The Great Predatory Birds of the Pleistocene of Cuba, in Olson, S.L. (Ed.), n.d. Collected Papers in Avian Paleontology Honoring the 90th Birthday of Alexander Wetmore. Smithsonian Contributions to Paleobiology 27, 244.

Backus, S.B., Sustaita, D., Odhner, L.U., Dollar, A.M., 2015. Mechanical analysis of avian feet: multiarticular muscles in grasping and perching. R. Soc. Open Sci. 2, 140350. https://doi.org/10.1098/rsos.140350

Barber, B.R., Robbins, M.B., 2002. Nest and eggs of the Tepui antpitta (Myrmothera simplex). Wilson Journal of Ornithology 1, 114, 287–288. https://doi.org/10.1676/0043-5643(2002)114[0287:NAEOTT]2.0.CO;2

Barbosa, A., Moreno, E., 1999. Hindlimb morphology and locomotor performance in waders: An evolutionary approach. Biological Journal of the Linnean Society, 67(3), 313–330. https://doi.org/10.1111/j.1095-8312.1999.tb01936.x

Baumel, J.J., Witmer, L.M., 1993. 4. Osteologia, in: Baumel, J.J. (Ed.), Handbook of Avian Anatomy: Nomina Anatomic Avium. Nuttall Ornithology Club, 45–132.

Becker, J.J., 1985. Pandion lovensis, A New Species Of Osprey From The Late Miocene Of Florida. Proceedings of the Biological Society of Washington 98, 314–320.

Bennett, M.B., 1996. Allometry of the leg muscles of birds. Journal of Zoology 238, 435–443. https://doi.org/10.1111/j.1469-7998.1996.tb05404.x

Benson, R.B.J., Starmer-Jones, E., Close, R.A., Walsh, S.A., 2017. Comparative analysis of vestibular ecomorphology in birds. J. Anat. 231, 990–1018. https://doi.org/10.1111/joa.12726

Benson, R.B.J., Hunt, G., Carrano, M.T., Campione, N., 2018. Cope's rule and the adaptive landscape of dinosaur body size evolution. Palaeontology 61, 13-48. doi: 10.1111/pala.12329

Berger, A.J., 1956. The Appendicular Myology of the Pygmy Falcon (Polihierax semitorquatus). The American Midland Naturalist, 55 (2), 326-333. https://www.jstor.org/stable/2422594

Berger, A.J., 1960. Some Anatomical Characters of the Cuculidae and the Musophagidae. The Wilson Bulletin, 72 (1), 60-104. http://www.jstor.com/stable/4158806

Berman, S.L., 1984. The hindlimb musculature of the White-fronted amazon (Amazona

albifrons, Psittaciformes). The Auk, 101, 74-92.
Berman S.L., Raikow R.J., 1982. The Hindlimb Musculature of the Mousebirds (Coliiformes). The Auk 99, 41–57.
Billerman, S.M., Keeney, B.K., Rodewald, P.G., Schulenberg, T.S. (Eds.), 2022. Birds of the World. Cornell Laboratory of Ornithology, Ithaca, NY, USA. https://birdsoftheworld.org/bow/home
Bock, W.J., 1994. Concepts and methods in ecomorphology. Journal of Biosciences 19 (4), 403-413. doi: 10.1007/BF02703177
Bock, W.J., Miller, W.D., 1959. The Scansorial Foot of the Woodpeckers, with Comments on the Evolution of Perching and Climbing Feet in Birds. American Museum Novitates 46.
Bookstein, F.L., 1991. Morphometric Tools for Landmark Data: Geometry and Biology. Cambridge University Press.
Botelho, J.F., Smith-Paredes, D., Nuñez-Leon, D., Soto-Acuña, S., Vargas, A.O., 2014. The developmental origin of zygodactyl feet and its possible loss in the evolution of Passeriformes. Proceedings of the Royal Society B: Biological Sciences 281, 20140765. https://doi.org/10.1098/rspb.2014.0765
Botelho, J.F., Smith-Paredes, D., Vargas, A.O., 2015. Altriciality and the Evolution of Toe Orientation in Birds. Evol Biol 42, 502–510. https://doi.org/10.1007/s11692-015-9334-7
Bourdon, E., Kristoffersen, A.V., Bonde, N., 2016. A roller-like bird (Coracii) from the Early Eocene of Denmark. Scientific Reports6 (34050). doi: 10.1038/srep34050
Bribiesca-Contreras, F., Parslew, B., Sellers, W.I., 2019. A Quantitative and Comparative Analysis of the Muscle Architecture of the Forelimb Myology of Diurnal Birds of Prey (Order Accipitriformes and Falconiformes). The Anatomical Record 302, 1808-1823.
Bright, J.A., Marugan-Lobon, J., Rayfield, E.J., Cobb, S.N., 2019. The multifactorial nature of beak and skull shape evolution in parrots and cockatoos (Psittaciformes). BMC Evolutionary Biology 19(1).
Brooks, A., 1945. The Under-Water Actions of Diving Ducks. The Auk 62, 517–523. https://doi.org/10.2307/4079802
Burnham, K.P., Anderson, D.R., 2002. Model Selection and Multimodel Inference: A Practical Information-Theoretic Approach, 2nd ed. Springer New York, NY, USA.
Burton, P.J.K., 1978. The intertarsal joint of the harrier-hawks Polyboroides spp. and the crane hawk Geranospiza caerulescens. Ibis 120, 171–177.
Burton, P.J.K., 1989. Birds of Prey. Gallery Books, New York.
Campione, N.E., Evans, D.C., 2012. A universal scaling relationship between body mass and proximal limb bone dimensions in quadrupedal terrestrial tetrapods. BMC Biology 10 (60), 1-21.
Carril, J., Mosto, M.C., Picasso, M.B.J., Tambussi, C.P., 2014. Hindlimb myology of the monk parakeet (Aves, Psittaciformes): Hindlimb Myology Of The Monk Parakeet. Journal of Morphology 275, 732–744. https://doi.org/10.1002/jmor.20253
Case, E.C., 1924. A possible explanation of fenestration in the primitive reptilian skull, with notes on the temporal region of the genus Dimetrodon. Contributions from the Museum of Geology University of Michigan 2 (1), 1-12.
Choiniere, J.N., Neenan, J.M., Schmitz, L., Ford, D.P., Chapelle, K.E.J., Balanoff, A.M., Sipla,

J.S., Georgi, J.A., Walsh, S.A., Norell, M.A., Xu, X., Clark, J.M., Benson, R.B.J., 2021. Evolution of vision and hearing modalities in theropod dinosaurs. Science 372, 610-613.
Clifton, G.T., Biewener, A.A., 2018. Foot-propelled swimming kinematics and turning strategies in common loons. Journal of Experimental Biology 221, jeb168831. https://doi.org/10.1242/jeb.168831
Collar, D.C., Schulte, J.A., O'Meara, B.C., Losos, J.B., 2010. Habitat use affects morphological diversification in dragon lizards. Journal of Evolutionary Biology 23, 1033-1049. doi: 10.1111/j.1420-9101.2010.01971.x
Collyer, M.L., Adams, D.C., 2018. RRPP: An R package for fitting linear models to high-dimensional data using residual randomization. Methods in Ecology and Evolution. 9(2), 1772-1779. https://besjournals.onlinelibrary.wiley.com/doi/10.1111/2041-210X.13029
Collyer, M.L., Adams, D.C., 2020. RRPP: Linear Model Evaluation with Randomized Residuals in a Permutation Procedure. R package version 0.4.1 https://cran.r-project.org/web/packages/RRPP
Cracraft, J., 1972. The Functional Morphology of the Hind Limb of the Domestic Pigeon, Columba livia. The Auk 89, 903–905. https://doi.org/10.2307/4084131
Crompton, R.H., Sellers, W.I., Thorpe, S.K.S., 2010. Arboreality, terrestriality and bipedalism. Phil. Trans. R. Soc. B 365, 3301-3314. doi: 10.1098/rstb.2010.0035
Crouch, N.M.A., Ramanauskas, K., Igić, B., 2019. Tip-dating and the origin of Telluraves. Molecular Phylogenetics and Evolution 131, 55-63. doi: 10.1016/j.ympev.2018.10.006
Csermely, D., Berte, L., Camoni, R., 1998. Prey Killing by Eurasian Kestrels: The Role of the Foot and the Significance of Bill and Talons. Journal of Avian Biology 29, 10. https://doi.org/10.2307/3677335
Cunningham, C.W., Omland, K.E., Oakley, T.H., 1998. Reconstructing ancestral character states: a critical reappraisal. Trends in Ecology & Evolution 13, 361–366. https://doi.org/10.1016/S0169-5347(98)01382-2
Dececchi, T.A., Larsson, H.C.E., 2011. Assessing Arboreal Adaptations of Bird Antecedents: Testing the Ecological Setting of the Origin of the Avian Flight Stroke. PLoS ONE 6 (8), e22292. doi: 10.1371/journal.pone.0022292
Degrange, F.J., 2017. Hind limb morphometry of terror birds (Aves, Cariamiformes, Phorusrhacidae): functional implications for substrate preferences and locomotor lifestyle. Earth and Environmental Science Transactions of the Royal Society of Edinburgh 106, 257–276. https://doi.org/10.1017/S1755691016000256
De Mendoza, R.S., Gómez, R.O., 2022. Ecomorphology of the tarsometatarsus of waterfowl (Anseriformes) based on geometric morphometrics and its application to fossils. The Anatomical Record. https://doi.org/10.1002/ar.24891
De Mendoza, R.S., Tambussi, C.P., 2015. Osteosclerosis in the Extinct Cayaoa bruneti (Aves, Anseriformes): Insights on Behavior and Flightlessness. Ameghiniana 52. 305–313.
Dollo, M.L., 1884. Cinquième note sur les dinosauriens de Bernissart. Bulletin du Musée Royal d'Histoire Naturelle de Belgique - Mededeelingen van het Koninklijk Natuurhistorisch Museum van België, 3 (8), 129-146.
Dyke, G.J., Cooper, J.H., 2000. A new psittaciform bird from the London Clay (Lower Eocene) of England. Palaeontology 43, 271–285. https://doi.org/10.1111/1475-4983.00126

Einoder, L.D., Richardson, A.M.M., 2007. Aspects of the hindlimb morphology of some Australian birds of prey: A comparative and quantitative study. Auk 124, 773–788. https://doi.org/10.1642/0004-8038(2007)124[773:AOTHMO]2.0.CO;2

Emslie, S.D., 1988. The Fossil History and Phylogenetic Relationships of Condors (Ciconiiformes: Vulturidae) in the New World. Journal of Vertebrate Paleontology, 8 (2), 212-228. https://www.jstor.org/stable/4523192

Feduccia, A., 1999. The Origin and Evolution of Birds: the architecture of flightless birds. Yale University Press.

Feduccia, A., Martin, L.D., 1976. The World's Oldest Owl: A New Strigiform from the Paleocene of Southwestern Colorado. In Olson, S.L. (Ed.), n.d. Collected Papers in Avian Paleontology Honoring the 90th Birthday of Alexander Wetmore. Smithsonian Contributions to Paleobiology 27, 244, 101–110.

Felsenstein, J., 1985. Phylogenies and the Comparative Method. The American Naturalist 125, 1–15.

Field, D.J., Bercovici, A., Berv, J.S., Dunn, R., Fastovsky, D.E., Lyson, T.R., Vajda, V., Gauthier, J.A., 2018. Early Evolution of Modern Birds Structured by Global Forest Collapse at the End-Cretaceous Mass Extinction. Current Biology 28, 1825-1831.e2. https://doi.org/10.1016/j.cub.2018.04.062

Finarelli, J.A., Flynn, J.J., 2006. Ancestral State Reconstruction of Body Size in the Caniformia (Carnivora, Mammalia): The Effects of Incorporating Data from the Fossil Record. Systematic Biology 55, 301–313. https://doi.org/10.1080/10635150500541698

Fowler, D.W., Freedman, E.A., Scannella, J.B., 2009. Predatory Functional Morphology in Raptors: Interdigital Variation in Talon Size Is Related to Prey Restraint and Immobilisation Technique. PLoS ONE 4, e7999. https://doi.org/10.1371/journal.pone.0007999

Frazzetta, T.H., 1968. Adaptive Problems and Possibilities in the Temporal Fenestration of Tetrapod Skulls. J. Morph. 125, 145-158.

Fry, C.H., Fry, K., 2010. Kingfishers, Bee-eaters and Rollers. A&C Black.

Gadow, H., ed. Bronn, H.G., 1893. Vögel, Vol. I. Klassen und Ordnungen des Thier-Reichs, Leipzig, 1-301.

Gál, E., Kessler, E., 2005. Songbird remains from the Miocene (Middle Sarmatian) site Credinţa (Dobrogea, south-east Romania). In Csiki, Z., (ed.) 'Volume dedicated to Dan Grigorescu on his 65th birthday', 117–125. Bucharest: University of Bucharest Printing House

Garland Jr., T., Midford, P.E., Ives, A.R., 1999. An Introduction to Phylogenetically Based Statistical Methods, with a New Method for Confidence Intervals on Ancestral Values. American Zoologist 39 (2), 374-388. https://doi.org.10.1093/icb/39.2.374

Garrod, A.H., 1874. On certain Muscles of Birds and their Value in Classification, Part II. Proceedings of the Zoological Society of London, 111-123.

Garthe, S., Benvenuti, S., Montevecchi, W.A., 2000. Pursuit plunging by northern gannets (Sula bassana) "feeding on capelin (Mallotus villosus)." Proceedings of the Royal Society of London. Series B: Biological Sciences 267, 1717–1722. https://doi.org/10.1098/rspb.2000.1200

Gaspar, J., Gibb, G.C., Trewick, S.A., 2020. Convergent morphological responses to loss of

flight in rails (Aves, Rallidae). Ecology and Evolution 10(13), 6186–6207.
Gatesy, S.M., Dial, K.P., 1996. Locomotor Modules and the Evolution of Avian Flight. Evolution 50, 331. https://doi.org/10.2307/2410804
Gatesy, S.M., Middleton, K.M., 1997. Bipedalism, flight, and the evolution of theropod locomotor diversity. Journal of Vertebrate Paleontology 17, 308–329. https://doi.org/10.1080/02724634.1997.10010977
Gebo, D.L., 1996. Climbing, Brachiation, and Terrestrial Quadrupedalism: Historical Precursors of Hominid Bipedalism. American Journal of Physical Anthropology 101, 55-92.
Goslow, G.E., 1971. The Attack and Strike of Some North American Raptors. The Auk 88, 815–827. https://doi.org/10.2307/4083840
Grafen, A., Hails, R., 2002. Modern Statistics for the Life Sciences: Learn to analyse your own data. Oxford University Press.
Grafen, A., Hamilton, W.D., 1989. The phylogenetic regression. Philosophical Transactions of the Royal Society of London. B, Biological Sciences 326, 119–157. https://doi.org/10.1098/rstb.1989.0106
Gregory, W.K., Adams, L.A., 1915. The Temporal Fossæ of Vertebrates in Relation to the Jaw Muscles. Science 41 (1064), 763-765. doi: 10.1126/science.41.1064.763
Grémillet, D., Argentin, G., Schulte, B., Culik, B.M., 1998. Flexible foraging techniques in breeding Cormorants Phalacrocorax carbo and Shags Phalacrocorax aristotelis: benthic or pelagic feeding? Ibis 140, 113–119. https://doi.org/10.1111/j.1474-919X.1998.tb04547.x
Gressler, D., Marini, M., 2008. Nest, eggs and nestling of the Collared Crescentchest Melanopareia torquata in the Cerrado region, Brazil. Revista Brasileira de Ornitologia 15.
Gunz, P., Mitteroecker, P., 2013. Semilandmarks: A method for quantifying curves and surfaces. Hystrix, the Italian Journal of Mammalogy 24. https://doi.org/10.4404/hystrix-24.1-6292
Hackett, S.J., Kimball, R.T., Reddy, S., Bowie, R.C.K., Braun, E.L., Braun, M.J., Chojnowski, J.L., Cox, W.A., Han, K., Harshman, J., Huddleston, C.J., Marks, B.D., Miglia, K.J., Moore, W.S., Sheldon, F.H., Steadman, D.W., Witt, C.C., Yuri, T., 2008. A Phylogenomic Study of Birds Reveals Their Evolutionary History.
Habib, M.B., Ruff, C.B., 2008. The effects of locomotion on the structural characteristics of avian limb bones. Zoological Journal of the Linnean Society 153, 601–624. Science 320 (5884), 1763-1768. doi: 10.1126/science.1157704
Harrison, C.J.O., Walker, C.A., 1972. The affinities of Halcyornis from the Lower Eocene. Bull Br Mus (Nat Hist) Geol 21, 153-170.
Hastie, T., Tibshirani, R., 2020. mda: Mixture and Flexible Discriminant Analysis. R package version 0.5-3. https://CRAN.R-project.org/package=mda
Hayes, G., Alexander, R.McN., 2009. The hopping gaits of crows (Corvidae) and other bipeds. Journal of Zoology 200, 205–213. https://doi.org/10.1111/j.1469-7998.1983.tb05784.x
Heers, A.M., Dial, K.P., 2015. Wings versus legs in the avian bauplan : Development and evolution of alternative locomotor strategies. Evolution 69, 305–320. https://doi.org/10.1111/evo.12576
Hertel, F., 1995. Ecomorphological indicators of feeding behavior in recent and fossil raptors. The Auk 112 (4), 890-903. https://www.jstor.org/stable/4089021
Hertel, F., Maldonado, J.E., Sustaita, D., 2015. Wing and hindlimb myology of vultures and

raptors (Accipitriformes) in relation to locomotion and foraging. Acta Zoologica 96, 283–295. https://doi.org/10.1111/azo.12074

Hinić-Frlog, S., Motani, R., 2010. Relationship between osteology and aquatic locomotion in birds: determining modes of locomotion in extinct Ornithurae. Journal of Evolutionary Biology 23, 372–385. https://doi.org/10.1111/j.1420-9101.2009.01909.x

Houde, P., Olson, S.L., 1992. A radiation of coly-like birds from the eocene of North America (Aves: Sandcoleiformes new order). Natural History Museum of Los Angeles County, Science Series 36, 137–160.

James, F.C., 1982. The ecological morphology of birds: a review. Annales Zoologici Fennici 19, 265–275.

Jarvis, E.D., Mirarab, S., Aberer, A.J., Li, B., Houde, P., Li, C., Ho, S.Y.W., Faircloth, B.C., Nabholz, B., Howard, J.T., Suh, A., Weber, C.C., Fonseca, R.R. da, Li, J., Zhang, F., Li, H., Zhou, L., Narula, N., Liu, L., Ganapathy, G., Boussau, B., Bayzid, M.S., Zavidovych, V., Subramanian, S., Gabaldón, T., Capella-Gutiérrez, S., Huerta-Cepas, J., Rekepalli, B., Munch, K., Schierup, M., Lindow, B., Warren, W.C., Ray, D., Green, R.E., Bruford, M.W., Zhan, X., Dixon, A., Li, S., Li, N., Huang, Y., Derryberry, E.P., Bertelsen, M.F., Sheldon, F.H., Brumfield, R.T., Mello, C.V., Lovell, P.V., Wirthlin, M., Schneider, M.P.C., Prosdocimi, F., Samaniego, J.A., Velazquez, A.M.V., Alfaro-Núñez, A., Campos, P.F., Petersen, B., Sicheritz-Ponten, T., Pas, A., Bailey, T., Scofield, P., Bunce, M., Lambert, D.M., Zhou, Q., Perelman, P., Driskell, A.C., Shapiro, B., Xiong, Z., Zeng, Y., Liu, S., Li, Z., Liu, B., Wu, K., Xiao, J., Yinqi, X., Zheng, Q., Zhang, Y., Yang, H., Wang, J., Smeds, L., Rheindt, F.E., Braun, M., Fjeldsa, J., Orlando, L., Barker, F.K., Jønsson, K.A., Johnson, W., Koepfli, K.-P., O'Brien, S., Haussler, D., Ryder, O.A., Rahbek, C., Willerslev, E., Graves, G.R., Glenn, T.C., McCormack, J., Burt, D., Ellegren, H., Alström, P., Edwards, S.V., Stamatakis, A., Mindell, D.P., Cracraft, J., Braun, E.L., Warnow, T., Jun, W., Gilbert, M.T.P., Zhang, G., 2014. Whole-genome analyses resolve early branches in the tree of life of modern birds. Science 346, 1320–1331. https://doi.org/10.1126/science.1253451

Jetz, W., Thomas, G., Joy, J., Hartmann, K., Mooers, A.O., 2012. The global diversity of birds in space and time. Nature 491, 444–448. https://doi.org/10.1038/nature11631

Johansson, L.C., Norberg, U.M.L., 2001. Lift-based paddling in diving grebe. Journal of Experimental Biology 204, 1687–1696.

Johansson, L.C., Norberg, R.Å., 2003. Delta-wing function of webbed feet gives hydrodynamic lift for swimming propulsion in birds. Nature 424, 65–68. https://doi.org/10.1038/nature01695

Johnson, J.A., Brown, J.W., Fuchs, J., Mindell, D.P., 2016. Multi-locus phylogenetic inference among New World Vultures (Aves: Cathartidae). Molecular Phylogenetics and Evolution 105, 193-199. doi: 10.1016/j.ympev.2016.08.025

Jollie, M., 1953. Are the Falconiformes a monophyletic group?. Ibis Short Communications, 95, 369-371.

Kirchner-Smith, M.E., 2015. 3D Geometric Morphometrics In Modern And Extinct Foot-

Propelled Diving Birds: An Evaluation Of The Tarsometatarsus For Species Identification. Master's Theses, 48, Fort Hays State University. https://scholars.fhsu.edu/theses/48
Ksepka, D.T., Clarke, J.A., 2012. A new stem parrot from the Green River Formation and the complex evolution of the grasping foot in Pan-Psittaciformes. Journal of Vertebrate Paleontology 32, 395–406. https://doi.org/10.1080/02724634.2012.641704
Ksepka, D.T., Balanoff, A.M., Bell, M.A., Houseman, M.D., 2013. Fossil grebes from the Truckee Formation (Miocene) of Nevada and a new phylogenetic analysis of Podicipediformes (Aves). Palaeontology 56 (5), 1149-1169. doi: 10.1111/pala.12040
Ksepka, D.T., Stidham, T.A., Williamson, T.E., 2017. Early Paleocene landbird supports rapid phylogenetic and morphological diversification of crown birds after the K–Pg mass extinction. Proc Natl Acad Sci USA 114, 8047–8052. https://doi.org/10.1073/pnas.1700188114
Kuhn-Schnyder, E., 1980. Observations on Temporal Openings of Reptilian Skulls and the Classification of Reptiles. Mitteilungen aus dem Paläontologischen Institut der Universität Zürich 135.
Kulemeyer, C., Asbahr, K., Gunz, P., Frahnert, S., Bairlein, F., 2009. Functional morphology and integration of corvid skulls - a 3D geometric morphometric approach. Frontiers in Zoology 6 (2). doi: 10.1186/1742-9994-6-2
Kurochkin, E.N., Dyke, G.J., 2011. The first fossil owls (Aves: Strigiformes) from the Paleogene of Asia and a review of the fossil record of Strigiformes. Paleontol. J. 45, 445–458. https://doi.org/10.1134/S003103011104006X
Leisler, B., Winkler, H., 1985. Ecomorphology, in: Johnston, R.F. (Ed.), Current Ornithology: Volume 2, Current Ornithology. Springer US, Boston, MA, pp. 155–186. https://doi.org/10.1007/978-1-4613-2385-3_5
Ligon, J.D., 1967. Relationships of the Cathartid Vultures. Occasional Papers of the Museum of Zoology University of Michigan, 651, 1-26.
Livezey, B.C., 1992a. Morphological Corollaries and Ecological Implications of Flightlessness in the Kakapo (Psittaciformes: Strigops habroptilus). Journal of Morphology 213, 105 -145.
Livezey, B.C., 1992b. An ecomorphological review of the dodo (Raphus cucullatus) and solitaire (Pezophaps solitaria), flightless Columbiformes of the Mascarene Islands. J. Zool., Lond. 230, 247-292.
Lovvorn, J. R. (1991). Mechanics of underwater swimming in foot-propelled diving birds. Proc. Int. Ornith. Cong. 20,1868-1874. https://internationalornithology.org/iocongress-proceedings
Lowi-Merri, T.M., Benson, R.B.J., Claramunt, S., Evans, D.C., 2021. The relationship between sternum variation and mode of locomotion in birds. BMC Biology 19:165. https://doi.org/10.1186/s12915-021-01105-1
Madan, M.A., Rayfield, E.J., Bright, J.A., 2017. Scaling and functional morphology in strigiform hind limbs. Sci Rep 7, 44920. https://doi.org/10.1038/srep44920
Maddison, W.P., Maddison, D.R., 2021. Mesquite: a modular system for evolutionary analysis. Version 3.70 http://www.mesquiteproject.org

Maloiy, G.M.O., Alexander, R.M., Njau, R., Jayes, A.S., 1979. Allometry of the legs of running birds. Journal of Zoology 187, 161–167. https://doi.org/10.1111/j.1469-7998.1979.tb03940.x
Manegold, A., 2008. Earliest fossil record of the Certhioidea (treecreepers and allies) from the early Miocene of Germany. J. Ornithol. 149, 223-228. doi: 10.1007/s10336-007-0263-9
Manegold, A., Mayr, G., Mourer-Chauviré, C., 2004. Miocene songbirds and the composition of the European passeriform avifauna. The Auk 121 (4) 1155-1160.
Martins, E.P., Hansen, T.F., 1997. Phylogenies and the Comparative Method: A General Approach to Incorporating Phylogenetic Information into the Analysis of Interspecific Data. The American Naturalist 149, 646–667.
Mayr, G., 2001. Comments on the systematic position of the putative Lower Eocene parrot Pulchrapollia gracilis. Senckenbergiana lethaea 81, 339–341. https://doi.org/10.1007/BF03042787
Mayr, G., 2002. On the osteology and phylogenetic affinities of the Pseudasturidae – Lower Eocene stem-group representatives of parrots (Aves, Psittaciformes). Zoological Journal of the Linnean Society 136, 715–729. https://doi.org/10.1046/j.1096-3642.2002.00042.x
Mayr, G., 2005. The Postcranial Osteology and Phylogenetic Position of the Middle Eocene Messelastur gratulator Peters, 1994: A Morphological Link between Owls (Strigiformes) and Falconiform Birds?. Journal of Vertebrate Paleontology 25 (3), 635-645. https:www.jstor.org/stable/4524483
Mayr, G., 2008. The phylogenetic affinities of the parrot taxa Agapornis, Loriculus and Melopsittacus (Aves: Psittaciformes): hypotarsal morphology supports the results of molecular analyses. Emu - Austral Ornithology 108 (1), 23-27. doi: 10.1071/MU07059
Mayr, G., 2009a. A small loon and a new species of large owl from the Rupelian of Belgium (Aves: Gaviiformes, Strigiformes). Paläontol. Z. 83, 247-254. doi: 10.1007/s12542-009-0019-3
Mayr, G., 2009b. Paleogene Fossil Birds. Springer-Verlag.
Mayr, G., 2010. Parrot interrelationships - morphology and the new molecular phylogenies. Emu - Austral Ornithology, 110 (4), 348-357. doi: 10.1071/MU10035
Mayr, G., 2011a. Well-preserved new skeleton of the Middle Eocene Messelastur substantiates sister group relationship between Messelasturidae and Halcyornithidae (Aves, ?Pan-Psittaciformes). Journal of Systematic Palaeontology, 9: 1, 159-171 doi: 10.1080/14772019.2010.505252
Mayr, G., 2011b. The phylogeny of charadriiform birds (shorebirds and allies) - reassessing the conflict between morphology and molecules. Zoological Journal of the Linnean Society 161, 916-934.
Mayr, G., 2015. A reassessment of Eocene parrotlike fossils indicates a previously undetected radiation of zygodactyl stem group representatives of passerines (Passeriformes). Zoologica Scripta 44, 587–602. https://doi.org/10.1111/zsc.12128
Mayr, G., 2016. Variations in the hypotarsus morphology of birds and their evolutionary significance. Acta Zool 97, 196–210. https://doi.org/10.1111/azo.12117
Mayr, G., 2017. Pectoral girdle morphology of Mesozoic birds and the evolution of the avian supracoracoideus muscle. J. Ornithol. 158, 859-867. doi: 10.1007/s10336-017-1451-x

Mayr, G., 2019. Hypotarsus Morphology of the Ralloidea Supports a Clade Comprising Sarothrura and Mentocrex to the Exclusion of Canirallus. Acta Ornithologica 54 (1), 51-58. doi: 10.3161/00016454AO2019.54.1.005

Mayr, G., 2021a. The coracoscapular joint of neornithine birds - extensive homoplasy in a widely neglected articular surface of the avian pectoral girdle and its possible functional correlates. Zoomorphology 140, 217-228. doi: 10.1007/s00435-021-00528-2

Mayr, G., 2021b. A partial skeleton of a new species of Tynskya Mayr, 2000 (Aves, Messelasturidae) from the London Clay highlights the osteological distinctness of a poorly known early Eocene "owl/parrot mosaic". PalZ 95, 337-357. https://doi.org/10.1007/s12542-020-00541-8

Mayr, G., Daniels, M., 1998. Eocene parrots from Messel (Hessen, Germany) and the London Clay of Walton-on-the-Naze (Essex, England). Senckenbergiana lethaea 78, 157–177. https://doi.org/10.1007/BF03042767

Mayr, G., Göhlich, U.B., 2004. A new parrot from the Miocene of Germany, with comments on the variation of hypotarsus morphology in some Psittaciformes. Belg. J. Zool., 134 (1), 47-54.

Mayr, G., Yang, J., De Bast, E., Li, C., Smith, T., 2013. A Strigogyps-like bird from the middle Paleocene of China with an unusual grasping foot. Journal of Vertebrate Paleontology 33 (4), 895-901. http://dx.doi.org/10.1080/02724634.2013.748059

Mayr, G., Smith, T., 2019. A diverse bird assemblage from the Ypresian of Belgium furthers knowledge of early Eocene avifaunas of the North Sea Basin. N. Jb. Geol. Paläont. Abh., 291 (3), 253-281. doi: 10.1127/njgpa/2019/0801

Mayr, G., Gingerich, P.D., Smith, T., 2020. Skeleton of a new owl from the Eocene of North America (Aves, Strigiformes) with an accipitrid-like foot morphology. Journal of Vertebrate Paleontology e1769116. 1-15. DOI: 10.1080/02724634.2020.1769116.

McClure, C.J.W., Schulwitz, S.E., Anderson, D.L., Robinson, B.W., Mojica, E.K., Therrien, J., Oleyar, M.D., Johnson, J., 2019. Commentary: Defining Raptors and Birds of Prey. Journal of Raptor Research, Short Communications 53 (4), 419-430.

McGowan, C., 1979. The hind limb musculature of the brown kiwi,Apteryx australis mantelli. J. Morphol. 160, 33–73. https://doi.org/10.1002/jmor.1051600105

Middleton, K.M., 2001. The morphological basis of hallucal orientation in extant birds. J. Morphol. 250, 51–60. https://doi.org/10.1002/jmor.1058

Midtgård, U., 1982. Patterns in the blood vascular system in the pelvic limb of birds. Journal of Zoology 196, 545–567. https://doi.org/10.1111/j.1469-7998.1982.tb03523.x

Miller, W.DeW., 1919. Notes on the Structure of Anseranas semipalmata. The Auk 36, 562–564. https://doi.org/10.2307/4073357

Mindell, D.P., Fuchs, J., Johnson, J.A., 2018. Phylogeny, Taxonomy, and Geographic Diversity of Diurnal Raptors: Falconiformes, Accipitriformes, and Cathartiformes. In: Sarasola, J.H., Grande, J.M., Negro, J.J., eds., Birds of Prey: Biology and conservation in the XXI century. Switzerland: Springer, 3-32.

Morrison, J.L., Dwyer, J.F., 2021. Crested Caracara (*Caracara plancus*), version 1.0. In Birds of the World (A. F. Poole, Editor). Cornell Lab of Ornithology, Ithaca, NY, USA. https://doi.org/10.2173/bow.y00678.01

Mosto, M.C., Carril, J., Picasso, M.B.J., 2013. The Hindlimb Myology of Milvago Chimango (Polyborinae, Falconidae). Journal of Morphology 274, 1191-1201.
Mosto, M.C., Cassini, G.H., Picasso, M.B.J., Krone, O., 2021. Grasping behaviour in the white-tailed sea eagle (Accipitridae, Aves) explained by muscle architecture. Journal of Zoology, 1-11. doi:10.1111/jzo.12876
Motani, R., Schmitz, L., 2011. Phylogenetic versus functional signals in the evolution of form-function relationships in terrestrial vision. Evolution 65 (8), 2245-2257. doi: 10.1111/j.1558-5646.2011.0127.x
Mourer-Chauviré, C., 1983. Les Gruiformes (Aves) des phosphorites du Quercy (France). 1. Sous-ordre Cariamae (Cariamidae et Phorusrhacidae). Systématique et biostratigraphie. Palaeovertebrata 13 (4), 18-143.
Mourer-Chauviré, C., 1987. Les Strigiformes (Aves) des Phosphorites du Quercy (France): Systématique, biostratigraphie et paléobiogéographie. In L'Evolution des oiseaux d'après le témoignage des fossiles: Table ronde internationale du CNRS, Lyon-Villeurbanne, 18-21 Septembre 1985. Docum. Lab. Géol. Lyon 99, 89-135.
Mourer-Chauviré, C., 1994. A Large Owl From the Palaeocene of France. Palaeontology 37, 339–348.
Navalón, G., Bright, J.A., Marugán-Lobón, J., Rayfield, E.J., 2018. The evolutionary relationship among beak shape, mechanical advantage, and feeding ecology in modern birds. Evolution 73, 422–435. https://doi.org/10.1111/evo.13655
Negro, J.J., Pertoldi, C., Randi, E., Ferrero, J.J., López-Caballero, J.M., Rivera, D., Korpimäki, E., 2006. Convergent evolution of Elanus kites and the owls. Journal of Raptor Research 40, 222–225. https://doi.org/10.3356/0892-1016(2006)40[222:CEOEKA]2.0.CO;2
Norberg, R.Å., 1986. Treecreeper Climbing; Mechanics, Energetics, and Structural Adaptations. Ornis Scandinavica (Scandinavian Journal of Ornithology) 17, 191–209. https://doi.org/10.2307/3676828
Norberg, U.M., 1979. Morphology of the Wings, Legs and Tail of Three Coniferous Forest Tits, The Goldcrest, and the Treecreeper in Relation to Locomotor Pattern and Feeding Station Selection. Philosophical Transactions of the Royal Society B: Biological Sciences 287, 131–165. https://doi.org/10.1098/rstb.1979.0054
Noriega, J.I., Areta, J.I., Vizcaíno, S.F., Bargo, M.S., 2011. Phylogeny and taxonomy of the Patagonian Miocene falcon Thegornis musculosis Ameghino, 1895 (Aves: Falconidae). Journal of Paleontology 85 (6), 1089-1104. doi: 10.2307/41409115
Olson, E.C., Miller, R.L., 1999. Morphological Integration. University of Chicago Press.
Olson, S.L., Wingate, D.B., 2001. A new species of large flightless rail of the Rallus longirostris/elegans complex (Aves: Rallidae) from the late Pleistocene of Bermuda. Proceedings of the Biological Society of Washington 114(2), 509-516.
Orkney, A., Bjarnason, A., Tronrud, B.C., Benson, R.B.J., 2021. Patterns of skeletal integration in birds reveal that adaptation of element shapes enables coordinated evolution between anatomical modules. Nature Ecology and Evolution 5, 1250-1258. https://doi.org/10.1038/s41559-021-01509-w
Ossa-Fuentes, L., Soto-Acuña, S., Bona, P., Sallaberry, M., Vargas, A.O, 2020. Developmental

evolution of the distal ankle in the dinosaur-bird transition. J. Exp. Zool. B. (Mol Dev Evol) 338, 119-128. doi: 10.1002/jez.b.23022
Ostrom, J.H., 1974. Archaeopteryx and the Origin of Flight. The Quarterly Review of Biology 49 (1), 27-47. https://www.jstor.org/stable/2821658
Ostrom, J.H., 1976. Archaeopteryx and the origin of birds. Biological Journal of the Linnean Society 8, 91-182.
Padian, K., Chiappe, L.M., 1998. The Origin of Birds and Their Flight. Scientific American 278 (2), 38-47. https://www.jstor.org/stable/26057663
Pagel, M., 1999. Inferring the historical patterns of biological evolution. Nature 401, 877-884.
Pavia, M., Mourer-Chauviré, C., 2011. Redescription of Tyto sanctialbani Lydekker, 1893 (Aves, Strigiformes), from its Type Locality of La Grive-Saint-Alban (Middle Miocene, France). Journal of Vertebrate Paleontology 31 (5), 1093-1101. doi: 10.1080/02724634.2011.595465
Peters, D.S., 1994. Messelastur gratulator n. gen. n. spec., ein Greifvogel aus der Grube Messel (Aves: Accipitridae). Courier forschungsinstitut Senckenberg 170, 3-9.
Pinheiro J, Bates D, DebRoy S, Sarkar D, R Core Team, 2020. _nlme: Linear and Nonlinear Mixed Effects Models_. R package version 3.1-145, URL: https://CRAN.R-project.org/package=nlme.
Provini, P., Simonis, C., Abourachid, A., 2013. Functional implications of the intertarsal joint shape in a terrestrial ( Coturnix coturnix ) versus a semi-aquatic bird ( Callonetta leucophrys ): Functional implications of the intertarsal joint shape. J Zool 290, 12–18. https://doi.org/10.1111/jzo.12007
Prum, R.O., Berv, J.S., Dornburg, A., Field, D.J., Townsend, J.P., Lemmon, E.M., Lemmon, A.R., 2015. A comprehensive phylogeny of birds (Aves) using targeted next-generation DNA sequencing. Nature 526, 569–573. https://doi.org/10.1038/nature15697
Purvis, A., Gittleman, J.L., Luh, H., 1994. Truth or Consequences: Effects of Phylogenetic Accuracy on Two Comparative Methods. Journal of Theoretical Biology 167, 293-300.
Quinn, T.H., Baumel, J.J., 1990. The digital tendon locking mechanism of the avian foot (Aves). Zoomorphology 109, 281–293. https://doi.org/10.1007/BF00312195
Raikow, R.J., 1973. Locomotor Mechanisms in North American Ducks. The Wilson Bulletin 85, 295–307.
Raikow, R.J., 1985. Locomotor System, in: Form and Function in Birds. Academic Press, pp. 57–147.
Revell, L. J. 2012. phytools: An R package for phylogenetic comparative biology (and other things). R package version 0.7-20. Methods Ecol. Evol. 3 217-223. doi:10.1111/j.2041-210X.2011.00169.x
Rich, P.V., Bohaska, D.J., 1976. The World's Oldest Owl: A New Strigiform from the Paleocene of Southwestern Colorado. Smithsonian Contributions to Paleobiology 27, 87–93.
Romer, A.S., Price, L.W., 1940. Review of the Pelycosauria. Special Paper - Geological Society of America 28, 1-538.
Schluter, D., 1995. Uncertainty in ancient phylogenies. Nature Scientific Correspondence 377, 108-109.
Schluter, D., Price, T., Mooers, A.Ø., Ludwig, D., 1997. Likelihood of Ancestor States in

Adaptive Radiation. Evolution 51, 1699–1711. https://doi.org/10.1111/j.1558-5646.1997.tb05095.x
Schmidt-Nielsen, Knut, 1984. Scaling: Why is Animal Size So Important?. Cambridge University Press. doi:10.1017/CBO9781139167826
Schmitz, L., Motani, R., 2011. Nocturnality in Dinosaurs Inferred from Scleral Ring and Orbit Morphology. Science 332 (705). doi: 10.1126/science.1200043
Schneider, C.A., Rasband, W.S., Eliceiri, K.W., 2012. NIH Image to ImageJ: 25 years of image analysis. Nature Methods, 9(7), 671–675. doi:10.1038/nmeth.2089
Silva, A.N., Nunes, R., Estrela, D.C., Malafaia, G., Castro, A.L.S., 2016. Behavioral repertoire of the poorly known Red-legged Seriema, Cariama cristata (Cariamiformes: Cariamidae). Revista Brasileira de Ornitologia 8.
Slater, G.J., Harmon, L.J., Alfaro, M.E., 2012. Integrating fossils with molecular phylogenies improves inference of trait evolution. Evolution 66-12, 3931-3944. doi: 10.1111/j.1558-5646.2012.01723.x
Spiess, A. 2018. qpcR: Modelling and Analysis of Real-Time PCR Data. R package version 1.4-1. https://CRAN.R project.org/package=qpcR
Sun, Y., Si, G., Wang, X., Wang, K., Zhang, Z., 2018. Geometric morphometric analysis of skull shape in the Accipitridae. Zoomorphology 137, 445-456. https://doi.org/10.1007/s00435-018-0406-y
Sustaita, D., 2008. Musculoskeletal underpinnings to differences in killing behavior between North American accipiters (Falconiformes: Accipitridae) and falcons (Falconidae). J. Morphol. 269, 283–301. https://doi.org/10.1002/jmor.10577
Sustaita, D., Hertel, F., 2010. In vivo bite and grip forces, morphology and prey-killing behavior of North American accipiters (Accipitridae) and falcons (Falconidae). Journal of Experimental Biology 213, 2617–2628. https://doi.org/10.1242/jeb.041731
Sustaita, D., Pouydebat, E., Manzano, A., Abdala, V., Hertel, F., Herrel, A., 2013. Getting a grip on tetrapod grasping: form, function, and evolution: Grasping in tetrapods. Biol Rev 88, 380–405.
Sustaita, D., Gloumakov, Y., Tsang, L.R., Dollar, A.M., 2019. Behavioral correlates of semi-zygodactyly in Ospreys (Pandion haliaetus) based on analysis of internet images. PeerJ 7, e6243. https://doi.org/10.7717/peerj.6243
Tarboton, W.R., 1978. Hunting and the Energy Budget of the Black-Shouldered Kite. The Condor 80, 88. https://doi.org/10.2307/1367793
Taylor, G., Thomas, A., 2014. Adaptation in avian wing design, in: Evolutionary Biomechanics. Oxford University Press. https://doi.org/10.1093/acprof:oso/9780198566373.001.0001
Thorp, B.H., 1988. Vascular pattern of the developing intertarsal joint in the domestic fowl. Research in Veterinary Science 44, 100–111. https://doi.org/10.1016/0034-5288(88)90020-3
Townsend, C.W., 1909. The Use of the Wings and Feet by Diving Birds. The Auk 26, 234–248. https://doi.org/10.2307/4070795
Tsang, L.R., McDonald, P.G., 2019. A comparative study of avian pes morphotypes, and the functional implications of Australian raptor pedal flexibility. Emu - Austral Ornithology 119, 14–23. https://doi.org/10.1080/01584197.2018.1483203

van der Loo, M., van der Laan, J., R Core Team, Logan, N., Muir, C., Gruber, J., Ripley, B., 2020. stringdist: Approximate String Matching, Fuzzy Text Search, and String Distance Functions. R package version https://CRAN.R-project.org/package=stringdist
Venables, W.N., Ripley, B.D., 2002. Modern Applied Statistics with S, Fourth edition. Springer, New York. https://www.stats.ox.ac.uk/pub/MASS4/.
Verstappen, M., Aerts, P., De Vree, F., 1998. Functional morphology of the hindlimb musculature of the black-billed magpie, Pica pica (Aves, Corvidae). Zoomorphology 118, 207–223. https://doi.org/10.1007/s004350050070
Vieillot, J.L.P., 1820-1830?. Faune française, ou Histoire naturelle, générale et particulière des animaux qui se trouvent en France, constamment ou passagèrement, à la surface du sol, dans les eaux qui le baignent, et dans le littoral des mers qui le bornent. Chez Rapet, Paris.
Vieillot, J.L.P., ed. Saunders, H., 1883. Vieillot's Analyse d'une nouvelle ornithologie élémentaire. The Willughby Society, London.
Volkov, S., 2004. The hindlimb musculature of the true owls (Strigidae: Strigiformes): Morphological peculiarities and general adaptations. Ornithologia 31. 154–174.
Voous, K.H., 1972. List of Recent Holarctic Bird Species Non-Passerines. Ibis Special Papers, 115:4, 612-638.
Walkinshaw, L.H., 1982. Observations on Limpkin Nesting. Florida Field Naturalist 10, 45–64.
Wanless, R., 2002. Frigatebirds: aerial attitude. Africa: Birds and Birding 7, 36–41.
Ward, A.B., Weigl, P.D., Conroy, R.M., 2002. Functional morphology of raptor hindlimbs: Implications for resource partitioning. The Auk 119(4). 1052–1063.
Waterhouse, D.M., 2006. Parrots in a nutshell: The fossil record of Psittaciformes (Aves). Historical Biology 18 (2), 227-238. doi: 10.1080/08912960600641224
Webster, M., Sheets, H.D., 2010. A practical introduction to landmark-based geometric morphometrics. The Paleontological Society Papers 16, 163–188.
Wetmore, A., 1960. A classification for the birds of the world. Smithsonian Miscellaneous Collections 139(11).
Wink, M., Seibold, I., Lotfikhah, F., Bednarek, W., 1998. Molecular Systematics of Holarctic Raptors (Order Falconiformes), in Chancellor, R.D., Meyburg, B.U., Ferrero, J.J. eds. "Holarctic Birds of Prey". ADENEX-WWGBP, 29-48.
Winkler, D. W., S. M. Billerman, and I. J. Lovette (2020a). Mousebirds (Coliidae), version 1.0. In Birds of the World (S. M. Billerman, B. K. Keeney, P. G. Rodewald, and T. S. Schulenberg, Editors). Cornell Lab of Ornithology, Ithaca, NY, USA. https://doi.org/10.2173/bow.coliid1.01
Winkler, D. W., S. M. Billerman, and I. J. Lovette (2020b). New Zealand Parrots (Strigopidae), version 1.0. In Birds of the World (S. M. Billerman, B. K. Keeney, P. G. Rodewald, and T. S. Schulenberg, Editors). Cornell Lab of Ornithology, Ithaca, NY, USA. https://doi.org/10.2173/bow.strigo1.01
Wright N.A., Steadman, D.W., Witt, C.C., 2016. Predictable evolution toward flightlessness in volant island birds. PNAS 113(17) 4765-4770.
Wu, Y., Yan, Y., Zhao, Y., Gu, L., Wang, S., Johnson, D.H., 2020. Genomic bases underlying

the adaptive radiation of core landbirds. bioRxiv 2020.07.29.222281; https://doi.org/10.1101/2020.07.29.222281

Yuri, T., Kimball,, R.T., Harshman, J., Bowie, R.C.K., Braun, M.J., Chojnowski, J.L., Han, K., Hackett, S.J., Huddleston, C.J., Moore, W.S., Reddy, S., Sheldon, F.H., Steadman, D.W., Witt, C.C., Braun, E.L., 2013. Parsimony and Model-Based Analyses of Indels in Avian Nuclear Genes Reveal Congruent and Incongruent Phylogenetic Signals. Biology 2, 419-444. doi: 10.3390/biology2010419

Zeffer A, Johansson LC, Marmebro Å., 2003. Functional correlation between habitat use and leg morphology in birds (Aves). Biol J Linn Soc. 79(3):461–484.

Zeffer, A., Norberg, U.M.L., 2003. Leg morphology and locomotion in birds: requirements for force and speed during ankle flexion. Journal of Experimental Biology 206, 1085–1097.

Zelditch, M.L., Swiderski, D.L., Sheets, H.D., Fink, W.L., 2004. Geometric Morphometrics for Biologists: A Primer. Elsevier.

Zelenkov, N.V., 2007. The structure and probable mechanism of evolutionary formation of the foot in piciform birds (Aves: Piciformes). Paleontol. J. 41, 290–297. https://doi.org/10.1134/S0031030107030082

Zhang, Z., Feduccia, A., James, H.F., 2012. A Late Miocene Accipitrid (Aves: Accipitriformes) from Nebraska and Its Implications for the Divergence of Old World Vultures. PLoS ONE 7 (11), e48842. doi: 10.1371/journal.pone.0048842